

EMPLACEMENT HISTORY OF THE PEARLY GATES
ANORTHOSITE PLUTON AND SPATIALLY RELATED
TESSIARSUYUNGOAKH INTRUSION, AND METAMORPHIC
PETROLOGY OF THE ADJACENT TASIUYAK
PARAGNEISS, NORTHERN LABRADOR

CENTRE FOR NEWFOUNDLAND STUDIES

**TOTAL OF 10 PAGES ONLY
MAY BE XEROXED**

(Without Author's Permission)

TANYA ANNE TETTELAAR

THE NATIONAL BUREAU OF STANDARDS
BUREAU OF CHEMISTRY
METHODS FOR THE DETERMINATION OF THE AMOUNT OF
SILICIC ACID IN SILICATES

By THOMAS W. WOODS, JR.



U.S. GOVERNMENT PRINTING OFFICE
WASHINGTON, D. C.
1924

Department of Commerce
BUREAU OF CHEMISTRY
WASHINGTON, D. C.

1924

**EMPLACEMENT HISTORY OF THE PEARLY GATES ANORTHOSITE PLUTON AND
SPATIALLY RELATED TESSIARSUYUNGOAKH INTRUSION, AND METAMORPHIC
PETROLOGY OF THE ADJACENT TASIUYAK PARAGNEISS, NORTHERN LABRADOR**

By: Tanya Anne Tettelaar, B.Sc. Honours



A thesis submitted to the School of Graduate Studies
in partial fulfillment of the requirements for
the degree of Master of Science

Department of Earth Sciences
Memorial University
St. John's, Newfoundland and Labrador

November, 2004



Library and
Archives Canada

Bibliothèque et
Archives Canada

0-494-06664-4

Published Heritage
Branch

Direction du
Patrimoine de l'édition

395 Wellington Street
Ottawa ON K1A 0N4
Canada

395, rue Wellington
Ottawa ON K1A 0N4
Canada

NOTICE:

The author has granted a non-exclusive license allowing Library and Archives Canada to reproduce, publish, archive, preserve, conserve, communicate to the public by telecommunication or on the Internet, loan, distribute and sell theses worldwide, for commercial or non-commercial purposes, in microform, paper, electronic and/or any other formats.

The author retains copyright ownership and moral rights in this thesis. Neither the thesis nor substantial extracts from it may be printed or otherwise reproduced without the author's permission.

AVIS:

L'auteur a accordé une licence non exclusive permettant à la Bibliothèque et Archives Canada de reproduire, publier, archiver, sauvegarder, conserver, transmettre au public par télécommunication ou par l'Internet, prêter, distribuer et vendre des thèses partout dans le monde, à des fins commerciales ou autres, sur support microforme, papier, électronique et/ou autres formats.

L'auteur conserve la propriété du droit d'auteur et des droits moraux qui protègent cette thèse. Ni la thèse ni des extraits substantiels de celle-ci ne doivent être imprimés ou autrement reproduits sans son autorisation.

In compliance with the Canadian Privacy Act some supporting forms may have been removed from this thesis.

Conformément à la loi canadienne sur la protection de la vie privée, quelques formulaires secondaires ont été enlevés de cette thèse.

While these forms may be included in the document page count, their removal does not represent any loss of content from the thesis.

Bien que ces formulaires aient inclus dans la pagination, il n'y aura aucun contenu manquant.


Canada

ABSTRACT:

The Mesoproterozoic Nain Plutonic Suite consists of anorthositic and granitic intrusions, which were emplaced along an older suture zone marked by the Torngat Orogen in northern Labrador. This study concerns the western margin of the Nain Plutonic Suite where the Pearly Gates Anorthosite pluton and spatially related Tessiarsuyungoakh intrusion, and the Makhavinekh Lake pluton, were intruded into the Paleoproterozoic Tasiuyak paragneiss of the Southeastern Churchill Province. Detailed geological mapping, petrography and U-Pb Thermal Ionization Mass Spectrometry dating of zircon and baddeleyite of the Pearly Gates Anorthosite pluton and Tessiarsuyungoakh intrusion were used to ascertain the mode of emplacement and crystallization ages of the major intrusive units. In addition, studies of the Paleoproterozoic regional metamorphism and Mesoproterozoic contact metamorphism of the Tasiuyak paragneiss were performed using the NaKFMASH petrogenetic grid to determine *P-T* conditions. The results of this thesis project indicate the following geological history of the study area.



The Tasiuyak paragneiss contains evidence of the Paleoproterozoic regional metamorphic mineral sub-assembly garnet + biotite + sillimanite. Detailed petrography of this sub-assembly indicated that the prograde and retrograde history of this unit occurred within the sillimanite stability field and peak *P-T* conditions were constrained in the range of 7.2 to 10.2 kbar and 800° to 830°C. Prior to ca. 1363 Ma, reactivation of structures in the paragneiss provided fractures into which monzonitic and monzodioritic magmas intruded as sheets. The 1363 ± 3 Ma monzonite and 1360 ± 4 Ma monzodiorite formed the composite Tessiarsuyungoakh intrusion. This intrusion produced a small (< 20 m) contact aureole in the Tasiuyak paragneiss. Incipient development of the contact metamorphic sub-assembly cordierite + orthopyroxene + spinel replaced the regional sub-assembly of garnet + biotite + sillimanite. This suggests that the Tessiarsuyungoakh intrusion was a small body with a short-lived emplacement and crystallization history. The *P-T* estimate of this contact aureole is between 3 and 4 kbar and 775° and 800°C.

Prismatic zircons included in plagioclase crystals from the Pearly Gates Anorthosite pluton yielded a maximum concordant crystallization age of 1370 ± 5 Ma. These crystals are

interpreted as having formed at depth at ca. 1370 Ma, prior to emplacement at a mid-crustal level. The earliest evidence of anorthosite emplacement is a relatively undeformed anorthosite body, herein called the Fraser Canyon Anorthosite, which intruded into the Tessiarsuyungoakh intrusion at 1355 ± 1.3 Ma. It is unknown if the Fraser Canyon Anorthosite is a part of the Pearly Gates Anorthosite pluton, however, both have similar characteristics such as an inner zone of massive anorthosite and an outer zone of layers of anorthosite and norite. The outer zone is interpreted as having crystallized relatively fast and the inner zone as having cooled relatively slowly. During crystallization of the outer zone, syn-emplacement deformation occurred along the contact between the Tessiarsuyungoakh intrusion and Pearly Gates Anorthosite pluton. Anhedral zircon fragments from the Pearly Gates Anorthosite pluton yielded an age of $1335 +7/-3$ Ma, of which the uppermost error limit of 1342 Ma is interpreted as approximating the final crystallization age of the pluton. Norite bodies that intruded the Pearly Gates Anorthosite pluton at ca. 1340 Ma are undeformed and indicate that the anorthosite had completely crystallized and deformation had ceased by this time.

At ca. 1322 Ma, the Makhavinekh Lake pluton intruded into the Tasiuyak paragneiss and produced a contact aureole 4 km wide with cordierite + orthopyroxene + spinel replacing regional garnet + biotite + sillimanite. The temperature gradient along this aureole ranged from 675°C at the 4 km limit of the contact aureole, to at least 850°C at the contact with the pluton, and isobaric conditions were between 3 to 4 kbar.

ACKNOWLEDGEMENTS:

This thesis is dedicated in memory of my mother Renate Tettelaar, who introduced me to the beauty of rocks. This work was supported by VBNC/Inco and NSERC through a CRD grant (CRDPJ 233669-99) to John Myers. The following people are thanked for their contributions to this project. My supervisor John Myers, who not only supported my work but also taught me a lot about geological mapping, as well as the importance of clear and concise writing. My "unofficial" supervisory committee members, Greg Dunning and Aphrodite Indares are thanked. Both of these individuals entered the murky and mystical waters and guided me through to clarity while developing my analytical skills. The Earth Sciences department is very lucky to have a terrific support staff. I would like to thank Gerry Ford, the multidisciplinarian, for his help in numerous situations, and the following people for their technical expertise: Pam King, Sherri Jordan and Mike Schaffer at Memorial University, and Pat Hunt at the GSC. My gratitude goes to Bruce Ryan and Don James for sharing their wealth of knowledge and invoking enthusiastic discussions that facilitated the direction and development of my ideas. My two field seasons would not have been possible without the logistical support from Voisey's Bay Nickel Company and a special thanks goes to Dan Lee, Rob Wheeler and Dawn Evans-Lamswood. I was extremely lucky to have two amazing field assistants, Brenda Obina and Tammy Perry, who made living out in the middle of nowhere a truly memorable experience. How they put up with the bears, wolves, bugs and worst of all, me, I'll never know! My time at MUN was enhanced by the friendship and support I've found in Istar Isler, Stephanie Papadimitriou, Cindy O'Driscoll, Marianne Mader, Don Wright and the Franklyn Inn gang. The preservation of my sanity during this adventure is due to Randy Batten for his strength and support during the good, the bad and the ugly. Finally, words cannot express what the support of my family has meant, particularly the enduring faith that my father has always had in me.

TABLE OF CONTENTS

TITLE PAGE	i
ABSTRACT	ii
ACKNOWLEDGMENTS	iv
TABLE OF CONTENTS	v
LIST OF TABLES	x
LIST OF FIGURES	xi
LIST OF PLATES	xiii
LIST OF MAPS	xvi
LIST OF ABBREVIATIONS AND SYMBOLS	xvii

CHAPTER 1 - INTRODUCTION TO THE THESIS STUDY

1.1 INTRODUCTION	1-1
1.1.1 Geological Importance of Anorthosites	1-1
1.1.2 Anorthosites of the Nain Plutonic Suite	1-2
1.1.3 Study Area	1-4
1.2 PETROGENESIS OF AMCG SUITES	1-5
1.2.1 Magmatic Source(s)	1-5
1.2.1.1 Depth of source(s)	1-5
1.2.1.2 Liquid versus crystal mush	1-6
1.2.1.3 AMCG suites – parental magma(s) and source region(s)	1-7
1.2.2 Emplacement Mechanisms – NPS	1-10
1.3 OUTSTANDING PROBLEMS	1-12
1.4 THESIS GOALS	1-12
1.5 METHODOLOGY	1-13

1.5.1 Field Mapping and Sampling	1-13
1.5.2 U-Pb Geochronology	1-14
1.5.2.1 U-Pb systematics theory	1-14
1.5.2.2 Analytical techniques	1-16
1.5.3 Metamorphism	1-18
1.5.3.1 Electron microprobe analytical conditions	1-18
1.5.3.2 Petrogenetic grids	1-19
1.6 THESIS STRUCTURE	1-19
 CHAPTER 2 - REGIONAL AND LOCAL GEOLOGY	
2.1 INTRODUCTION	2-1
2.2 REGIONAL GEOLOGY	2-1
2.3 STUDY AREA	2-4
2.3.1 Introduction	2-4
2.3.2 Previous Work	2-4
2.3.3 Location and Access	2-5
2.3.4 Field Component of the Project	2-5
2.3.5 Local Geology	2-6
2.3.5.1 Pearly Gates Anorthosite pluton	2-6
2.3.5.2 Tessiarsuyungoakh intrusion	2-7
2.3.5.3 Tasiuyak paragneiss	2-7
2.3.5.4 Makhavinekh Lake pluton	2-8
2.3.5.5 Local minor dykes and faulting	2-9

**CHAPTER 3 – EMPLACEMENT HISTORY OF THE PEARLY GATES ANORTHOSITE PLUTON
AND TESSIARSUYUNGOAKH INTRUSION: PETROLOGICAL AND GEOCHRONOLOGICAL
EVIDENCE**

ABSTRACT	3-1
3.1 INTRODUCTION	3-2
3.2 REGIONAL GEOLOGY	3-4
3.3 GEOLOGY OF THE STUDY AREA	3-5
3.3.1 Pearly Gates Anorthosite Pluton	3-5
3.3.2 Tessiarsuyungoakh Intrusion	3-8
3.3.3 Exposed Anorthosite Bodies	3-9
3.3.4 Faults and Dykes	3-11
3.4 PETROGRAPHY	3-11
3.4.1 Pearly Gates Anorthosite Pluton	3-11
3.4.2 Tessiarsuyungoakh Intrusion	3-13
3.5 U-Pb GEOCHRONOLOGY	3-14
3.5.1 Sample Selection	3-14
3.5.2 Sample Preparation and Analytical Methods	3-15
3.5.3 Results	3-16
3.5.3.1 Pearly Gates Anorthosite pluton	3-17
3.5.3.2 Tessiarsuyungoakh intrusion	3-21
3.5.4 Overview of U-Pb Geochronology Ages	3-22
3.6 DISCUSSION	3-24
3.7 MODEL FOR EMPLACEMENT OF THE TI AND PGA	3-27
3.8 SUMMARY OF CONCLUSIONS	3-28

**CHAPTER 4 – STUDY OF REGIONAL AND CONTACT METAMORPHISM OF THE TASIUYAK
PARAGNEISS BETWEEN THE MAKHAVINEKH LAKE PLUTON AND THE
TESSIARSUYUNGOAKH INTRUSION, NAIN PLUTONIC SUITE, NORTHERN LABRADOR**

ABSTRACT	4-1
4.1 INTRODUCTION	4-2
4.2 GEOLOGICAL SETTING	4-2
4.3 GEOLOGY OF THE STUDY AREA	4-4
4.4 PREVIOUS WORK	4-5
4.5 GENERAL APPROACH	4-6
4.6 ANALYTICAL TECHNIQUES	4-8
4.7 SAMPLE SELECTION	4-8
4.8 REGIONAL METAMORPHISM	4-9
4.8.1 Petrography	4-9
4.8.1.1 Bulk composition	4-11
4.8.2 Mineral Chemistry	4-11
4.8.2.1 Garnet	4-11
4.8.2.2 Biotite	4-12
4.8.2.3 Plagioclase	4-12
4.8.3 Interpretation	4-12
4.8.4 <i>P-T</i> Conditions	4-16
4.8.5 Discussion	4-16
4.8.5.1 Comparison with previous work	4-18
4.9 CONTACT METAMORPHIC GRADIENT BETWEEN THE TI AND MLP	4-19
4.9.1 Petrography	4-19
4.9.1.1 Regional metamorphic assemblage in the study area	4-19
4.9.1.2 Progressive development of the contact metamorphic assemblage	4-20

4.9.2 Bulk Composition	4-23
4.9.3 Mineral Chemistry of Sample TL01-147	4-23
4.9.3.1 Cordierite	4-24
4.9.3.2 Orthopyroxene	4-24
4.9.3.3 Plagioclase	4-25
4.9.4 Interpretation	4-25
4.9.4.1 Regional and contact metamorphic assemblage of the Tasiuyak paragneiss in the northern part of the study area	4-25
4.9.4.2 Contact metamorphic assemblage	4-26
4.9.5 Discussion	4-29
4.9.5.1 Comparison with previous work	4-30
4.10 CONTACT METAMORPHISM OF TASIUYAK PARAGNEISS SCREENS IN THE TI	4-32
4.10.1 Petrography	4-32
4.10.1.1 Interpretation	4-33
4.11 SUMMARY OF CONCLUSIONS	4-34
CHAPTER 5 - COMPILATION OF CONCLUSIONS FROM THE THESIS RESEARCH	
5.1 SUMMARY OF THESIS GOALS	5-1
5.2 SUMMARY OF CONCLUSIONS	5-1
REFERENCES	R-1
APPENDIX A	A-1

LIST OF TABLES

Table 1.1: Compilation of U-Pb ages of intrusive rocks of the Nain Plutonic Suite	1-20
Table 3.1: U-Pb geochronology analytical data	3-38
Table 3.2: Summary of zircon crystallization ages	3-24
Table 4.1: Mineralogy of samples from the regional and contact metamorphosed Tasiuyak paragneiss	4-36
Table 4.2: Bulk composition analyses from thin sections of Tasiuyak paragneiss	4-36

LIST OF FIGURES

Figure 1.1:	Geological map of the Nain Plutonic Suite showing the location of intrusions dated by U-Pb geochronology	1-21
Figure 2.1:	Regional geological map of northern Labrador	2-10
Figure 2.2:	Geological map of the study area	2-11
Figure 3.1:	Regional geological map of northern Labrador	3-30
Figure 3.2:	Geological map of the study area showing location of geochronology samples	3-31
Figure 3.3:	Cathodoluminescence images of zircons from geochronology samples	3-33
Figure 3.4:	Concordia diagrams of the six major units sampled for U-Pb geochronology	3-34
Figure 3.5:	Schematic drawing depicting a proposed model of emplacement of the Pearly Gates Anorthosite pluton and Tessiarsuyungoakh intrusion	3-37
Figure 4.1:	Simplified regional geological map of northern Labrador	4-37
Figure 4.2:	Geological map of the study area showing location of metamorphic samples	4-38
Figure 4.3:	Petrogenetic grid of the NaKFMASH system for anatectic pelites	4-40
Figure 4.4:	Bulk composition of studied samples plotted on AFM diagram	4-41
Figure 4.5:	NaKFMASH petrogenetic grid showing possible metamorphic reactions of the Tasiuyak paragneiss regional metamorphic assemblage	4-42
Figure 4.6:	Mineral and chemical composition plots of regional metamorphic garnet	4-43
Figure 4.7:	Mineral and chemical composition plots of regional metamorphic biotite	4-46
Figure 4.8:	Mineral and chemical composition plots of regional metamorphic plagioclase	4-47
Figure 4.9:	Staurolite-out reaction shown on AFM diagrams	4-49
Figure 4.10:	Schematic AFM diagrams showing shifting of the garnet-sillimanite-biotite triangle with a change in temperature	4-50
Figure 4.11:	Fe/Fe+Mg garnet isopleths plotted on the NaKFMASH petrogenetic grid	4-51
Figure 4.12:	NaKFMASH petrogenetic grid depicting the <i>P-T</i> conditions of regional metamorphism of the Tasiuyak paragneiss	4-52
Figure 4.13:	Photomicrograph showing location of spot and transect microprobe analyses of contact metamorphic minerals	4-53

Figure 4.14: NaKFMASH petrogenetic grid showing possible metamorphic reactions of the Tasiuyak paragneiss contact metamorphic assemblage	4-54
Figure 4.15: Chemical composition plots of contact metamorphic cordierite	4-55
Figure 4.16: Chemical composition plots of contact metamorphic orthopyroxene	4-56
Figure 4.17: Mineral composition plots of plagioclase adjacent to contact metamorphic minerals	4-58
Figure 4.18: <i>P-T</i> conditions of the regional and contact metamorphic events plotted on the NaKFMASH petrogenetic grid	4-59

LIST OF PLATES

Plate 3.1:	Megacrystic plagioclase in the inner zone of the Pearly Gates Anorthosite pluton	3-40
Plate 3.2:	Partially recrystallized megacrystic plagioclase in the inner zone of the Pearly Gates Anorthosite pluton	3-40
Plate 3.3:	Foliated compositional layers of anorthosite and norite in the outer zone of the Pearly Gates Anorthosite pluton	3-41
Plate 3.4:	Heterogeneous deformation along foliation plane in the outer zone of the Pearly Gates Anorthosite pluton	3-41
Plate 3.5:	Norite dyke cross-cutting gneissic norite of the Pearly Gates Anorthosite pluton near the contact	3-42
Plate 3.6:	Plagioclase xenocryst in monzodiorite	3-42
Plate 3.7:	Foliated compositional layers of monzonite and monzodiorite of the Tessiarsuyungoakh intrusion	3-43
Plate 3.8:	Monzodiorite dyke in quartz monzonite of the Tessiarsuyungoakh intrusion	3-43
Plate 3.9:	Anorthosite dyke cutting quartz monzonite of the Tessiarsuyungoakh intrusion	3-44
Plate 3.10:	Undeformed norite at the roof of the Fraser Canyon Anorthosite	3-44
Plate 3.11:	Plagioclase xenocrysts in monzodiorite of the Tessiarsuyungoakh intrusion	3-45
Plate 3.12:	Brecciated quartz monzonite in pseudotachylite fault gouge	3-45
Plate 3.13:	Primary igneous plagioclase showing recrystallized grain boundaries	3-46
Plate 3.14:	Partially recrystallized plagioclase showing bent deformation twins and minor alteration	3-46
Plate 3.15:	Foliated norite from the outer zone of the Pearly Gates Anorthosite pluton showing deformation textures and partial recrystallization	3-47
Plate 3.16:	Ophitic orthopyroxene and antiperthitic plagioclase of the undeformed intrusive norite body	3-47
Plate 3.17:	Minor recrystallization of plagioclase and ophitic orthopyroxene from the roof of the Fraser Canyon Anorthosite	3-48
Plate 3.18:	Adcumulate plagioclase of the undeformed Fraser Canyon Anorthosite	3-48
Plate 3.19:	Mesoperthite and recrystallized minerals in deformed orthopyroxene-bearing monzonite	3-49

Plate 3.20: Minor recrystallization of undeformed olivine-bearing quartz monzonite	3-49
Plate 3.21: Zircon fragments from sample 1 - Pearly Gates Anorthosite pluton	3-50
Plate 3.22: Photomicrograph of sample 1 showing interstitial, anhedral zircon	3-50
Plate 3.23: Prismatic zircon from sample 1 - Pearly Gates Anorthosite pluton	3-51
Plate 3.24: Photomicrograph of sample 1 showing prismatic zircon inclusion in plagioclase	3-51
Plate 3.25: Highly resorbed cusped zircon from sample 1 - Pearly Gates Anorthosite pluton	3-52
Plate 3.26: Photomicrograph of sample 1 showing highly resorbed zircon partially included in plagioclase	3-52
Plate 3.27: Prismatic zircon from sample 2 - Fraser Canyon Anorthosite	3-53
Plate 3.28: Zircon fragments from sample 2 - Fraser Canyon Anorthosite	3-53
Plate 3.29: Baddeleyite from sample 1 - Pearly Gates Anorthosite pluton	3-54
Plate 3.30: Baddeleyite from sample 2 - Fraser Canyon Anorthosite	3-54
Plate 3.31: Zircon fragments from sample 3 - Norite dyke	3-55
Plate 3.32: Zircon fragments from sample 4 - Norite intrusive body	3-55
Plate 3.33: Prismatic zircon from sample 5 - Olivine-bearing monzodiorite	3-56
Plate 3.34: Photomicrograph of sample 5 showing interstitial prismatic zircon	3-56
Plate 3.35: Prismatic zircon from sample 6 - Orthopyroxene-bearing monzonite	3-57
Plate 3.36: Photomicrograph of sample 6 showing interstitial prismatic zircon	3-57
Plate 4.1: Photograph of the regional metamorphic Tasiuyak paragneiss	4-60
Plate 4.2: Photograph of the Tasiuyak paragneiss in the northern part of the study area	4-60
Plate 4.3: Photograph of the contact metamorphic assemblage partially replacing the regional assemblage	4-61
Plate 4.4: Photograph of the contact metamorphic assemblage completely replacing the regional assemblage	4-61
Plate 4.5: Photomicrograph of garnet in quartz-rich Domain I	4-62
Plate 4.6: Porphyroblastic feldspars in quartzofeldspathic Domain II	4-62
Plate 4.7: Grt2 embayed by vermicular quartz and feldspars	4-63

Plate 4.8:	Vermicular quartz and feldspar patches in quartzofeldspathic Domain II	4-63
Plate 4.9:	Randomly oriented Sil1 inclusions in Grt1 surrounded by Grt2 and coarse-grained, relict Sil2	4-64
Plate 4.10:	Fabric-parallel Sil1 inclusions in rotated Grt1 surrounded by Grt2 and coarse-grained, relict Sil2	4-64
Plate 4.11:	Bent Sil2 overgrown by Grt2 abutting Grt1	4-65
Plate 4.12:	Polymineralic inclusion of biotite, quartz, and K-feldspar in Grt2	4-65
Plate 4.13:	Photomicrograph of retrograde biotite, Sil3 and quartz replacing Sil2 and Grt2	4-66
Plate 4.14:	Small Grt3 adjacent to xenomorphic Grt2 rims and Sil2 rims	4-66
Plate 4.15:	Sample TL02-80 of the Tasiuyak paragneiss in the northern part of the study area showing preservation of the regional metamorphic assemblage	4-67
Plate 4.16:	Sample TL02-66b of the Tasiuyak paragneiss in the northern part of the study area showing incipient development of the contact metamorphic assemblage	4-67
Plate 4.17:	Sample TL02-79 showing development of contact metamorphic orthopyroxene rims replacing biotite and Grt2	4-68
Plate 4.18:	Cathodoluminescence microscopy of sample TL02-74 showing crystallized melt along feldspar grain boundaries	4-68
Plate 4.19:	Photomicrograph of contact metamorphic assemblage which has partially replaced regional metamorphic assemblage	4-69
Plate 4.20:	Photomicrograph showing textural relationships of partially developed contact metamorphic assemblage spinel + cordierite + orthopyroxene replacing Grt1, Grt2 and Sil2	4-70
Plate 4.21:	Photomicrograph showing textural relationships of completely developed contact metamorphic assemblage spinel + cordierite + orthopyroxene	4-71
Plate 4.22:	Garnet and biotite partially replaced by coarse-grained intergrowths of spinel + cordierite + orthopyroxene from a paragneiss screen exposed in the T1	4-72
Plate 4.23:	Symplectic orthopyroxene + spinel after biotite and symplectic cordierite + spinel after garnet from a paragneiss screen exposed in the T1	4-72
Plate 4.24:	Garnet and biotite partially replaced by cordierite + spinel + orthopyroxene from a paragneiss screen exposed in the T1	4-73
Plate 4.25:	Garnet and biotite partially replaced by cordierite + K-feldspar + spinel from a paragneiss screen exposed in the T1	4-73

LIST OF MAPS

1. A 1:20 000 solid geological map of a portion of the western margin of the Nain Plutonic Suite, northern Labrador, with emphasis on geological units, structure and geochronological sample sites. This map includes the southwest margin of the Pearly Gates Anorthosite pluton, the Tessiarsuyungoakh intrusion, the Tasiuyak paragneiss and the northern part of the Makhavinekh Lake pluton. (Located in pocket, inside back cover.)

2. A 1:20 000 geological map of a portion of the western margin of the Nain Plutonic Suite, northern Labrador, with emphasis on sample locations and delineation of outcrop. This map includes the southwest margin of the Pearly Gates Anorthosite pluton, the Tessiarsuyungoakh intrusion, the Tasiuyak paragneiss and the northern part of the Makhavinekh Lake pluton. (Located in pocket, inside back cover.)

LIST OF ABBREVIATIONS AND SYMBOLS

Mineral Abbreviations:

Ab – Albite

Alm – Almandine

An – Anorthite

Ap – Apatite

As – Aluminosilicate

Bt – Biotite

Cpx – Clinopyroxene

Crd – Cordierite

Grt – Garnet

Grs – Grossular

Ilm – Ilmenite

Ms – Muscovite

Kfs – K-Feldspar

OI – Olivine

Opx – Orthopyroxene

Plg – Plagioclase

Prp – Pyrope

Qtz – Quartz

Sil – Sillimanite

Sps – Spessartine

Spl – Spinel

St – Staurolite

Zrn – Zircon

Other Abbreviations:

ASZ – Abloviak Shear Zone

MLP – Makhavinekh Lake pluton

NPS – Nain Plutonic Suite

PGA – Pearly Gates Anorthosite

SECP – southeastern Churchill Province

TI – Tessiarsuyungoakh intrusion

TIMS – Thermal Ionization Mass

Spectrometry

L – liquid (melt)

kV – kilovolts

nA – nanoamperes

pg – picograms

μm – micrometre

CHAPTER 1 - INTRODUCTION TO THE THESIS STUDY

1.1 INTRODUCTION

1.1.1 Geological Importance of Anorthosites

Anorthosite is an igneous, plutonic rock characterized by at least 90% plagioclase and minor components of mafic minerals, such as orthopyroxene, clinopyroxene, and/or olivine. The majority of large bodies of anorthosite are typically Archean or Proterozoic in age. The paucity of younger anorthosite bodies indicates that their production is related to ancient geological events and parameters that do not appear to exist after the late Proterozoic. Therefore, understanding the mechanism and environment that produced anorthosites could provide insight into geological processes related to the temporal evolution of the Earth.

Archean anorthosites and Proterozoic anorthosites each have distinct characteristics. Archean anorthosites typically contain very calcic plagioclase, An_{80-100} , and are usually stratiform units in basic layered intrusions. These intrusions are typically associated with greenstone belts and meager evidence suggests that these anorthosites formed as sills within these oceanic basic meta-volcanic complexes (Ashwal, 1993). In contrast, Proterozoic anorthosites typically consist of intermediate plagioclase compositions, An_{35-60} , and formed as large complexes, hundreds to thousands of square kilometres in area, within cratons, usually in or near orogenic belts. These anorthosite complexes are contemporaneous with acidic and intermediate rocks (Emslie, 1985) and are often referred to as anorthosite-mangerite-charnockite-granite (AMCG) suites. AMCG suites consist of anorthosite and related granitoid rocks, which contain anhydrous mafic minerals, usually orthopyroxene, as well as minor amounts of clinopyroxene, olivine and oxides. Minor amounts of intermediate rocks are also associated with this suite and comprise ferrodiorite, ferrogabbro, jotunite and monzodiorite. Most AMCG suites formed between 2200 and 900 Ma, and well-known bodies are found in Norway, Finland, Greenland, Canada and the United States.

In the past, the genesis of Proterozoic anorthosite complexes was considered 'problematic' because the mechanisms that produced and transported such large volumes of

plagioclase could not be compared with any relatively recent analogous geological processes. However, combining detailed geological mapping and well-constrained field relationships with improvements of geological techniques in petrology, geochemistry, geochronology, geothermobarometry and geophysics, can shed new insight into the petrogenesis of anorthosites.

1.1.2 Anorthosites of the Nain Plutonic Suite

The Nain Plutonic Suite (NPS) of northern Labrador is a renowned Mesoproterozoic AMCG suite. It is one of the largest, best-exposed suites in the world, covering an area of ~ 20,000 km². Exposure is spectacular due to the sub-arctic climate, and topographic relief of up to 1000 m from sea level. Therefore the plutons and their structures are well exposed in three dimensions. Considering the fame, size and exposure of the NPS, it is surprising that the emplacement and parental magma(s) of this relatively unusual, time constrained (ca. 1360-1290 Ma) magmatism are still unresolved. Many regional studies have been undertaken to answer these questions but until recently, there has been little detailed work. However, such detailed studies are essential in order to recognize the similarities and differences between plutons and therefore give a better understanding of the regional geological history of the NPS.

There have been more detailed studies of the eastern portion of the NPS than the western portion because it is more accessible. Previous work by Wheeler (1960, 1969), Ryan (1991, 1993, 1997, 2001), Xue and Morse (1993) and Emslie et al. (1994) shows that there are compositional, geochemical and temporal differences between the western and eastern parts of the NPS. Typically the western half is older (Table 1.1) and comprises orthopyroxene-bearing anorthosite and norite, whereas in the younger eastern half, gabbro and leucotroctolite are associated with olivine-bearing anorthosite. Emslie et al. (1994) also divided the NPS into eastern and western zones on the basis of Nd isotope geochemistry of intrusions, which they attributed to contamination by the underlying Archean Nain Province and Paleoproterozoic Churchill Province, respectively. The western NPS plutons typically have deformed and recrystallized margins especially where adjacent to rocks other than pure anorthosite, whereas the eastern NPS plutons

generally exhibit pristine igneous textures and contacts (Ryan, 1991, 1993; Berg et al., 1994; Royse and Ryan, 1995, Royse and Park, 2000).

Previous work by Ryan (1991), Emslie and Stirling (1993), and Emslie et al. (1994) has described the relationships between the anorthositic, granitic, and ferrodioritic components of the NPS. Debate about the temporal relationships of spatially related anorthositic and granitoid intrusives is ongoing.

Many intrusions (ca. 28) of the NPS have been dated by zircon and/or baddeleyite using the U-Pb thermal ionization mass spectrometry technique. However, only a few ages and U-Pb data sets are available in publications. The other ages are quoted in conference abstracts or papers. Hamilton et al. (1994, 1998) dated many of the NPS intrusions with other contributions by Krogh & Davis (1973); Simmons et al. (1986); Simmons & Simmons (1987); Ryan (1991); Ryan et al. (1991); Emslie & Loveridge (1992); Connelly (1993); Connelly & Ryan (1994); Hamilton (1997) and Amelin et al. (1999). A compilation of these U-Pb ages is found in Table 1.1 and the location of the intrusions is found in Figure 1.1. The plethora of emplacement ages determined by Hamilton et al. (1994) indicated that the magmatic interval for anorthositic, granitoid and ferrodiorite intrusions was the same (ca. 1333 to 1294 Ma). The interval of granitic intrusions was increased by dates acquired by Connelly, (1993) for the 1351 ± 3 Ma Hare Hill monzonite and Connelly & Ryan (1994) for the 1343 ± 3 Ma monzonite adjacent to the eastern margin of the Mt. Lister Anorthosite pluton. The youngest intrusion of the NPS is the 1292 ± 4 Ma granitic Voisey Bay – Notakwanon batholith (Ryan et al., 1991). Therefore, prior to this thesis (Table 1.1), the known age range for emplacement of the NPS was ca. 1350 to 1290 Ma. Recent graduate thesis studies at Memorial University of Newfoundland have obtained new U-Pb emplacement ages such as the 1318 ± 6 Ma Hosenbein Lake complex (R. Voordouw, per comm., 2004), and the ca. 1360 Ma Tessiarsuyungoakh intrusion and ca. 1340 Ma Pearly Gates Anorthosite pluton (herein, see Chapter 3). In addition, U-Pb dating of zircon and baddeleyite from two units within the Barth Island composite intrusion has provided an older age than was previously reported by Hamilton et

al. (1994). These new older ages are, 1332 ± 2 Ma from a leucotroctolite unit and 1333 ± 4 Ma from a leuconorite unit (O. Gaskill, per comm., 2004).

Studies by Berg (1977b, 1979), Speer (1982), Berg and Docka (1983), Lee (1987) and McFarlane et al. (2003) concentrated on the contact metamorphic affects of NPS intrusions to determine peak metamorphic pressures and temperatures. However, account was not always taken of the other surrounding plutons, which do not *appear* to have caused contact metamorphism. In addition, none of these studies reported details of the regional metamorphic assemblage to provide a better understanding of the regional context in which contact metamorphism occurred.

1.1.3 Study Area

The thesis study area lies in the western margin of the NPS and consists of the southwestern portion of the Pearly Gates Anorthosite pluton (PGA) (Ryan, 1993), the adjacent Tessiarsuyungoakh intrusion (TI) (Wheeler, 1969), the host Tasiuyak paragneiss (Wardle, 1983) of the Southeastern Churchill Province, and the northeastern margin of the Makhavinekh Lake pluton. The PGA is an ~ 900 km², ovoid body consisting of an inner zone of massive anorthosite and outer zone of deformed layers of anorthosite and norite. Along the southwestern margin of the PGA lies the composite monzonite (mangerite) and monzodiorite (jotunite) TI. Detailed field mapping was conducted on the rocks of the PGA and the TI. The Tasiuyak paragneiss is exposed between the TI to the east and Makhavinekh Lake pluton to the southwest. The paragneiss has undergone contact metamorphism during emplacement of the Makhavinekh Lake pluton but *appears* to have been unaffected by the intrusion of the TI or the very large PGA. The northeastern margin of the Makhavinekh Lake pluton is composed of olivine- and orthopyroxene-bearing granite with rapakivi texture. This pluton was not studied in detail and only locations along transects through the Tasiuyak paragneiss were examined. Geological details of the above mentioned units are briefly described in Chapter 2. More thorough descriptions of the PGA and TI

are reported in Chapter 3 and descriptions of the Tasiuyak paragneiss and Makhavinekh Lake pluton are reported in Chapter 4.

1.2 PETROGENESIS OF AMCG SUITES

There has been much speculation about the geological processes that produced AMCG suites, the magmatic source(s), and the mechanisms that produced such large amounts of plagioclase and emplaced these rocks at mid-crustal levels. This section will summarize the most common theories regarding AMCG suite development, mainly focusing on anorthosite genesis.

1.2.1 Magmatic Source(s)

The main problem in determining the magmatic source(s) of AMCG suites is that they are cumulate rocks. Therefore whole rock geochemistry is not easily interpretable because during relatively long-term crystallization, processes like fractionation, filter-pressing, assimilation and contamination will change the original magmatic characteristics. However, studies of field relationships, mineral chemistry and whole-rock isotopic signatures have provided clues about potential magmatic source(s), assimilation/contamination and the depth at which the parental magmas were generated.

1.2.1.1 Depth of source(s)

Some anorthosite complexes contain minor amounts of highly aluminous orthopyroxene megacrysts (HAOM) with exsolved lamellae of plagioclase (Emslie, 1975; Morse, 1975; Dymek & Gromet, 1984; Duchesne, 1984). The HAOM are typically 20 cm to 1 m in diameter and much more magnesium- and aluminum-rich than orthopyroxene in the matrix (Emslie, 1975). Since aluminum content increases in orthopyroxene with increasing pressure, Emslie (1975), Wiebe (1986) and Longhi et al. (1993) proposed that the HAOM were formed deep in the lithosphere. Geobarometric studies of these megacrysts by Emslie (1975) and Wiebe (1986) suggested that they crystallized at ~ 11 kbar, equivalent to ~ 36 km. Although it is inconclusive whether the

HAOM formed from the same parental magma as anorthosite, the depth at which these orthopyroxene megacrysts formed could provide an indication of the depth of anorthosite formation.

Proterozoic anorthosites contain intermediate plagioclase compositions ranging from andesine to labradorite (An_{35} to An_{60}). This indicates a relatively sodic magma, however with increasing pressure sodium, rather than calcium, is more readily incorporated into plagioclase. Therefore, the relatively albitic plagioclase could be interpreted to represent either a melting of lower crustal material already rich in sodic plagioclase or crystallization of plagioclase at a depth conducive to the preferred incorporation of sodium into the crystal, or a combination of both.

1.2.1.2 Liquid versus crystal mush

Anorthosite bodies contain various amounts of plagioclase phenocrysts indicating that the magma contained plagioclase crystals in suspension during emplacement. However, the question is: what was the relative proportion of crystals to liquid? If the intrusive magmas were mostly liquid, they would have to have been anorthositic in composition with relatively high amounts of sodium and aluminum to account for the crystallization of intermediate plagioclase after emplacement. If these bodies intruded with large amounts of plagioclase crystals (a crystal mush), how and where were these crystals formed?

Wiebe (1979) reported chilled margins in undeformed anorthositic bodies and anorthosite dykes, and later proposed that they formed from hyperfeldspathic liquids (Wiebe, 1990). He proposed that these liquids could be produced by fractionation and segregation of mafic magma in the lower crust. Fractionation of olivine and pyroxene from this magma would leave a more aluminous residual liquid, which would begin to form plagioclase crystals. The plagioclase would float in the mafic magma near the top of the chamber while the olivine and pyroxene would settle to the chamber floor. Continued plagioclase production and occasional partial resorption of these crystals by replenishment of mafic magma would produce a liquid enriched in plagioclase components. Fram and Longhi (1992) experimented on one of Wiebe's dykes in which they fused

and crystallized the dyke sample under assumed environmental conditions of the NPS dyke and compared it to the original. The experimental sample had a different mineralogy and the plagioclase crystals were more calcic than the original sample suggesting that the dyke was not formed from a liquid. Rather, Fram and Longhi (1992) indicated that the dyke intruded as a crystal mush and that most of the plagioclase crystals were formed at ~ 11 kbar, equivalent to ~ 36 km, in the lower crust.

It is widely accepted that anorthosite bodies formed from intrusion of a plagioclase crystal mush produced at depth, however, the proportion of plagioclase crystals to liquid in such a mush is debated and may be different from one pluton to the next. It is thought that the younger, undeformed anorthositic bodies of the NPS possibly contained more liquid since the margins of some of these plutons show troughs, scours, and compositional and graded layering (Wiebe, 1990; D. Wright, per comm., 2002). However, the older deformed plutons also appear to have compositional layers at the margins and other layering structures may possibly be obscured by the deformation.

1.2.1.3 AMCG suites – parental magma(s) and source region(s)

There are currently two principal schools of thought on the parental source(s) and formation of AMCG suites. One is that mantle-derived basaltic magma is parental to the anorthositic rocks and granitic rocks are derived from partial melting of lower crust; and the other more recent theory is that AMCG suites originated from partial melting and fractionation of lower crustal granulites. Morse (1982), Wiebe (1990), Ashwal (1993) and Xue and Morse (1993) believed that an anorthositic crystal mush formed during fractional crystallization of a juvenile basaltic magma at the base of the crust. Emslie et al. (1994) suggested that heat from this ponding of basaltic magma caused partial melting of the lower crust, and formed the granitic intrusions.

Regional studies of major- and trace-element geochemistry were conducted by Xue and Morse (1993) of anorthositic plutons, and by Emslie et al. (1994) of anorthositic, granitoid and

ferrodiorite intrusions. Both studies have shown that anorthositic rocks are characterized by high Ba, Pb, K, Sr, Ti, Eu and low Rb, Nb, Zr. Both authors suggested that these anomalies were consistent with a mantle-derived basaltic magma that had been contaminated with depleted lower crust. Emslie et al. (1994) also reported that ferrodioritic intrusions were geochemically similar to anorthositic intrusions. In addition, ferrodioritic rocks are characterized by evolved Fe/Mg, depleted concentrations of Cr and Ni and moderate Sr content. Emslie et al. (1994) attributed this to protracted fractionation of mafic minerals (enriched in Mg, Cr, Ni) and plagioclase (enriched in Sr) and suggested that ferrodioritic liquid was residual to anorthositic magmas. The Emslie et al. (1994) study of the granitoid rocks showed that they were geochemically distinct from the anorthositic and ferrodioritic rocks. The granitoid rocks were characterized by low Rb, Nb, Sr, P, Eu, Ti contents and high Zr. They proposed that the depleted elements reflected a lower crustal source, which underwent dehydration partial melting and that the restite contained residual plagioclase (Sr- and Eu-rich). Emslie et al. (1994) suggested that this restite, possibly a pyroxene + (plagioclase) granulite, was the contaminant that assimilated with the basaltic magma to produce anorthositic rocks (discussed further below).

Isotopic studies by Emslie et al., (1994) showed that neodymium isotopic signatures (ϵ_{Nd} , calculated at 1.3 Ga) in all the NPS rock types differed depending on whether they intruded into rocks of the Archean Nain Province (east) or rocks of the Archean and Paleoproterozoic Churchill Province (west). A rock with a longer crustal residence time will have a more negative ϵ_{Nd} value and this appears to be reflected in the lower ϵ_{Nd} value of -21.9 for the older Nain Province (east) compared to -14.6 for the younger Churchill Province (west). In general, the NPS rocks in the east have ϵ_{Nd} values < -10 and in the west ϵ_{Nd} values are > -10 . This is interpreted to represent crustal assimilation and contamination of the NPS intrusive magmas depending on which structural province they intruded. It was also shown that the granitoid rocks typically had slightly more negative ϵ_{Nd} values (west $\epsilon_{Nd} = -5.8$ to -9.7 ; east $\epsilon_{Nd} = -12.5$ to -14.1) than the ferrodiorite

units (west $\epsilon_{Nd} = -3.6$ to -8.7 ; east $\epsilon_{Nd} = -9.8$ to -14.8) while anorthositic rocks had the widest range of values (west $\epsilon_{Nd} = -3.7$ to -10.2 ; east $\epsilon_{Nd} = -8.9$ to -17.4).

Strontium isotopic signatures (I_{Sr}) in the same studies did not show a geographical distribution related to the country rocks, instead the I_{Sr} values were consistent with specific rock types. Emslie et al. (1994) divided the rocks into 3 groups; 1) anorthosite and related mafic components, $I_{Sr} = 0.7038$ to 0.7087 ; 2) ferrodiorite, $I_{Sr} = 0.7054$ to 0.7090 ; and 3) granitoid rocks, $I_{Sr} = 0.7047$ to 0.7104 . They suggested that based on the isotopic evidence, the granitoid rocks were derived from significant partial melting of the lower crust with relatively short crustal residence time, possibly a fractionate from basic magma underplating. They indicated that this would account for the higher I_{Sr} values and lower ϵ_{Nd} values in the granitoid rocks. A plagioclase + pyroxene restite from the partial melting event was proposed to have been assimilated by a mantle-derived basaltic magma. This contamination of the basaltic magma would have increased the Al and Si content to levels that could have produced plagioclase crystals. These plagioclase phenocrysts would then have segregated by floatation leaving a residual liquid. Ferrodiorite, which has similar isotopic, chemical and mineral compositions to the anorthosite, was thought by Emslie et al. (1994) to represent this residual liquid. This interpretation was also based on their observation that the ferrodiorite appeared to have been intruded after the anorthosite. However more recent field evidence compiled by the MUN Nain Plutonic Suite Transect Project has shown that although some ferrodiorite bodies are isolated entities, others form composite bodies with mangerite (orthopyroxene-bearing monzonite). These composite units typically show gradational contacts and mingling textures suggesting that they were contemporaneous. Studies of other AMCG suites in the Rogaland anorthosite province, Norway, by Bolle et al. (2003) and the Laramie anorthosite complex, United States, by Scoates and Chamberlain (2003) suggested that the mangeritic rocks were derived by fractional crystallization of ferrodiorite (jotunite). All of these authors proposed that the ferrodiorite might have undergone various amounts of assimilation/contamination by lower crustal granulites prior to fractional crystallization. Scoates

and Chamberlain (2003) interpreted the ferrodiortite to represent residual liquid from the formation of anorthosite at depth.

Petrological experimental work done by Longhi et al. (1999) has suggested that mantle-derived basaltic magma alone could not generate anorthosite via fractionation and density driven segregation of mafic minerals and plagioclase. They presented evidence to suggest that in order for the basic magma to produce plagioclase on the liquidus in volume or for a protracted period of time, the magma would either have to contain sufficient amounts of water or assimilate $\geq 20\%$ of granitic rock at ≤ 4 kbar. Since NPS rocks are anhydrous and evidence suggests that at least some plagioclase crystals formed at ~ 11 kbar the two aforementioned criteria are not met. Longhi et al. (1999) suggested that anorthosite was formed from melting of a gabbro-noritic unit, which was either a lower crustal granulite or a "foundering mafic pluton", which possibly sank down through the crust.

1.2.2 Emplacement Mechanisms - NPS

Emplacement of NPS anorthosites from a lower crustal level of ~ 33 km to mid-crustal levels of between 10-15 km (Berg, 1977; Lee, 1987; Ryan, 1991) requires a plausible ascent mechanism. This mechanism must move a liquid or crystal mush relatively quickly through the crust in order to maintain its internal heat. The two most commonly proposed mechanisms are: the transport of magma by conduit systems and diapiric ascent.

Diapirism was suggested as the most plausible mechanism to transport large volumes of crystal mush (Wiebe, 1990; Ashwal, 1993; Emslie et al., 1994). The ovoid shape and outward dipping contact of the larger anorthosite plutons appear to suggest a diapiric (balloon-like) structure. In order for this mechanism to work the semi-solid mass must rise due to buoyancy and vertically displace the country rock, without substantial heat loss during ascent. Royse and Park (2000) conducted theoretical calculations using known parameters from NPS intrusions. They suggested that diapiric ascent would be extremely slow, ~ 31 Ma to ascend 30 km. This sluggish

ascent would make it very difficult for the diapiric mass to retain enough heat to continue its ascent and also provide enough heat to ductily deform the surrounding rock. Royse and Park (2000) showed that at this slow ascent rate the crystal mush would be unable to carry the dense HAOM to emplacement levels and this will be discussed later.

Ascent via conduit systems was considered plausible if the rising magma was mostly liquid (Longhi et al., 1993). The argument against conduit ascent is that if anorthosite ascended as a crystal mush, transport through fractures in the crust would be difficult and that the plagioclase phenocrysts should show evidence of fracturing and deformation. Studies have shown little evidence of protoclastic plagioclase. However, evidence of plagioclase resorption, possibly occurring during ascent (Wiebe, 1990), may mask this feature. Longhi et al. (1993) have suggested that a crystal mush as much as 65% crystalline ascending under shear stress could act like a liquid and therefore show no evidence of protoclasia. Royse and Park (2000) proposed that the NPS anorthosite plutons were emplaced via conduit systems formed by dilation of pre-existing shear zones. Their evidence for this is three-fold. Firstly, dykes in the eastern portion of the NPS cross-cut host gneisses but are not deformed by cross-cutting anorthosite plutons, which would be expected if anorthosites were diapirically emplaced. Secondly, these dykes are heterogeneously affected by shear zones and have similar emplacement ages (1316 to 1327 Ma) as the eastern NPS anorthosite bodies, indicating that deformation occurred during emplacement. Finally, as mentioned earlier, terminal velocity rates were calculated for the HAOM and compared against diapiric versus conduit system ascent rates. They determined that a 50 cm HAOM in a crystal mush with a solid fraction ranging from 0 to 50% would settle out of the system at between 8.2 and 5.0 cm/s, respectively. Calculated ascent rates were 7.5×10^{-8} cm/s for a diapir with a diameter of 5 km (smaller than is typical for the NPS) and 0.09 to 7.56 cm/s for dykes ranging from 2 – 18 m, respectively. Therefore, according to these calculations conduit ascent is the only mechanism fast enough to transport the HAOM to emplacement levels. Royse and Park (2000) suggested that the elongate, ovoid structure of the large plutons is not a diapiric balloon but rather a reflection of sill-like emplacement and elongation during deformation.

1.3 OUTSTANDING PROBLEMS

Reconnaissance mapping in the study area has been done by Wheeler (1969), Taylor (1977a), Ryan (1991, 2001) and Ryan and James (2003), in which they provided an outline of the location, structure and description of the main geological units. Previous studies have investigated the temporal relationship between some NPS anorthosite and adjacent granitic intrusions but none have concentrated on the PGA and TI. The contact between the PGA and TI is deformed, both rock units share a common foliation parallel with the contact and the primary contact relations are obscured. The PGA is a large, ~2275 km², generally homogeneous body of anorthosite. How was the space created for this large pluton and what was the nature of the magma?

Previous studies of the Tasiuyak paragneiss have compared the regional and contact metamorphic mineral assemblages and used geothermobarometry to calculate *P-T* conditions of the contact metamorphism. In these studies the regional assemblage was described from rocks just outside the contact aureole. Although these rocks do not contain contact metamorphic assemblages they have still been subjected to thermal effects and therefore do not best represent regional metamorphism of the paragneiss. *P-T* constraints determined by geothermobarometry also have flaws since the contact mineral assemblages show disequilibrium textures and mineral chemistry indicates homogenization and resetting during cooling. Since geothermobarometric calculations are based on equilibrium reactions, the quantitative constraints produced from the previous studies most likely do not represent maximum *P-T* conditions. It has been recognized that the contact aureole in the Tasiuyak paragneiss was caused by thermal effects during the intrusion of the Makhavinekh Lake pluton (Ryan, 1991; McFarlane et al., 2003). However, to date there is no explanation why the adjacent TI appears not to have had the same effect.

1.4 THESIS GOALS

This study was designed to provide a better understanding of the spatially and structurally related PGA and TI, their mode of emplacement and deformation history, on the basis

of detailed 1:20 000 mapping, petrography and geochronological studies. The documentation of field relationships and determination of crystallization ages are essential in unraveling any temporal and possibly cogenetic relationships of the units selected. Understanding the geological history of the PGA and TI may also provide insight into why these intrusions, in contrast to the Makhavinekh Lake pluton, did not cause large-scale contact metamorphism of the adjacent Tasiuyak paragneiss.

A comprehensive study of the Paleoproterozoic regional metamorphic assemblage of the Tasiuyak paragneiss was attempted in order to produce better constraints towards understanding the Mesoproterozoic contact metamorphic assemblages. A representative sample of the regional assemblage was collected from a location unaffected by the NPS. Information gathered from petrographic studies of the mineral assemblages and textures combined with mineral and bulk chemistry were used to plot *P-T* conditions on a petrogenetic grid. These results were then used to determine if the Tasiuyak paragneiss outside the Makhavinekh Lake pluton contact aureole but adjacent to the TI did not reach sufficiently high temperatures to cause contact metamorphism or whether other factors, such as bulk composition, played a role.

1.5 METHODOLOGY

1.5.1 Field Mapping and Sampling

Geological mapping was carried out in the field on 1:20 000 airphotos. Information such as sample location, photograph location, rock types, contacts and structural measurements were recorded directly onto the airphotos. Detailed information was recorded in a fieldbook. Samples were labeled as TL01-# and TL02-# depending on the year they were collected (2001 and 2002, respectively). Measurements were recorded using the right-hand rule method. Oriented samples were collected by first measuring the strike and dip of the planar fabric, then marking the orientation on the sample before extraction from its location.

The contact aureole in the Tasiuyak paragneiss was studied along three transects from the margin of the Makhavinekh Lake pluton to the margin of the TI. Samples were collected along

these transects for petrographic studies to examine the changes in contact metamorphism assemblages and construct petrogenetic grids to determine P - T conditions. In addition, one sample was collected ~ 10 km from the NPS-Tasiuyak margin. This sample contains an undisturbed regional metamorphic assemblage and was used for comparison with samples adjacent to the TI that appear to be unaffected by contact metamorphism.

Sample locations of the major rock units were selected for geochronology after well-constrained field relationships were established. The rock was broken up and the weathered surfaces trimmed away at the sampling site to reduce possible contamination. About 20 to 40 kg of rock was collected for each geochronological sample. A total of 11 geochronological samples were collected, of which 6 were actually dated.

1.5.2 U-Pb Geochronology

1.5.2.1 U-Pb systematics theory

U-Pb geochronology is based on the radioactive decay of a parent atom of uranium (U) via α -decay producing a series of meta-stable daughter isotopes and ending with a stable daughter isotope of lead (Pb). U has three natural isotopes, ^{238}U , ^{235}U and ^{234}U . All three are unstable, however, ^{234}U exists as a step in the decay series of ^{238}U . The decay of ^{238}U and ^{235}U produces stable ^{206}Pb and ^{207}Pb , respectively. Pb has four natural isotopes, ^{208}Pb , ^{207}Pb , ^{206}Pb , and ^{204}Pb , of which only the last is nonradiogenic.

The law of radioactive decay states that the rate of decay of an unstable parent isotope to a stable daughter product is proportional to the number of atoms, n , present at time t :

$$dn/dt = -\lambda n, \quad (1.1)$$

where λ is the decay constant and dn/dt is the rate of change of the number of parent atoms. The equation contains a negative since the rate is decreasing with time.

The equation is integrated from $t=0$ to t , assuming that at time $t=0$, the number of atoms present is n_0 :

$$\ln n/n_0 = -\lambda t \text{ or } n = n_0 e^{-\lambda t} \quad (1.2)$$

Since the number of daughter atoms produced, D^* , is equal to the number of parent atoms consumed:

$$D^* = n_0 - n \quad (1.3)$$

Therefore combining equations 1.2 and 1.3 to replace n_0 gives:

$$D^* = n(e^{-\lambda t} - 1) \quad (1.4)$$

Taking into account the number of daughter atoms at $t=0$, D_0 , then the total number of daughter atoms after time t is:

$$D = D_0 + n(e^{-\lambda t} - 1) \quad (1.5)$$

In the case of the U-Pb system the equation becomes:

$$\frac{^{206}\text{Pb}}{^{238}\text{U}} = (e^{\lambda_{238}t} - 1) \text{ and} \quad (1.6)$$

$$\frac{^{207}\text{Pb}}{^{235}\text{U}} = (e^{\lambda_{235}t} - 1), \quad (1.7)$$

where Pb denotes strictly radiogenic lead.

Minerals such as zircon, monazite and baddeleyite, that acquire U, but not Pb, into the crystal structure during crystallization can be used to provide absolute ages for the event (i.e. igneous, metamorphic, deformation) in which the mineral was formed. If the mineral has remained a closed system for U and Pb, equations 1.6 and 1.7 will yield concordant ages, which can be plotted on a concordia diagram. The concordia curve graphically represents the isotopic compositions in a closed system for the two U/Pb isotopic systems with relation to the decay constant and successive values of t (Wetherill, 1956a).

Correction for common lead is made by measuring the initial ^{204}Pb in the mineral, and subtracting common lead of a composition defined by the model of Stacey & Kramers (1975) for the age of the rock. The model calculated $^{204}\text{Pb}/^{206}\text{Pb}$ and $^{204}\text{Pb}/^{207}\text{Pb}$ are subtracted from the measured values. This yields values for total radiogenic ^{206}Pb and ^{207}Pb , which are used in the age calculation.

Lead loss is a common problem in mineral dating. Lead may be leached out of the system from metamict domains along fractures. In this case the U-Pb ages do not lie on the concordia curve (discordant) but they often form a linear array on the diagram. The discordia line intersects the concordia curve at two points, 1) at the time of original crystallization, and 2) at a younger age which may represent the time when the grain was disturbed (Wetherill, 1956b) or at a meaningless "young age" which is the result of lead loss integrated over time. Tilton (1960) suggested that, over time, Archean minerals undergo continuous lead loss by diffusion. The discordant data yield a straight line that intersects at or near the origin. However, without geological evidence of a specific lead loss event, no age-significance should be inferred from the lower intersection of the discordia line (Dickin, 1995).

1.5.2.2 Analytical techniques

Samples were fragmented in a jaw crusher and then reduced to powder in a disc mill. The powder was panned on a Wilfley table where the heaviest minerals were concentrated and collected; then further concentrated by passing these separates through methylene iodide. The heavy mineral separate contains the desired minerals for U-Pb geochronological studies.

Lead loss effects in analyses can be reduced by passing the heavy mineral separates through a magnetic separator. This removes metamict minerals, which typically incorporate iron along fractures as well as inclusions containing impurities (Krogh, 1982a). In this study, the magnetic field of a Frantz isodynamic separator was strengthened, increasing the field current from 0.2 to 1.8 A, using an initial chute side-slope of 10°. Then, with the magnet at maximum strength, the side-slope of the separation tray was decreased from 10° to 0°. After each pass through the separator the magnetic concentrate was collected and saved and the non-magnetic material was passed through again. The final concentrated highest quality, non-magnetic grains were handpicked under a binocular microscope and then treated with air abrasion in a pneumatic mill. This technique removes any other minerals still attached to the zircon, baddeleyite, or monazite. Air abrasion also removes the outer layer of the crystal, which may be the highest in U

and therefore metamict (Krogh, 1982b) or may be more altered from fluids passing along grain boundaries.

Close inspection under a microscope may not always ensure selection of the best quality grains. Problems such as detecting inherited inclusions of older radioactive minerals in the selected grains and microscopic internal structures must be resolved to fully understand the data after analysis. Therefore another important tool is imaging grains using back-scattered electron and/or cathodoluminescence imaging techniques, which can show internal structures that are not visible to the naked eye. Selection of grains for isotope dilution geochronology may be improved by determining if there are factors such as inheritance, overgrowths, or annealed fractures in representative grains of the selected populations. Back-scattered electron imaging of zircon was carried out using the Cameca SX50 ion microprobe at Memorial University. Operating conditions for imaging were: 15 kV acceleration potential, and a beam current of 10 nA. Later imaging was conducted at 25 nA, which better revealed internal structures in the zircon grains.

Cathodoluminescence imaging was performed on the Leica Cambridge Instruments S-360 scanning electron microscope at the Geological Survey of Canada. Operating conditions for cathodoluminescence imaging were 20 kV accelerating voltage, 25 mm working distance and a beam current of 2 nA.

Minerals selected for analyses, either multiple- or single-grain fractions, were dissolved in HF and HNO₃ in teflon capsules at 210 C for 5 days. The aliquot was passed through ion exchange chemistry (Krogh, 1973) to extract purified U and Pb. Phosphoric acid was added to the extracted U and Pb and this mixture was then dried. Each sample was prepared for mass spectrometry by adding a drop of phosphoric acid and loading the mixture onto silica gel on rhenium filaments.

Thermal ionization mass spectrometry was performed on a MAT 262 multi-collector at Memorial University. Multiple sets of data were measured in the temperature ranges of 1400°C to 1550°C for Pb and 1550°C to 1650°C for U, and the sets that best agreed with each other and had the lowest errors were calculated to give a mean value for each ratio. The ratios were also

corrected for laboratory procedure blanks (typically 2-5 pg for Pb and 1 pg for U) and for common lead above the laboratory blank with lead of the composition predicted by the two-stage model of Stacey and Kramers (1975) according to the age of the sample. Uncertainties of ages are quoted at the 95% confidence level.

1.5.3 Metamorphism

Oriented samples collected for metamorphic petrology and microprobe studies were cut on a rock saw perpendicular to the foliation and parallel to strike or lineation. Polished sections were examined under the petrological microscope to determine metamorphic textures and mineral reactions/assemblages.

1.5.3.1 Electron microprobe analytical conditions

A set of polished sections from a transect through the contact aureole was analyzed on the Cameca SX50 electron microprobe at Memorial University. The polished sections were carbon coated to improve conductivity of electrons from the sample. Two types of analyses were performed: 1) bulk compositions of polished sections, and 2) quantitative spot analyses of minerals. Bulk composition analyses were conducted using the EDX method with an acceleration potential of 15 kV and a beam current of 250 nA. A task command was created to account for dead time and the overall area to be scanned and then calculate the real-time allotted to scan the polished section. Quantitative spot analyses of minerals were conducted by selecting transects across grains and in adjacent grains at grain boundaries to test for chemical zoning. Analyses were performed by spot collection, where the electron beam was concentrated on one spot over a period of time. Operating conditions for mineral compositional studies were: acceleration voltage: 15 kV, beam current: 20 nA, beam size: 1 μm , and counting time: 50 seconds for garnet, 75 seconds for all other minerals. In the case of plagioclase, a lower beam current of 10nA and a larger beam diameter of 3 μm were used due to feldspar's sensitivity to damage by the beam.

1.5.3.2 Petrogenetic grids

The NaKFMASH petrogenetic grid from Spear et al. (1999) was used to determine the pressure and temperature fields in which the different regional and contact metamorphic assemblages were equilibrated. This grid is appropriate for pelitic rocks like the Tasiuyak paragneiss, which have undergone partial melting in the P - T range of amphibolite to granulite facies metamorphism.

1.6 THESIS STRUCTURE

The thesis contains five chapters of which Chapters 3 and 4 represent stand-alone papers intended for journal submission. Chapter 1 introduces the scope of the project and Chapter 2 contains an overview of the regional and local geology and information on relevant field components. Chapter 3 represents a paper, which contains a study of field relationships and geochronology used to propose a model of emplacement of the PGA and T1. The manuscript represented in Chapter 4 consists of a regional and contact metamorphic study of the Tasiuyak paragneiss and its relationship to the surrounding intrusive rocks. Chapter 5 is a compilation of the conclusions drawn from the manuscripts and provides a synthesis of the research. This structure therefore contains details that are unavoidably repeated between some chapters. All references are located at the end of the thesis rather than after each manuscript. The thesis version of the papers contains additional figures and plates, which will not be included in the manuscripts submitted for publication.

Table 1.1: Compilation of U-Pb ages of intrusive rocks of the Nain Plutonic Suite. The location of intrusions is provided in Figure 1.1.

Intrusion/Location	Location in the NPS	Rock type	Mineral dated	Age	Reference
Voisey Bay–Notakwanon batholith (VB-N)	East	Granite	Zircon	1292 ± 4 Ma	Ryan et al., 1991 *
Sango Bay (SB)	East	Leucotroctolite	Zircon	1294 ± 1 Ma	Hamilton et al., 1994
Dog Island (DI)	East	Granite	Zircon	ca. 1295 Ma	Krogh & Davis, 1973 *
Cabot Lake (CL)	West	Ferrodiorite	Zircon & baddeleyite	1298 ± 2 Ma	Hamilton et al., 1994
Satorsoakulluk dyke (SD)	East	Ferrodiorite	Baddeleyite	1301 ± 2 Ma	Hamilton et al., 1994
Koiktalik Island (Ko)	East	Anorthosite	Zircon	1305 ± 2 Ma	Hamilton et al., 1994
Newark Island (NW)	East	Granodiorite	Zircon	1305 ± 5 Ma	Simmons et al., 1986
Goodnews complex (GN)	East	Granite	Zircon	1305 ± 10 Ma	Simmons & Simmons, 1987
Tigalak intrusion (Tg)	East	Ferrodiorite	Zircon	1306 ± 3 Ma	Hamilton et al., 1994
Kiglapait intrusion (KG)	East	Gabbroic pegmatite	Baddeleyite	1307 ± 1 Ma	Hamilton, 1997
Kikkertavak Island (KI)	East	Anorthosite and leuconorite	Zircon	1311 ± 2 Ma	Hamilton et al., 1994
Tabor Island (Tb)	East	Anorthosite and leuconorite	Zircon	1311 ± 2 Ma	Hamilton et al., 1994
Johnathan Island intrusion (JI)	East	Diorite & troctolite	Zircon	1312 ± 3 Ma	Hamilton et al., 1994
Satorsoakulluk dyke (SD)	East	Ferrodiorite	Zircon (xenocrystic)	1315 ± 2 Ma	Hamilton et al., 1994
Umiakovik batholith (UK)	West	Granite	Zircon	1316 ± 3 Ma	Emslie & Loveridge, 1992 *
Hosenbein Lake complex (HL)	East	Leucogabbro	Zircon	1318 ± 6 Ma	R. Voordouw, per comm., 2004
Umiakovik batholith (UK)	West	Quartz monzodiorite	Zircon	1319 ± 2 Ma	Emslie & Loveridge, 1992 *
Paul Island intrusion (PI)	East	Massive anorthosite	Zircon	1319 ± 1 Ma	Hamilton et al., 1994
Makhavinekh Lake pluton (MK)	West	Leuconorite	Zircon	1322 ± 1 Ma	Hamilton et al., 1994
Makhavinekh Lake pluton (MK)	West	Granite	Zircon	1322 ± 1 Ma	Ryan, 1991
Puttuaalu Brook intrusion (PB)	West	Leuconorite	Zircon	1322 ± 1 Ma	Hamilton et al., 1998*
Barth Island intrusion (BI)	East	Ferrodiorite	Zircon	1322 ± 2 Ma	Hamilton et al., 1994
Anaktalik Brook dyke (AB)	West	Monzonite	Zircon	ca. 1326 Ma	R.F. Emslie, quoted in Ryan and James, 2003
Iglusuataliksiak Lake (IL)	East	Quartz monzodiorite	Zircon	1330 ± 1 Ma	Hamilton et al., 1998*
Ukpaume intrusion (Up)	Central	Leuconorite	Zircon	1330 ± 2 Ma	Hamilton, 1997
Barth Island intrusion (BI)	East	Leucotroctolite	Zircon & baddeleyite	1332 ± 2 Ma	O. Gaskill, per comm., 2004
Barth Island intrusion (BI)	East	Leuconorite	Zircon	1333 ± 4 Ma	O. Gaskill, per comm., 2004
Voisey's Bay intrusion (VB) (also called Reid Brook intrusion)	Central	Troctolite & gabbro	Zircon & baddeleyite	1333 ± 1 Ma	Amelin et al., 1999 *
Ukpaume intrusion (Up)	Central	Diorite	Zircon	1333 ± 2 Ma	Hamilton et al., 1994
Pearly Gates pluton (PG)	West	Anorthosite	Zircon	1335 ± 7/-3 Ma	This thesis (see Chapter 3)
Pearly Gates pluton (PG)	West	Leuconorite	Zircon	1342 ± 1 Ma	This thesis (see Chapter 3)
Mt. Lister region (ML)	Central	Monzonite (adjacent to Mt. Lister pluton)	Zircon	1343 ± 3 Ma	Connelly & Ryan, 1994
Hare Hill Monzonite (HH)	West	Monzonite	Zircon	1351 ± 3 Ma	Connelly, 1993
Fraser Canyon intrusion (FC)	West	Anorthosite	Zircon	1355 ± 1 Ma	This thesis (see Chapter 3)
Tessiarsuyungoakh intrusion (TI)	West	Monzodiorite	Zircon	1360 ± 4 Ma	This thesis (see Chapter 3)
Tessiarsuyungoakh intrusion (TI)	West	Monzonite	Zircon	1363 ± 3 Ma	This thesis (see Chapter 3)

* The U-Pb ages and supporting data have been published. (All others refer to ages quoted in papers or conference abstracts.)

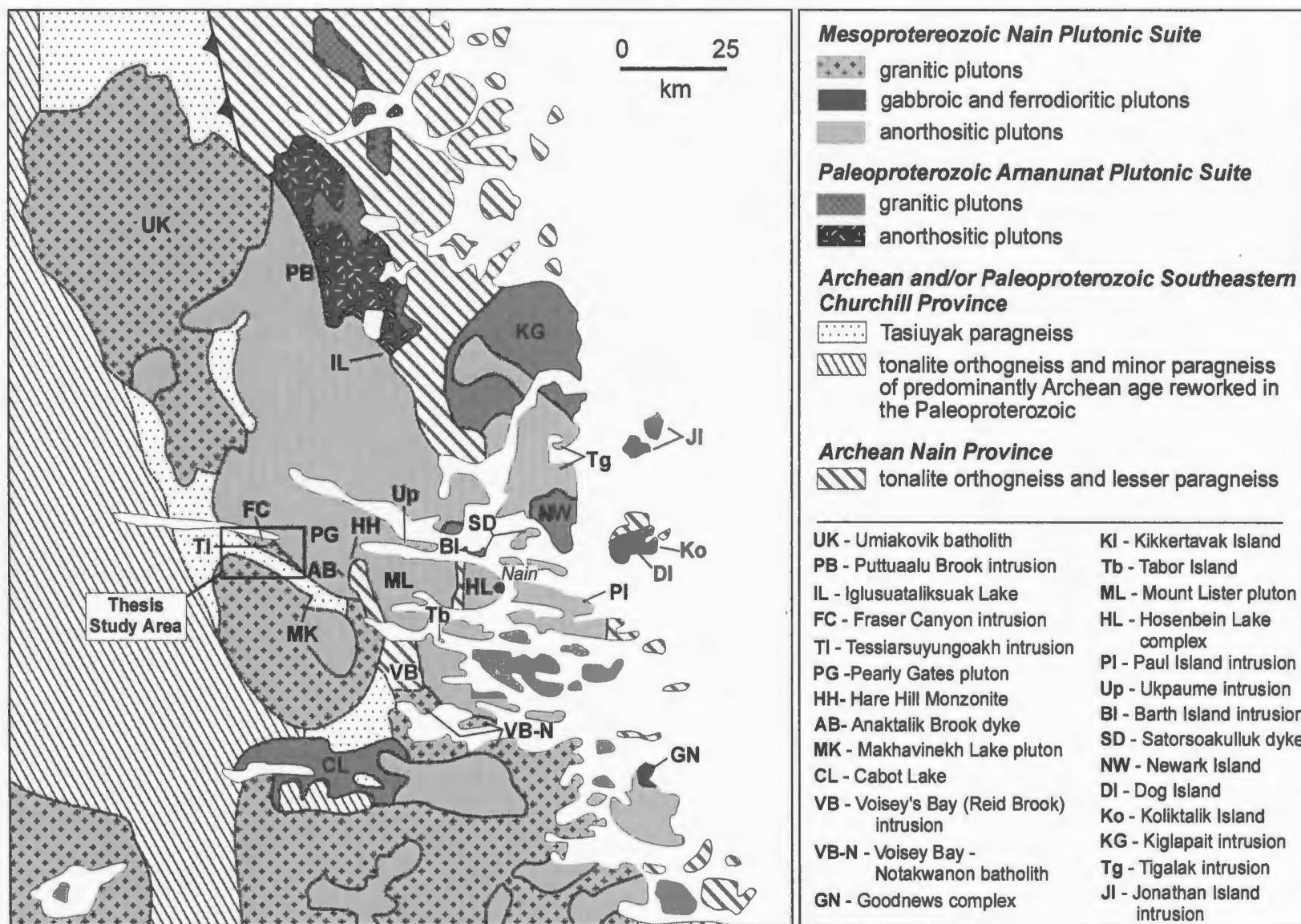


Figure 1.1: Simplified geological map of the Nain Plutonic Suite showing the location of dated intrusions from Table 1.1 (modified from Ryan & James, 2003). VB, SD, Up, AB, HH, ML monzonite, IL, Tg, Ko and FC units are too small to show on this map. Sango Bay is south of this map area.

CHAPTER 2 - REGIONAL AND LOCAL GEOLOGY

2.1 INTRODUCTION

This chapter describes the regional geological setting in detail and gives a brief overview of the geology of the study area. Detailed geological descriptions and interpretation of the study area are found in the respective manuscripts represented as Chapters 3 and 4 to reduce repetition. This section also provides information about previous work and field components related to the research of the study area.

2.2 REGIONAL GEOLOGY

The host rocks of the Mesoproterozoic Nain Plutonic Suite (NPS) are part of two structural provinces ranging in age from Archean to Paleoproterozoic (Fig. 2.1). These are the Archean Nain Province and the Archean and Paleoproterozoic southeastern Churchill Province (SECP). The Nain Province is part of the North Atlantic Craton that extends eastwards through Greenland, Scotland and Baltica. The SECP is the southeastern extent of the Churchill Province proper, which can be traced through northwestern Canada, northward through the Arctic islands and into northwestern Greenland. The Churchill Province is part of the Rae Craton, in which the SECP portion was sandwiched between the North Atlantic Craton to the east and Superior Craton to the west during ca. 1.87 – 1.80 successive, oblique collision. The collision along the western margin between the Superior and the Rae Cratons formed the New Quebec Orogen along the margin of the Superior Craton. The North Atlantic Craton and the eastern margin of the Rae Craton were accreted together during the Paleoproterozoic Torngat Orogen, a 1.87-1.86 Ga oblique continent-continent collision zone. The suture zone divides Archean orthogneiss of the Nain Province to the east from the SECP to the west.

The Archean Nain Province (3.8 – 2.5 Ga) is subdivided into the Saglek Block in the north and the Hopedale Block in the south. The Saglek and the Hopedale blocks have different geological characteristics, which imply that they were originally separate Archean cratons.

Connelly and Ryan (1996) suggested that they were accreted in the Late Archean although the suture has been obscured by the intrusion of NPS. The older Saglek Block (ca. 3.8 – 2.5 Ga) comprises tonalitic orthogneisses and deformed diabase dykes as well as three supracrustal units that unconformably overlie the orthogneisses. The supracrustal units are: 1) the metasedimentary Snyder Group (>1800 Ma) (Barton & Barton, 1975), 2) the metavolcanic Mugford Group (ca. 1950 Ma) (M.A. Hamilton, per comm., 2004) and 3) the metasedimentary Ramah Group (<2135 Ma) (Ermanovics & Van Kranendonk, 1990). Recently, Ryan & Hamilton (1998) recognized a Paleoproterozoic anorogenic AMCG suite, which is locally deformed and metamorphosed, within the Saglek Block. This group of anorthositic, noritic and granitic bodies was previously mapped as part of the Mesoproterozoic Nain Plutonic Suite. However, U-Pb dating indicated that this group of rocks, called the Annanunat Plutonic Suite (B. Ryan, per. comm., 2002), intruded between ca. 2135 and 2110 Ma (Hamilton et al., 1998). The Saglek Block rocks were subjected to regional metamorphism that produced amphibolite to granulite facies assemblages. The younger Hopedale Block consists of ca. 3.1 Ga orthogneiss and volcanic belts and a ca. 2.8 Ga tonalite-trondhjemite-granite suite. Regional metamorphism in this block has produced greenschist to amphibolite facies assemblages.

The eastern portion of the SECP related to the Torngat orogenic event is often referred to as the Rae Province (Hoffman, 1988; Hoffman 1990; Mengel and Rivers, 1991; Van Kranendonk, 1996, Van Kranendonk and Wardle, 1997). However, for simplicity this region will be referred to herein as the SECP. The SECP consists of Paleoproterozoic paragneiss and minor amounts of orthogneiss as well as Archean orthogneiss reworked in the Paleoproterozoic. The Tasiuyak paragneiss is interpreted to represent an accretionary wedge of detritus (Van Kranendonk et al., 1994; Wardle and Van Kranendonk, 1996; Rivers et al., 1996) shed from an unidentified Paleoproterozoic source (Scott and Machado, 1994) prior to subduction-related volcanic arc magmatism. The detritus underwent amphibolite to granulite facies metamorphism at ca. 1860 Ma (Bertrand et al., 1993) during the Torngat orogen collision and crustal thickening. Bertrand et al. (1993) reported maximum peak metamorphic conditions of 9-10 kbar and 950°C.

The evolution of the Torngat orogen involved transpressional collision and crustal thickening beginning at ca. 1860 Ma. Crustal thickening produced a doubly vergent structural fan with the axis centred in the Tasiuyak paragneiss (Rivers et al., 1996). Peak metamorphism reached granulite and amphibolite facies shortly after collision. There is some debate about which continent underwent subduction. Van Kranendonk (1996) suggested that the Nain Province was subducted under the SECP. Scott (1998) argued that the SECP (Rae Province) was subducted under the Nain Province. Scott (1998) also presented a model suggesting that the Tasiuyak paragneiss was accreted to the Nain Province (North Atlantic Craton) after its sedimentary source underwent complete subduction. Wardle and Van Kranendonk (1996) proposed the possibility that neither craton had undergone subduction but rather that a separate crustal sliver subducted under both cratons. All parties, however, agree on the relative timing and oblique nature of collision.

Sinistral shear zones related to continued orogenic deformation were formed between ca. 1845 and 1820 Ma. The Abloviak shear zone (ASZ) (Fig. 2.1) is one of these sinistral transpressional zones that formed along the suture within the Tasiuyak paragneiss producing a strong foliation trending 160-180°. A U-Pb geochronological study of zircons from syntectonic granitic intrusions in the Tasiuyak paragneiss by Bertrand et al. (1993) suggested ASZ deformation at ca. 1844 Ma. Post-collisional uplift (and erosion) occurred ca. 1.79 to 1.71 Ga with the development of the sinistral Komaktorvik shear zone, folding of the ASZ and a series of east-verging thrust-fold and thrust belts in the Nain Province (North Atlantic Craton).

The anorogenic ca. 1360 to 1290 Ma NPS (Fig. 2.1) intruded along part of the Torngat Orogen suture zone. The NPS consists of numerous intrusive bodies that were emplaced at mid-crustal level, at depths of ~10-15 km (Berg, 1979; Lee, 1987; Ryan, 1991; Emslie and Stirling, 1993). It comprises two major rock groups: 1) anorthosite, norite, gabbro and troctolite; and 2) charnockite, mangerite, granite and ferrodiorite. These igneous bodies are generally well preserved, however some older intrusions have been partially recrystallized and deformed at their margins (Ryan, 1993). Some of the regionally metamorphosed host gneisses of both the Nain

Province and the SECP have been subjected to contact metamorphism by NPS intrusions (Berg, 1977b). The region has been subjected to faulting and minor hydrothermal alteration. The NPS is also known for hosting the Voisey's Bay Ni-Cu deposit, southwest of Nain.

2.3 STUDY AREA

2.3.1 Introduction

The study area spans the deformed contact between the PGA and TI of the NPS and the intrusive contacts into the Tasiuyak paragneiss (SECP) by the TI to the east and the Makhavinekh Lake pluton to the southwest. This section discusses previous work and field components, and introduces the geology of the study area.

2.3.2 Previous Work

The first geological and geographical mapping of the thesis area was pioneered by E.P. Wheeler (1942, 1960, 1969). Wheeler (1969) also published a study of the TI describing petrography and mineral chemistry as well as suggesting the geometry and emplacement of the intrusion relative to the PGA. Further regional mapping has been done at 1:250 000 scale by Taylor (1977a) and by Ryan and James (2003) at 1:50 000 and 1:100 000 scale. Reconnaissance mapping by Bruce Ryan of the Newfoundland and Labrador Department of Mines and Energy over the last 13 years has added more detail to Wheeler's work. Ryan (1991) investigated the Makhavinekh Lake pluton and the surrounding contact metamorphosed Tasiuyak paragneiss, and described the rock units and field relationships. Ryan (1993) and Ryan and James (2003) also described the geological units of the PGA, TI and Tasiuyak paragneiss and field relationships. A preliminary investigation of labradorite occurrences was conducted in the area by Watson (1980) with particular attention to the Pearly Gates "quarry" for which the pluton is named by Ryan (1993). The "quarry" is actually a talus slope in a narrow east-west valley along a fault zone. The valley walls and talus contain large centimetre- to metre-scale blue-green and rarely seen yellow, iridescent labradorite.

Berg (1977a,b) did a regional study of contact metamorphic assemblages in the host rocks and incorporated two samples (2-1716, 2-1572) from this thesis area in his metamorphic study. These samples produced *P-T* results of 5.6 kbar and 910°C to 915°C. McFarlane et al. (2003) carried out a study with samples from the contact aureole to model geothermometry techniques using Al-solubility of orthopyroxene. The authors collected samples along two transects; the first was oriented northward from the northern margin of the Makhavinekh Lake pluton (within this thesis area), and the second was oriented eastward from the southeastern margin of this pluton (outside this thesis area). Only samples from the second transect were used to determine the contact metamorphic *P-T* paths. However, McFarlane et al. (2003) reported that due to the similarity in assemblages with increasing distance from the contact, the *P-T* conditions should be the same for both transects. Reported temperatures were 700°C to 900°C at distances ranging from 5750 to 20 m, respectively, from the contact.

2.3.3 Location and Access

The study area is located approximately 60 km west of Nain, northern Labrador (Fig. 2.1) and encompasses approximately 100 km² on NTS map sheets 14D/9 and 10. The area (Fig. 2.2) incorporates the western margin of the Nain Plutonic Suite and its Paleoproterozoic host, the Tasiuyak paragneiss of the SECP. The area was investigated on foot from camps established by helicopter. A zodiac was used in 2002 for more rapid access along Tessiarsuyungoakh Lake and to cover the shoreline and islands.

2.3.4 Field Component of the Project

The aim of the field component was to provide a detailed 1:20 000 map of the study area (Map 1 and Map 2), with particular attention to defining: 1) intrusive mechanisms and relationships of the Pearly Gates Anorthosite pluton and Tessiarsuyungoakh intrusion, and 2) determining the distribution and conditions of contact metamorphism of the Tasiuyak paragneiss.

A total of twelve weeks of fieldwork was carried out in the summers of 2001 and 2002 with logistical support from Voisey's Bay Nickel Company. Samples were collected for petrographic studies, mineral chemistry, U-Pb geochronology, and metamorphic studies.

2.3.5 Local Geology

The research area (Figs. 2.1 and 2.2) encompasses the western margin of the PGA, the adjacent TI, the Tasiuyak paragneiss host rocks and the northern margin of the Makhavinekh Lake pluton. (To avoid repetition, detailed geological descriptions and interpretations are found in Chapters 3 and 4, which represent manuscripts.) A brief description of the geology follows from east to west.

2.3.5.1 Pearly Gates Anorthosite pluton

The PGA consists of an inner zone of massive anorthosite and a deformed outer zone with foliated and recrystallized layers of anorthosite and norite. The inner zone contains various sizes of grey plagioclase megacrysts, averaging about 30 to 70 cm. These megacrysts are fractured and typically have thin rims of recrystallized, white plagioclase between grain boundaries and along fractures. The outer zone rocks are increasingly deformed and recrystallized towards the contact with the TI and the foliation is parallel to this contact.

The PGA was intruded by norite. A relatively large body of leuconorite and norite located along the southeastern shore of Tessiarsuyungoakh Lake is relatively undeformed and contains xenoliths of anorthosite. Norite dykes are found throughout the PGA study area and are weakly foliated or undeformed. A weakly foliated norite dyke crosscuts the gneissic PGA rocks at the contact with the TI. Minor intrusions of monzodiorite were also observed cutting anorthosite in the southwestern part of the outer zone (Map 1 & 2).

2.3.5.2 Tessiarsuyungoakh intrusion

The TI is a composite body of monzonite and monzodiorite which both contain various amounts of orthopyroxene, olivine and/or clinopyroxene. The TI is also strongly foliated along the contact with the PGA. The fabric weakens away from this contact and the TI rocks are relatively undeformed along the contact with the Tasiuyak paragneiss. Two contact relationships were observed between the monzonite and monzodiorite: the first is a compositional gradation, and the second is a sharp contact with irregular, lobate or cusped boundaries. In some cases, cusped contacts show monzodiorite pinching into the monzonite and no change in grain-size toward the contact. Along the western margin of the TI, monzonite was intruded as sheets into the Tasiuyak paragneiss.

Two bodies of megacrystic anorthosite are exposed in the TI. The first body is located on the north shore of the Tessiarsuyungoakh Lake and the second body is located along the southern cliffs of the Fraser Canyon (Fig. 2.2). Like the PGA, both anorthosite bodies have an inner zone of anorthosite and outer zone of layers of anorthosite and norite. However, only the Tessiarsuyungoakh Lake anorthosite body is deformed in its outer zone like the PGA.

2.3.5.3 Tasiuyak paragneiss

The Tasiuyak paragneiss is a relatively homogeneous metapelitic diatexite. The regional metamorphic assemblage comprises leucosome layers of quartz ribbons, K-feldspar, plagioclase and garnet and mesosome layers of plagioclase, K-feldspar, biotite, quartz, garnet and sillimanite. Minor amounts of pyrite, pyrrhotite, ilmenite, graphite, zircon, monazite and rutile are also present. Garnet porphyroblasts are round or elongate parallel to the foliation. Sillimanite grains form trains in the foliation plane and wrap around some garnet grains. Screens of unfoliated, granulite facies orthopyroxene-bearing meta-tonalite (enderbite) are distributed throughout the paragneiss but make up only a minor portion of the mapped area. The regional foliation broadly trends 160°SSE and is sub-vertical, however, locally the foliation can diverge from 110° to 165°

and dips range from 26° to 65° southwestwards. In the southern part of the map area changes in foliation orientation have been interpreted as a fold structure (Fig. 2.2).

In the study area the Tasiuyak paragneiss has been subjected to contact metamorphism during intrusion of the Makhavinekh Lake pluton. The contact aureole extends 4 km radially from the margin of the Makhavinekh Lake pluton. This intrusion has produced cordierite + orthopyroxene pseudomorphs replacing garnet + biotite and cordierite + spinel pseudomorphs replacing garnet + sillimanite along most of the study area with the exception of the northern most region along the Tasisuak Lake (Fig. 2.2). In this area the regional metamorphic assemblage appears to be intact and therefore unaffected by the emplacement of either the Makhavinekh Lake pluton or the TI.

2.3.5.4 Makhavinekh Lake pluton

Only small areas of the northern margin of the Makhavinekh Lake pluton were investigated during this study, as part of transects from this pluton through the Tasiuyak paragneiss. In these areas the pluton consists of undeformed rapakivi granite. The rock contains medium- to coarse-grained K-feldspar rimmed by plagioclase, with interstitial, pale blue quartz, olivine, orthopyroxene, clinopyroxene and minor amounts of hornblende. The attitude of the contact was not observed in this study, but was reported by Ryan (1991) and McFarlane et al. (2003) as sub-vertical. The margin of the pluton contains abundant xenoliths of Tasiuyak paragneiss which have undergone contact metamorphism producing a metamorphic assemblage of cordierite + orthopyroxene + spinel from garnet + biotite + sillimanite. Along the northeastern margin of the pluton, dykes of coarse-grained, white weathered granite with pale blue quartz were observed. However, these dykes were not observed along the northern margin of the Makhavinekh Lake pluton or in the Tasiuyak paragneiss.

2.3.5.5 Local minor dykes and faulting

Dykes of pegmatitic to aplitic syenite and granite as well as gabbro cut through all of the above-mentioned units. These dykes generally trend east-west, north-south or northwest-southeast parallel to major faults that also cut all the units. Five localities of fault breccia were found. One location was along the north shore of Tessiarsuyungoakh Lake, three locations were along the river system following the NW-SE contact between the TI and the Tasiuyak paragneiss and one was along an east-west river system, which cuts through the TI and PGA. In every case the fault gouge was located in the TI units and contained sub-rounded to rounded monzonitic fragments.

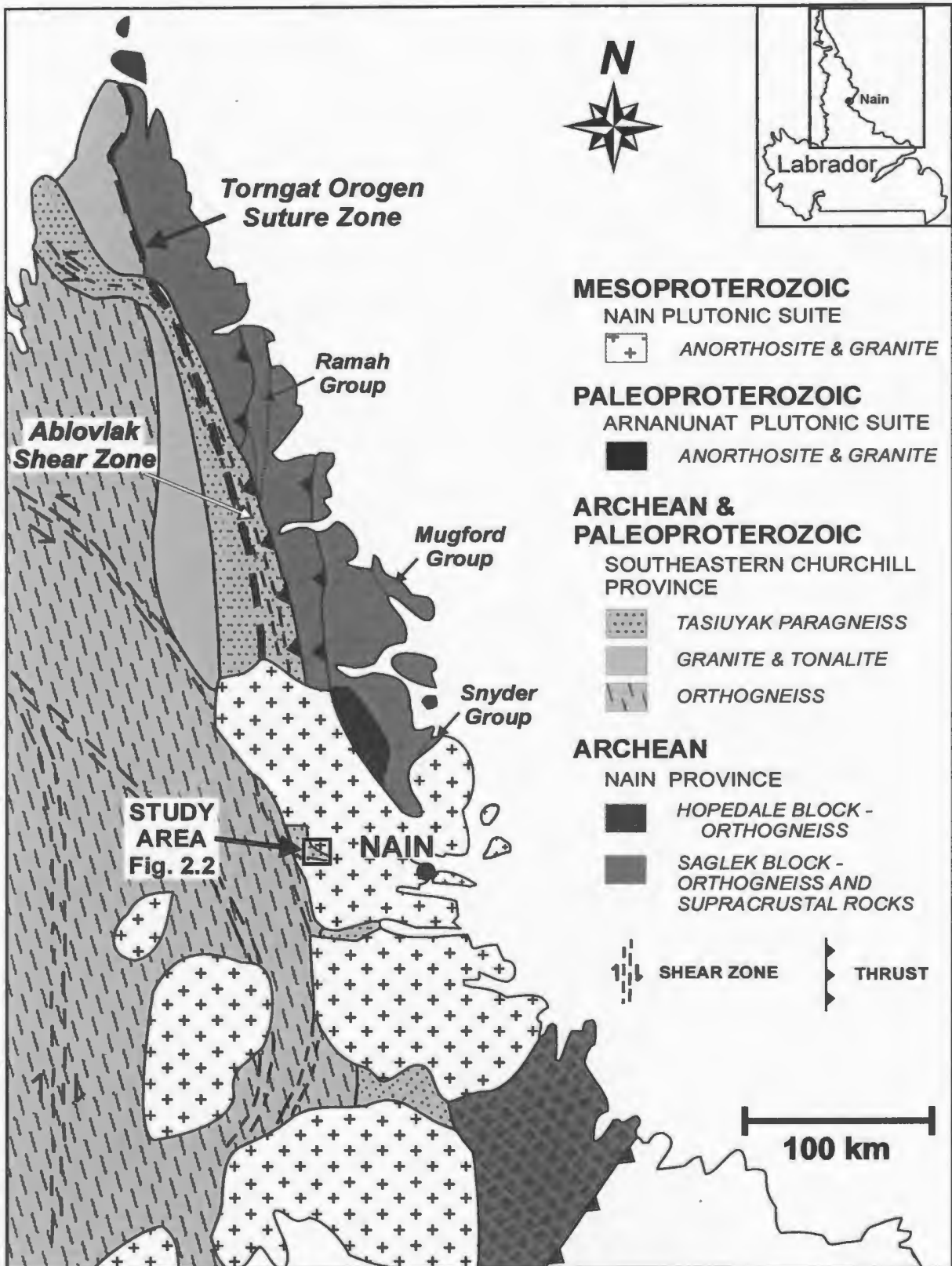
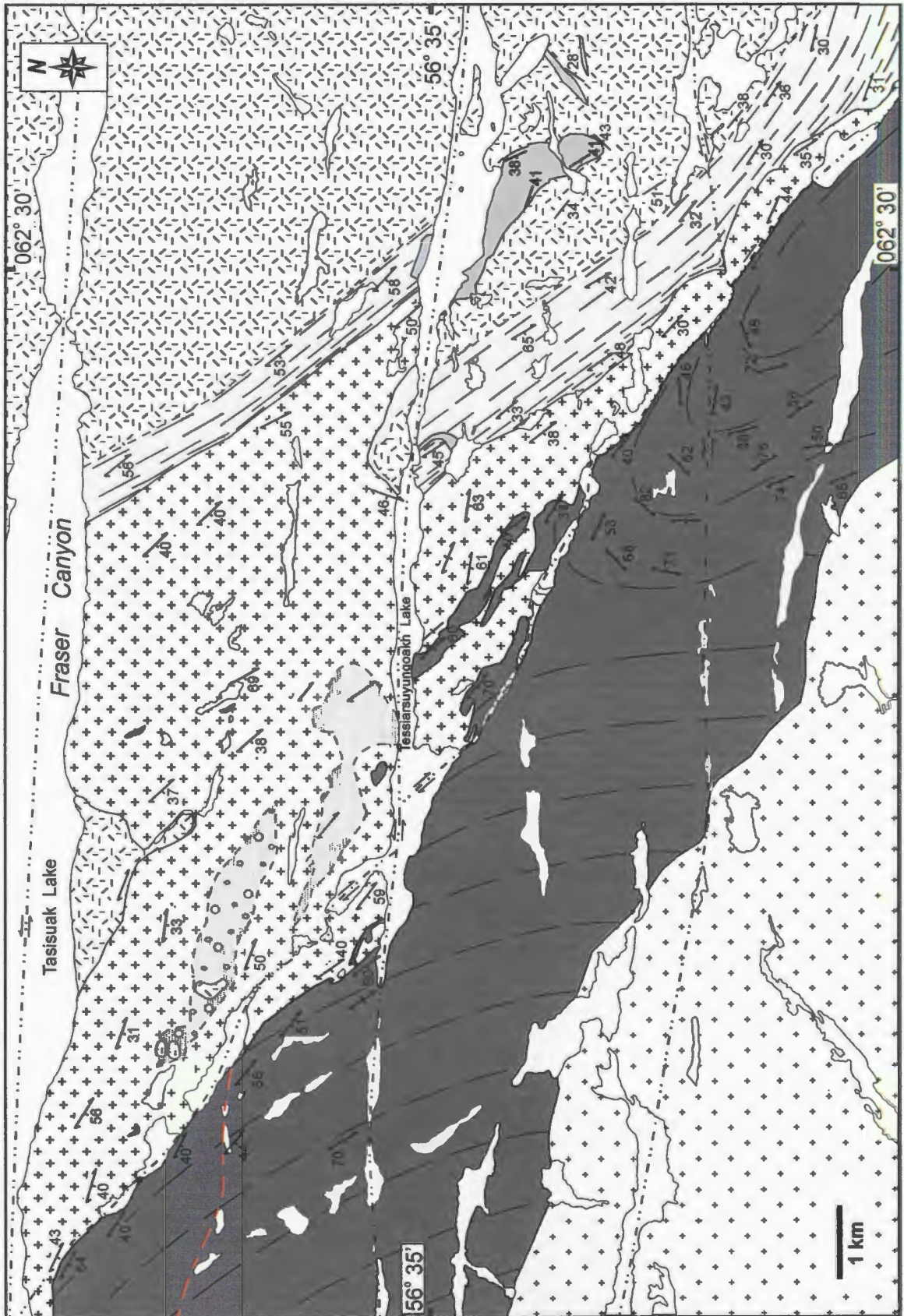


Figure 2.1: Simplified geological map of the major structural and intrusive units in northern Labrador (modified after Hall et al., 1995).



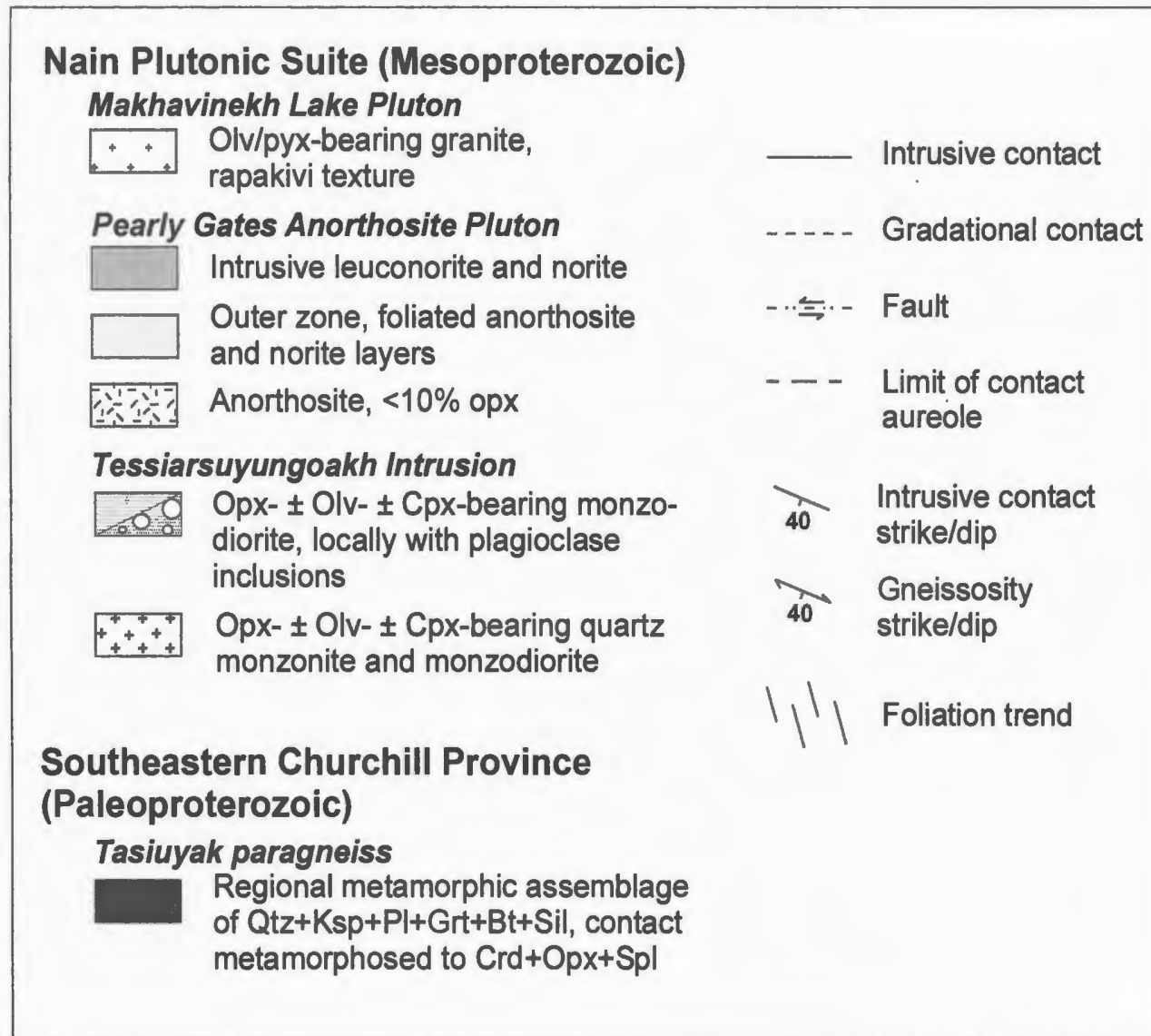


Figure 2.2: Geological map of the study area.

**CHAPTER 3 – EMPLACEMENT HISTORY OF THE PEARLY GATES ANORTHOSITE PLUTON
AND TESSIARSUYUNGOAKH INTRUSION:
PETROLOGICAL AND GEOCHRONOLOGICAL EVIDENCE**

Abstract:

The Pearly Gates Anorthosite pluton and the spatially related monzonite and monzodiorite Tessiarsuyungoakh intrusion are located along the western margin of the Mesoproterozoic Nain Plutonic Suite. Syn-emplacement deformation along the contact of these two bodies has masked the intrusive relationships. Norite bodies were intruded into the Pearly Gates Anorthosite pluton during and after deformation. U-Pb thermal ionization mass spectrometry dating of zircon and baddeleyite from units within these intrusions has yielded the oldest crystallization ages to date for magmatic components of the Nain Plutonic Suite. The Tessiarsuyungoakh intrusion has the oldest intrusive ages with concordant zircon data of 1363 ± 3 Ma for the monzonite and 1360 ± 4 Ma for the monzodiorite. The Pearly Gates Anorthosite pluton contained prismatic zircons and anhedral zircon fragments. The prismatic zircons, which were included in plagioclase phenocrysts gave an age of 1370 ± 5 Ma, and are interpreted to represent the time of growth of plagioclase crystals at depth, prior to emplacement. The zircon fragments, which formed between plagioclase grain boundaries yielded an age of 1335 ± 3 Ma, and are interpreted to represent the time of final crystallization of the Pearly Gates Anorthosite pluton. The Fraser Canyon Anorthosite that is exposed in the Tessiarsuyungoakh intrusion contained anhedral zircon fragments and baddeleyite grains, which gave the oldest intrusive age of 1355 ± 1.3 Ma for an anorthosite body in the NPS. An undeformed intrusive norite body in the Pearly Gates Anorthosite contained anhedral zircon fragments, which yielded a crystallization age of 1342 ± 1.2 Ma. Anhedral zircon fragments from a norite dyke that cuts the gneissosity of the Pearly Gates Anorthosite rocks at the contact gave a crystallization age of 1341 ± 1.8 Ma. The norite intrusive ages indicate that deformation in this area had terminated by ca. 1341 Ma.

Intermittent reactivation of older structures in the host Tasiuyak paragneiss formed conduit systems along which magmas were transported. These magmas were intruded as sheets, and stoping possibly occurred during emplacement. The Pearly Gates Anorthosite pluton and Tessiarsuyungoakh intrusion are not contemporaneous. Deformation along the contact between these intrusions most likely occurred during intrusion of the Pearly Gates Anorthosite pluton and after crystallization along its margins.

3.1 INTRODUCTION

The Mesoproterozoic Nain Plutonic Suite (NPS) is a 20,000 km² Anorthosite-Mangerite-Charnockite-Granite (AMCG) suite located in northern Labrador (Fig. 3.1). The area studied is located 60 km west of Nain on NTS map sheets 14D/9 and 10, and incorporates the western margin of the NPS and the Paleoproterozoic Tasiuyak paragneiss of the Southeastern Churchill Province that locally forms the host rocks of the NPS.

The Pearly Gates Anorthosite pluton (PGA) (Ryan, 1993) (Fig. 3.1) is part of the ca. 1360-1290 Ma NPS. This pluton is ovoid and extends at least 65 km in a north-south direction and 35 km east-west (Ryan and James, 2003). The PGA consists of an inner zone of massive, very coarse-grained anorthosite bounded by a kilometre-wide outer zone of foliated anorthosite and norite layers. The foliation is defined by heterogeneously strained, medium- to coarse-grained, partially recrystallized layers of leuconorite and norite. The PGA is intruded by bodies of deformed and undeformed leuconorite and norite (Fig. 3.2). To the west, the pluton is bounded by a concentric composite body of olivine- and/or pyroxene-bearing monzonite and monzodiorite, called the Tessiarsuyungoakh intrusion (TI), named by Wheeler (1969) (Fig. 3.2). The contact between the PGA and the TI is strongly deformed, obscuring intrusive relationships.

The TI comprises a wide variety of anhydrous rock types. These rocks contain various amounts of primary quartz + plagioclase + K-feldspar + orthopyroxene ± clinopyroxene ± olivine and some rocks contain relatively high quantities of ilmenite and magnetite. These relatively unusual rocks are found throughout the NPS and have often been referred to as monzonite,

manganite and ferrodiorite. The term ferrodiorite was used to describe anhydrous dioritic rocks with Si-content of ~47%, high Fe, Ti and P, and inverted pigeonite. In this study the name ferrodiorite has been replaced with more descriptive rock names using the IUGS recommendations for granitic rocks. Using this terminology the rock types are monzonite and minor quartz monzonite (manganite equivalent if orthopyroxene-bearing) and monzodiorite (ferrodiorite equivalent).

There have been many suggestions about possible magma sources and modes of emplacement associated with these AMCG suites. Suggestions of the possible parental magma vary from underplated or mantle-plume derived basaltic magmas (Berg, 1977b; Ashwal, 1993; Emslie, 1985; Emslie et al., 1994), to jotunitic or gabbro-noritic material melted in the lower crust (Taylor et al., 1984; Longhi et al., 1999; Bolle et al., 2003). Determining whether the anorthosite and granitic counterparts are comagmatic, inferring fractionation from the same parental magma, or whether components of the AMCG suite are derived from different source regions further complicates an interpretation of the magmatic history. It has been widely accepted that anorthosite massifs were emplaced as a plagioclase crystal and liquid "mush" (Emslie, 1985, Emslie et al., 1994, Wiebe, 1990, Longhi et al., 1999); however, there is still much debate about the proportion of crystals to liquid.

Assuming that anorthosite intruded as a crystal mush, the next problem is to determine a viable transport mechanism. There are two schools of thought regarding ascent mechanisms. Berg (1979), Wiebe (1990), Ashwal, (1993) and Emslie et al. (1994) suggested that diapiric transport is needed to move such large volumes of crystal mush through the crust. However there appears to be no evidence of vertical displacement of the country rocks adjacent to anorthosite plutons in the NPS. Xue and Morse (1993), Scoates and Chamberlain (1997, 2003) and Royse and Park (2000) favoured ascent via conduit systems and the latter group suggested evidence that shear zones were active during anorthosite emplacement in the eastern NPS.

There are two proposed tectonic settings for the emplacement of AMCG suites. The first is failed rifting along an older structural weakness, i.e. the Paleoproterozoic Torngat orogen

suture zone, (Berg, 1977b; Morse, 1982; Emslie, 1985; Dushesne, 1984) although no field evidence has corroborated this hypothesis. The second and perhaps more viable scenario is reactivation of transpressional shear zones, which provided conduit systems to transport and emplace AMCG suites (Scoates and Chamberlain, 1997; Royse and Park, 2000).

Two main questions addressed by this research are: 1) how were the TI and PGA emplaced and the inner and outer zones of the PGA formed, and 2) are the structurally related anorthosite-monzonite-monzodiorite intrusions temporally related? U-Pb geochronology studies were conducted to determine absolute igneous ages of six major rock units where field relationships were well constrained. The geochronological results were combined with field evidence to develop a model for the emplacement and formation of these intrusions.

3.2 REGIONAL GEOLOGY

The anorogenic Mesoproterozoic NPS intruded along part of the Paleoproterozoic Torngat Orogen, a 1.87-1.86 Ga continent-continent collision zone (Fig. 3.1). This suture zone joins Archean orthogneiss of the Nain Province to the east with the Southeastern Churchill Province to the west. Recently, a Paleoproterozoic (ca. 2135-2110 Ma) AMCG suite, called the Arnanunat Plutonic Suite, was recognized as part of the Nain Province (Hamilton et al., 1998). This suite lies adjacent to the northeastern margin of the NPS and, like the NPS, consists of anorthositic and granitic rocks. However, the Arnanunat Plutonic Suite was affected by regional amphibolite facies metamorphism and deformation during the Torngat orogenic event (Ryan & Hamilton, 1998). The Southeastern Churchill Province consists of Paleoproterozoic Tasiuyak paragneiss (Wardle, 1983) and Archean orthogneiss reworked in the Paleoproterozoic (Wardle and Van Kranendonk, 1996). The quartz-K-feldspar-plagioclase-rich Tasiuyak paragneiss with a regional metamorphic sub-assembly of garnet-biotite-sillimanite has been subjected to contact metamorphism by NPS intrusions producing cordierite-opx-spinel sub-assemblages (Berg, 1977a,b; Ryan, 1991, Ryan and James, 2003, McFarlane et al., 2003).

The NPS consists of numerous intrusive bodies that were emplaced at a mid-crustal level at depths of ~10-15 km (Berg, 1979; Lee, 1987; Ryan, 1991). It comprises two major rock groups: 1) basic rocks, such as anorthosite, norite, gabbro and troctolite, and 2) acidic rocks, such as granite, monzonite, and monzodiorite. Most NPS granitic rocks are anhydrous consisting of olivine + quartz, and/or pyroxene except for a few hornblende-bearing granitic intrusions (Ryan, 1991). The NPS has not been subjected to regional metamorphism and deformation and therefore is generally well preserved. However some of the older intrusions are partially recrystallized and deformed at their margins (Ryan, 1993). The NPS has been subjected to faulting and minor hydrothermal alteration. The NPS is best known as one of the world's best exposed AMCG suites and for hosting the Voisey's Bay Ni-Cu-Co deposit, southwest of Nain (Fig. 3.1).

3.3 GEOLOGY OF THE STUDY AREA

The research area (Fig. 3.2) encompasses the western margin of the PGA and adjacent TI. A description of the geology follows from east to west.

3.3.1 Pearly Gates Anorthosite Pluton

The PGA consists of an inner zone of massive anorthosite and an outer zone of foliated, partially recrystallized layers of anorthosite and norite. The inner zone typically contains very coarse-grained, grey plagioclase (An_{30} to An_{55}) (Pl. 3.1) with <10% similar sized interstitial orthopyroxene, generally a half a metre to a metre in length, and minor medium-grained ilmenite. Internal contacts were not observed, however, large metre-scale zones where plagioclase grains either increase or decrease in size, may suggest multiple intrusions. Orthopyroxene is ophitic and kink-banded. Plagioclase exhibits pervasive fracturing and minor white fine-grained recrystallization at grain boundaries (Pl. 3.2). North of Tessiarsuyungoakh Lake, many plagioclase crystals display labradorite schiller. This labradorite is typically iridescent with green, blue and yellow colours however some grains also show purple, red and bronze colours. The

crystals are typically fractured and altered and therefore are poor quality for use as gemstones or facing stone.

The kilometre-wide outer zone of the PGA is increasingly deformed and recrystallized towards the contact with the TI (Fig. 3.2). The anorthosite and norite layers range between centimetre- to metre-scale and have diffuse to sharp contacts in the less deformed areas. These layers are interpreted as igneous layering. This interpretation is most likely since relatively undeformed margins of anorthosite plutons in the eastern NPS show slump folding, gradational layering, troughs and scours (Wiebe, 1979; Royse and Ryan, 1995; D. Wright, per. com. 2002). The foliation is not obvious in the anorthosite layers, except for augen of relict igneous plagioclase in a matrix of sugary, recrystallized plagioclase. The fabric is best defined by norite layers, which contain attenuated coarse-grained, partially recrystallized, orthopyroxene and ilmenite surrounding lenticular coarse-grained plagioclase (Pl. 3.3). At the contact, the medium- to fine-grained anorthosite and norite rocks are gneissose with a foliation parallel to the boundary, striking 120° to 150°, dipping 30° to 50° SW. Where the dip surface of the foliation is exposed, textures and compositions are heterogeneous (Pl. 3.4). Highly strained, recrystallized orthopyroxene appears to form a weakly oriented lineation, plunging ~ 20° WNW, within the foliation. The PGA appears to have a domal shape, with the western, southern and eastern contacts dipping outwards from the intrusion (Ryan, 1993; Ryan and James, 2003).

The PGA was intruded by a medium- to coarse-grained, brown-weathering body of leuconorite and norite at the southeast end of Tessiarsuyungoakh Lake (Fig. 3.2). Xenoliths of anorthosite were observed in the leuconorite at the margin. The noritic body displays igneous textures and only minor evidence of deformation with kink-banded orthopyroxene and minor recrystallization of plagioclase. This unit can be traced continuously north and northwest of the lake as well as on some of the islands (too small to be shown on Fig. 3.2). The contact of the noritic body north of Tessiarsuyungoakh Lake does not contain anorthosite xenoliths and the contact can be diffuse or sharp with no chilled margin.

Coarse-grained, weak to moderately foliated, discontinuous norite dykes intruded into the PGA, of which most of the dykes are found in the outer zone. Some dykes display reaction rims of coarse-grained opx extending along the dyke margins. Most dykes are sub-concordant with the PGA foliation/boundary. However one dyke, located within a few metres of the TI-PGA contact, crosscuts the anorthosite/norite gneissosity (Pl. 3.5). Both the noritic dykes and intrusive norite body contain high concentrations of interstitial ilmenite (~5 – 15%).

Minor bodies and dyklets of monzodiorite intruded the PGA, south of Tessiarsuyungoakh Lake. One 25 m² monzodiorite body contains xenoliths of anorthosite. The xenoliths range from metre-sized blocks to centimetre-sized, rounded fragments, which are often fractured and in-filled with the surrounding monzodiorite. A 15 cm plagioclase xenocryst shows evidence of having been fractured and rotated during resorption (Pl. 3.6). This xenocryst is round, with a grey core and white rim and the monzodiorite matrix filled the fractures. No intrusive monzonite was observed in the PGA.

East-west and north-south trending hornblende- and biotite-bearing granitic to syenitic pegmatite and aplite dykes intrude the PGA and are associated with pink alteration along fractures. The alteration minerals consist of hematized epidote, white mica and calcite formed from the breakdown of plagioclase, and amphibole and chlorite formed from the breakdown of orthopyroxene. In many cases the alteration minerals are medium-grained which suggests pervasive fluid transport along these fractures. East-west, north-south and northwest-southeast trending gabbro dykes also intrude the PGA. Only a few gabbro dykes were seen and were mostly observed in valleys and riverbeds suggesting that they intruded along faults. Most of the gabbro dykes have undergone serpentinization of olivine. Both acidic and basic dykes have chilled margins indicating intrusion after cooling of the PGA. Alteration fractures in the PGA and serpentinization of the gabbro dykes indicate that hydrous fluids interacted with these rocks, possibly derived from the crystallization of the hydrous granitic dykes.

3.3.2 Tessiarsuyungoakh Intrusion

The TI is a composite body consisting of fine-to medium-grained, orthopyroxene-olivine-clinopyroxene-bearing, oxide-rich monzodiorite and a medium- to coarse-grained orthopyroxene-olivine-clinopyroxene-bearing monzonite. The weathered surface of the monzonite is white and the fresh surface has a colour index of 15 to 25. The monzonite typically has medium- to coarse-grained, ovoid, K-feldspar phenocrysts and rarely seen coarse-grained, elongate K-feldspar phenocrysts, which are oriented parallel to the foliation. The monzodiorite has a rusty weathered surface and a colour index of 25 to 50. Although monzodiorite units are generally homogeneous in outcrop-scale, minor, millimetre-scale layering, defined by more mafic and more felsic compositions, was observed in fine-grained units. These layers are interpreted as igneous compositional layering.

Like the anorthosite, these units are gneissic at the contact with the PGA with alternating centimetre- to metre-scale bands of monzonite and monzodiorite (Pl. 3.7). However, although the fabric weakens away from the contact with the PGA, it can be traced throughout most of the intrusion. This weak foliation represents igneous layering and the elongate oriented K-feldspar phenocrysts in this region are interpreted to represent a magmatic flow foliation. Both the igneous and gneissic foliations are generally parallel to this contact except in the centre of the intrusion where the igneous foliation swings to east-west. This deflection appears to mimic the gneissosity in the Tasiuyak paragneiss to the south (Fig. 3.2) suggesting reactivation of older structures during deformation of these younger intrusive bodies.

Where the fabric is weakest, two different contact relationships between the monzonite and monzodiorite were observed: 1) the contact is diffuse and the two rock units appear to have a gradational contact; and 2) intrusion of monzodiorite into the monzonite was observed and the irregular to cusped contact (Pl. 3.8) indicates that the monzonite had not completely crystallized when the monzodiorite intruded. In both cases the evidence suggests that the monzonite and monzodiorite are temporally related. The different contact relationships could be interpreted as two or possibly three magma pulses. In this scenario, the earliest intrusion of monzonitic and

monzodioritic magma formed gradational contacts during crystallization. A second pulse of monzodioritic magma may have intruded the partially crystallized earlier intrusives. There is no evidence of monzodiorite intruding monzodiorite but this relationship would be difficult to observe. A few decimetre- to metre-scale anorthosite dykes intruded the TI and have no chilled margins but have straight contacts. Although these anorthosite dykes could not be traced back to the PGA, they do suggest that the anorthosite intruded after the TI crystallized but while the TI was still hot (Pl. 3.9).

The western margin of the TI is typically coarse-grained monzonite, which intruded as sheets into the Tasiuyak paragneiss. The monzonite is generally undeformed but minor metre-scale shear zones trend parallel to the contact with the paragneiss. In addition, the TI-Tasiuyak paragneiss contact is generally parallel to the gneissosity in the Tasiuyak paragneiss.

Screens of Tasiuyak paragneiss are found throughout the TI. The gneissosity in the screens is almost parallel ($< 20^\circ$) to the contact and the foliation of this intrusive unit, suggesting that the TI intruded as sheets parallel to the older structures in the paragneiss. Most of the Tasiuyak screens *appear* to have retained the regional metamorphic assemblage except for those within the 4 km range of the contact aureole produced by the Makhavinekh Lake pluton (see Chapter 4, section 4.10).

3.3.3 Exposed Anorthosite Bodies

Two bodies of anorthosite are exposed within the TI (Fig. 3.2). Like the PGA, these bodies generally have an inner zone of anorthosite and an outer zone of noritic and anorthositic layers. The anorthosite on the north shore of Tessiarsuyungoakh Lake (Fig. 3.2) has structures, textures and fabrics similar to the PGA. A foliation in the outer zone is defined by leuconorite and norite layers associated with anorthosite layers. The contact and foliation dips east at the eastern margin and dips west at the western margin suggesting this anorthosite body has a domal shape. The eastern margin of this anorthosite body was intruded by coarse- to very coarse-grained,

undeformed norite, with similar compositional and textural characteristics as the norite body within the PGA. This anorthosite body is interpreted as a portion of the PGA.

The other anorthosite, south of Tasisuak Lake, is exposed along the vertical face of the Fraser Canyon, herein called the Fraser Canyon Anorthosite. The view from the other side of the canyon shows that it also has a domal structure. The roof of the Fraser Canyon Anorthosite was easy to access since it is near the top of the canyon, however access to the walls was difficult to impossible to reach on foot. This anorthosite, although partially recrystallized, is relatively undeformed. It consists of an inner zone of massive, very coarse-grained anorthosite, and an outer zone of medium- to coarse-grained norite. The norite exposed at the roof of the Fraser Canyon Anorthosite contains tabular plagioclase with interstitial orthopyroxene and ilmenite (Pl. 3.10).

A kilometre north of the Fraser Canyon Anorthosite, in a marshy valley, small outcroppings of undeformed anorthosite and norite are exposed in monzodiorite. These small units of anorthosite and norite are interpreted as exposed portions of the Fraser Canyon Anorthosite roof. The overlying monzodiorite is fine- to medium-grained and contains plagioclase inclusions (Fig. 3.2) ranging from a few millimetres to 20 cm in size (Pl. 3.11). The plagioclase inclusions are sub-angular to sub-round, and the smaller inclusions are white whereas the larger inclusions are grey with white, recrystallized rims. The plagioclase inclusions could indicate that the monzodiorite intruded after the anorthosite. However, if the monzodiorite is part of the anorthosite intrusive package then the plagioclase crystals could be from the anorthositic magma and therefore were not plucked from the anorthosite by later intrusion.

Field evidence suggests that the anorthosite body on the north shore of Tessiarsuyungoakh Lake is an exposed part of the PGA. However, on the basis of field relationships, the Fraser Canyon Anorthosite cannot be conclusively included or excluded as part of the PGA.

3.3.4 Faults and Dykes

Faulting in the study area is best exposed along, and trending northwest-southeast, parallel to the TI-Tasiuyak paragneiss contact. The fault lies within the monzonite of the TI, and was seen as fault breccia and fault gouge (Pl. 3.12). A garnet-bearing syenite dyke intruded along this fault zone. A 2 m wide gabbro dyke intruded along the margin of the fault and the monzonite. The dyke appears unaffected by faulting and therefore was intruded after this event. Syenite, granite, aplite and gabbro dykes in the PGA and TI generally trend east-west, north-south or northwest-southeast as do other major faults that cut these two intrusions. At least some of the granitic and gabbro dykes are younger than the faulting but it is unknown how many generations of these dykes exist.

3.4 PETROGRAPHY

3.4.1 Pearly Gates Anorthosite Pluton

Due to the very coarse grain size of the inner zone of the PGA only the outer zone layers of anorthosite were selected for petrography. In the outer zone the anorthosite comprises adcumulate plagioclase containing minor inclusions of needle-like oxide and prismatic zircon. Plagioclase grains are recrystallized along grain boundaries showing development of subgrains and serrated boundaries (Pl. 3.13). Deformation twinning and undulose extinction is typical in both cumulate and recrystallized plagioclase. At the contact of the PGA, the anorthosite is completely recrystallized and granoblastic with sharp grain boundaries and triple junctions. Some cumulate plagioclase is antiperthitic with lamellae forming along cleavage planes. In a few places these lamellae were bent (Pl. 3.14). The interstitial minerals show a crystallization order of apatite, followed by ilmenite or magnetite, then orthopyroxene and clusters of anhedral zircon crystallizing last. Ilmenite is typically the dominant Fe-oxide and magnetite was rarely seen.

The PGA noritic layers in the outer zone also show increasing recrystallization and deformation textures and fabrics towards the contact. Although the norite is heterogeneously deformed, ophitic and sub-ophitic orthopyroxene indicate that plagioclase crystallized first. At the

contact with the TI, orthopyroxene and plagioclase are completely recrystallized with only minor relict igneous cores in the largest original grains. In the schistose region of the outer zone away from the contact, relict igneous plagioclase is anti- to meso-perthitic and the lamellae appear to be elongated due to strain. In rare cases the albitic lamellae were bent. In this region, coarse-grained orthopyroxene appears to be single crystals in hand sample but petrographic observations indicate that they are typically recrystallized (Pl. 3.15).

The norite intrusive body and dykes generally have the same mineralogy and similar characteristics. These rocks are composed of cumulate plagioclase and ophitic orthopyroxene. The orthopyroxene also contains inclusions of apatite and ilmenite. Strong deformation textures and fabrics were absent in the norite intrusive body indicating that the rock is relatively undeformed (Pl. 3.16). This intrusion also contained minor clinopyroxene lamellae in orthopyroxene indicating the presence of a minor amount of inverted pigeonite. The norite dykes have been heterogeneously deformed. Some dykes were highly strained containing attenuated, recrystallized orthopyroxene and bent antiperthitic lamellae, while others contained no deformation fabric and only minor fine-grained, recrystallized grains mantling primary orthopyroxene and plagioclase.

Samples from the two exposed bodies of anorthosite show the same petrographic characteristics as the anorthosite and norite from the PGA with one exception. The anorthosite and norite sampled at the roof of the Fraser Canyon Anorthosite show undulose extinction in both orthopyroxene and plagioclase, and deformation twinning in plagioclase (Pl. 3.17). However, the lack of foliation, major recrystallization and bent crystals and crystal structures indicate that the Fraser Canyon Anorthosite was not subject to major deformation. This anorthosite comprises adcumulate plagioclase defined by triple-junctions and very little recrystallization (Pl. 3.18). Minor amounts of primary biotite mantling orthopyroxene also indicate hydrous fluids accumulated at the roof of this anorthosite.

H₂O alteration throughout the units in the PGA is indicated by heterogeneous saussuritization of plagioclase, secondary calcite and epidote, and fibrous amphibole and chlorite

replacing orthopyroxene. Alteration fractures are most prominent in the anorthosite and contain calcite, scapolite, muscovite and epidote and the adjacent plagioclase walls have undergone over 50% saussuritization.

3.4.2 Tessiarsuyungoakh Intrusion

The monzodiorite and monzonite units of this intrusion generally consist of K-feldspar, plagioclase, quartz (< 5%) and orthopyroxene with lesser clinopyroxene and/or olivine. Accessory minerals include ilmenite, magnetite, apatite, rutile and relatively abundant prismatic zircon.

The monzonite is medium- to coarse-grained and typically contains ovoid K-feldspar phenocrysts. The alkali feldspars are typically microcline and mesoperthitic orthoclase and albite. The felsic minerals make up between 60 to 80%. The fine- to medium-grained monzodiorite has a felsic to mafic mineral ratio of 50/50, and rarely contain K-feldspar phenocrysts. Interstitial orthopyroxene, fayalitic olivine, pigeonite and augite are typical in both the monzonite and monzodiorite. Where orthopyroxene is present it is generally the dominant mafic mineral and is usually the product of pigeonite exsolving lamellae of augite. Fayalite, inverted pigeonite and augite are typically present together in various amounts. In some cases fine-grained augite and plagioclase were observed mantling inverted pigeonite and the textures indicate that the augite/plagioclase aggregate crystallized late. Both rock types show slow cooling textures, such as mesoperthitic feldspars and inverted pigeonite.

Deformation and recrystallization textures are dominant in samples collected within about 200 m from the contact with the PGA. These textures include serrated grain boundaries, subgrain development, bent exsolution lamellae, deformation twinning and bent albite twinning and undulose extinction (Pl. 3.19). Evidence of deformed antiperthite and inverted pigeonite lamellae indicates that exsolution occurred before deformation. Further away from the PGA contact, minerals show little evidence of deformation. Only minor recrystallization, undulose extinction and deformation twinning were observed (Pl. 3.20). Exsolution lamellae such as mesoperthite and inverted pigeonite are typical in all the rocks of the TI.

In the Fraser Canyon Anorthosite the margin is noritic and has a sharp contact against monzodiorite of the TI. Petrographic studies of this monzodiorite indicated that the monzodiorite composition grades outward from the contact with the norite. This gradation ranges from an orthopyroxene-monzodiorite adjacent to the norite, to an orthopyroxene-clinopyroxene-olivine-bearing monzodiorite to a clinopyroxene-olivine-bearing monzonite. This compositional gradation was also observed at the margin of the anorthosite exposed in the marshy valley, north of the Fraser Canyon Anorthosite. The compositional gradation seen in thin sections suggests that the monzonite and monzodiorite could have been immiscible liquids and that perhaps minor mixing occurred at the liquid boundaries to form this compositional gradation.

3.5 U-Pb GEOCHRONOLOGY

3.5.1 Sample Selection

Samples for geochronology were selected from the major rock units where relationships were well established by field evidence. The samples were broken up and the weathered surfaces trimmed away, then double-bagged and sealed at the sampling site to prevent contamination. About 20 kg of rock was collected for each sample. A total of 11 geochronological samples were collected. The PGA and the monzonite were sampled twice at two different locations in case one sample did not contain the desired U-Pb-bearing minerals, such as zircon and baddeleyite. A sample of the Makhavinekh Lake pluton was discarded after discovering that McFarlane (per comm., 2002) had previously dated the pluton and produced a well-constrained crystallization age of 1322 ± 2 Ma. Two samples of Tasiuyak paragneiss were also discarded due to the complexity of the paragneiss and time constraints. Therefore only 6 of the 11 geochronological samples were actually dated. Sample locations are shown in Figure 3.2. The six samples selected for U-Pb geochronological study are numbered as follows: 1 – outer zone of the PGA, 2 – the Fraser Canyon Anorthosite, 3 – norite dyke cross-cutting gneissic outer zone of the PGA, 4 – norite body intruding inner zone of the PGA, 5 – olivine-bearing monzodiorite, and 6 – orthopyroxene-bearing monzonite.

3.5.2 Sample Preparation and Analytical Methods

The rock samples were crushed with a jaw crusher and then reduced to powder in a disc mill. The powder was panned using a Wilfley table and passed through methylene iodide to extract the heaviest minerals. A Frantz magnetic separator was used to extract the least magnetic, and therefore highest quality, zircon and baddeleyite. All zircon and baddeleyite grains were removed from non-magnetic separates at 0° side-slope (horizontal), except for sample 4 which had very little non-magnetic material left after processing at a 2° side-slope. Zircon and baddeleyite grains were hand picked under a binocular microscope and the clearest grains with minimal fracturing were selected. If more than one crystal morphology was observed in a sample, each morphology was picked and separated for analysis. This was done to determine if the different morphologies would produce the same crystallization age. If different crystallization ages were obtained from different morphologies this would suggest a complex crystallization history of the unit sampled.

Selected zircons were mounted in epoxy resin, polished, and imaged using back-scattered electron (BSE) first and later cathodoluminescence (CL) techniques to determine internal structures. Baddeleyite grains were too small and too few were recovered to sacrifice using any to mount and image. Some of the BSE imaged zircons were removed from the mount and used for TIMS analyses. It was later discovered that BSE imaging revealed less information regarding zoning or other structures than CL imaging. However, CL imaging indicated that the zircons selected for U-Pb geochronology were of igneous origin and did not contain inherited grains to warrant concern about previous zircon analyses. Zircons in most samples were either large 3:1 prisms or large fragments, with the exception of samples 1 and 2, which contained both. Sample 1 also contained highly resorbed cusped zircons. Baddeleyite grains were small stubby and euhedral. Zircons were abraded for periods ranging from 8 to 40 hours depending on their size and hardness to enhance concordance according to procedures found in Krogh (1982a). Softer baddeleyite grains were abraded for 2 to 3.5 hours.

After abrasion of morphologically similar zircon or baddeleyite, grains were separated into fractions for analyses. Fractions either contained multiple grains if the grains were small and/or extremely low in radiogenic lead or contained one large single grain with enough radiogenic lead to provide data on the mass spectrometer. The fractions were dissolved in HF and HNO₃ over 5 days at 210°C and each aliquot was passed through ion exchange chemistry (Krogh, 1973) to extract purified U and Pb.

Thermal ionization mass spectrometry was performed on a MAT 262 multi-collector instrument. Data were acquired on either the faraday multi-collector or single ion counter depending on the intensity of ion beams for U and Pb. Multiple sets of data were measured in the temperature ranges of 1400°C to 1550°C for Pb and 1550°C to 1650°C for U, and the best sets were calculated to give a mean value for each ratio. The ratios were also corrected for laboratory procedure blanks (2-5 pg for Pb and 1 pg for U) and for common lead above the laboratory blank with lead of the composition predicted by the two-stage model of Stacey and Kramers (1975) for the age of the sample. Uncertainties for ages are quoted with a 95% confidence level, but, do not include uncertainties in the U decay constants.

Where possible, the petrographic observations of zircon populations used in dating are described. However, the anorthosite and norite samples contained relatively small amounts of zircon and smaller amounts of baddeleyite and therefore these minerals were not always observed in thin section.

3.5.3 Results

The six samples selected yielded prismatic and/or angular fragmented zircon, and samples 1 and 2 also contained baddeleyite. Angular fragments typically had planar zones of dusty inclusions and these were avoided during the selection process. Grains typically exhibited less detail in BSE therefore descriptions of internal structures are based on CL images. Zircon was only observed in thin sections from samples 1, 5, and 6. No baddeleyite grains were

identified in thin section. The U-Pb geochronology analytical data set is listed in Table 3.1 and concordia diagrams are shown in Figure 3.4.

3.5.3.1 Pearly Gates Anorthosite pluton

Sample 1, PGA outer zone: The sample was taken from the foliated margin of the PGA and incorporates both anorthosite and norite layers. The sample has a complicated zircon population including pale brown, angular fragments with no crystal faces (Pl. 3.21, 3.22); pale brown, slightly resorbed prisms (Pl. 3.23, 3.24); and highly resorbed, pale brown cusped grains (Pl. 3.25, 3.26). Baddeleyite grains were chocolate brown, euhedral, and stubby (Pl. 3.29). Three zircon populations were observed in thin section. They are: slightly resorbed prisms as inclusions in plagioclase grains (Pl. 3.24), interstitial cusped zircons located at plagioclase-plagioclase boundaries (Pl. 3.26), and clusters of interstitial anhedral zircon (fragments) located at plagioclase-plagioclase and plagioclase-ilmenite grain boundaries (Pl. 3.22). Typically the cluster of anhedral zircons is in optical continuity indicating that they are parts of one large grain extending in the third dimension.

CL imaging of prismatic zircons showed that no inherited cores were present. These zircon prisms typically display igneous zoning as well as irregular and patchy zoning (Fig. 3.3a-c). The two latter zoning patterns seem to suggest redistribution of heavy elements by either diffusion or recrystallization. These diffusion or recrystallization zones in the grains and evidence of minor resorption of crystal faces may indicate a thermal event, which has affected these prisms. The U concentration is extremely low in these grains ranging from 2.5 - 5.4 ppm. Two multi-grain fractions (P1 and P4) are concordant and gave overlapping $^{207}\text{Pb}/^{206}\text{Pb}$ ages of 1373 and 1368, respectively. Multi-grain fractions P2 and P3 are also concordant but yield younger ages, which suggests that there has been minor lead loss. Therefore, using P1 and P4, the oldest minimum crystallization age of the prismatic zircons from the weighted average of the $^{207}\text{Pb}/^{206}\text{Pb}$ age is 1370 ± 5 Ma.

The cusped zircons are interpreted to be highly resorbed prismatic grains. Evidence for this is the relict, elongate shape of the cusped zircons and CL imaging where the sharp boundary of a terminating prismatic tip was observed (Fig. 3.3e). If the edge of the relict crystal shape is extended to include the remnant cusped shape, this indicates that at least 50% of the original grain has been resorbed possibly due to changing magma composition. Typically, CL imaging shows very complex zoning patterns attributed to internal diffusion during resorption (Fig. 3.3d-f). Six single-grain analyses lie on or almost on concordia and $^{207}\text{Pb}/^{206}\text{Pb}$ ages range from 1355 to 1335 Ma. The cusped grains have a much higher U concentration (39-188 ppm) than the slightly resorbed prisms (2.5-5.4 ppm) and prisms from samples 5 (4.8-14.8 ppm) and sample 6 (0.5-27.1)(Table 3.1). Therefore it is suggested that the prisms that were later highly resorbed to form the cusped population are not xenocrystic from the other prismatic zircon-bearing rocks but may have originally crystallized from a younger than 1370 Ma plagioclase crystallization event. The range of concordant $^{207}\text{Pb}/^{206}\text{Pb}$ ages and the evidence of strongly resorbed grains with major internal diffusion, indicates that minor lead loss occurred, reconfirming the evidence for at least a single, if not multiple, thermal event(s).

CL imaging of zircon fragments shows some grains have igneous zoning and others have been highly fractured and annealed with a diffusion pattern relative to the annealed fractures (Fig. 3.3g-h). Four multi-grain fractions yielded F3 and F4 overlapping on concordia with $^{207}\text{Pb}/^{206}\text{Pb}$ ages of 1333 and 1337 Ma, and concordant F1 overlapping F4 with a $^{207}\text{Pb}/^{206}\text{Pb}$ age of 1343 Ma. F2 is discordant with a $^{207}\text{Pb}/^{206}\text{Pb}$ age of 1331 Ma. Fractions F2, F3 and F4 define a recent lead-loss regression line with an upper intercept of 1335 \pm 7/-3 Ma (44% probability of fit, lower intercept = 340 Ma). Based on petrographic observations, the interstitial fragmental zircon was one of the last minerals to crystallize. Therefore, the final igneous crystallization age of this rock based on the upper intercept of the F2, F3 and F4 discordia line is 1335 \pm 7/-3 Ma.

Two single grain fractions of small, brown, euhedral baddeleyite gave concordant and overlapping $^{207}\text{Pb}/^{206}\text{Pb}$ ages of 1358 and 1362 Ma. However both analyses were relatively imprecise and therefore do not provide a good age constraint on their crystallization age.

Sample 2, Fraser Canyon Anorthosite: Sample 2 represents a massive, heterogeneously recrystallized anorthosite from the exposed body adjacent to the Tasisuak Lake (Fraser Canyon). The sample contained four zircon populations, which include very large (400-800 μm), clear, colourless, fractured and fluid inclusion-filled, euhedral prisms; large (200-400 μm), clear, colourless, euhedral prisms (Pl. 3.27); and brown and colourless angular fragments with no crystal faces (Pl. 3.28). The very large prisms lacked either one terminating end or both. Both populations of prismatic zircon have pristine crystal faces with no evidence of resorption. The fractures and clear fluid inclusions are parallel to the c-axis and give the crystals a columnar appearance. The large prisms show no evidence of resorption and no internal structures when viewed under the microscope. There were relatively few prismatic zircons and only 34 grains were recovered from the non-magnetic separate. CL imaging of both types of prismatic zircons show igneous zoning and no evidence of inheritance or diffusion/ recrystallization (Fig. 3.3i-j). One single grain fraction, P3, is concordant giving a $^{207}\text{Pb}/^{206}\text{Pb}$ age of 1345 ± 2 Ma. Fractions P2, P3 and P4 fall on a recent lead-loss trajectory for the same age. The weighted average for the $^{207}\text{Pb}/^{206}\text{Pb}$ age of fractions, P2, P3 and P4, gives a crystallization age of 1344 ± 3.5 Ma, consistent with the concordant point P3.

The fragmental zircons were either homogeneous or showed internal structures such as annealed fractures and recrystallized patches, as well as fine-scale igneous zoning at high angles (Fig. 3.3k-n). The most concordant data with the smallest error is fraction F2 with a $^{207}\text{Pb}/^{206}\text{Pb}$ age of 1356 Ma. A regression line for recent lead-loss using fractions F2 – F5 gives an age of 1355.1 Ma, with 49% probability of fit and lower intercept = 0 Ma. F1 was the most discordant point and did not fit on the recent lead loss line suggesting that one or both of the two grains in this fraction may have been affected by more complicated lead loss. The weighted average of the $^{207}\text{Pb}/^{206}\text{Pb}$ age for fractions F2 – F5, inclusive, gives a crystallization age of the 1355 ± 1.3 Ma.

Baddeleyite grains are chocolate brown, and either subhedral and stubby (Pl. 3.30) or angular with sugary zircon overgrowths. The latter morphology was not used for dating.

Baddeleyite was not observed in thin section. The multi-grain fractions B2 and B3 are concordant

and slightly overlap each other. B1 is above concordia and this is interpreted as incomplete dissolution in HF and HNO₃ during preparation. The B2 (1358 Ma) and B3 (1362 Ma) analyses were relatively imprecise, providing only minor constraints on the crystallization age.

Although zircon grains were not observed in thin section, the zircon fragments show similar characteristics to the fragments found in sample 1, such as colour, general size and internal structures and therefore are considered to be an interstitial phase. The baddeleyite ages, 1358 and 1362 Ma, are also generally consistent with the zircon fragments ²⁰⁷Pb/²⁰⁶Pb age. Therefore the ²⁰⁷Pb/²⁰⁶Pb age of the zircon fragments is interpreted to represent the crystallization age of the rock at 1355 ± 1 Ma. The 1344 ± 4 Ma prismatic zircons are unlike from those of the PGA. The Fraser Canyon Anorthosite prisms are pristine, colourless, and some contain fluid inclusions. The fluid inclusions in the largest prismatic zircons suggest that they could have formed within a pegmatitic (anorthositic?) vein. However, such veins were not observed in this sample either during collection or the crushing process. These prismatic zircons are interpreted as a later phase of igneous crystallization, most likely unrelated to the crystallization of the Fraser Canyon Anorthosite.

Sample 3, cross-cutting norite dyke: This sample was taken from the centre of the weakly foliated, cross-cutting norite dyke, away from the intruded gneissic norite outer zone of the PGA. Pale yellow, clear, angular zircon fragments were recovered (Pl. 3.31). CL images of the fragmental zircon show that some grains appear homogeneous, while others show igneous zoning, fracturing and annealing textures and partial diffusion or recrystallization (Fig. 3.3o-p). No evidence of inheritance was observed under the microscope or in BSE and CL imaging. All three multi-grain fractions (F1, F2 and F4) are either sub-concordant or just below concordia. The weighted average of the ²⁰⁷Pb/²⁰⁶Pb ages gives a crystallization age of 1341 ± 1.8 Ma.

Sample 4, intrusive norite body: The medium-grained, undeformed norite intrusive was sampled near the interior of the body away from the anorthosite xenolith-bearing margin. Yellow-

brown, clear, angular zircon fragments were recovered (Pl. 3.32). CL images show no evidence of inheritance and have the same complex internal characteristics as described in sample 3 (Fig. 3.3q-r). Multi-grain fraction F3 is concordant at 1346 ± 11 Ma, and multi-grain fractions F1, F2 and F4 are sub-concordant to discordant. All fractions lie on a recent lead-loss regression line with an upper intercept of 1341.3 Ma (58% probability of fit, lower intercept = -20 Ma). The weighted average of fractions F1, F2 and F4 $^{207}\text{Pb}/^{206}\text{Pb}$ ages provides a crystallization age of 1342 ± 1.2 Ma. Due to the larger 2-sigma error of F3 compared to the other fractions, it was not used in the weighted average of the $^{207}\text{Pb}/^{206}\text{Pb}$ ages.

3.5.3.2 Tessiarsuyungoakh intrusion

Sample 5, olivine monzodiorite: The fine-grained olivine monzodiorite was taken 20 m from the contact with the PGA. The sample contained abundant, large (200 – 400 μm), pale yellow, slightly resorbed, prismatic zircon (Pl. 3.33). In thin section, zircons were observed at grain boundaries (Pl. 3.34). Many zircon grains contain oxide and sulphide inclusions and these were avoided during selection for analyses. Zircons appear fracture-free when viewed under the microscope but both BSE and CL imaging revealed internal fractures parallel to the c-axis. 17 zircons were imaged using BSE and CL techniques. Two zircons contained inherited zircon and were not used for analyses. CL imaging was more successful than BSE imaging in revealing internal structures, however some grains appeared homogeneous while the other zircons only show minor igneous zonation with an enriched heavy element (darker) core (Fig. 3.3s).

All four multi-grain fractions lie on concordia and overlap each other. The weighted average of the $^{207}\text{Pb}/^{206}\text{Pb}$ ages provide a well-constrained crystallization age of 1360 ± 4 Ma.

Sample 6, orthopyroxene-bearing monzonite: The coarse-grained orthopyroxene-bearing monzonite was taken about 40 m from the contact with the PGA and about 30 m from sample 5. The sample yielded large (200 – 300 μm) pale yellow-brown, slightly resorbed prismatic zircon (Pl. 3.35). Large zircon tips were also recovered and used for dating. In thin section, zircons were

observed at grain boundaries (Pl. 3.36). As with sample 5, many zircon grains have oxide and sulphide inclusions and were avoided during selection. Zircons appear fracture-free when viewed under the microscope but both BSE and CL imaging revealed internal fractures parallel to the c-axis. CL imaging also shows an enriched heavy element (darker) core and igneous zoning with minor diffusion at grain rims (Fig. 3.3t).

Three multi-grain fractions, P1, P2 and P3, and one single grain fraction, T2, overlap concordia and each other. The weighted average of the $^{207}\text{Pb}/^{206}\text{Pb}$ age for the four fractions is 1363 ± 3 Ma. The multi-grain fraction T1 has a $^{207}\text{Pb}/^{206}\text{Pb}$ age of 1447 Ma and is assumed to contain inherited zircon. Therefore, the minimum age of crystallization of the orthopyroxene-bearing monzonite is well constrained at 1363 ± 3 Ma.

3.5.4 Overview of U-Pb Geochronology Ages

Based on the ages obtained from the six samples (Table 3.2), there appear to be 4 temporally distinct events. 1) The earliest event is the growth of prismatic zircons in the PGA sample 1 at 1370 ± 5 Ma. In thin section prismatic zircons were observed as inclusions in plagioclase crystals indicating that plagioclase phenocrysts, growing in a liquid, included the already present slightly resorbed prismatic zircons. The fact that the prismatic zircon fractions are reproducibly concordant and that the zircons all exhibit the same morphological and internal characteristics with only minimal resorption further suggests that these zircons formed in the anorthosite producing magma. There is also no known rock in this area with an age of ca. 1370 Ma to provide the zircon. Therefore, this is interpreted to represent the first zircon crystallization from the PGA magmatic system, possibly during the production of a crystal mush at depth before emplacement of the anorthosite. 2) At ca. 1360 Ma, the intrusion and crystallization of the T1 composite body occurred. The $^{207}\text{Pb}/^{206}\text{Pb}$ crystallization age of the monzonite and monzodiorite at 1363 ± 3 and 1360 ± 4 Ma, respectively, overlap within error and the irregular to cusped contacts mentioned earlier indicates that at least some monzodiorite intruded the monzonite before it had completely solidified. 3) At ca. 1355 Ma anorthosite began to intrude into the area

represented by the Fraser Canyon Anorthosite. Although it is impossible to say conclusively that this anorthosite intrusion is part of the PGA it does suggest that multiple intrusions were occurring locally considering the Fraser Canyon Anorthosite is older than the final crystallization age of the PGA. 4) At ca. 1340, the PGA had completely crystallized, norite intruded the PGA and deformation had terminated in the area. The interstitial, fragmental zircon recovered from the PGA sample provides a final crystallization age of 1335 ± 3 Ma, which places it within error of the crystallization age of the norite. The fact that the fragmental zircons appear slightly resorbed in thin section and some grains are fractured and annealed suggests that there was minor lead loss. Therefore it is probable, considering the intrusive nature of the norite into the PGA that the final crystallization of the PGA occurred at the age defined by the concordant analysis F1 at 1343 ± 3 Ma.

As mentioned, zircon grains from the anorthosite and norite units showed resorption, internal recrystallization and/or annealed fractures. These grains were: prisms, fragments and cusped grains from the PGA; fragments from both the norite dyke and norite intrusive body; and fragments from the Fraser Canyon Anorthosite. There is no evidence of contemporaneous or younger intrusions in close proximity to these units. The closest intrusion is the ca. 1322 Ma Makhavinekh Lake pluton, which is more than 5 km away. Therefore, it is unlikely that disturbance of these grains was due to local metamorphic processes. Rather, it is suggested that disturbance of these zircons may have been caused by changing magma composition (resorption), syn-emplacment deformation (fracturing, annealing and recrystallization) and re-heating caused by intermittent magmatic pulses (recrystallization).

Table 3.2: Summary of zircon crystallization ages

Sample Unit	Zircon Morphology	Age in Ma (2 σ error)	Interpretation
1: PGA	Angular fragments	1335 +7/-3	- Final crystallization of PGA
3: Norite dyke	Angular fragments	1341 \pm 2	- Crystallization of unit - Minimum age of deformation
4: Intrusive Norite body	Angular fragments	1342 \pm 1	- Crystallization of unit - PGA must have been solid
2: Fraser Canyon Anorthosite	Prismatic	1344 \pm 4	- Pegmatitic patch (?)
2: Fraser Canyon Anorthosite	Angular fragments	1355 \pm 1	- Crystallization of unit
5: TI (Monzodiorite)	Prismatic	1360 \pm 4	- Crystallization of unit
6: TI (Monzonite)	Prismatic	1363 \pm 3	- Crystallization of unit
1: PGA	Prismatic	1370 \pm 5	- Formation of plagioclase crystal mush at depth

3.6 DISCUSSION

The field relationships and geochronology in this study confirm that the monzonite and monzodiorite components of the TI are contemporaneous and were emplaced before the anorthosite bodies. At least some of the monzodiorite intruded the monzonite before the monzonite had completely crystallized forming cusped contacts. Geochemical and isotopic studies on other AMCG suites by Bolle et al. (2003) (Rogaland, Norway) and Scoates and Chamberlain (2003) (Laramie, USA) have suggested that monzonitic rocks could have been derived by fractional crystallization from jotunite or ferrodiorite (both referred to here as monzodiorite). The fact that the TI units are temporally related would support the notion that they are also genetically linked. K-feldspar phenocrysts typically found in the monzonite imply partial crystallization prior to emplacement and therefore at least some fractional crystallization from monzodiorite could have occurred prior to emplacement. There are gradational contacts between the monzonite and monzodiorite that could reflect in situ fractionation. Likewise, the monzodiorite dykes that intruded the monzonite could also reflect fractionation within a deeper magma chamber. However, there could be other interpretations of these observations of field relationships. These hypotheses need to be tested by further research, especially geochemical and isotopic studies.

The timing of emplacement of the PGA is not as straightforward as the TI. The Hare Hill monzonite, which is located at the eastern margin of the PGA, has been studied by Wheeler (1960), Ryan (1993), T.A. Tettelaar and J.S. Myers (unpublished mapping, 2000) and Ryan and James (2003). The mineralogy, textures and foliation parallel to the contact with the PGA are similar to the TI except for the presence of garnet in the Hare Hill monzonite (Ryan, 1993). Ryan and James (2003) questioned the possibility that the eastern and western monzonites rimming the PGA were part of one continuous intrusion. However, they have continued to refer to each intrusion by their individual names pending further evidence to suggest that they are not separate bodies. The Hare Hill monzonite was dated using U-Pb TIMS method on zircon, which gave a crystallization age of 1351 ± 3 Ma (Connelly, 1993). This age is younger than the TI ages of 1363 ± 3 and 1360 ± 4 Ma determined in this study. The PGA obscured any contact that may have existed between these two composite monzonite/monzodiorite bodies. However, based on the different ages of the TI and Hare Hill monzonite these bodies are interpreted to represent separate sheets rather than one large body. An anorthosite dyke with sharp contacts was observed cutting the Hare Hill monzonite in close proximity to the contact with the PGA (Tettelaar and Myers, field observations, 2000). This may indicate that the PGA intruded the Hare Hill monzonite after 1351 ± 3 Ma. The oldest anorthosite is the Fraser Canyon Anorthosite at 1355 ± 1 Ma and this age overlaps within error of the Hare Hill monzonite age of 1351 ± 3 Ma. Although it is uncertain whether this anorthosite body is part of the PGA, it does indicate that anorthosite began intruding into this region ca. 1355 Ma and that intermittent magma pulses continued to intrude until final crystallization of the PGA at ca. 1343 Ma.

The domal shape of the PGA and exposed anorthosite bodies as well as the deformed outer zone could be used to advocate a diapiric emplacement mechanism. However, closer examination of field evidence argues against diapirism. If the PGA were intruded in this manner the surrounding host rock would be vertically displaced and deformed. In the study area the TI is deformed parallel to the contact with the PGA. However, the east and west contacts of the TI are broadly parallel and the TI intruded as sheets parallel to the local gneissosity of the Tasiuyak

paragneiss. The contact between the TI and the Tasiuyak paragneiss is relatively undeformed and there is no distortion or overprinting of the paragneiss fabric. The same relationship exists at the eastern margin of the PGA. Here the contact between the PGA and the Hare Hill monzonite is parallel to the foliation of the country rock. The foliation in screens of Tasiuyak paragneiss is parallel to the foliation in the surrounding TI and there is no evidence that these screens have been rotated.

The combined evidence seems to indicate that emplacement of both the monzonitic and anorthositic intrusions was controlled by older structures. Northwest-southeast trends are common to all contacts, igneous and gneissic foliations in all rock units, as well as faults and dykes. This is further corroborated by the deflection of the fabric from the typical northwest-southeast direction to east-west direction in the central region of the TI, which appears to mimic the east-west deflection of the gneissosity in the Tasiuyak paragneiss. Weakly oriented orthopyroxene in the foliation of the outer zone of the PGA also suggests shearing. Therefore, the evidence seems to indicate emplacement along weakness in the structures in the Tasiuyak paragneiss, possibly in a transpressional regime, which were intermittently reactivated and provided conduits for magmatic ascent. The anorthosite dykes that cut the TI and Hare Hill monzonite indicate small-scale fracturing and intrusion further implying conduit emplacement. If the plagioclase-rich magma intruded as sheets like the TI, these conduits would have formed parallel to the foliation in the country rock. Fracturing of the country rock would likely have been accompanied by stoping, providing space for intrusion of the plagioclase-rich magma. It is therefore suggested that the domal shape of the exposed anorthosite bodies and PGA could be attributed to a sill-like body rather than a balloon-shaped diapir.

The intermittent reactivation of structures affected the TI and the PGA differently. The TI magmas, transported by conduits, intruded as sheets along weak structures in the Tasiuyak paragneiss, which was most likely triggered by a deformation event. However, the central and western portion of the TI is relatively undeformed suggesting that during crystallization, deformation had ceased. It is possible that a second reactivation opened up the earlier formed

conduits to transport the crystal mush that formed the PGA. Igneous layers of anorthosite and norite formed along the chamber walls and were then subject to deformation. The question then is whether this deformation was related to reactivation of structures or emplacement mechanisms? Considering that the inner zone of the PGA is relatively undeformed, the latter choice, possibly related to stoping, is more likely the cause of deformation along the margins. It is also uncertain whether the deformation occurred during sub-liquidus and/or sub-solidus state. However, considering the final crystallization age of the PGA is temporally consistent with the age of the norite dyke that cross-cuts the gneissic PGA outer zone and igneous layering is present along the margins, syn-emplacement deformation most likely occurred while the margins were sub-solidus. Later reactivation caused faulting and emplacement of granitic and gabbroic dykes.

The 1370 Ma prismatic zircons included in plagioclase phenocrysts probably date crystallization stages at depth prior to the PGA emplacement. Although geochemical studies were not performed in this study, field evidence suggests that the PGA magma incorporated plagioclase crystals suspended in a noritic liquid. This could explain the origin of the noritic and anorthositic layers in the outer zone as products of relatively rapid cooling at the plagioclase-orthopyroxene cotectic. The insulated inner zone remained hot, and continued to crystallize only plagioclase, and possibly filter pressing most of the residual liquid towards the chamber margins. This is speculative since the roof of the PGA is not observed and is interpreted to have been above the current level of exposure. However, the roof and walls of the Fraser Canyon Anorthosite are noritic and undeformed, whereas the inner zone is massive anorthosite. The relatively undeformed norite bodies that intruded the PGA could represent the final pulse of the PGA.

3.7 MODEL FOR EMPLACEMENT OF THE TI AND PGA

The proposed model for emplacement of the TI and PGA is shown in Figure 3.5. Prior to 1363 Ma, reactivation of older structures in the country rock provided conduit systems into which monzonitic and monzodioritic magma ascended. These magmas intruded as sheets parallel to

the gneissosity of the Tasiuyak paragneiss, possibly forming separate, large sills at different times (Fig. 3.5A). During crystallization of the monzonite and monzodiorite there may have been a second intrusion of monzodioritic magma. All the components of the TI had completely crystallized by 1360 Ma, prior to emplacement of anorthosite.

At ca. 1355 Ma, noritic magma with plagioclase phenocrysts ascended through the re-activated conduit system (Fig. 3.5B). This magma intermittently intruded as sheets into and between the margins of the surrounding TI and Hare Hill monzonite. The culmination of these anorthositic intrusive sheets and stoping of country rock formed elongate, sill-like bodies. Compositional layering and rapid crystallization formed a 'chilled margin' represented by the outer zone of the anorthosite bodies. The crystallized outer zone of the PGA and the adjacent TI rocks were subjected to strain during syn-emplacement deformation. It appears that deformation was localized along the margins of the PGA and did not affect the Fraser Canyon Anorthosite. The inner zone of the anorthosite bodies cooled relatively slowly, which allowed for continued plagioclase crystal growth and possibly removal of residual liquid from the inner chamber.

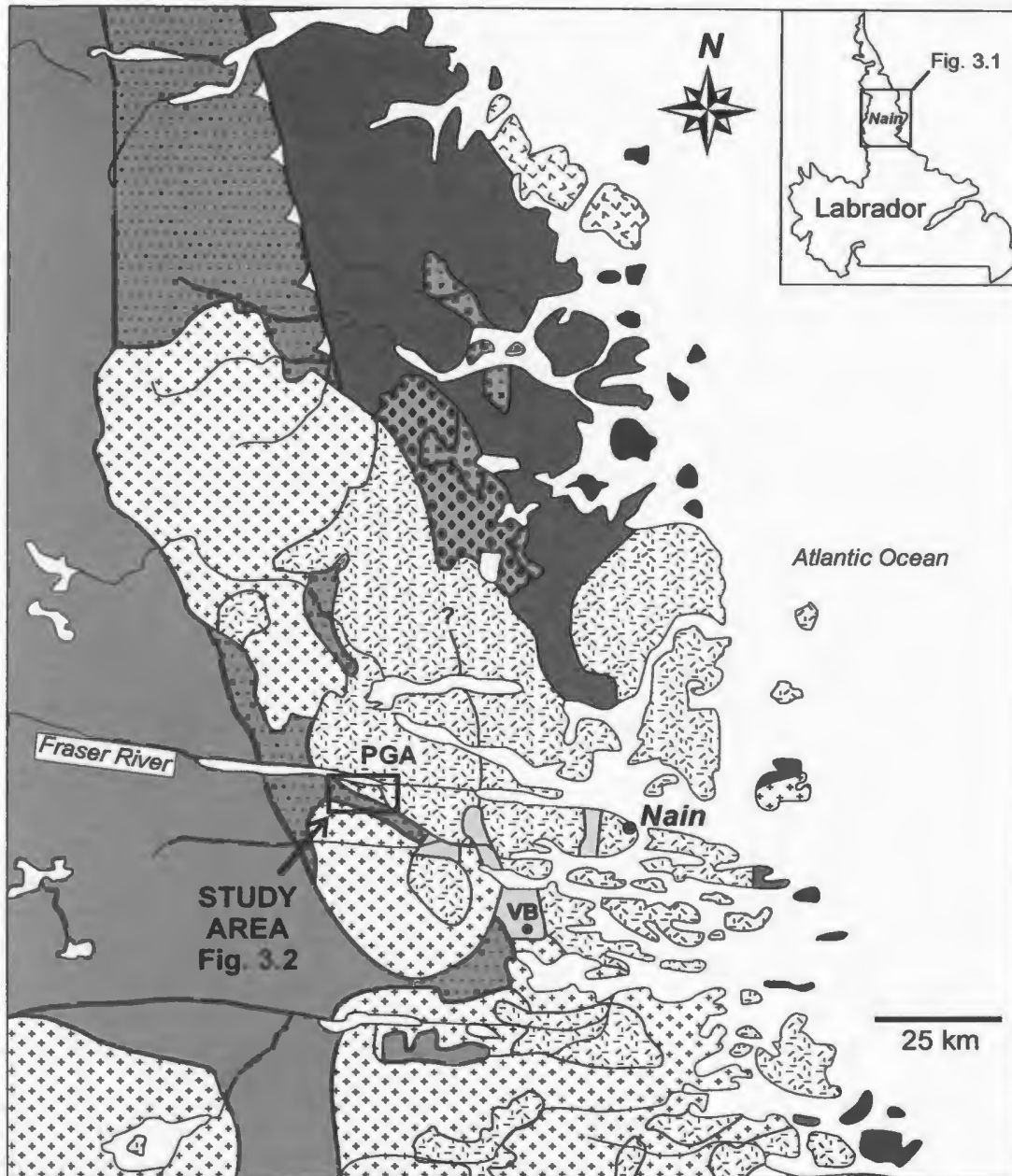
At ca. 1340 Ma, the PGA had completely crystallized (Fig. 3.5C), noritic magma intruded along cooling fractures in the PGA forming the norite body and dykes and deformation had terminated in the area.

3.8 SUMMARY OF CONCLUSIONS

This study has produced the oldest known emplacement ages for rocks of the NPS, which are the monzonite, at 1363 ± 3 Ma, and monzodiorite, at 1360 ± 4 Ma of the TI. It has also produced the oldest known zircon crystallization ages of the NPS of 1370 ± 5 Ma from prismatic zircons included in plagioclase phenocrysts in the PGA. These ages suggest that the magmas of the TI and the spatially related anorthosite bodies are broadly contemporaneous. The geochronological evidence suggests that anorthosite genesis of the PGA has had a long-lived magmatic history of about 30 million years. The 1370 ± 5 Ma prismatic zircons included in plagioclase phenocrysts from the PGA were most likely formed at depth, prior to emplacement at

mid-crustal levels. The oldest intrusive age of anorthosite in the NPS is the Fraser Canyon Anorthosite at 1355 ± 1.3 Ma. It is unknown whether this anorthosite is a part of the PGA. However, it indicates that anorthosite intrusion in the study area began around this time and ended with the crystallization of the PGA at ca. 1340 Ma.

Prior to 1363 Ma reactivation of older structures in the country rock provided conduit systems, along which monzonitic and monzodioritic magma ascended and were emplaced as sheets into the Tasiuyak paragneiss. At ca. 1360 Ma, the TI had completely crystallized. At ca. 1355 Ma, intermittent intrusion of noritic magma with plagioclase phenocrysts was emplaced by reactivating conduits and stoping and formed the sill-like bodies of the Fraser Canyon Anorthosite and PGA. The outer zone of the anorthosite bodies is interpreted to represent a chilled margin, where compositional layers of anorthosite and norite cooled quickly. The inner zone of massive anorthosite is interpreted to represent relatively slow cooling where plagioclase crystals continued to grow and possibly filtered out the noritic magma towards the margins of the chamber. Shearing of the crystallized margins of the PGA and the adjacent TI was caused by syn-emplacment deformation but had little effect on the hot, partially crystallized inner zone. By ca. 1340 Ma the PGA had completely crystallized, noritic magma intruded the PGA and deformation in the area had terminated.



MESOPROTEROZOIC
Nain Plutonic Suite

- anorthositic plutons
- granitic to dioritic plutons

PALEOPROTEROZOIC
Armanuat Plutonic Suite

- anorthositic plutons
- granitic plutons

PALEOPROTEROZOIC
Southeastern Churchill Province

- Tasiuyak paragneiss
- reworked Archean orthogneiss
- undivided, Archean and Paleoproterozoic ortho- and paragneiss

ARCHEAN

- Mugford Group volcanics
- Nain Province**
- tonalitic orthogneiss and minor paragneiss
- VB** Voisey's Bay Ni-Cu-Co deposit
- PGA** Pearly Gates Anorthosite
- Torngat orogen thrust zone

Figure 3.1: Geological map of the Nain region, Labrador (modified from Ryan & James, 2003). The eastern margin of the Pearly Gates Anorthosite pluton is based on 1:50 000-scale reconnaissance mapping by Ryan & James (2003).



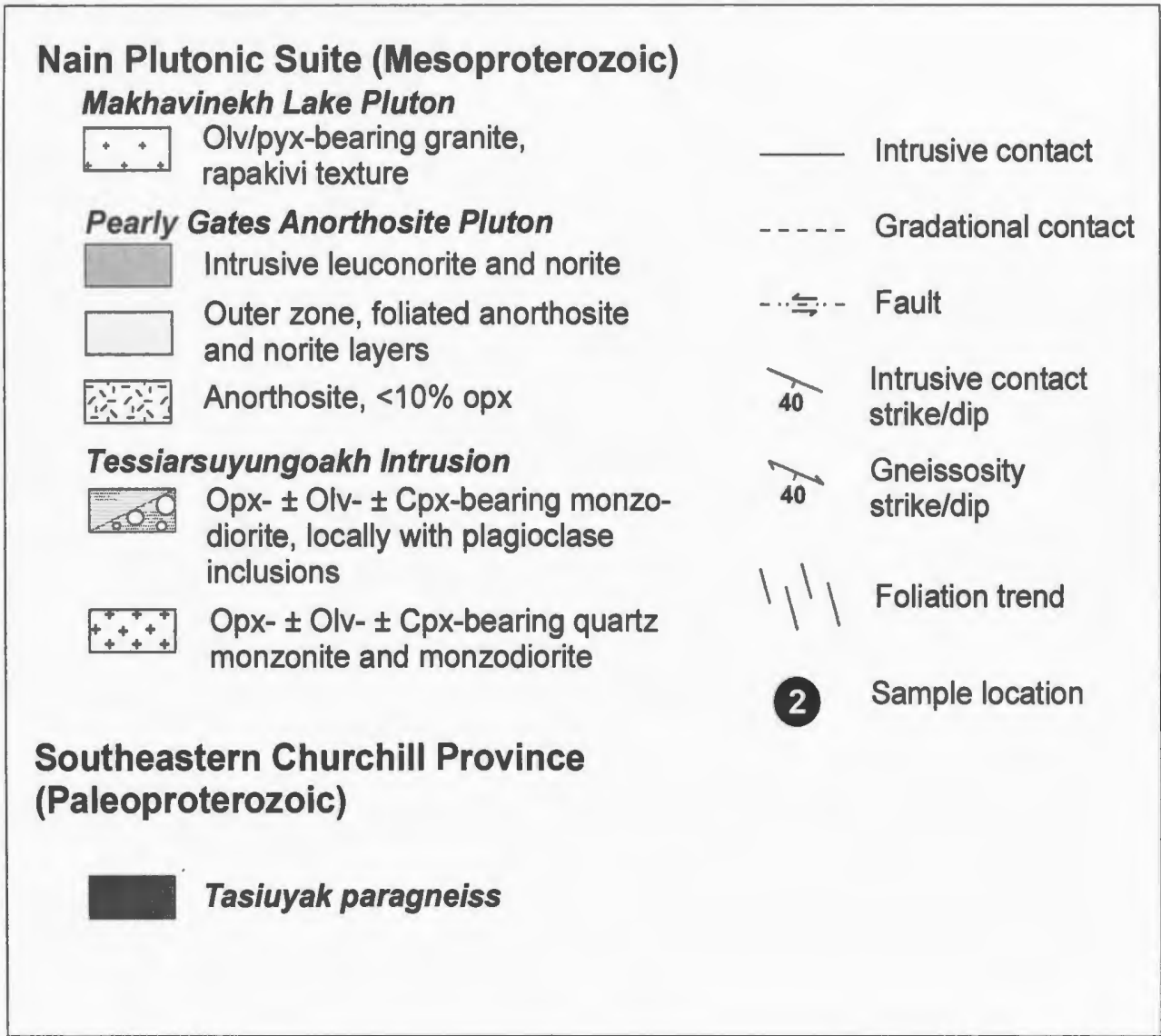


Figure 3.2: Geological map of the study area.

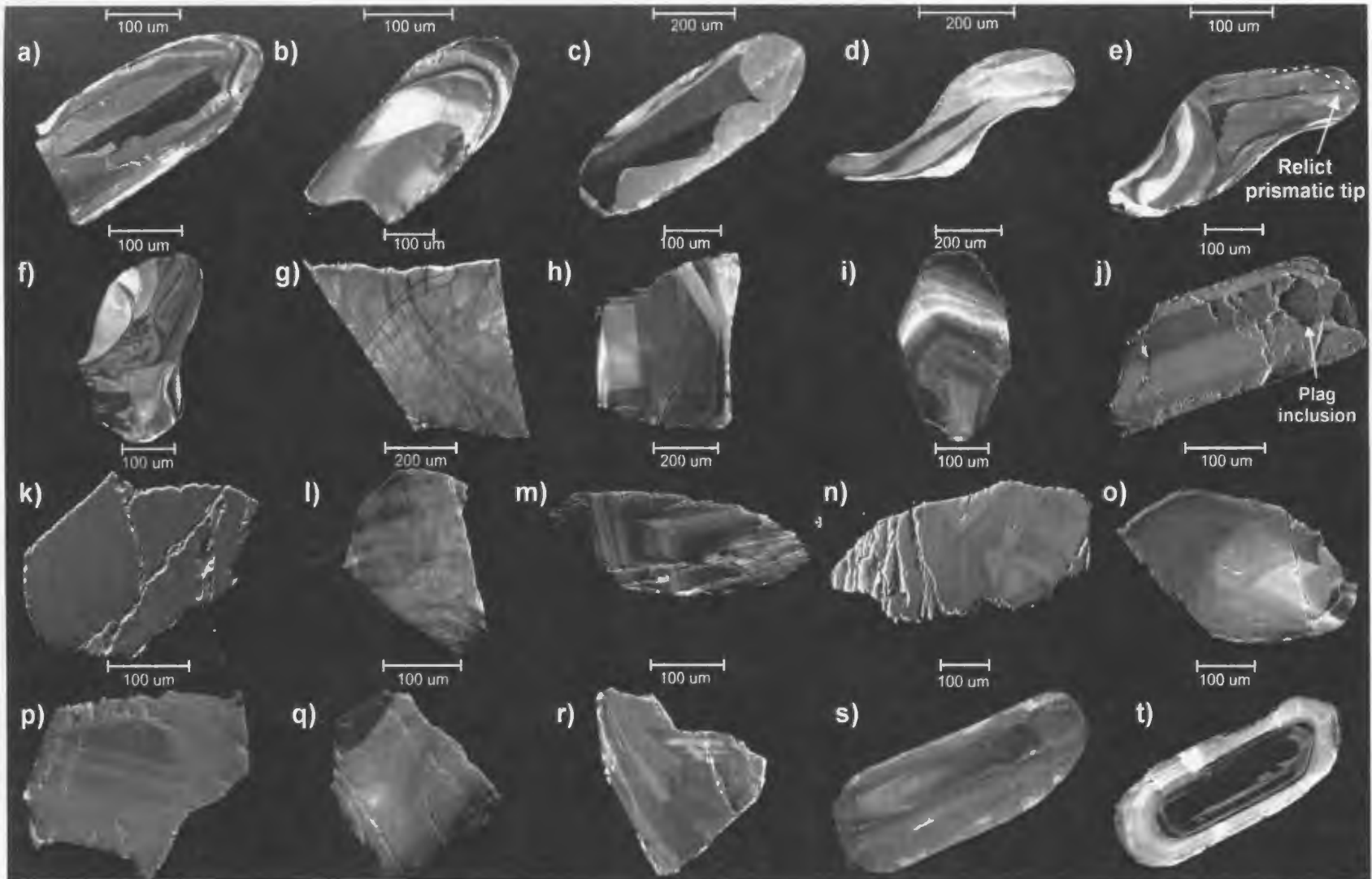


Figure 3.3: Cathodoluminescence images of zircons. Sample 1 zircons from a) to h). a)-c) are prisms with relict igneous growth zones but are partially recrystallized and/or internal diffusion has occurred. d)-f) are cusped, showing zones that cross-cut and are not parallel to or reflect grain boundaries. Fragment g) indicates diffusion and annealing while h) shows primary igneous zoning. Sample 2 zircons from i) to n). Both i) and j) show relatively undisturbed growth zoning and j) contains a plagioclase inclusion. Fragments range from k) appearing homogenous; l) diffusion and annealing textures; m) igneous growth zoning; to n) recrystallization textures. Samples 3(o, p), 4(q, r), 5(s) and 6(t) consist of igneous zoning and partial recrystallization.

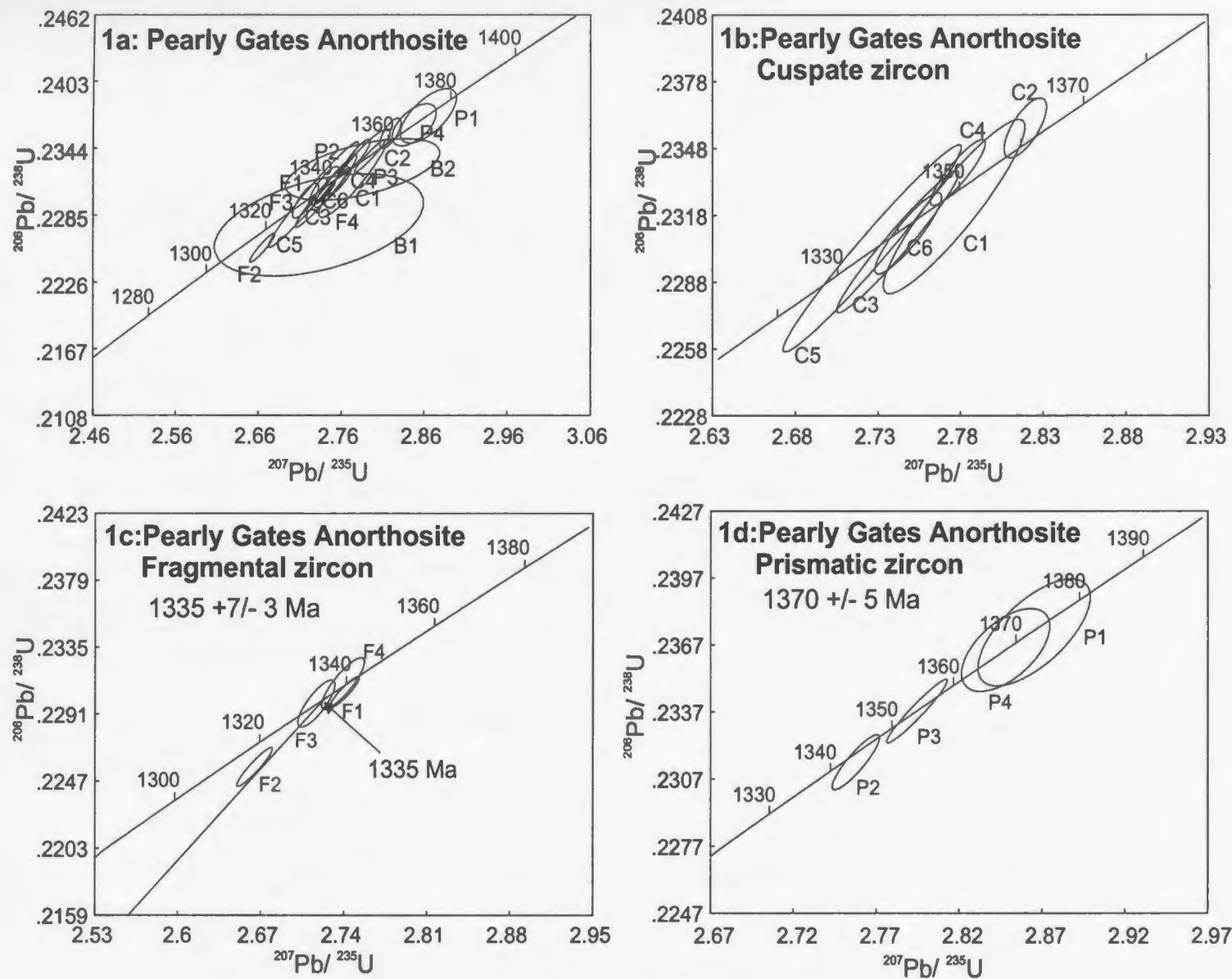
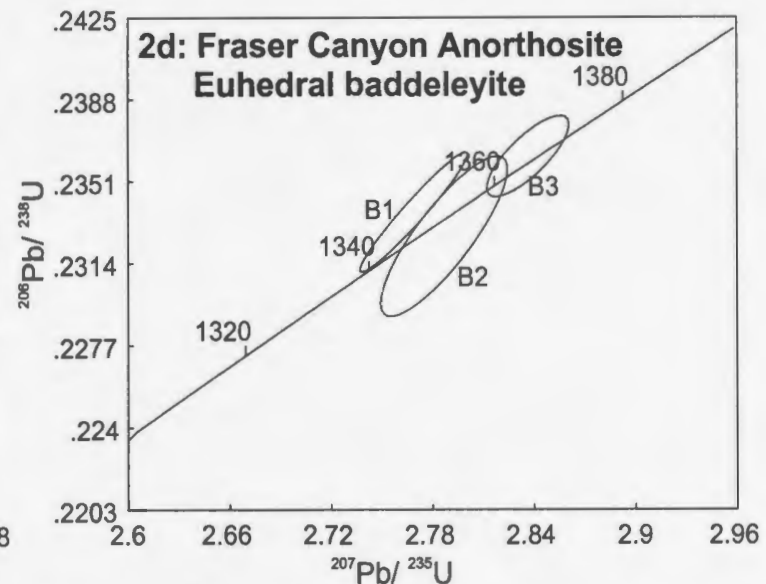
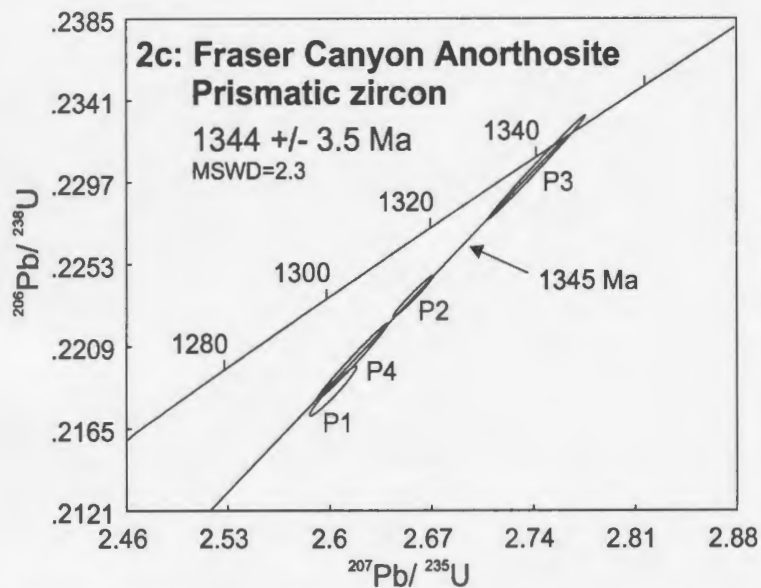
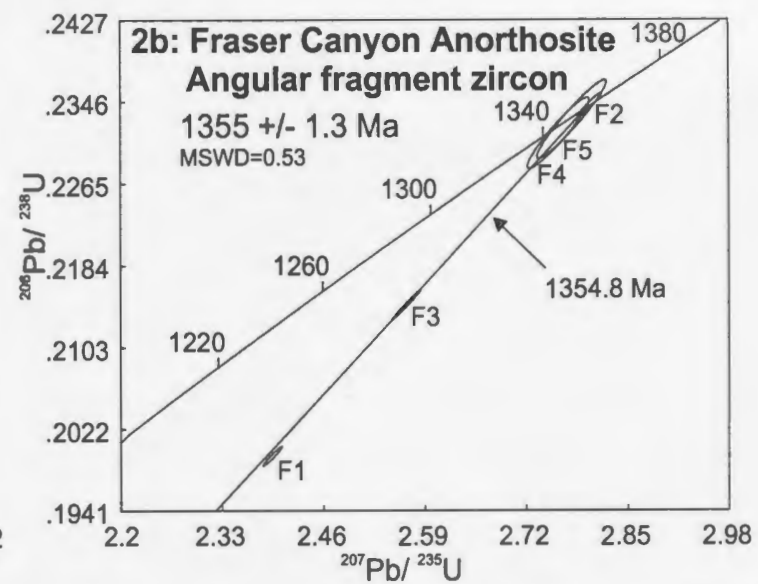
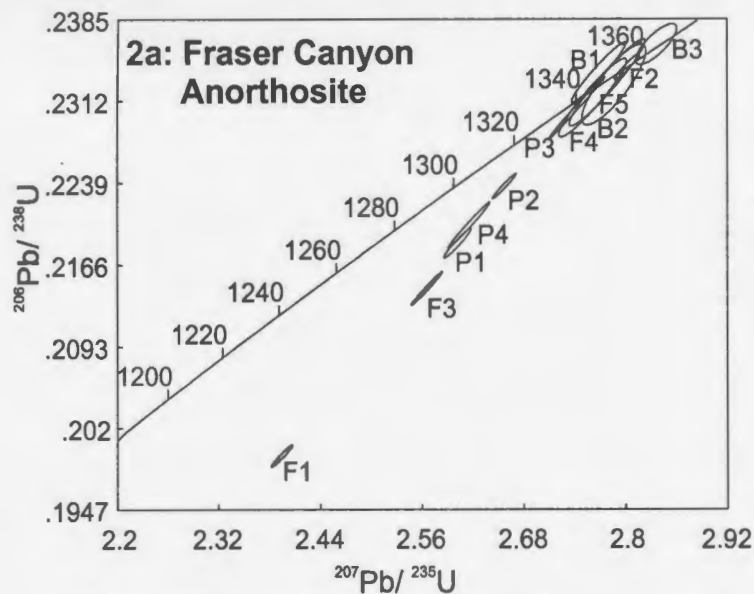
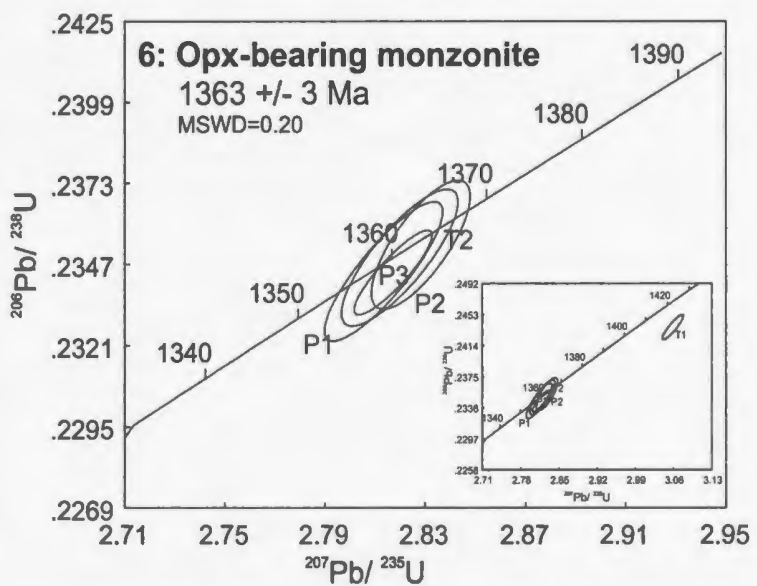
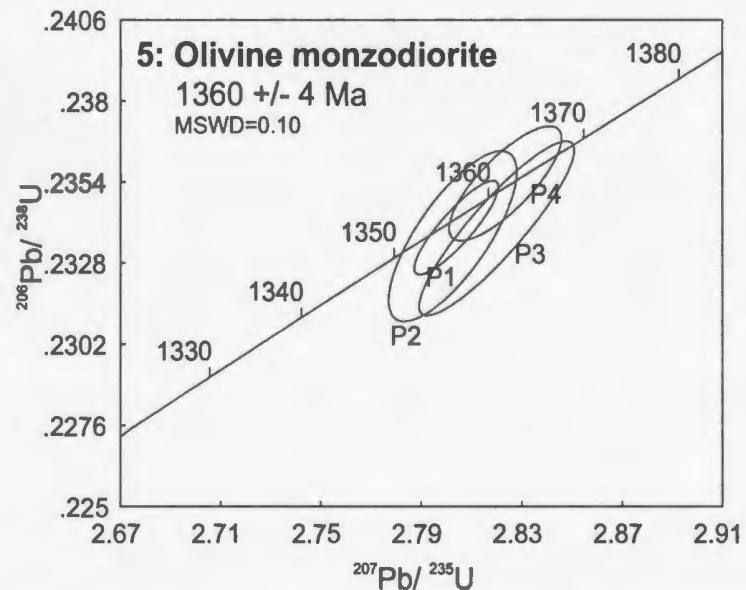
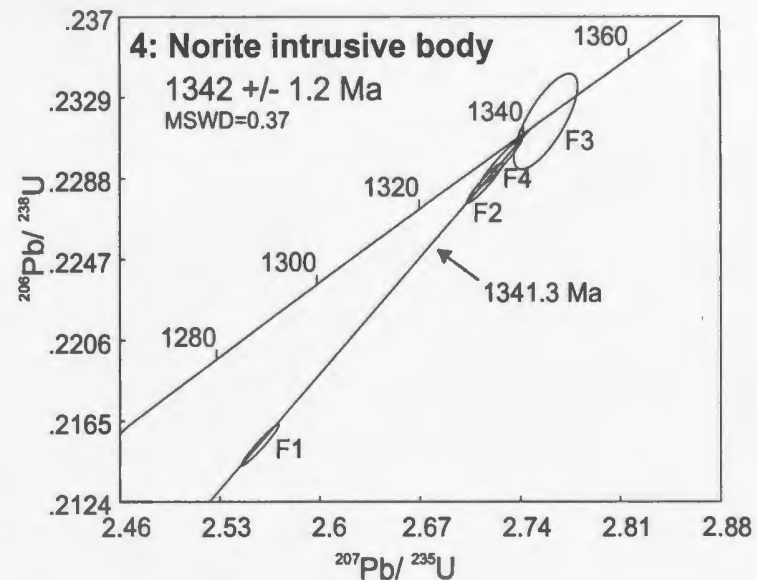
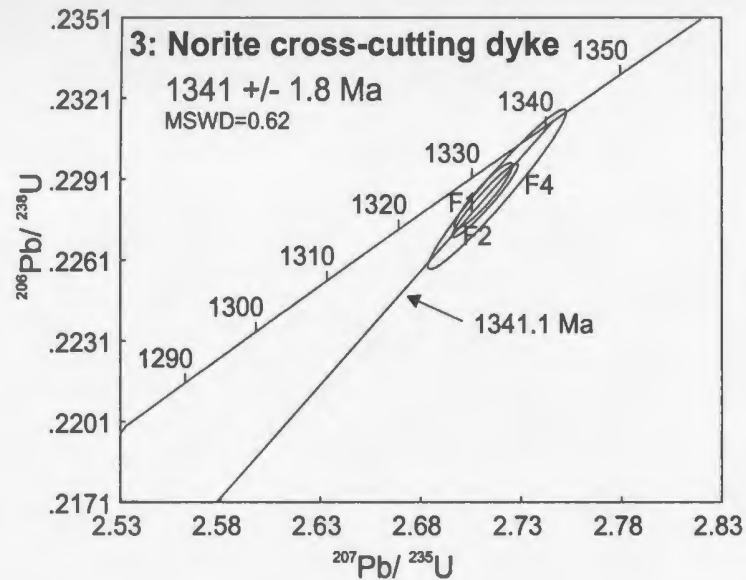


Figure 3.4: Concordia diagrams of samples 1-6. Sample 1, the Pearly Gates Anorthosite, where 1a) and shows data from all analyses, 1b) represents the data for cusate zircons, 1c) fragmental zircon data, and 1d) prismatic zircon data.



Sample 2, the Fraser Canyon Anorthosite, where 2a) represents data for all zircon and baddeleyite analyses, 2b) angular fragment zircon data, 2c) prismatic zircon data, and 2d) baddeleyite data.



Samples 3 (norite dyke) and 4 (norite intrusive body) represent data from zircon fragments. Samples 5 (olivine monzodiorite) and 6 (opx-bearing monzonite) represent data from prismatic zircon.

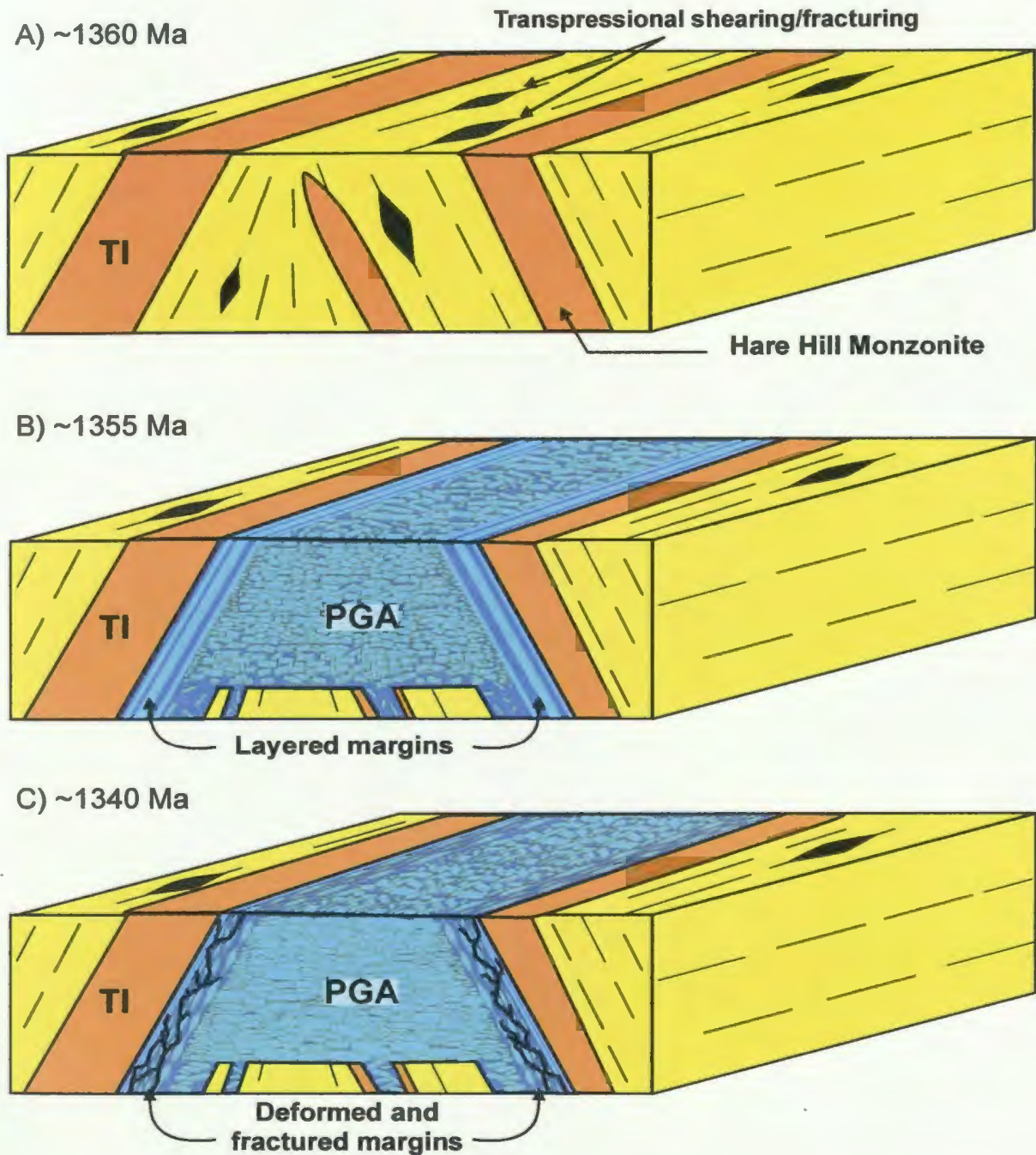


Figure 3.5: Schematic drawing showing the proposed model of emplacement for the Pearly Gates Anorthosite pluton and the Tessiersuyungoakh intrusion. A) At ca. 1360 Ma, monzonitic and monzodioritic magmas ascended through conduits and were emplaced along pre-existing structural weaknesses in the Tasiuyak paragneiss. B) At ca. 1355 Ma, plagioclase crystals and noritic magma were intruded by reactivation of the conduit system and stoping of country rock to form a magma chamber. Rapid crystallization of the outer zone formed a 'chilled margin' that was subsequently deformed. The inner zone cooled slowly and plagioclase crystals continued to grow, possibly squeezing out the noritic magma. C) At ca. 1340 Ma, deformation ended, the Pearly Gates Anorthosite pluton completely crystallized and was intruded by norite along fractures.

Table 3.1: U-Pb geochronology analytical data.

Fraction	Weight [mg]	Concentration		Measured		Corrected Atomic Ratios *						Age [Ma]				
		U [ppm]	Pb rad [ppm]	Total common Pb [pg]	²⁰⁶ Pb/ ²⁰⁴ Pb	²⁰⁸ Pb/ ²⁰⁶ Pb	²⁰⁶ Pb/ ²³⁸ U	+/-	²⁰⁷ Pb/ ²³⁵ U	+/-	²⁰⁷ Pb/ ²⁰⁶ Pb	+/-	²⁰⁶ Pb/ ²³⁸ U	²⁰⁷ Pb/ ²³⁵ U	²⁰⁷ Pb/ ²⁰⁶ Pb	
Sample 1: Pearly Gates Anorthosite (N 56° 32.990', W 062°29.000')^c																
F1	6 lrg clr ang	0.090	23.5	6.2	5.5	5605	0.2445	0.23054	82	2.741	10	0.08622	12	1337	1340	1343
F2	5 clr ang	0.094	62.8	17.0	4.6	18321	0.3077	0.22563	104	2.665	12	0.08566	14	1312	1319	1331
F3	6 clr ang	0.295	9.2	2.4	2.4	16149	0.2087	0.22979	126	2.717	13	0.08575	28	1333	1333	1333
F4	7 clr ang	0.090	14.5	3.8	3.0	6262	0.2136	0.23111	138	2.739	15	0.08597	28	1340	1339	1337
C1	1 str rsb	0.020	38.8	9.9	2.7	4177	0.1865	0.23220	320	2.776	35	0.08671	48	1346	1349	1354
C2	1 str rsb	0.020	188.0	50.0	4.6	11997	0.2230	0.23572	110	2.819	11	0.08675	28	1364	1361	1355
C3	1 str rsb	0.020	52.3	13.4	2.7	5580	0.2003	0.23062	260	2.742	30	0.08623	24	1338	1340	1343
C4	1 str rsb	0.020	57.9	14.6	2.2	7585	0.1699	0.23373	120	2.778	14	0.08622	20	1354	1350	1343
C5	1 str rsb	0.020	87.2	24.8	4.0	6238	0.3484	0.23032	380	2.727	44	0.08586	30	1336	1336	1335
C6	1 str rsb	0.020	41.4	10.7	2.0	6163	0.2152	0.23100	148	2.748	17	0.08628	24	1340	1342	1345
P1	5 lrg clr	0.055	2.5	0.7	7.1	303	0.2013	0.23726	196	2.865	28	0.08759	66	1372	1373	1373
P2	14 fract clr	0.343	4.0	1.1	2.3	8656	0.2641	0.23145	100	2.758	12	0.08641	18	1342	1344	1347
P3	9 clr	0.100	5.4	1.4	3.4	2355	0.2192	0.23373	116	2.795	15	0.08672	14	1354	1354	1354
P4	8 clr	0.100	5.0	1.3	22.8	338	0.2047	0.23647	152	2.848	22	0.08735	58	1368	1368	1368
B1	1 sm euh brn	0.003	41.3	8.9	4.1	467	0.0141	0.22764	368	2.733	103	0.08708	296	1322	1338	1362
B2	1 sm euh brn	0.002	54.3	12.2	30.0	70	0.0338	0.23253	222	2.786	76	0.08689	204	1348	1352	1358
Sample 2: Fraser Canyon Anorthosite (N 56° 37.402', W 062°38.434')																
P1	1 lrg clr fract	1.233	7.3	2.1	3.0	40697	0.4474	0.21852	108	2.602	13	0.08636	12	1274	1301	1346
P2	9 lrg clr cls	1.120	25.5	7.4	3.5	115013	0.4275	0.22359	92	2.658	11	0.08620	8	1301	1317	1343
P3	1 lrg clr fract	0.080	304.2	87.0	6.4	54747	0.3544	0.23051	228	2.743	27	0.08630	8	1337	1340	1345
P4	1 lrg clr fract	0.080	165.0	49.2	6.9	26466	0.4853	0.22010	170	2.616	20	0.08618	10	1282	1305	1342
F1	2 lrg clr ang brn	0.404	25.4	7.4	5.6	23119	0.6133	0.19953	80	2.394	10	0.08703	8	1173	1241	1361
F2	8 lrg clr ang brn	0.301	31.2	8.6	4.4	31083	0.2863	0.23421	96	2.802	12	0.08678	10	1357	1356	1356
F3	9 lrg clr ang	0.288	199.0	51.2	2.9	266294	0.3055	0.21451	122	2.566	15	0.08676	8	1253	1291	1355
F4	6 clr brn ang	0.175	42.4	11.7	5.7	18693	0.3056	0.23023	254	2.751	27	0.08667	44	1336	1342	1353
F5	7 clr brn ang	0.205	37.9	10.5	5.6	20124	0.2951	0.23281	318	2.779	37	0.08657	34	1349	1350	1351
B1	1 sm euh stub brn	0.017	19.5	4.3	1.8	2737	0.0050	0.23371	220	2.769	26	0.08593	22	1354	1347	1337
B2	3 sm euh stub brn	0.009	74.6	16.4	2.8	3679	0.0104	0.23261	294	2.787	31	0.08689	60	1348	1352	1358
B3	2 sm euh stub brn	0.004	117.3	26.3	44.7	172	0.0150	0.23622	150	2.837	20	0.08709	38	1367	1365	1362

Table 3.1: U-Pb geochronology analytical data (continued).

Fraction	Concentration			Measured		Corrected Atomic Ratios *						Age [Ma]			
	Weight [mg]	U [ppm]	Pb rad [ppm]	Total common Pb [pg]	²⁰⁶ Pb/ ²⁰⁴ Pb	²⁰⁸ Pb/ ²⁰⁶ Pb	²⁰⁶ Pb/ ²³⁸ U	+/-	²⁰⁷ Pb/ ²³⁵ U	+/-	²⁰⁷ Pb/ ²⁰⁶ Pb	+/-	²⁰⁶ Pb/ ²³⁸ U	²⁰⁷ Pb/ ²³⁵ U	²⁰⁷ Pb/ ²⁰⁶ Pb
Sample 3: Norite cross-cutting dyke (N 56°34.050', W 062°31.500')⁵															
F1 6 lrg ang	0.160	39.3	10.3	14.9	6033	0.2428	0.22848	100	2.711	12	0.08607	14	1327	1332	1340
F2 6 lrg ang	0.169	40.6	10.4	7.1	13841	0.2193	0.22831	112	2.712	13	0.08616	12	1326	1332	1342
F4 7 clr ang	0.185	43.2	11.4	5.3	21624	0.2516	0.22872	242	2.718	28	0.08619	24	1328	1333	1342
Sample 4: Norite intrusive body															
F1 5 clr ang	0.179	53.3	16.1	7.0	18321	0.5419	0.21530	86	2.558	11	0.08618	10	1257	1289	1342
F2 5 clr ang	0.197	48.4	14.6	3.1	43507	0.4495	0.22858	84	2.716	10	0.08616	10	1327	1333	1342
F3 4 clr ang	0.081	9.6	3.0	1.4	8095	0.4827	0.23168	198	2.758	18	0.08634	48	1343	1344	1346
F4 11 clr ang	0.320	33.0	10.3	5.1	30057	0.4850	0.22962	102	2.726	12	0.08612	10	1332	1336	1341
Sample 5: Olivine-bearing monzodiorite (N 56°34.060', W 062°31.500')⁵															
P1 5 clr euh 4:1	0.113	12.3	3.2	3.6	5775	0.1942	0.23393	124	2.804	14	0.08693	22	1355	1357	1359
P2 6 clr euh 4:1	0.057	10.4	2.8	2.1	4220	0.2279	0.23366	224	2.803	21	0.08699	54	1354	1356	1360
P3 5 clr euh 4:1	0.096	14.6	3.9	4.6	4496	0.2225	0.23391	228	2.820	25	0.08744	38	1355	1361	1370
P4 7 clr euh 4:1	0.134	4.8	1.3	8.8	1097	0.2411	0.23535	150	2.823	18	0.08701	36	1362	1362	1361
Sample 6: Orthopyroxene-bearing monzonite (N 56°34.065', W 062°31.505')⁵															
P1 11 clr	0.068	27.1	7.3	5.5	4953	0.2365	0.23443	110	2.817	13	0.08716	20	1358	1360	1364
T1 9 clr tip	0.069	34.1	9.3	22.2	1632	0.2102	0.24371	128	3.059	16	0.09103	20	1406	1422	1447
P2 30 fract clr	0.860	0.5	0.1	2.2	3010	0.2151	0.23491	180	2.820	19	0.08706	38	1360	1361	1362
T2 1 lrg clr tip	0.154	3.5	0.9	2.5	3241	0.2419	0.23532	168	2.828	16	0.08717	40	1362	1363	1364
P3 15 clr	0.160	11.4	3.1	2.9	9371	0.2507	0.23447	182	2.814	19	0.08703	34	1358	1359	1361

Notes: C, cusped zircon; F, zircon fragment; P, prismatic zircon; B, baddeleyite; T, prism tips; str, strongly; rsb, resorbed; clr, clear; ang, angular; tip, prismatic tip; fract, fractured; brn, brown; cls, colourless; euh, euhedral; stub, stubby; lrg, large; sm, small. All zircon and baddeleyite grains were abraded.

*Corrected for fractionation, spike, laboratory procedure blank of 1-5 pg of common lead and initial common lead at the age of the sample calculated from the model of Stacey and Kramers (1975) and 1 pg U blank. Two sigma uncertainties calculated with an unpublished error propagation program are reported after the ratios and refer to the final digits.

⁵ co-ordinates for sample locations are approximate, referenced from NTS 14D/10 map. Only Sample 2 was recorded using a GPS.

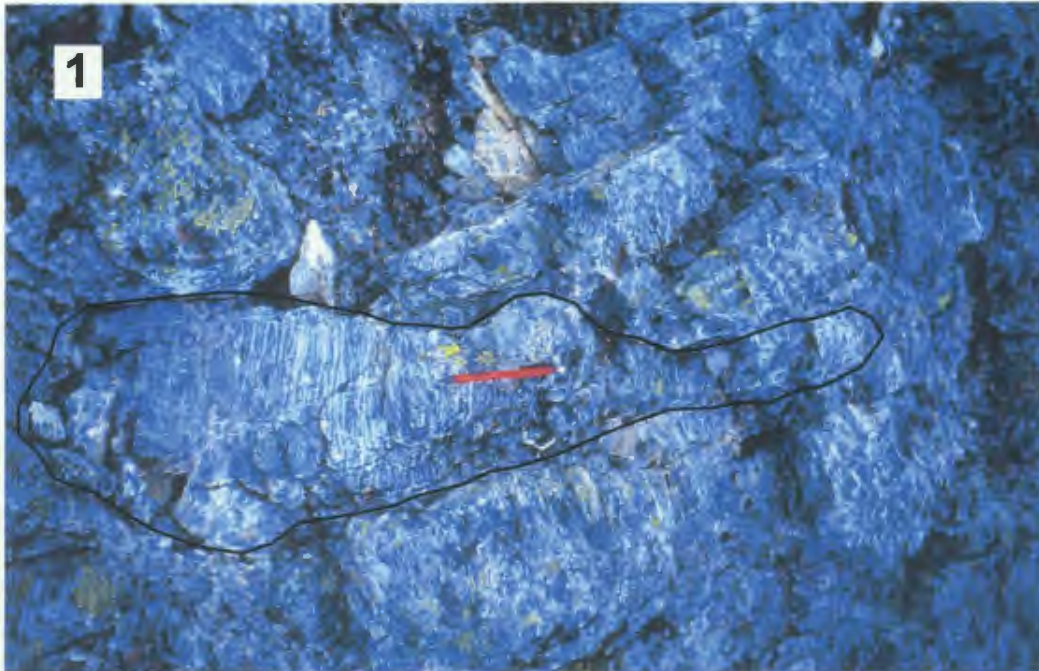


Plate 3.1: Photo of metre-long, dark grey, elongate plagioclase crystals (one outlined) in the inner zone of the PGA. Crystals are fractured perpendicular to length. Pencil is 15 cm long.



Plate 3.2: Pale grey plagioclase crystals of various sizes with white, recrystallized margins in the inner zone of the PGA.



Plate 3.3: Outer zone of the PGA with foliated igneous layers of anorthosite and leuconorite. Boundaries between compositional layers are undulose. Location of geochronological sample 1.



Plate 3.4: View onto the foliation plane in the outer zone of the PGA, about 50 m from the contact with the TI. Note the heterogeneity in composition and strain. Geological hammer is 30 cm long.



Plate 3.5: Norite dyke cross-cutting gneissic norite in the outer zone of the PGA, a few metres from the contact with the T1. Location of geochronological sample 3.



Plate 3.6: Rounded, fractured and resorbed plagioclase crystal in monzodiorite which intruded into the southwest margin of the PGA. The plagioclase crystal has a grey core and a white, recrystallized rim.



Plate 3.7: Compositional layers of quartz monzonite (light) and monzodiorite (dark) with parallel foliation in the eastern margin of the Tessiarsuyungoakh intrusion. Arrow is pointing to geological hammer.



Plate 3.8: Photo of fine-grained monzodiorite (dark) with an undulose intrusive contact into medium-grained quartz monzonite (light). Pencil is oriented roughly perpendicular to this contact.



Plate 3.9: Medium-grained, half-metre wide, anorthosite dyke cutting medium-grained clinopyroxene- and olivine-bearing quartz monzonite. Contact is relatively sharp with no chilled margins.

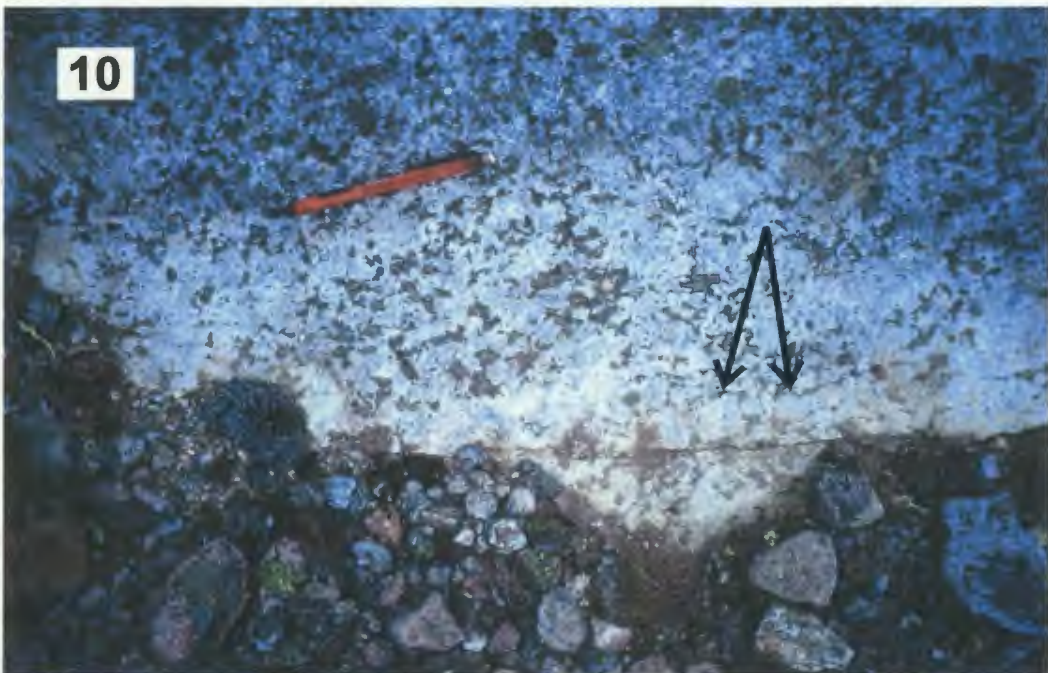


Plate 3.10: Undeformed norite at the margin of the Fraser Canyon Anorthosite, south of Tasisuak Lake. Arrows point to tabular, cumulate plagioclase crystals, surrounded by interstitial orthopyroxene and ilmenite.



Plate 3.11: Monzodiorite with plagioclase xenocrysts of various shape and size. Plagioclase crystals have grey cores and white recrystallized rims.



Plate 3.12: Brecciated quartz monzonite in pseudotachylite fault gouge. The fault is located in the Tessiarsuyungoakh intrusion near the contact with the Tasuiyak paragneiss, south of Tessiarsuyungoakh Lake.

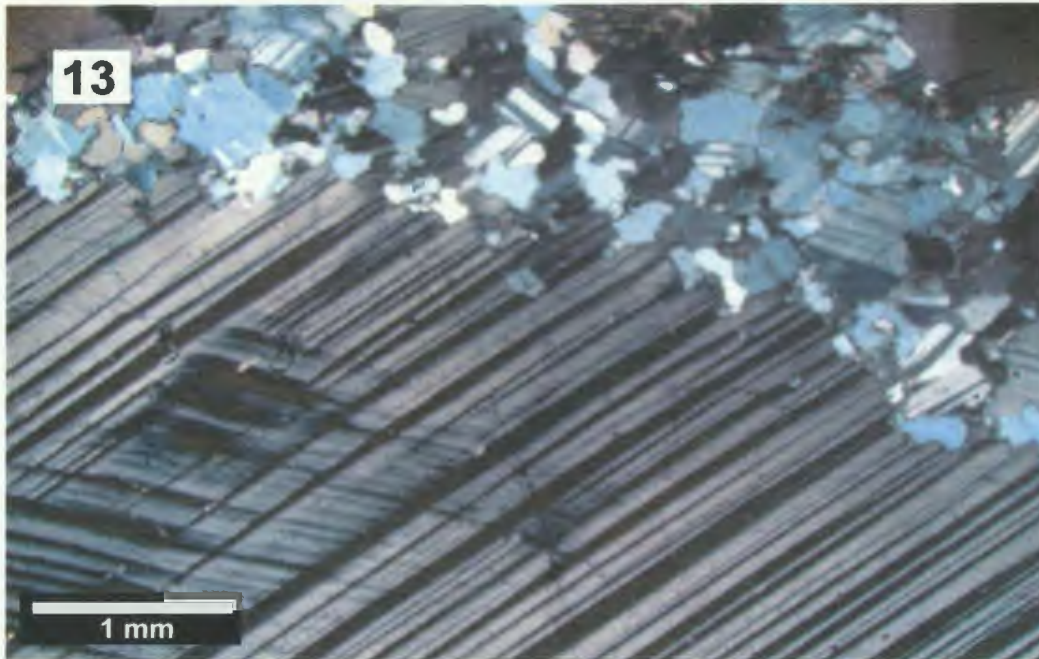


Plate 3.13: Sample TL02-11 of anorthosite showing partial recrystallization along the boundary of a plagioclase grain. Photomicrograph shows deformation twin development in primary, large plagioclase grain with sub-grains formed at the boundary.

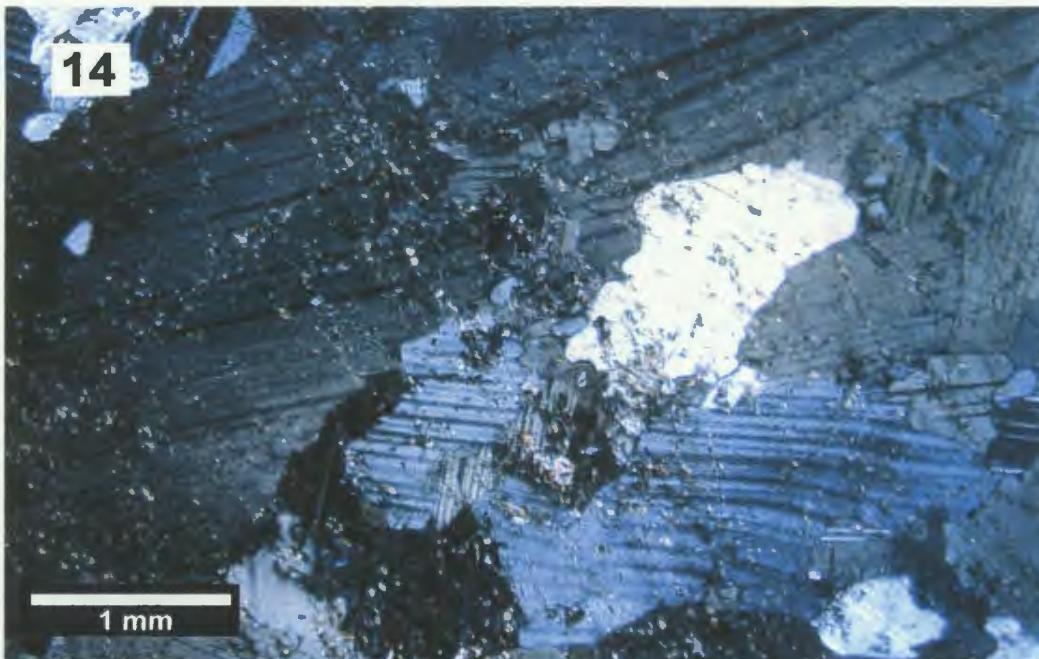


Plate 3.14: Photomicrograph of sample 1 anorthosite in the outer zone of the Pearly Gates Anorthosite. This sample shows partially recrystallized plagioclase, bent deformation twins, and minor alteration.

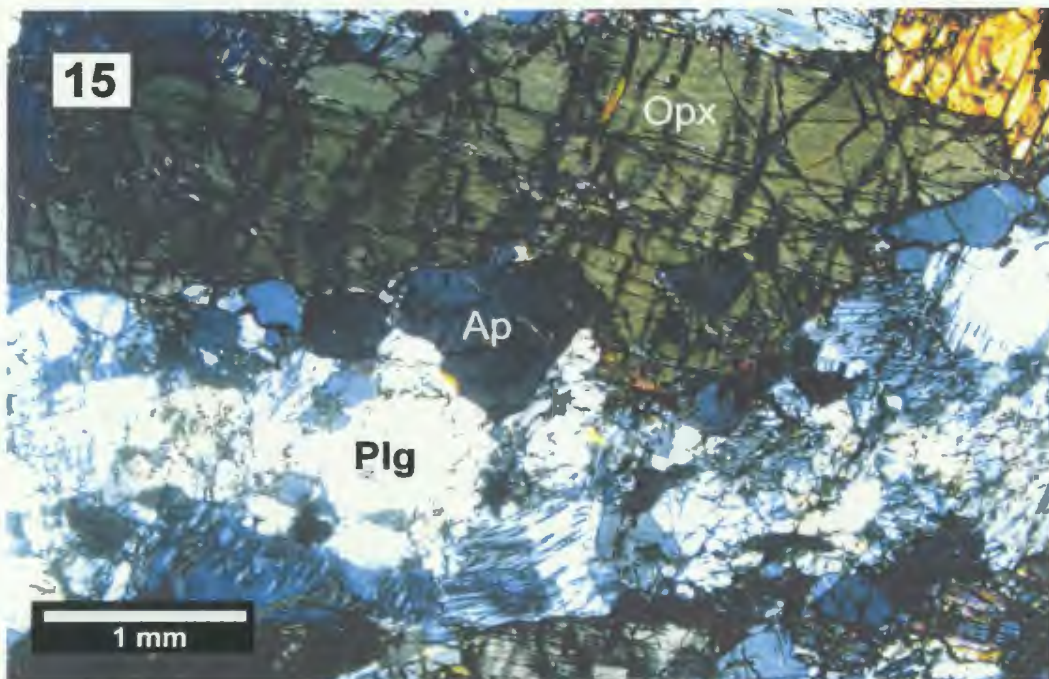


Plate 3.15: Photomicrograph of sample TL01-45 norite in the foliated outer zone of the Pearly Gates Anorthosite. Trains of apatite are partially overgrown by recrystallized orthopyroxene and partially recrystallized plagioclase has deformation twins and exsolution lamellae, which are bent.

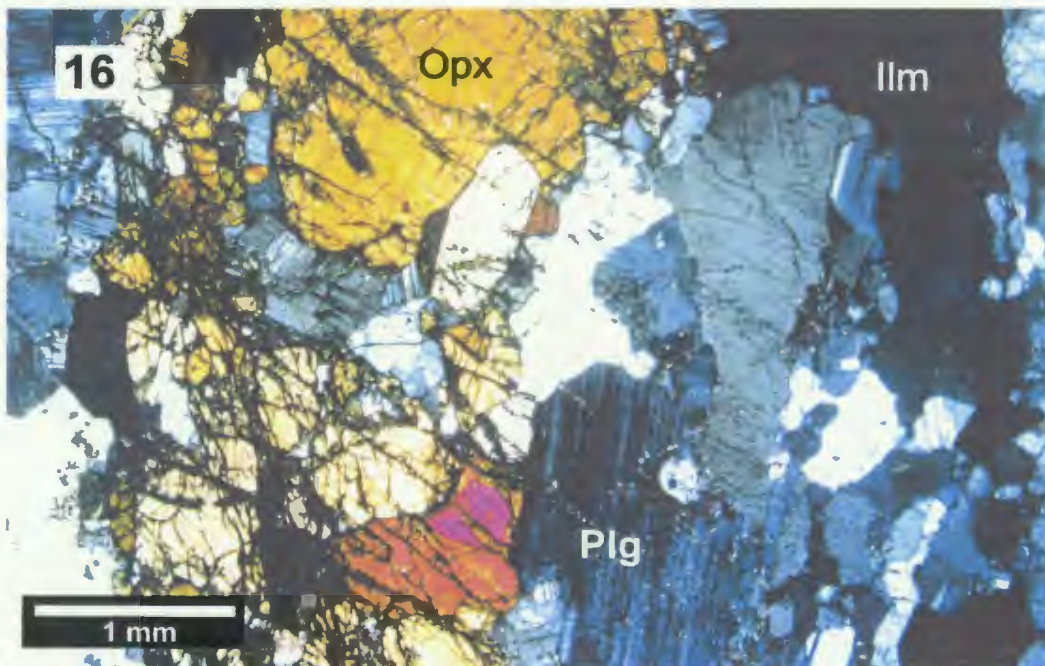


Plate 3.16: Photomicrograph of geochronological sample 4 from the intrusive, undeformed norite body in the Pearly Gates Anorthosite. Orthopyroxene is ophitic and plagioclase shows deformation twinning.

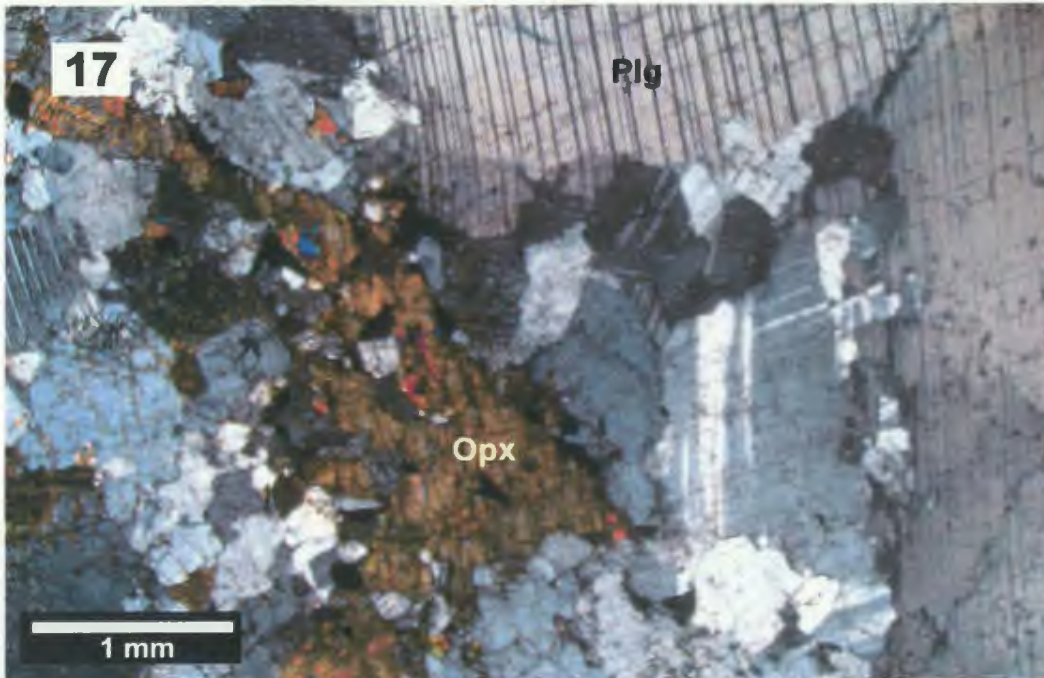


Plate 3.17: Photomicrograph of sample TL02-60a undeformed norite at the roof of the Fraser Canyon Anorthosite. Minor recrystallization occurred along plagioclase grain boundaries and interstitial orthopyroxene is ophitic.

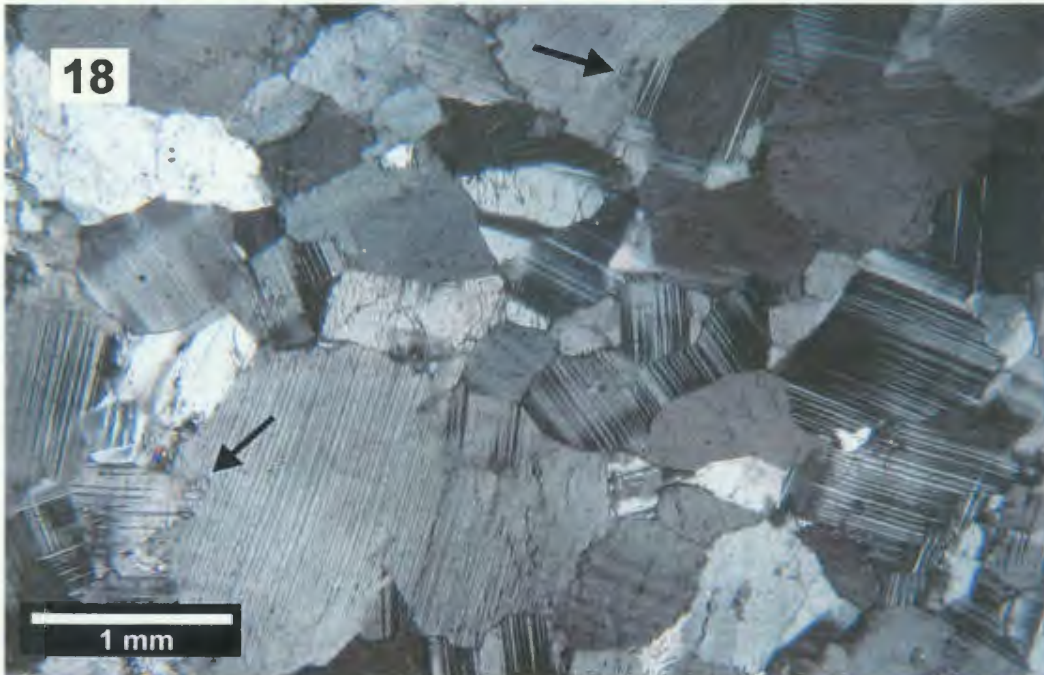


Plate 3.18: Photomicrograph of sample TL02-60c from the roof of the Fraser Canyon Anorthosite. Plagioclase is adcumulus and undeformed. There is only minor recrystallization at grain boundaries shown by arrows.

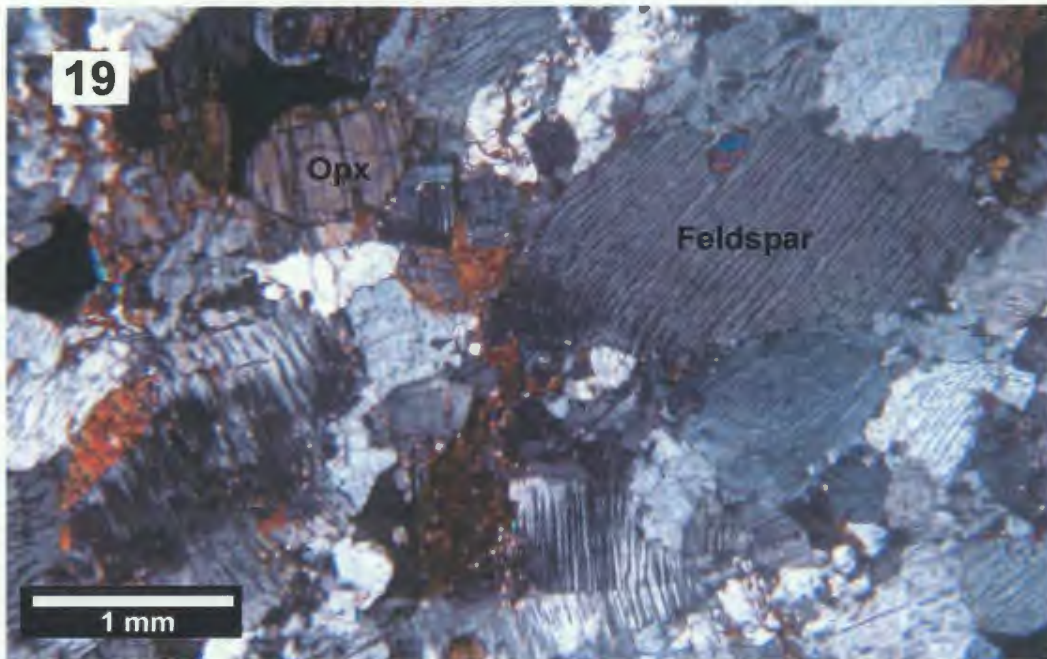


Plate 3.19: Photomicrograph of orthopyroxene-bearing monzonite sample TL02-32b. Sample location is ~200 m from the Tessiarsuyungoakh intrusion/Pearly Gates Anorthosite pluton contact. Feldspars are mesoperthitic and the lamellae are deformed. Grains are recrystallized along their boundaries.

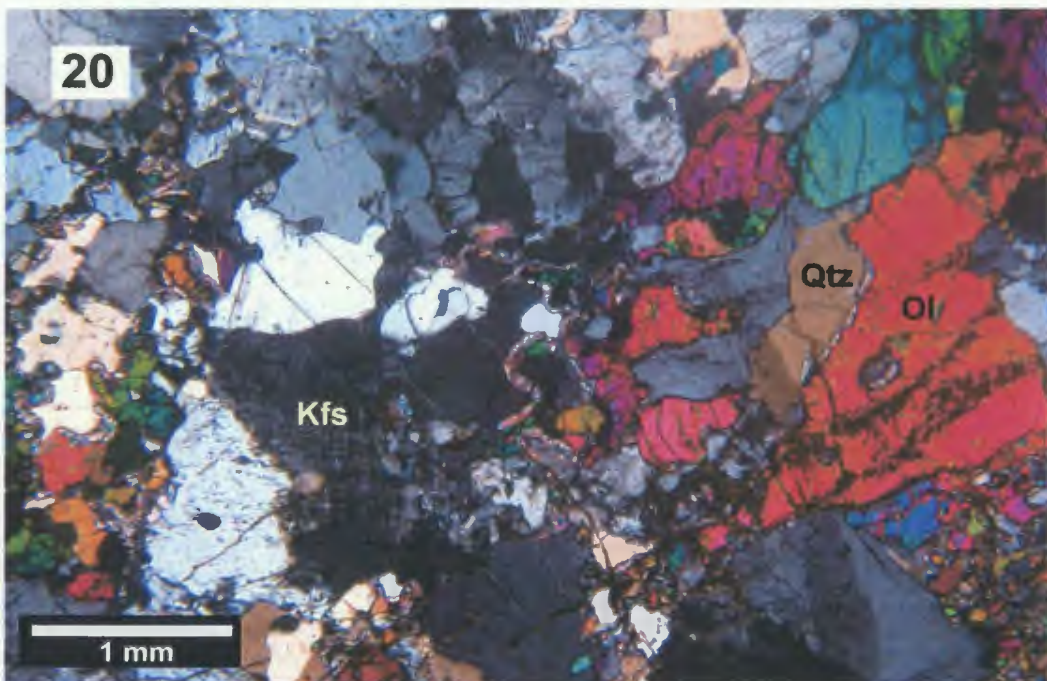


Plate 3.20: Photomicrograph of olivine-bearing quartz monzonite sample TL02-30. Sample location is ~2000 m from the Tessiarsuyungoakh intrusion/Pearly Gates Anorthosite pluton contact. The minerals have undergone minor recrystallization but are undeformed.



Plate 3.21: Photomicrograph of zircon fragments from sample 1. Zircon is pale brown, clear and angular to subangular suggesting slight resorption.

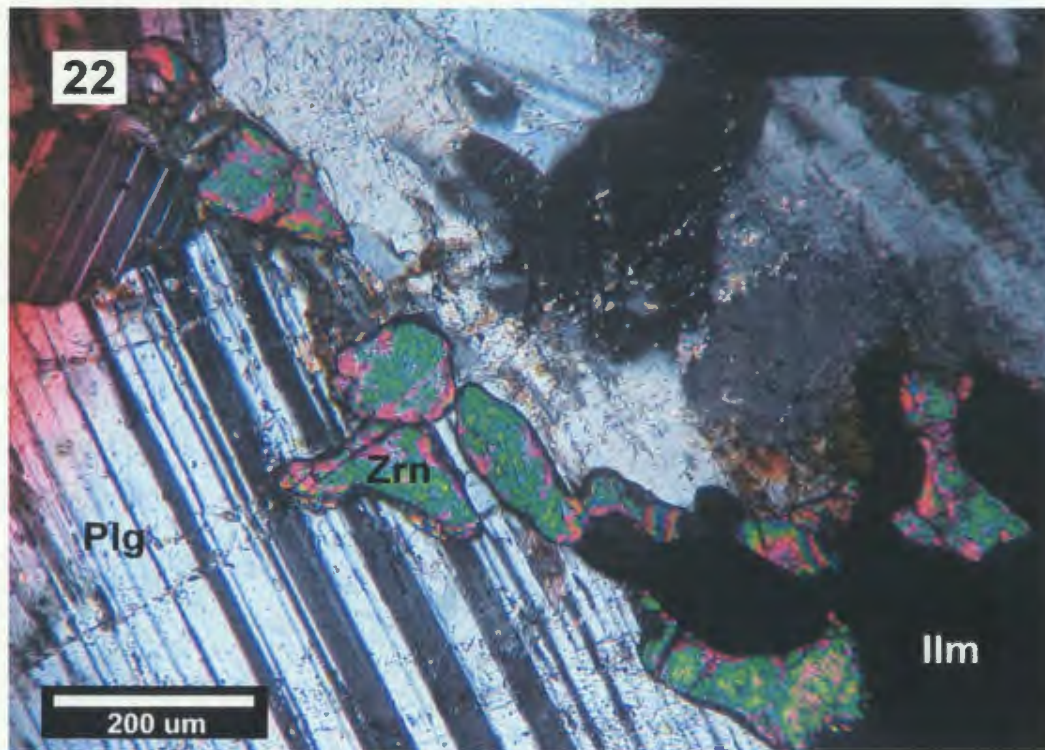


Plate 3.22: Photomicrograph showing clusters of interstitial, anhedral zircon from sample 1. Zircon shows high birefringence and crystallized together with or after ilmenite.



Plate 3.23: Photomicrograph of slightly resorbed prismatic zircons from sample 1. Zircon is pale brown, clear and inclusion-free.

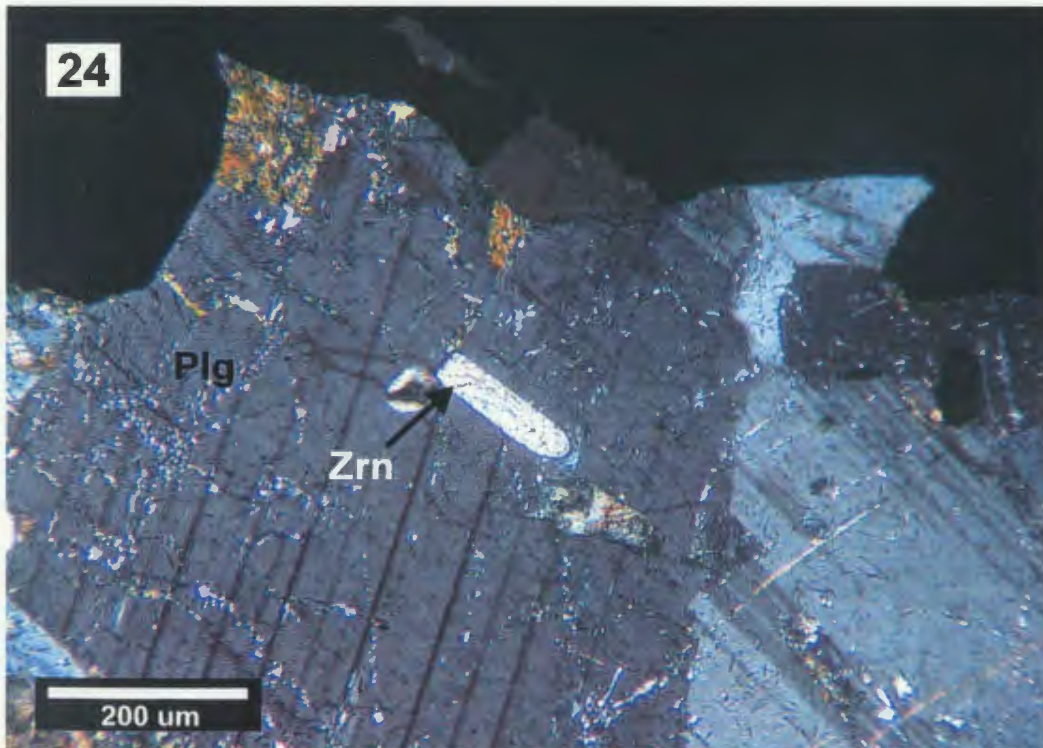


Plate 3.24: Photomicrograph of slightly resorbed, prismatic zircon included in plagioclase from sample 1.



Plate 3.25: Photomicrograph of highly resorbed, cusped zircon from sample 1. Zircon is pale brown, clear and inclusion-free.

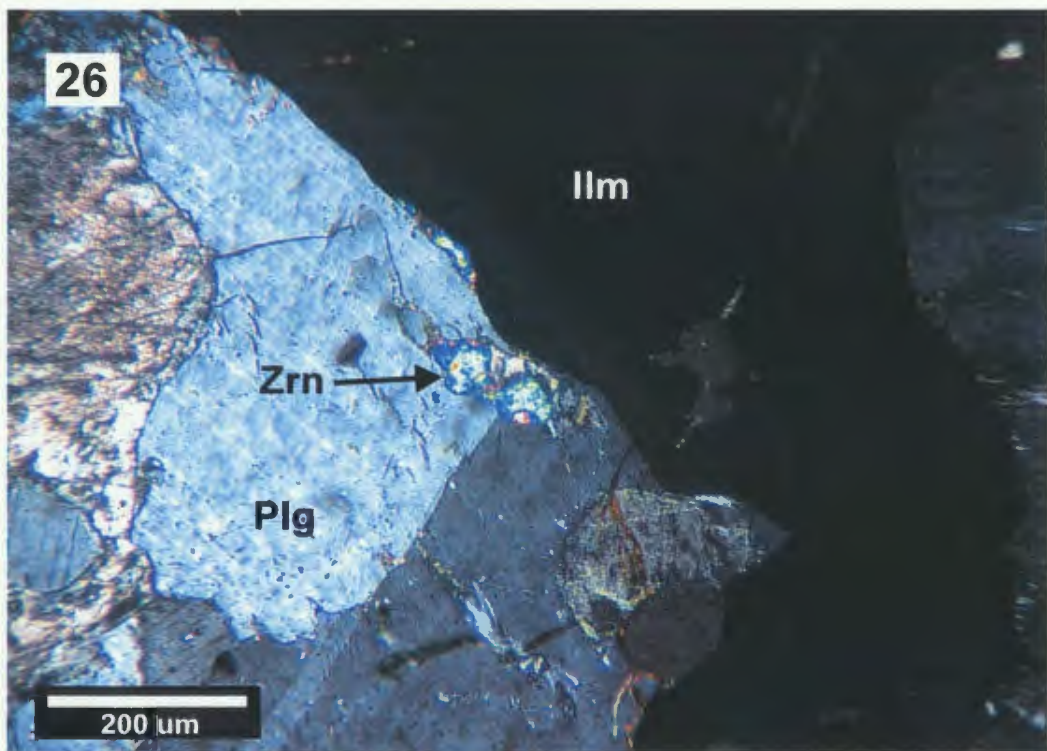


Plate 3.26: Photomicrograph of highly resorbed, zircon from sample 1, partially included in plagioclase at grain boundary.

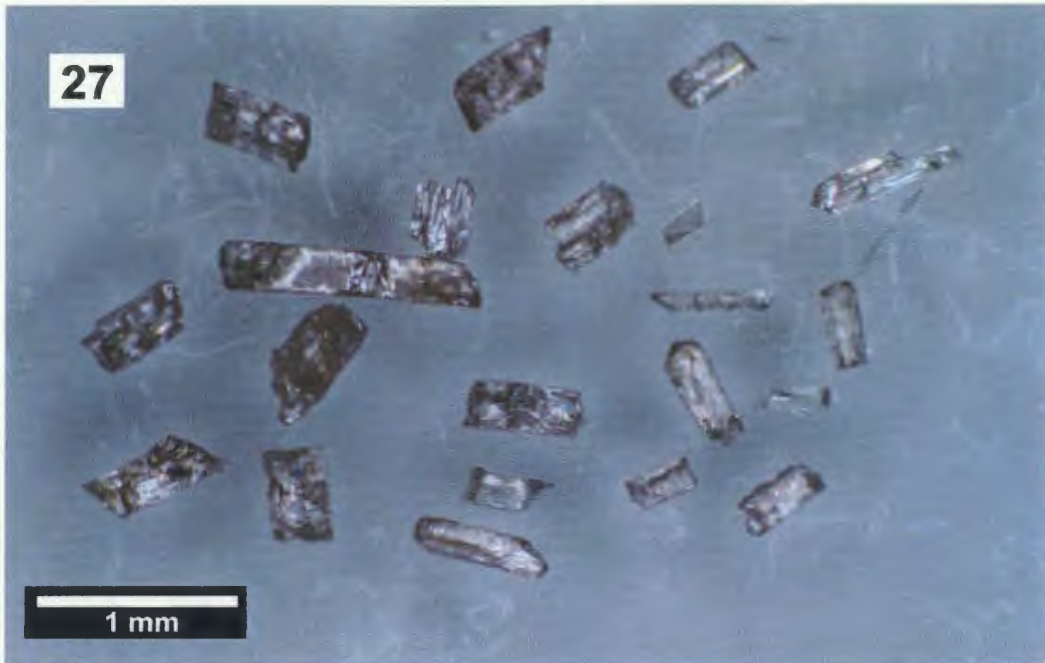


Plate 3.27: Photomicrograph of large, euhedral, prismatic zircon from sample 2. Zircons selected for analyses were colourless, clear, fractured and inclusion-free, however, many of the largest grains contained fluid inclusions.

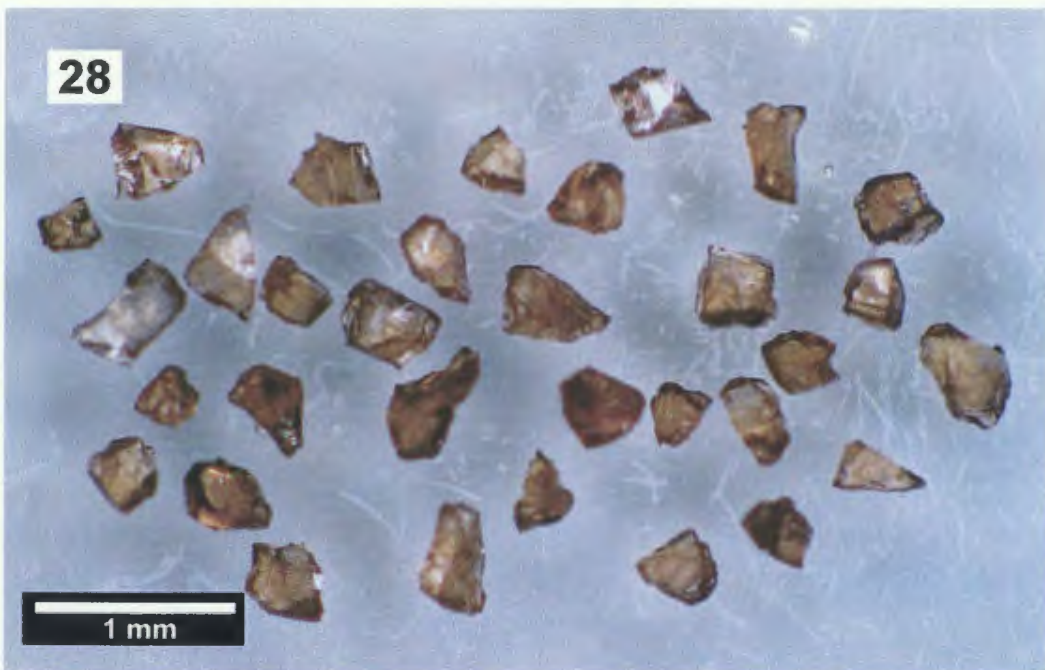


Plate 3.28: Photomicrograph of angular zircon fragments from sample 2. Zircons selected for analyses were colourless or brown, clear, angular and inclusion-free.

29



Plate 3.29: Photomicrograph of stubby, euhedral baddeleyite grains and fragments from sample 1. Baddeleyite is chocolate brown and clear.

30

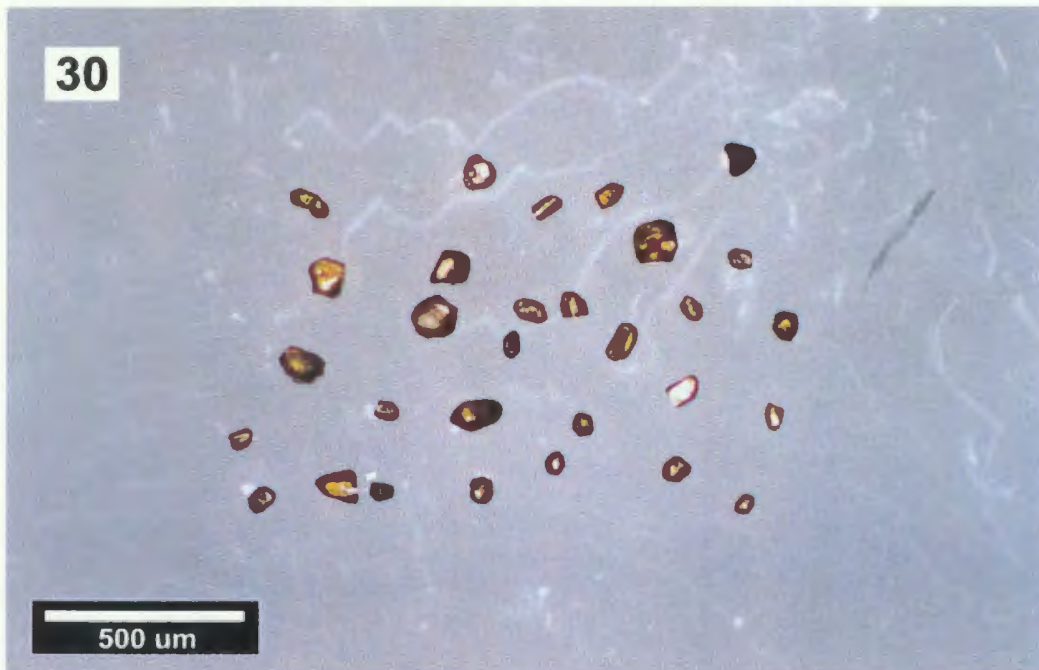


Plate 3.30: Photomicrograph of stubby, euhedral baddeleyite from sample 2. Baddeleyite is chocolate brown and clear.

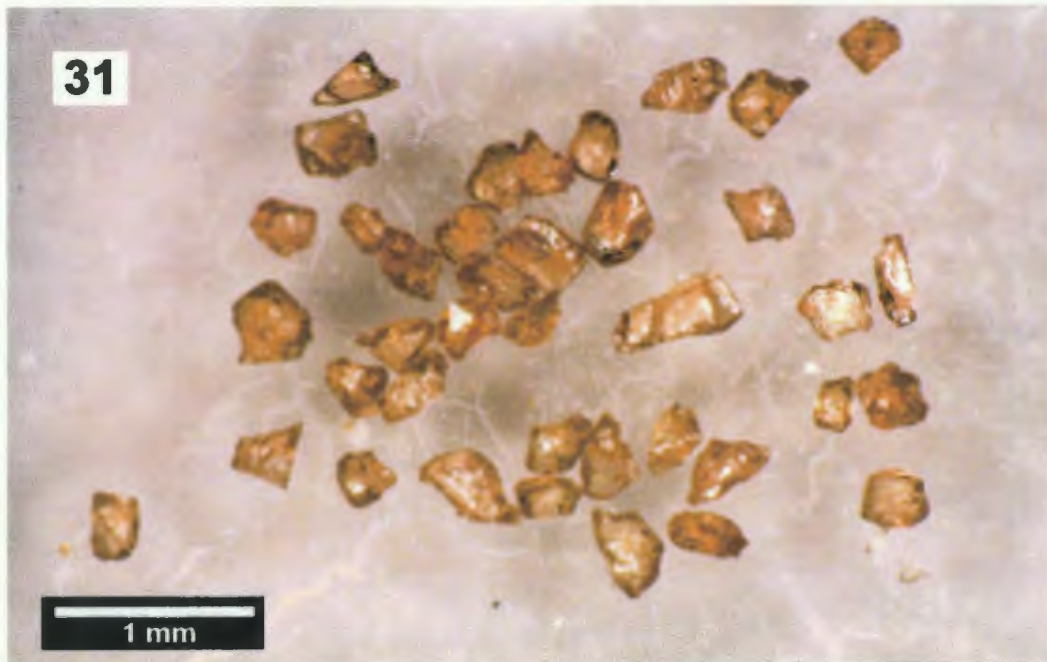


Plate 3.31: Photomicrograph of angular zircon fragments from sample 3. Zircons selected for analyses were pale yellow, clear, angular and inclusion-free.



Plate 3.32: Photomicrograph of angular zircon fragments from sample 4. Zircons selected for analyses were pale yellow-brown, clear, angular and inclusion-free.



Plate 3.33: Photomicrograph of slightly resorbed, prismatic zircon from sample 5. Zircons selected for analyses were pale yellow, clear and inclusion-free.

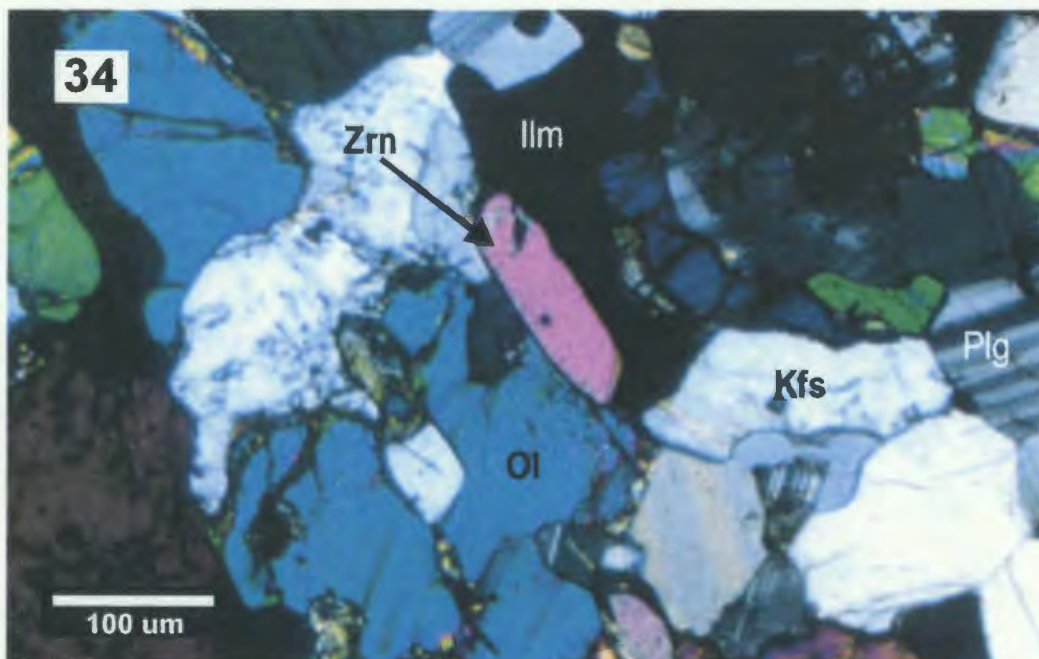


Plate 3.34: Photomicrograph of interstitial prismatic zircon in sample 5.



Plate 3.35: Photomicrograph of slightly resorbed, prismatic zircon from sample 6. Zircons selected for analyses were pale yellow-brown, clear and inclusion-free, although minor inclusions are typical in this sample.

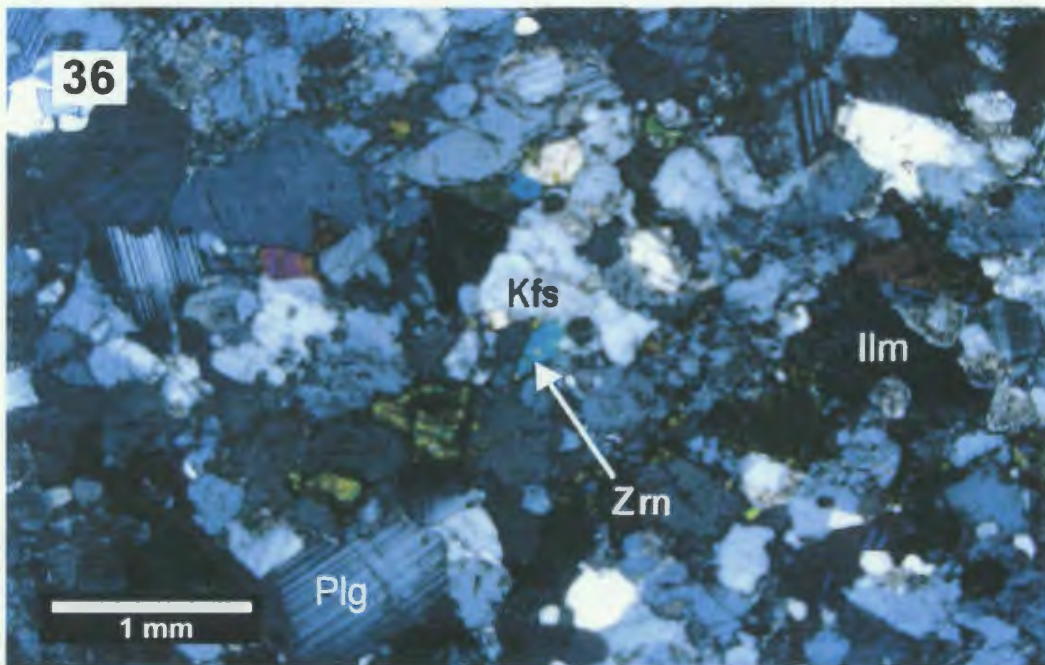


Plate 3.36: Photomicrograph of interstitial, slightly resorbed, large, prismatic zircon from sample 6.

**CHAPTER 4 - STUDY OF REGIONAL AND CONTACT METAMORPHISM OF THE
TASIUYAK PARAGNEISS BETWEEN THE MAKHAVINEKH LAKE PLUTON AND THE
TESSIARSUYUNGOAKH INTRUSION, NAIN PLUTONIC SUITE, NORTHERN LABRADOR**

Abstract:

The Tasiuyak paragneiss adjacent to the western margin of the Nain Plutonic Suite has been subjected to high-temperature regional metamorphism associated with the Paleoproterozoic Torngat orogen, and contact metamorphism associated with emplacement of the Mesoproterozoic Nain Plutonic Suite. This metamorphic study of the paragneiss used petrogenetic grids to determine the nature and conditions of each metamorphic event. The regional metamorphic mineral sub-assembly of garnet-biotite-sillimanite indicates a prograde evolution within the sillimanite stability field and peak *P-T* conditions ranging from 7.2 to 10.2 kbar and 800° to 830°C. The ca. 1360 Ma Tessiarsuyungoakh composite body of monzonite and monzodiorite intruded as sheets into the paragneiss. A small contact aureole (< 20 m wide) was formed along this contact and was marked by incipient development of the metamorphic sub-assembly cordierite + orthopyroxene + spinel after garnet-biotite-sillimanite. This suggests that the Tessiarsuyungoakh intrusion is a relatively small body that intruded and crystallized quickly. The *P-T* estimate of the contact metamorphism in this aureole is between 3 to 4 kbar and 775° to 800°C. The large Makhavinekh Lake pluton consisting of olivine-pyroxene-hornblende-bearing rapakivi granite formed a substantial (~ 4 km) contact aureole in the Tasiuyak paragneiss. The progressive development of the contact metamorphic assemblage cordierite + orthopyroxene + spinel after garnet-biotite-sillimanite with decreasing distance toward the intrusion, is interpreted to represent a temperature gradient along the contact aureole. Temperatures ranged from 675°C at the 4 km limit of the contact aureole, to at least 850°C at the Makhavinekh Lake pluton contact, and isobaric conditions are estimated to have between 3 to 4 kbar.

4.1 INTRODUCTION

Most of the anorthositic and granitic intrusions along the margins of the Mesoproterozoic Nain Plutonic Suite (NPS) (Fig. 4.1) have caused contact metamorphism of the surrounding country rocks. However, other than a reconnaissance contact metamorphic study done by Berg (1977a, 1977b) of the whole NPS region, there are very few detailed studies. These comprise the metamorphic studies by Speer (1982) and Berg and Docka (1983) of the contact aureole surrounding the Kiglapait intrusion in the east (Fig. 4.1), and studies by Lee (1987) and McFarlane et al. (2003) of the contact aureole surrounding the Makhavinekh Lake pluton (MLP), in the west (Fig. 4.1).

Along the western margin of the NPS, several intrusions were emplaced into the Tasiuyak paragneiss that had previously been regionally metamorphosed to garnet-biotite-sillimanite during the Paleoproterozoic Torngat Orogeny. Adjacent to the MLP (Fig. 4.2) composed of rapakivi granite, a contact metamorphic assemblage of cordierite + orthopyroxene + spinel has replaced this regional metamorphic assemblage. To the northeast of the MLP, there is a large body of anorthosite (Pearly Gates Anorthosite pluton), bordered by the composite Tessiarsuyungoakh intrusion (TI) of monzonite and monzodiorite (Fig. 4.2). It was previously unknown whether the TI had also contributed to contact metamorphism of the paragneiss.

The metamorphic study of the Tasiuyak paragneiss described below combines field evidence, textural interpretations and petrogenetic grids to determine three main points: 1) the regional metamorphic *P-T* evolution, 2) if the TI has caused contact metamorphism, and 3) the thermal gradient and isobaric conditions of the contact aureole surrounding the MLP. The latter part of the present study also compliments and compares *P-T* conditions with previous studies by Lee (1987) and McFarlane et al. (2003), southeast of the present study area.

4.2 GEOLOGICAL SETTING

Northern Labrador comprises remnants of two Archean cratons (North Atlantic Craton to the east and the Rae Craton to the west) that were amalgamated during the ca. 1.8 Ma Torngat

Orogeny. The remnant of the North Atlantic Craton in Labrador is known as the Nain Province and is composed of orthogneiss with minor amounts of paragneiss and metavolcanic rocks. To the west of the Torngat Orogen, the Rae Craton was extensively intruded by Paleoproterozoic tonalite, granite and gabbro and was intensely deformed and interleaved with Paleoproterozoic metasedimentary rocks during the Paleoproterozoic. This region was metamorphosed to upper amphibolite to granulite facies and is commonly referred to as the Southeastern Churchill Province. Along the western margin of the Torngat Orogen there is a belt of metasedimentary rocks called the Tasiuyak paragneiss (Wardle, 1983). The Tasiuyak paragneiss was metamorphosed to granulite facies grade during the late stages (ca. 1860 to 1840 Ma) of the Torngat Orogeny (Bertrand et al., 1993). Between ca. 1845-1820 Ma (Rivers et al., 1996), the NNW trending Abloviak Shear Zone developed along the eastern margin of the Tasiuyak paragneiss and defines the eastern edge of the Torngat Orogen.

The Mesoproterozoic (ca. 1360-1290 Ma) NPS was intruded along the collisional suture marked by the Torngat Orogen. The western boundary lies adjacent to the Tasiuyak paragneiss of the Southeastern Churchill Province and the eastern boundary lies adjacent to the rocks of the Nain Province. The NPS comprises composite bodies of anhydrous, anorthositic and granitic rocks. Some of these intrusions have produced contact aureoles in the country rocks. Along the western margin of the NPS, some plutons have produced granulite facies contact metamorphic assemblages that overprint the regional granulite facies assemblage of the Tasiuyak paragneiss.

The Tasiuyak paragneiss is dominated by highly deformed, layers of semi-pelitic rocks with minor pelitic components and is locally interlayered with sheets of orthopyroxene-bearing tonalitic orthogneiss and garnet-bearing quartzofeldspathic orthogneiss. The paragneiss is migmatitic and the regional metamorphic assemblage mainly consists of quartz + K-feldspar + plagioclase + garnet + biotite \pm sillimanite (Pl. 4.1). Contact metamorphism of the Tasiuyak paragneiss by intrusions of the NPS has produced cordierite, orthopyroxene and spinel at the expense of garnet, biotite and sillimanite.

4.3 GEOLOGY OF THE STUDY AREA

In the study area, the Tasiuyak paragneiss (Fig. 4.2) was intruded by the TI in the east and by the MLP in the southwest. The ca. 1360 Ma TI (this study, Chapter 3) intruded into the paragneiss as sheets and formed pyroxene- and/or olivine-bearing monzonite and monzodiorite. The composite TI separates the ca. 1340 Ma Pearly Gates Anorthosite pluton (this study, Chapter 3), to the east, from the Tasiuyak paragneiss, to the west. The ca. 1322 Ma MLP (McFarlane et al., 2003) is a pyroxene-olivine-hornblende-bearing granite with rapakivi texture. This pluton intruded as a sheet-like cylindrical body into the paragneiss (Ryan, 1991).

Metre-thick sheets of foliated, granulite facies orthopyroxene-bearing tonalite and sub-concordant garnet-bearing quartzofeldspathic dykes are distributed throughout the paragneiss but make up only a minor portion of the mapped area. The regional gneissosity of the paragneiss broadly trends 160°SSE and is sub-vertical. Close to the TI contact, this gneissosity is parallel to the TI contact ranging from 110° to 165° and dipping 26° to 65° southwestwards. In the southern part of the study area near the TI contact, the north-south trending foliation in the paragneiss is deflected by east-west trending shear zones.

The intrusion of the MLP produced a contact aureole in the Tasiuyak paragneiss. Contact metamorphism is marked by cordierite + orthopyroxene ± plagioclase pseudomorphs after garnet and biotite, and cordierite + spinel ± orthopyroxene ± plagioclase pseudomorphs after garnet and sillimanite (Pl. 4.3 and 4.4). In the field, this aureole appears to extend ~ 4 km radially from the MLP contact (Fig. 4.2). The intensity of these transformations increases towards the contact of the MLP. Recrystallization associated with the contact metamorphism has obscured the foliation in the paragneiss near the MLP contact. Beyond the contact aureole, the regional metamorphic assemblage of the paragneiss appears to be well preserved (Pl. 4.2). However, new petrographic evidence (see section 4.9.4.1) indicates that the regional metamorphic assemblage has been perturbed.

Minor screens of paragneiss, generally 10's of metres in length and width, were observed in the TI. The gneissosity of the paragneiss is concordant to the layering and magmatic flow foliation of the TI (see Chapter 3, section 3.3.2). In the field, these screens appear to contain only the regional metamorphic assemblage but new petrographic evidence (see section 4.10.1) indicates the presence of a contact metamorphic assemblage of cordierite + spinel ± orthopyroxene.

4.4 PREVIOUS WORK

North of the NPS, the regional metamorphism of the Tasiuyak paragneiss has been studied by Ermanovics and Van Kranendonk (1998) and Rivers et al. (1996) (Fig. 4.1). The regional metamorphic assemblages of the paragneiss described in these studies are generally the same as those in this study area. Ermanovics and Van Kranendonk (1998) reported *P-T* conditions of 7 kbar and 510 to 700°C. Rivers et al. (1996) reported *P-T* conditions of 6 to 7 kbar and 650 to 750°C from the paragneiss and 10 to 12 kbar and 800°C from interlayered mafic rocks. Rivers et al. (1996) suggested that the lower *P-T* conditions of the paragneiss were due to “more pervasive post-peak re-equilibration”.

Ryan (1991) described the structure, petrography and geochemistry of the MLP and discussed the contact metamorphic assemblage in the Tasiuyak paragneiss. Berg (1977a, 1977b) conducted a study of the contact metamorphism in paragneisses, ironstone formations and ultramafic rocks in both the Nain Province and Southeastern Churchill Province adjacent to NPS intrusions and provided the first data set on contact mineral assemblages and *P-T* conditions in the NPS region. This study included a sample of the Tasiuyak paragneiss (sample 2-1572), which was collected in the present study area (Fig. 4.2). The mineral assemblage of this sample was garnet + cordierite + orthopyroxene (+ quartz) and *P-T* conditions were determined as 5.3 kbar, 780° to 785°C (from garnet rim analyses) and 5.6 kbar, 910° to 915°C (from garnet core analyses) (Berg, 1977b). Berg (1977a, 1977b) suggested that minor zoning in garnet rims

formed during retrograde re-equilibration and therefore, interpreted the garnet core analyses to represent peak *P-T* conditions.

A B.Sc. honours thesis by Lee (1987) focused on the contact aureole southeast of the present study area. This thesis reported *P-T* estimates of 6 to 9 kbar, 850 to 900°C for the regional metamorphism and of 3.5 to 4.5 kbar, 600 to 760°C for the (isobaric) thermal gradient of the contact metamorphism. Lee (1987) also suggested that the temperature estimate close to the MLP contact was a minimum because of retrograde Fe-Mg exchange.

McFarlane et al. (2003) studied the contact aureole related to the MLP along two transects. The contact metamorphic assemblage was used to test whether Al solubility in orthopyroxene, which replaced garnet, could be used as a reliable geothermometer for high-temperature metamorphic rocks. One of the transects was done in the same region as Transect 3 of the present study. However, the data and results presented by McFarlane et al. (2003) are from a second transect, south of the present study area at the eastern boundary of the MLP. They stated that their results from both transects were the same and that the sample used to describe the regional metamorphic assemblage was located along their first transect. The results of McFarlane et al. (2003) indicated a temperature gradient from 900°C at the MLP contact to 700°C at a distance of 5750 m from the contact.

4.5 GENERAL APPROACH

A petrographic study was carried out to determine the mineral compositions and textures of the regional and contact metamorphic assemblages. This information was used in conjunction with a petrogenetic grid, bulk composition, mineral composition, and AFM diagrams to interpret the metamorphic reaction textures and estimate *P-T* conditions. The NaKFMASH petrogenetic grid of Spear et al. (1999) (Fig. 4.3), which illustrates high temperature phase relationships in pelitic systems, was used to constrain the reaction history and *P-T* evolution of the analyzed samples. The role of bulk composition in the textural evolution was addressed using AFM diagrams. The main metamorphic phases, garnet, biotite, plagioclase, cordierite and

orthopyroxene were analyzed for chemical zoning in order to provide additional constraints on the metamorphic evolution.

For the regional metamorphism, *P-T* conditions were further constrained by using garnet X_{Fe} ($X_{Fe} = Fe/Fe+Mg$) isopleths and GASP (Garnet + Aluminosilicate + Silica + Plagioclase) geobarometry. Spear et al. (1999) calculated garnet X_{Fe} isopleths in the NaKFMASH system for a number of mineral assemblages (Fig. 4.11). Therefore, the range of calculated garnet X_{Fe} values from the studied samples helps to confine the thermal peak to within a specific range of isopleths.

The chemical compositions of garnet and plagioclase were used to constrain pressure limits in the NaKFMASH petrogenetic grid. The peak pressure estimates were determined using the GASP reaction:



The GASP reaction is a robust geobarometer since it is relatively unaffected by late exchange during cooling along the *P-T* path. Geobarometric calculations were performed using the TWEEQU 2.02 program (Berman, 1991). The intersection of the garnet X_{Fe} and GASP isopleths ideally provides quantitative *P-T* conditions.

TWEEQU is a computational database which contains thermodynamic data and activities (Berman, 1988; Berman and Aranovich, 1996; unpublished data from Berman and Aranovich, 1997) for many common minerals. This application calculates all equilibrium reactions for a given mineral assemblage and produces a graphical output of pressure and temperature. The above-mentioned GASP equilibrium reaction was used with mineral compositions to calculate a univariant reaction line and plotted on the NaKFMASH petrogenetic grid to further constrain the pressure conditions during regional metamorphism.

Geothermobarometric studies were not done on the contact metamorphic assemblages for two reasons: 1) previous studies (see section 4.4) have already provided extensive analytical data and geothermobarometric *P-T* conditions of the contact metamorphic assemblage in the

paragneiss adjacent to the MLP; and 2) these same studies have suggested that resetting of Fe-Mg phases occurred. Therefore, the petrogenetic study described here is designed to complement and compare *P-T* conditions with those estimated in the previous work.

The use of petrogenetic grids in conjunction with X_{Fe} isopleths is a powerful and relatively new approach. This technique helps to constrain the metamorphic peak *P-T* conditions in high temperature metapelites because it avoids the limitations of the traditional geothermobarometry in high-grade rocks, i.e. Fe-Mg resetting by garnet-biotite or garnet-cordierite Fe-Mg exchange during cooling (Spear, 1991).

4.6 ANALYTICAL TECHNIQUES

Bulk composition of polished sections and mineral chemical analyses were conducted on the Cameca SX50 electron microprobe at Memorial University. Bulk composition analyses were conducted using the EDX method with an acceleration potential of 15 kV, a beam current of 250 nA and a scanning beam size of .8 mm x 1 mm while the stage was moving between specified limits. Spot analyses, also conducted using EDX, were performed along transects across grains of garnet, biotite, plagioclase, cordierite and orthopyroxene to detect chemical zoning. Operating conditions for mineral analyses were: acceleration voltage: 15 kV, beam current: 20 nA, beam size: 1 μ m, and counting time: 50 seconds for garnet, 75 seconds for all other minerals. In the case of plagioclase, a lower beam current of 10nA and a larger beam diameter of 3 μ m were used due to feldspar's sensitivity to damage by the beam. Ferric iron cannot be distinguished from ferrous iron by the microprobe but is considered to be negligible in the analyzed minerals.

4.7 SAMPLE SELECTION

46 samples of Tasiuyak paragneiss were selected for a study of the regional and contact metamorphism. All samples were oriented and thin sections were cut perpendicular to the foliation and along strike. Samples were collected along three transects at high angles to the

boundaries of the paragneiss (Fig. 4.2). In addition, sample TL01-146 was collected ~ 10 km west of the TI and 5 km north of the MLP, in order to represent the pristine Paleoproterozoic regional metamorphic assemblage of the Tasiuyak paragneiss. This sample was used in a detailed petrographic study to constrain the regional peak *P-T* conditions in the study area.

Samples collected along Transect 3 (Fig. 4.2) display a gradational change between the TI and MLP from regional to contact metamorphic assemblages, respectively. Therefore samples from this transect (samples TL02-73 to -80 and TL02-66a, -66b) were used to best describe the entire variation of metamorphic assemblages across the aureole.

This study of the contact metamorphism mainly focuses on textural interpretations using the petrogenetic grid and AFM diagrams. Therefore it complements the studies of Lee (1987) and McFarlane et al. (2003), which included detailed determination of mineral chemistry and geothermobarometry but did not place the results in a petrogenetic *P-T* framework. In the context of this thesis, only sample TL01-147 (Transect 2) was analyzed for mineral chemistry to constrain the location of phases on AFM diagrams. The mineralogy of key samples is shown in Table 4.1.

In addition, three samples, TL02-29, -44 and -48 (Fig. 4.2), were collected from Tasiuyak paragneiss screens within the TI. These samples were studied in order to determine whether spinel is a result of a contact metamorphic overprint on the regional assemblage.

4.8 REGIONAL METAMORPHISM

4.8.1 Petrography

Thirteen polished sections taken from different compositional layers in sample TL01-146 were examined to document the regional metamorphic mineral assemblage (Table 4.1). The sample is highly strained and heterogeneously recrystallized. Two textural domains were distinguished: domain I is mostly composed of large quartz ribbons and domain II consists of fine-grained biotite-bearing quartzofeldspathic matrix with feldspar porphyroblasts, large sillimanite prisms, and garnet porphyroblasts. Garnet is generally several mm to 7 cm in diameter

and locally abuts and deflects quartz ribbons of domain I (Pl. 4.5). The foliation is defined by biotite, quartz ribbons and sillimanite prisms. Minor amounts of rutile, ilmenite, pyrite, chalcopyrite, zircon and monazite are found in both domains, whereas titanite is only found in domain II.

Domain I is dominated by coarse-grained, partially recrystallized, highly attenuated quartz ribbons that are locally separated by thin lenses of attenuated quartzofeldspathic matrix (Pl. 4.5). The quartz ribbons show minor recrystallization as serrated grain boundaries perpendicular to the length of the ribbons.

Domain II is characterized by fine-grained, granoblastic K-feldspar + plagioclase + quartz + biotite (Pl. 4.6). In addition, fine-grained patches of vermicular quartz and feldspars were found at or close to (within 200 μm) garnet grain boundaries (Pl. 4.7 and 4.8). Relatively large feldspar porphyroblasts (0.7 mm to 2 mm) consist of augen-shaped, partially recrystallized, mesoperthite (Pl. 4.6). Throughout the rock, feldspars are moderately saussauritized and have a dirty-brown appearance in plane-polarized light (Pl. 4.5).

Within domain II, complex textural relationships were observed between garnet and sillimanite. There are three textural types of sillimanite, fine-grained needles (Sil1), coarse-grained sillimanite prisms (Sil2) and fibrolite (Sil3). Sil1 was found as inclusions in the core of some garnet porphyroblasts (Grt1) and is either randomly oriented (Pl. 4.9), or forms trains parallel to the existing fabric (Pl. 4.10). Sil2 (0.5 to 1 mm) consists of euhedral prisms that are locally bent (Pl. 4.11). Sil2 occurs as: a) clustered trains parallel to the foliation in the matrix from which they are separated by a garnet rim (Pl. 4.9), and b) as inclusions in the outer part of large xenomorphic garnet porphyroblasts, some of which developed around Grt1 (Pl. 4.9 and 4.10). Therefore, the garnet associated with Sil2 postdates Grt1 and will be referred to as Grt2. The matrix surrounding the sillimanite-garnet assemblage (Domain II) is generally plagioclase-rich.

In addition to Sil2, Grt2 contains inclusions of quartz, plagioclase, K-feldspar, biotite and polymineralic quartz \pm biotite \pm plagioclase \pm K-feldspar (Pl. 4.12). Grt2 is locally resorbed and

rimmed by fine-grained intergrowths of Sil3, quartz and biotite. This intergrowth was also found along garnet fractures and grain boundaries between Grt2 and Sil2 (Pl. 4.13). Locally, biotite (50 to 500 μm) was observed embayed into Grt2 (Pl. 4.11). The largest garnet porphyroblasts (up to 7cm) are those completely enclosed in domain II. In contrast, garnet porphyroblasts associated with thin lenses of quartzofeldspathic matrix in domain I either abut quartz ribbons or do not exceed 1 cm in diameter. Lesser amounts of fine-grained (100 μm to 200 μm), euhedral garnet usually rims Grt2 (Pl. 4.14). This euhedral garnet, referred to as Grt3 (reason discussed in interpretation section), contains quartz inclusions (Pl. 4.14) and in a few cases, euhedral Grt3 was observed as inclusions in biotite.

4.8.1.1 Bulk composition

The bulk compositions of sections TL01-146c, d, j and k are shown in Table 4.2 and plotted on an AFM diagram in Figure 4.4. Sections c and d are characterized by larger proportions of domain II relative to sections j and k, in which domain I is dominant. X_{Fe} ranges from .58 to .62 and the Al index ranges between .40 and .49. The Al index is highest in sections c and d (.48 - .49 versus .40 - .44 in sections j and k), which also have the highest modal amount of sillimanite. The bulk compositions of all the sections cluster within the Grt-Sil-Bt triangle of the AFM diagram, close to the Grt-Sil tie line (Fig. 4.5, AFM diagram labelled Field I).

4.8.2 Mineral Chemistry

Analytical data for garnet, biotite and plagioclase is located in Table A.1 of Appendix A.

4.8.2.1 Garnet

Garnet porphyroblasts were analyzed in sections TL01-146c, d, j and k (Fig. 4.6a-f). These porphyroblasts include Grt1 rimmed by Grt2, xenomorphic Grt2 and euhedral Grt3. All these garnet grains are relatively homogeneous and are characterized by high almandine and low

grossular contents (X_{Alm} .57 – .64, X_{Prp} .33 – .38, X_{Grs} .023 – .031, X_{Sps} .002 – .005). Minor X_{Fe} zoning exists at the rims of some xenomorphic Grt2 and adjacent to biotite inclusions. Both X_{Ca} and X_{Mn} generally show no change across garnet. X_{Mn} is very low and was not plotted.

4.8.2.2 Biotite

Biotite adjacent to garnet, and biotite inclusions in garnet were analyzed in section TL01-146j (Fig. 4.7a-c). X_{Fe} of biotite ranges from ~ .22 to .25 with maximum values typically at rims adjacent to garnet. X_{Ti} depends on the textural setting: it is highest in biotite inclusions, .54 to .65 per formula unit (p.f.u.), whereas it ranges from .48 to .55 p.f.u. in biotite adjacent to garnet. X_{Al}^{VI} ranges from .23 to .45 p.f.u. and decreases towards the rim of biotite adjacent to garnet.

4.8.2.3 Plagioclase

Small, matrix plagioclase adjacent to garnet was analyzed in sections TL01-146j and k (Fig. 4.8a-f). Plagioclase is homogeneous with a composition of X_{An} .28 - .30 and a K-feldspar component (X_{Or}) between .01 and .02.

4.8.3 Interpretation

The metamorphic assemblage and textures observed in sample TL01-146 can be best interpreted by using the NaKFMASH petrogenetic grid of Spear et al. (1999) that illustrates phase relationships in high-temperature muscovite-free pelitic rocks.

The absence of muscovite and the co-existence of K-feldspar and Sil2 in sample TL01-146 indicates that the metamorphic temperatures exceeded those required for muscovite dehydration melting and reached the biotite dehydration field (Fig. 4.5). In this context, the fine-grained quartzofeldspathic matrix of domain II, that mainly has a granitic composition, is interpreted as leucosome. The associated porphyroblasts of garnet, sillimanite and feldspars

likely represent peritectic phases and/or unmolten residue. Finally, the large quartz ribbons of domain I are interpreted as excess quartz that escaped melting.

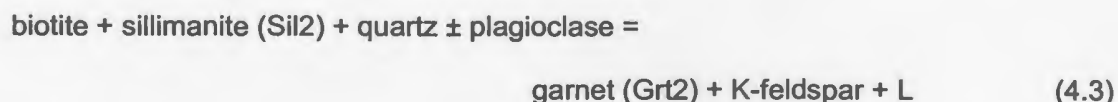
The observed mineral assemblages and textures suggest the following evolution. The garnet cores with Sil1 inclusions (Grt1) represent the earliest preserved assemblage. The evidence of both random and foliation-parallel orientation of Sil1 suggests that Grt1 formed during the early stage of fabric development. The bulk composition of TL01-146c and 146d, the only sections that contained Grt1, were plotted on AFM diagrams projected from muscovite representing the staurolite-out reaction (Fig. 4.9). Both sections lie within the Grt-St-Bt and Grt-Sil-Bt triangles, and have relatively high X_{Fe} and aluminum index close to that of garnet. Their location suggests that Grt1 and Sil1 may have been produced, at least in part, by the NaKFMASH discontinuous reaction (Fig. 4.5):



The formation of coarse-grained sillimanite prisms (Sil2) took place during a later stage of deformation of the paragneiss. Evidence for this deformation is the presence of bent crystals and that Sil2 is oriented within the foliation, and exhibits strained extinction. Sil2 is likely the product of dehydration melting of muscovite (Fig. 4.5):



A second generation of xenomorphic garnet growth (Grt2) formed rims around Sil2 and Grt1. The inclusions of K-feldspar, plagioclase, quartz and Sil2 are consistent with growth of Grt2 by the biotite dehydration melting reaction:

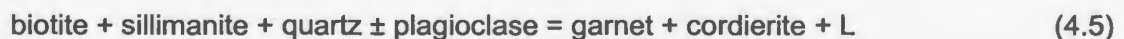


Reaction 4.3 is continuous in the NaKFMASH system and occurs within the field denoted by "I" in Fig. 4.5. The xenomorphic Grt2 most likely reflects pseudomorphic overprinting of Sil2 trains and clusters. The lack of sillimanite in the quartzofeldspathic lenses of the quartz-rich domain is likely due to the lower Al content of these lenses. This is reflected in the bulk composition of sections TL01-146j and k, which had the lowest Al index.

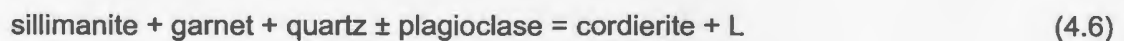
Patches of vermicular leucosome that locally corrode garnet (Pl. 4.7) indicate that at some stage of partial melting garnet became a reactant. This can happen if biotite was entirely consumed in Field I. This reaction is:



The bulk composition of this sample lies within the Grt-Sil-Bt triangle and near the Grt-Sil tie line. If during cooling new biotite was produced by melt crystallization, this biotite would have higher X_{Fe} than that of the biotite at the P - T peak. Then the calculated X_{Fe} (that is plotted in the AFM diagram) would be higher than the peak X_{Fe} . If this were the case, then during the thermal peak the Grt-Sil-Bt triangle may have shifted to the right of the bulk compositions, leaving them in the Grt-Sil tie line region and marking the end of reaction 4.3 (Fig. 4.10). This poses a problem in constraining temperature conditions since without biotite the higher temperature discontinuous reaction:



could not occur. However, in the divariant Field II the bulk composition of the analyzed samples lies in the Grt-Sil-Crd triangle, suggesting that the continuous reaction:



would occur. Because cordierite is absent, the *P-T* conditions for the thermal peak are interpreted to have been restricted to Field I (Fig. 4.5).

The small, euhedral Grt3 that locally rim xenomorphic Grt2 and are found as inclusions in biotite are suggested to have formed during melt crystallization. If, as proposed earlier, garnet was partially consumed by reaction 4.4 following elimination of biotite in Field I, then during the early stages of melt crystallization garnet would be the first ferromagnesian phase to crystallize by reaction 4.4 in the reverse sense. Biotite crystallized later and occasionally grew around Grt3 grains.

Grt2 rims resorbed by sillimanite, quartz and biotite intergrowths are consistent with reaction 4.3 occurring in the opposite direction during cooling:



The absence of muscovite indicates that the reverse of reaction 4.2 did not take place, suggesting that melt crystallization occurred during cooling in Field I. The preservation of delicate vemicular textures of granitic composition in Domain II indicates that at least the last stage of melt crystallization occurred after deformation.

The homogeneous composition of garnet is attributed to intracrystalline cation diffusional homogenization at high temperatures. Therefore, any potential compositional differences between the three generations of garnet, Grt1, Grt2 and Grt3, have been obliterated by diffusion. The minor increase of X_{Fe} at the rims of garnet and decrease at the rims of adjacent biotite are attributed to retrograde intercrystalline Fe-Mg exchange across grain boundaries prior to reaching Fe-Mg diffusional closure temperatures.

The small plagioclase grains adjacent to garnet are interpreted to represent crystallized melt. This plagioclase is also homogeneous, which is attributed to rapid crystallization during cooling shortly after peak metamorphic conditions were reached.

4.8.4 *P-T* Conditions

The small range of X_{Fe} in garnet cores was plotted along the X_{Fe} isopleths calculated for the Grt + Bt + Sil + Kfs + Qtz + L divariant assemblage (Field I, Fig. 4.5) on the NaKFMASH petrogenetic grid (Fig. 4.11). The parameters used to calculate slopes of contours are described in Spear et al., Figure 5 (1999). The slope of the isopleths indicates that during garnet growth in Field I Fe/Fe+Mg decreases with increasing temperature, whereas during garnet consumption the reverse is true. Therefore these isopleths can be used as a thermometer. The area shaded in dark grey in Figure 4.11 further constrains the *P-T* conditions that produced the regional assemblage, giving a *P-T* range of 6.7 to 10.2 kbar and 780° to 830° C.

Grt2 was formed during prograde metamorphism by reaction 4.3, within Field I and therefore was present during the metamorphic peak. Textural evidence and the relatively high sodic content of plagioclase ($X_{Ab} \sim .69$) suggest that the felsic material adjacent to the garnet represents crystallized melt that formed during cooling. Therefore, assuming that cooling was accompanied by decompression, garnet and plagioclase compositions would give a minimum pressure limit on the metamorphic peak conditions. Based on this assumption, minimum pressure estimates can be calculated using the GASP reaction (see section 4.5).

GASP isopleths were calculated by the TWEEQU v. 2.02 program (Berman, 1991) using two sets of representative garnet and plagioclase compositions (#7Grt-Plg and #9Grt-Plg). See Figure A.1 in Appendix A for TWEEQU generated pressure plots.

The location of the calculated GASP isopleths is shown in Field I of Figure 4.12. The intersection of these isopleths with the Fe/Fe+Mg garnet isopleths defines a range of metamorphic *P-T* conditions of 7.2 to 10.2 kbar and 800°C to 830°C (striped region in Figure 4.12).

4.8.5 Discussion

Textural evidence helps to constrain part of the prograde reaction history of the Tasiuyak paragneiss. The earliest preserved textures of Grt1 with random or foliation-parallel Sil1

inclusions suggest that they were formed during the onset of deformation. The absence of muscovite and the presence of textural domain II (fine-grained matrix) of granitic composition with coarse-grained sillimanite prisms (Sil2) indicate: a) that temperatures surpassed the muscovite-out dehydration melt reaction, and b) the rocks reached the *P-T* field of biotite dehydration melting (Fig. 4.12).

Sil2 is bent and oriented in the foliation and therefore grew during deformation. Grt2 partially or completely replaced Sil2 during the biotite dehydration melting reaction 4.3. The lack of cordierite in these rocks suggests that temperature conditions did not exceed those required for the univariant reaction 4.5 and divariant reaction 4.6 in Field II (Fig. 4.5). In addition, there is evidence that biotite may have been entirely consumed in Field I. In this context, local corrosion of garnet in contact with leucosome suggests partial dissolution of garnet in the melt by reaction 4.4 after the elimination of biotite, whereas small euhedral Grt3 formed during melt crystallization by the same reaction in the opposite direction. Minor local resorption of Grt2 by intergrowths of Sil3, biotite and quartz indicates that relatively short-lived back-reaction of 4.3 occurred during cooling within Field I (Fig. 4.12). In addition, the local preservation of delicate vermicular leucosome patches and euhedral Grt3 grains imply that melt crystallization occurred after deformation.

Garnet, biotite and plagioclase are all relatively homogeneous suggesting that intragranular diffusional homogenization took place at high temperatures. This homogenization could also be the reason why Grt1, Grt2, which typically rims Grt1, and Grt3 have the same composition. The minor Fe/Fe+Mg increase at Grt2 rims and Fe/Fe+Mg decrease at adjacent biotite rims most likely reflect limited retrograde intercrystalline Fe-Mg exchange.

In conclusion, this study has combined mineral assemblages and textures, petrogenetic grids, and bulk and mineral compositions, to determine the range of regional metamorphic *P-T* conditions as 7.2 to 10.2 kbar and 800°C to 830°C (Fig. 4.12).

4.8.5.1 Comparison with previous work

Most of the published metamorphic studies of the Tasiuyak paragneiss were located north of the NPS (Fig. 4.1). The regional metamorphic assemblages of the paragneiss described in these studies is generally the same as the study area. Ermanovics and Van Kranendonk (1998) reported P - T conditions of 510° to 700°C and a pressure of 7 kbar for the Tasiuyak gneiss outside of the Abloviak shear zone. At 7 kbar, these temperature estimates are generally below those required for reaction 4.2 (Fig. 4.12). Therefore, the P - T estimates of Ermanovics and Van Kranendonk (1998) most likely reflect retrograde re-equilibration. P - T conditions reported by Rivers et al. (1996) from the paragneiss within the Abloviak Shear Zone along the Saglek transect (labelled S in Fig. 4.1) are 6 to 7 kbar and 650° to 750°C. These conditions are intermediate between those of Ermanovics and Van Kranendonk (1998) and those estimated in this study. However, interlayered mafic rocks yielded P - T conditions of 10 to 12 kbar and 800°C that indicate equilibration mostly within the kyanite stability field (Fig. 4.12). Rivers et al. (1996) suggested that the lower P - T conditions of the Tasiuyak paragneiss were due to pervasive retrograde re-equilibration since previous work by Mengel and Rivers (1991) had recognized textures related to decompression reactions in the surrounding rocks.

This study has shown that garnet was produced during prograde metamorphism, whereas biotite and plagioclase were products of retrograde metamorphism (crystallization of melt during cooling). In addition, garnet and biotite have re-equilibrated during cooling. Both Ermanovics and Van Kranendonk (1998) and Rivers et al. (1996) used garnet-biotite thermometry. It is proposed that the lower metamorphic temperatures obtained in both studies reflect Fe-Mg exchange closure temperatures rather than peak temperature conditions, as suggested by Rivers et al. (1996) in their study.

Since plagioclase formed by melt crystallization, it is also probable that the pressure estimates in both studies (calculated using the GASP reaction) represent minimum pressures, if cooling was accompanied by decompression. The high- P estimates from the mafic rocks (10-12 kbar) in the study of Rivers et al. (1996) place the paragneiss in the kyanite stability field.

However, they also state that the paragneiss contains sillimanite. In the present study, the paragneiss contains multiple generations of sillimanite indicating that these rocks have undergone both prograde and retrograde metamorphism in the sillimanite stability field.

The present study provides a method of overcoming the limitations of geothermobarometry in high-temperature metapelites by establishing P - T ranges of equilibration based on the interpretation of textures and a relevant petrogenetic grid. Although this approach provides a range of P - T conditions rather than P - T points, it is more rigorous and reliable than geothermobarometry for the study of high temperature rocks.

4.9 CONTACT METAMORPHIC GRADIENT BETWEEN THE TI AND MLP

The Tasiuyak paragneiss between the TI and MLP is characterized by progressive development of cordierite-orthopyroxene-spinel after garnet-biotite-sillimanite. The intensity of overprinting increases towards the MLP suggesting that this intrusion was responsible for producing the contact aureole. Table 4.1 lists the mineral assemblages for samples collected across this contact aureole and their distance from the MLP contact.

4.9.1 Petrography

4.9.1.1 Regional metamorphic assemblage in the study area

The regional metamorphic assemblage is best preserved in samples TL02-66a, b and TL02-80 that were collected adjacent to the TI contact in the northern part of the study area (Fig. 4.2). However, the texture of this assemblage shows a number of differences compared to the “reference” regional assemblage of sample TL01-146, which was discussed in the previous section.

The main differences are: 1) Large, recrystallized quartz grains pseudomorph the original quartz ribbons of Domain I. 2) The quartzofeldspathic minerals of Domain II are coarser grained. 3) In addition, the rims of quartz and feldspars have serrated grain boundaries and show subgrain development; the rims of large feldspars are recrystallized into smaller grains with triple-

junction grain boundaries; and large plagioclase is recrystallized to augen-shaped aggregates. 4) Garnet is highly fractured and partially replaced by biotite and/or plagioclase along grain boundaries and fractures (Pl. 4.15). 5) Sillimanite was not observed. 6) Biotite is more abundant and larger. It occurs in the matrix, generally oriented parallel to the foliation, but is randomly oriented adjacent to garnet rims and fractures (Pl. 4.15).

Sample TL02-80 does not show any development of contact metamorphic phases, whereas samples TL02-66a and -66b show development of symplectic orthopyroxene + cordierite and spinel + cordierite (Pl. 4.16) (see next section).

4.9.1.2 Progressive development of the contact metamorphic assemblage

Contact metamorphism of the regional assemblage has produced new phases of cordierite, orthopyroxene and spinel at the expense of biotite, garnet and sillimanite. At outcrop-scale, cordierite is granular and blue-grey in colour and forms a symplectic overgrowth with orthopyroxene. The cordierite and orthopyroxene symplectite is typically rimmed by orthopyroxene, which may or may not be rimmed by cordierite + spinel symplectic ribbons. These symplectites typically rim garnet, which is progressively replaced towards the MLP contact.

In thin sections, cordierite displays radial sector twinning and contains minuscule inclusions giving it a dusty appearance. Spinel is typically dark green and orthopyroxene exhibits pleochroic colours of green and pink. Progressive breakdown of the regional metamorphic phases to the point of complete replacement can be best seen in the samples taken along Transect 3, where only contact metamorphic phases are present in samples adjacent to the MLP contact.

In samples furthest from this contact, large Grt2 porphyroblasts are typically adjacent to either plagioclase and/or biotite. Samples TL02-79 to -77 show blebs and/or needles of orthopyroxene forming an outer rim at garnet boundaries adjacent to biotite and between biotite, plagioclase and quartz ribbons (Pl. 4.17, 4.19 & 4.20). The orthopyroxene needles are formed at the outermost rim and are perpendicular to grain boundaries, whereas the orthopyroxene blebs

formed between the needles and the reactant (either garnet or biotite). With decreasing distance towards the MLP contact (TL02-76 to – 73) the grain size of orthopyroxene increases, averaging 50 to 100 μm , at the outer rim of reactant garnet, and biotite disappears from the reactants (Pl. 4.21, Fig. 4.13). However, locally minor amounts of secondary biotite have replaced orthopyroxene. In samples TL02-74 and 73, large orthopyroxene grains have recrystallized forming clusters of polygonal grains (Pl. 4.21).

Inside the orthopyroxene outer rim, Grt2 show progressive consumption forming symplectic cordierite and orthopyroxene. In samples TL02-79 to –77, symplectic cordierite and orthopyroxene developed along garnet grain boundaries and fractures (Pl 4.19, 4.20). Orthopyroxene grains form as very small, wormy projections perpendicular to grain boundaries. Cordierite is anhedral, relatively large and typically contains inclusions of the orthopyroxene worms. Samples TL02-75 to 73 show almost complete to complete consumption of garnet. The symplectite shows progressive formation from rim to core of polygonal cordierite and small isolated orthopyroxene blocks or chains of orthopyroxene blocks (Pl 4.21). In sample TL02-73, minor amounts of garnet were observed rimming coarse-grained orthopyroxene and pyrite adjacent to cordierite. Quartz and biotite inclusions in Grt2 were progressively replaced by coarse-grained, orthopyroxene. In samples closest to the MLP contact, large clusters of orthopyroxene grains were found within the symplectic cordierite and orthopyroxene and are assumed to represent complete replacement of quartz and biotite inclusions. Samples TL02-77 and –78 contain still recognizable Grt1 surrounded by Grt2 (see section 4.8.1). Grt1 (with Sil1 inclusions) is partially replaced by symplectic cordierite and spinel, which in turn is enclosed by symplectic cordierite and orthopyroxene (Pl. 4.20). The texture of the symplectic cordierite and spinel is described below.

Grt2 associated with coarse-grained Sil2 is progressively replaced by symplectic cordierite + spinel. In general, Sil2 and associated Grt2 have typically undergone complete replacement even in samples furthest from the contact. However, sample TL02-77 does contain relict Grt2 and associated Sil2. Grt2 is preserved adjacent to the quartzofeldspathic matrix and a

cluster of cordierite grains replaces the other side (Pl. 4.19). Adjacent to the cordierite mass is symplectic cordierite + spinel. Regions of Sil₂ are partially replaced by symplectic cordierite + spinel (Pl. 4.19). Samples TL02-78 through -73 contain elongate pods of symplectic cordierite + spinel with or without a rim of massive cordierite. These pods are generally surrounded by polygonal plagioclase (Pl. 4.18). In the cordierite + spinel symplectite, spinel formed as small spheres or vermicular worms and cordierite is interstitial. The spinel worms delineate interlocking networks and/or radiate from the core as well as forming a thin continuous outer rim. A minor amount of tiny, colourless, spheroids with high relief were observed in the cordierite + spinel symplectite and are assumed to be corundum. In the rims of massive cordierite, grains are typically polygonal. In samples TL02-74 and -73 small blocks and chains of spherical spinel replace spinel worms.

The matrix minerals also show changes toward the contact of the MLP. Furthest from this contact, quartz ribbons are observed. Domain II generally consists of anhedral feldspars and quartz with serrated grain boundaries and all minerals show subgrain development (Pl. 4.20b). K-feldspar porphyroblasts are very coarse-grained (2 to 4 mm, one grain was ~ 1 cm), mesoperthitic and exhibits subgrain development along serrated grain boundaries.

Within a kilometre of the MLP contact, quartz ribbons are replaced by clusters of large, anhedral quartz. Domain II is coarser grained and is generally granoblastic (Pl. 4.18, 4.21b). The size of K-feldspar porphyroblasts decreases (.5 - 1 mm), and exsolution lamellae are scarcely seen. In addition, pervasive vermicular plagioclase and quartz are found between plagioclase - K-feldspar and K-feldspar - K-feldspar grain boundaries in all samples throughout Transect 3 (Pl. 4.18).

In addition, samples TL02-66a and -66b (see previous section), collected within a few metres from the TI, exhibit incipient development of symplectic orthopyroxene and cordierite (~ 10 µm wide) between garnet and biotite. Sample TL02-66b also contains fully developed pods of symplectic cordierite and spinel (Pl. 4.16).

4.9.2 Bulk Composition

Bulk compositions are represented on the AFM diagram in Figure 4.4 with analytical data reported in Table 4.2. This includes samples TL02-80, -66A and -66B from the regional metamorphic assemblage in the study area and the contact metamorphic assemblage samples TL02-73 to -79 (except for TL02-76, which showed substantial alteration).

All samples had similar X_{Fe} values ranging from .53 to .65. Sample TL02-80 had the highest X_{Fe} , which ranged from .63 to .65. Al index of all the samples had a large range from .26 to .60. Samples TL02-73 to -79 ranged from .44 to .60 and generally showed that the Al index increased towards the contact. Petrographic evidence revealed that sample sections TL02-73 to -77 generally contained more symplectic spinel + cordierite (replacing sillimanite) than -78 and -79. Therefore the amount of original sillimanite in the samples was interpreted as the controlling factor for the increase in Al. Sample TL02-80 had the lowest Al index ranging from .26 to .33. The sections from sample TL02-80 were of poor quality because of exposed epoxy due to plucking out of garnet. However, since garnet has more [Fe+Mg] than Al, the Al index calculated for these sections is interpreted as a maximum value.

On the AFM diagram in Figure 4.4, bulk composition of samples TL02-66A and TL02-66B overlap with those of samples TL01-146, TL02-78 and -79, whereas the bulk composition of TL02-80 has the lowest Al index and the highest F values. The bulk composition of samples TL02-73 to -79 form a linear array with a range of Al index and have the lowest F values when compared to samples TL01-146, TL02-66 and -80.

4.9.3 Mineral Chemistry of Sample TL01-147

Sample TL01-147 was collected adjacent to the TI contact along Transect 2 (Fig. 4.2) and contains contact metamorphic phases and reactant garnet. Analytical data for cordierite, orthopyroxene, plagioclase and garnet are located in Table A.2 of Appendix A. Results of this sample are reported below and were used to constrain mineral compositions for AFM diagrams in Figure 4.14.

4.9.3.1 Cordierite

Analytical transects were conducted across two regions of symplectic cordierite and orthopyroxene (Fig. 4.13). Cordierite is Fe-rich with X_{Fe} ranging from .43 to .48 (transect 1) and from .46 to .49 (transect 2) (Fig. 4.15a, b). X_{Fe} increases at rims adjacent to symplectic orthopyroxene worms and towards coarse-grained orthopyroxene in the outer rim (point B in Fig. 4.15a). At the outer margin of the corona, cordierite locally shows a slight decrease of X_{Fe} towards the quartzofeldspathic matrix (point D in Fig. 4.15a, b).

In the core of the symplectic cordierite-orthopyroxene pod of Transect 1 there is relict garnet, 250 and 350 μm wide. The composition of this garnet is: X_{Alm} .81, X_{Prp} .13, X_{Grs} .02, X_{Sps} .03 and X_{Fe} of .86. The cordierite analyses from Transect 1 show a decrease of X_{Fe} , from .47 down to 0.42, toward the garnet rim (Fig. 4.15a). In addition, spot analyses of cordierite rims adjacent to the relict garnet are also characterized by relatively low X_{Fe} (0.43 and 0.44).

4.9.3.2 Orthopyroxene

Three large orthopyroxene grains, Opx1, Opx2 and Opx3, which rim the symplectic cordierite + orthopyroxene pod and six symplectic orthopyroxene grains were analyzed (Fig. 4.13). The Opx1 grain displays a decrease of X_{Fe} from core (.68) to rim adjacent to cordierite (.63), whereas Opx2 and Opx3 are relatively homogenous, X_{Fe} = .66 to .67 (Fig. 4.16a-c). Al_2O_3 ranges between 4.0 and 5.1 with most values clustering between 4.5 and 4.9 (Fig. 4.16d). Opx1 and Opx3 decrease in Al_2O_3 towards the rim, whereas Opx2 is homogenous in terms of Al_2O_3 .

Most analyses of symplectic orthopyroxene grains were of poor quality due to the small size of the grains. The high-quality analyses of these grains show that X_{Fe} (.66 to .68) falls within the same range as X_{Fe} of the large orthopyroxene, whereas Al_2O_3 of the symplectic orthopyroxene ranges from 3.6 to 5.6.

4.9.3.3 Plagioclase

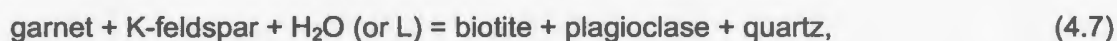
Three large plagioclase grains, Plg1, Plg2 and Plg3, adjacent to the corona were analyzed along transects perpendicular to corona boundaries (Fig. 4.13). The composition of these grains falls in the range of X_{Ab} .68 - .72, X_{An} .27 - .30 and X_{Or} .003 - .018, with the exception of a core analysis of Plg1 that exhibits higher X_{Ab} of .77 (X_{An} .22) (Fig. 4.17a-c). In general, all grains show a slight X_{An} increase towards the rims.

4.9.4 Interpretation

4.9.4.1 Regional and contact metamorphic assemblage of the Tasiuyak paragneiss in the northern part of the study area

Coarsening and recrystallization of matrix minerals indicates that these rocks have been subjected to static recrystallization. The augen-shaped plagioclase mats are interpreted as recrystallized plagioclase porphyroblasts like those observed in the regional assemblage of sample TL01-146.

The randomly oriented biotite aggregates that replaced garnet indicate that these rocks were subjected to rehydration, either by the introduction of water or melt (+ H₂O). There is no clear evidence to discern how rehydration occurred. However the pervasive fractures in garnet may have been formed during fluid influx. The production of biotite and plagioclase from garnet are consistent with the multivariant reaction:

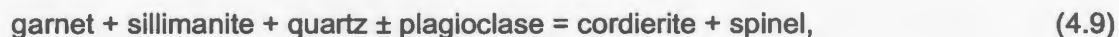


which is pressure sensitive and requires decompression (Vielzeuf and Schmidt, 2001).

Samples TL02-66a and -66b, collected less than a metre from the TI contact, show incipient development of symplectic cordierite + orthopyroxene and TL02-66b also contains pods of symplectic cordierite + spinel. These symplectic assemblages are interpreted to be the result of the discontinuous NaKFMASH reactions (Fig. 4.14):



and,

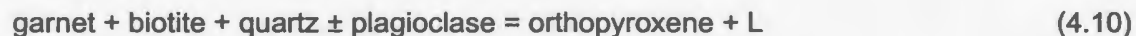


and the bulk composition of these samples fall within the appropriate fields of mineral assemblages (Fig. 4.14).

Sample TL02-80, collected ~ 20 m from the contact of the TI, does not contain contact metamorphic assemblages even though the bulk composition falls within the appropriate fields of contact mineral assemblages (Fig. 4.14). This suggests that samples TL02-66a and -66b underwent contact metamorphism during intrusion of the TI but that the thermal effects were minimal. These rocks were probably also affected by the contact metamorphism produced by the intrusion of the MLP. However, it is suggested that during intrusion of the MLP, temperature gradients in this location were not high enough to produce contact metamorphic assemblages but may have caused static recrystallization. The possible reasons why the TI did not produce a major contact metamorphic affect on these rocks like the MLP are discussed later.

4.9.4.2 Contact metamorphic assemblage

Samples furthest from the MLP contact show local replacement of Grt2 rim and adjacent biotite by coarse-grained orthopyroxene. This is interpreted to represent the continuous NaKFMASH reaction in Field II (Fig. 4.14), where:



The AFM diagram for Field II shows that the bulk composition of the contact metamorphic samples (Fig. 4.14, black dots) does not lie within the triangle for the assemblage Grt-Opx-Bt. However, garnet and biotite rims that are replaced by orthopyroxene likely represent a bulk

composition that is close to the Grt-Bt tie line, which makes this reaction possible in this restricted microtextural domain.

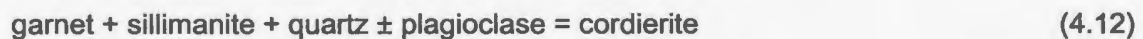
It is also proposed that the rocks closer to the MLP contact (TL02-73 to -78) underwent the higher temperature (than Field II, reaction 4.10 in Fig. 4.14) discontinuous reaction 4.8:



Once biotite is eliminated or isolated from garnet by a continuous orthopyroxene corona (the product of reaction 4.10), further development of cordierite + orthopyroxene symplectite within the garnet domain may occur in Field III and IV (Fig. 4.14) by the continuous reaction:



The replacement of Grt1 (+ Sil1 inclusions) and Grt2 associated with coarse-grained Sil2 typically forms pods of symplectitic cordierite + spinel that may or may not be rimmed by cordierite. This outer cordierite rim is probably the product of the continuous reaction in Fields II and III, where:



The symplectitic cordierite + spinel is the product of the discontinuous reaction 4.9 (Fig. 4.14):



Grt1, and Grt2 associated with trains of Sil2 are smaller than the Grt2 porphyroblasts. Therefore, it is proposed that garnet and associated sillimanite were quickly consumed during

reaction 4.9, before Grt2 porphyroblasts were completely replaced by symplectic cordierite + orthopyroxene of reaction 4.11. Pods of cordierite + spinel were rarely seen to contain orthopyroxene near the rims of the pods. This suggests that in a few cases sillimanite was exhausted and residue garnet produced cordierite + orthopyroxene during reaction 4.11.

The vermicular quartz and plagioclase patches observed along both plagioclase - K-feldspar and K-feldspar - K-feldspar grain boundaries are interpreted as crystallized melt. This melt was most likely the result of dehydration melting of biotite related to reactions 4.8, 4.10 and 4.11. The relatively minor amount of biotite in the rock suggests that only small amounts of melt were produced and therefore remained in situ. Further evidence of in situ melt is that biotite is observed replacing orthopyroxene in samples closest to the contact indicating retrogression (rehydration), possibly by reaction 4.8 in the opposite direction. This back-reaction may also be responsible for producing garnet, which replaced orthopyroxene + cordierite in sample TL02-73.

Mineral chemistry indicates that cordierite X_{Fe} decreases toward rims adjacent to garnet and increases at rims adjacent to orthopyroxene. The large orthopyroxene grain labelled Opx1 shows a decrease of X_{Fe} in rims adjacent to cordierite, whereas Opx2 and Opx3 are homogeneous. Garnet X_{Fe} is higher (by $\sim .15$) than the regional metamorphic garnet in sample TL01-146, which is consistent with X_{Fe} increasing by Fe-Mg partitioning during garnet consumption (Spear et al., 1999). Therefore, these results indicate preferential partitioning of Mg into cordierite during consumption of garnet and possible late intercrystalline Fe-Mg exchange between cordierite and orthopyroxene during cooling.

The contact metamorphic assemblages and their textures suggest that a range of metamorphic reactions occurred along a temperature gradient. In the contact aureole surrounding the MLP the range of reactions beginning in Field II (reaction 4.10) and extending into Field IV (reactions 4.8 and 4.11). The contact aureole associated with the TI shows the same range of reactions but only minor development of the contact metamorphic assemblage. Since the contact metamorphic mineral assemblages produced from these reactions appear to occur together, it is proposed that this can be used to further constrain the isobaric P -estimate. At ~ 3 kbar reactions

4.8 and 4.9 intersect and it is likely that the contact metamorphic assemblages were formed at a pressure near the intersection of these two reactions.

Assuming that the reactions occurred during isobaric conditions, Figure 4.18 constrains the possible *P-T* conditions from the petrographic evidence and use of petrogenetic grids. These *P-T* estimates suggest that the contact aureoles of the MLP and TI developed under isobaric *P*-conditions ranging between 3.0 to 4.0 kbar (Fig. 4.18). The ~ 4 km wide contact aureole surrounding the MLP had a temperature gradient ranging from 675°C to at least 850°C, whereas the narrow TI contact aureole probably only raised temperatures from 750° to 825°C, defined by the close proximity of reactions 4.8 and 4.9 (Fig. 4.18).

4.9.5 Discussion

The samples along Transect 3 show progressive development of cordierite + orthopyroxene and cordierite + spinel towards the contact with the MLP, with the exception of sample TL02-80. The bulk composition of this sample falls within the triangle Grt + Bt + Opx in the AFM diagram for Field II (Fig. 4.14). This suggests that, locally, the temperature was insufficient to produce contact metamorphic assemblages for that bulk composition. Therefore the proposed limit of the contact aureole related to the MLP is placed between TL02-79 and -80 (Fig. 4.2). Samples TL02-66a and b, located further north and adjacent to the TI contact, show incipient development of symplectic orthopyroxene + cordierite and spinel + cordierite. This implies that the paragneiss along the TI contact was subjected to thermal overprinting during emplacement. Perturbation of the thermal gradient locally produced a small contact aureole (1 to 20 m) adjacent to the TI contact (too small to show on Fig. 4.2). Outside this aureole the paragneiss underwent partial recrystallization and coarsening of the quartzofeldspathic matrix. At this stage, fracturing and partial replacement of Grt₂ by biotite and plagioclase may have occurred.

The TI did not produce a substantial prograde contact aureole like the MLP. It is assumed that the intrusion temperatures of the TI and MLP would have been similar since both have

comparable (anhydrous) mineralogy, consisting of olivine + pyroxenes + feldspars + quartz. However, the MLP also contains minor amounts of hornblende and biotite. Since the TI did not appear to contain much water in the magma, conduction was most likely the main mechanism by which heat was transferred to the country rocks. This is a sluggish method of heat transfer and may be one of the reasons why this intrusion did not create an extensive contact aureole. Subsequent intrusion of the Pearly Gates anorthosite pluton has obscured the original shape and size of the TI. The contact of the TI dips under the paragneiss and strikes parallel to the paragneiss foliation. This implies that heat from the intrusion could have affected the overlying rocks, however, this does not appear to have been the case. This could suggest that the TI was a small body and cooled relatively quickly.

Another possibility is that the ambient temperature of the host rock was higher at ca. 1360 Ma (age of TI) than the ambient temperatures of between 350° to 450°C (McFarlane et al., 2003) estimated just prior to intrusion of the MLP. If the temperature gradient was insufficient then a major contact aureole would not be expected. Any one factor or a combination of the factors listed above could explain the relatively poor contact metamorphic affects of the TI.

4.9.5.1 Comparison with previous work

In addition to determining the nature and conditions of contact metamorphism of the Tasiuyak paragneiss by the TI and MLP, this study also focused on determining the regional metamorphic assemblage away from temperature disturbances of the NPS intrusions. This provided a better understanding of the 'original' mineral assemblages and the reactions that produced the contact metamorphic assemblages. Berg (1977a, 1977b) did not discuss the regional assemblage of the paragneiss and it appears as though he interpreted garnet as part of an earlier contact metamorphic assemblage (Berg, 1977a). Lee (1987) suggested that a sample north of his study area reflected the regional assemblage of the Tasiuyak paragneiss, but this sample contained orthopyroxene. Orthopyroxene does not appear to be part of the regional assemblage of the pelitic Tasiuyak paragneiss. It is possible that this sample was either another

unit interleaved with the paragneiss, such as the orthopyroxene-bearing meta-tonalite, or the paragneiss was most likely affected by lower temperature contact metamorphism within Field I (Fig. 4.14), where garnet + biotite + quartz formed orthopyroxene.

Lee (1987) and Berg (1977b) calculated isobaric P -estimates of the contact aureole surrounding the MLP and reported 3.5 to 4.5 kbar and 5.3 to 5.6 kbar, respectively. The P -estimates of Lee (1987) are consistent with those determined in this study (3 to 4 kbar), whereas the P -estimate by Berg (1977b) is higher. Berg (1977b) used garnet + cordierite geobarometers and it is possible that the garnet analyzed in this sample ($X_{Fe} = .76$, lower than this study) was in disequilibrium. This would produce a pressure isopleth that is relatively higher than the true pressure. The P -estimates determined by Lee (1987) and in this study suggest that the isobaric P -conditions for the MLP contact aureole fall somewhere in the range of 3.0 to 4.5 kbar.

Estimates of the temperature gradient by Lee (1987) are 600° to 760°C, which are lower than the temperatures determined in this study by using the NaKFMASH petrogenetic grid (675° to at least 850°C). T -estimates in this study are similar to those determined by McFarlane et al. (2003). Their test of Al solubility of orthopyroxene as a viable geothermometer in high-grade rocks provided a thermal gradient across the contact aureole from 700° to 900°C. These temperatures are only slightly higher than the results in this study and may be due to disequilibrium of Al in the phases orthopyroxene and cordierite. Berg (1977b) reported a T -estimate of 780° to 785°C from the one sample collected in this study area and this estimate is consistent with those of this study.

This comparative study of the MLP related contact aureole shows that well-constrained textural evidence, coupled with petrogenetic grids and bulk and mineral compositions can yield reliable P - T estimates. This can be especially useful in assemblages that have not reached equilibrium or have been affected by late Fe-Mg exchange, which limits the effectiveness of thermobarometric studies. This study of the contact metamorphism suggests isobaric conditions between 3 to 4 kbar and a temperature gradient ranging from 675° to at least 850°C to produce the contact metamorphic assemblage cordierite + orthopyroxene + spinel (Fig. 4.18). This study

also recognizes the limited contact metamorphic affects of the T1. Incipient development of cordierite + orthopyroxene + spinel represents similar isobaric *P*-conditions as the MLP (3 to 4 kbar) and a temperature gradient ranging from 675° to 830°C (Fig. 4.18).

4.10 CONTACT METAMORPHISM OF TASIUYAK PARAGNEISS SCREENS IN THE T1

A reconnaissance study was done on samples collected from screens of paragneiss exposed in the T1. These samples, TL02-29, -44 and -48, were used to determine whether the T1 had caused contact metamorphism of these screens. At outcrop-scale these rocks appear to contain the regional metamorphic assemblage of garnet + biotite, but also show 'black specks' along garnet rims and fractures.

4.10.1 Petrography

In thin section, garnet and biotite are partially replaced by spinel + cordierite ± orthopyroxene, which is interpreted as a contact metamorphic assemblage. This assemblage shows a range of development from symplectic textures adjacent to reactants to coarse-grained intergrowths.

Domains I and II (see section 4.8.1) are still recognizable. The quartz ribbons of Domain I have undergone heterogeneous recrystallization between samples. The quartzofeldspathic matrix of Domain II is relatively coarse-grained and K-feldspar grains are perthitic. This domain is almost granoblastic in texture, with both triple-junctions and serrated grain boundaries between relatively equigranular minerals.

Sillimanite is absent from all three samples. Randomly oriented, coarse-grained biotite is located in the matrix and surrounding garnet (Pl. 4.22). The contact metamorphic assemblage of cordierite + spinel ± orthopyroxene replacing garnet + biotite shows some textural differences between samples. In sample TL02-29, garnet and biotite are separated by three successive rims. The first is an inner rim of symplectic spinel + cordierite replacing isolated garnet; the second is a

rim of symplectic spinel + orthopyroxene replacing garnet + biotite (Pl. 4.23); and the third is an outer rim of coarse-grained intergrowths of cordierite + spinel and this spinel may or may not be rimmed by orthopyroxene (Pl. 4.24). Sample TL02-48, however, only contains the coarse-grained intergrowths of cordierite + spinel with spinel rimmed by orthopyroxene (Pl. 4.24).

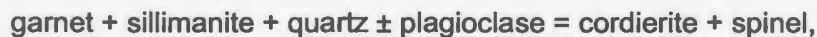
In sample TL02-44, orthopyroxene is absent, and instead, the intergrowths of cordierite + spinel are associated with spinel rimmed by cordierite (Pl. 4.25). In addition, symplectic cordierite + K-feldspar have replaced isolated garnet (Pl. 4.25).

4.10.1.1 Interpretation

The replacement of garnet + biotite by spinel and orthopyroxene and the replacement of garnet by either cordierite + spinel or cordierite + K-feldspar is not clearly understood. Semi-quantitative analyses of spinel show high X_{Fe} (.83) (and low ZnO = .11 - .14%), which is indicative of high temperature spinel (Yardley et al., 1990). It is possible that the contact metamorphic phases cordierite + orthopyroxene in samples TL02-29 and -48 may have been produced by the discontinuous reaction 4.8:



If sillimanite had been present, it is possible that it was completely consumed during the discontinuous reaction 4.9:



and would explain the presence of cordierite + spinel, found in all samples.

Reactions 4.8 and 4.9 would have occurred simultaneously, which may have been possible at around 3 kbar where these univariant reaction lines meet, and could have been controlled by microdomains of specific compositions. Even with these uncertainties, the textural

evidence and the presence of hercynitic spinel (Fe-rich) suggests that these screens of paragneiss have undergone high temperature contact metamorphism during intrusion of the T1.

The partial preservation of regional metamorphic garnet and biotite implies that high temperatures were not sustained for a long period of time, which would indicate quick crystallization of the T1 magma. The preservation of quartz ribbons of Domain I and the almost granoblastic texture of Domain II most likely represent static recrystallization during cooling of the T1.

Although the screens of Tasiuyak paragneiss were not studied in detail, petrographic evidence seems to corroborate the interpretation made in the previous section (4.9.5.1). The contact metamorphic assemblages and textures of these screens and sample TL02-66 seem to indicate that the duration of magmatism, crystallization and cooling of the T1 was short. Therefore it is likely that this intrusive body was relatively small and unable to produce a substantial contact aureole.

4.11 SUMMARY OF CONCLUSIONS

This study shows that the use of an appropriate petrogenetic grid along with bulk composition constraints is a useful tool for determining P - T conditions of high temperature metamorphic rocks. The range of P - T conditions determined here are either consistent or slightly higher than P - T estimates from other metamorphic studies in which geothermobarometry was applied. In cases where other studies had lower T -estimates than determined in this study, the author(s) suggested that these were closure temperatures and not peak P - T conditions. The following points summarize the conclusions of this study:

- The regional metamorphic assemblage preserves evidence of the prograde reaction history. This includes: a) the formation of Grt1 with Sil1 inclusions before the onset of partial melting; b) growth of Sil2 during muscovite dehydration melting; c) growth of Grt2 at the expense of

Sil2 during biotite dehydration melting; and d) limited development of retrograde biotite and Sil3 after garnet during melt crystallization. Peak *P-T* conditions are constrained in the range of 7.2 to 10.2 kbar and 800° to 830°C.

- The intrusion of the TI at ca. 1360 Ma caused incipient development of the contact metamorphic assemblage (cordierite + orthopyroxene + spinel) only in the Tasiuyak paragneiss directly adjacent (< 20 m) to this intrusion. The *P-T* estimate of the contact metamorphism at the TI contact is between 3 and 4 kbar and 775° and 800°C.
- Textural evidence from the paragneiss adjacent to the TI and screen of paragneiss exposed in the TI imply that this intrusive body had a short-lived history of emplacement and crystallization. Since the eastern margin of the TI was intruded by the Pearly Gates Anorthosite pluton, the above-mentioned evidence may indicate that the TI is relatively small.
- Intrusion of the large (~ 1900 km²) MLP at ca. 1322 Ma produced a substantial high-grade metamorphic contact aureole in the Tasiuyak paragneiss, which radiates ~ 4 km from the MLP contact. The temperature gradient along the contact aureole probably ranged from 675°C at the limit of the contact aureole, to at least 850°C at the MLP contact. Contact metamorphism took place under isobaric conditions and the pressure is estimated at between 3 and 4 kbar.

Table 4.1: Mineralogy of samples from the regional and contact metamorphosed Tasiuyak paragneiss.

Sample #	Distance from MLP contact (m)	Regional Metamorphic Assemblage						Contact Metamorphic Assemblage						
		Qtz	Kfs	Pl	Sil	Bt	Grt	Crd	Opx	Spl	Ilm			
TL02-29	screen in Tl	X	X	X		X	X			tr	X	tr		
TL02-44	screen in Tl	X	X	X		X	X				X	tr		
TL02-48	screen in Tl	X	X	X		X	X				X	tr		
TL01-147*	2670	X	X	X							X	X	tr	
TL02-73	71	X	X	X	a						X	X	X	tr
TL02-74	555	X	X	X	a	tr	tr				X	X	X	tr
TL02-75	1107	X	X	X	a	tr	tr				X	X	X	tr
TL02-76	1607	X	X	X	a	X	tr				X	X	X	tr
TL02-77	2571	X	X	X	X	tr	X				X	X	X	tr
TL02-78	3268	X	X	X	X	tr	X				X	X	X	tr
TL02-79	3893	X	X	X	a	X	X				X	X		tr
TL02-80	4696	X	X	X		X	X							tr
TL02-66a	4768	X	X	X		X	X				tr	tr		tr
TL02-66b	4875	X	X	X		X	X				tr	tr	tr	tr
TL01-146	5000	X	X	X	X	X	X						tr	tr

TL01-146 was collected ~ 10 km from the Tessiarsuyungoakh intrusion (N 56°35.991', W 062°50.308')

tr - indicates trace amounts (1% or less) present.

tr - indicates trace amounts (1% or less) present but not related to MLP contact metamorphism.

a - indicates assumed in original regional assemblage but completely consumed by contact assemblage.

* - sample from Transect 2, data collected on microprobe.

Table 4.2: Bulk composition analytical data of Tasiuyak paragneiss sample sections. Both regional and contact assemblages are included, "*" denotes regional assemblages.

OXIDE	TL02-73	TL02-74a	TL02-74b	TL02-75	TL02-77	TL02-78	TL02-79	TL02-80a	TL02-80b	TL02-80c	TL02-86A	TL02-86Bb	TL02-86Bc	TL01-146c	TL01-146d	TL01-146j	TL01-146k
Na ₂ O	1.54	2.49	2.12	2.62	1.88	1.09	3.53	3.78	3.93	4.15	2.44	2.46	2.51	2.41	2.43	2.55	2.09
MgO	4.26	4.62	5.62	4.57	5.66	4.79	1.84	1.84	3.03	2.76	2.19	3.38	2.72	3.08	3.26	1.68	2.16
Al ₂ O ₃	25.38	26.82	25.01	22.04	27.70	17.94	14.92	12.54	13.86	13.69	12.02	18.33	15.50	18.72	17.85	11.79	12.67
SiO ₂	51.98	50.06	47.50	71.06	53.71	56.13	68.97	69.64	57.61	62.37	74.41	57.19	61.69	59.14	62.03	71.18	70.07
P ₂ O ₅	0.05	0.02	0.17	0.04	0.09	0.10	0.04	0.04	0.12	0.00	0.08	0.10	0.00	0.00	0.00	0.08	0.01
S	0.51	0.14	0.23	0.20	0.59	0.45	0.34	0.17	0.23	---	0.21	0.22	---	---	---	0.17	0.14
K ₂ O	3.79	1.92	1.18	2.72	2.74	4.28	1.62	2.03	2.67	2.69	2.11	3.49	2.84	3.30	2.51	2.51	3.44
CaO	0.69	2.34	1.95	1.63	1.69	1.10	2.85	1.21	1.01	0.80	1.37	1.44	1.18	1.48	1.59	1.22	1.33
TiO ₂	0.59	0.55	0.54	0.64	0.66	0.29	0.34	0.57	0.96	0.74	0.57	0.81	0.42	0.47	0.49	0.52	0.43
Cr ₂ O ₃	0.04	0.03	0.06	0.03	0.04	0.05	0.02	0.03	0.06	---	0.05	0.06	---	---	---	0.04	0.01
MnO	0.11	0.09	0.14	0.08	0.15	0.11	0.04	0.08	0.13	0.00	0.07	0.11	0.00	0.00	0.01	0.07	0.06
FeO	9.80	9.49	11.68	9.26	11.81	10.46	4.08	5.98	9.11	8.84	4.90	8.75	7.33	9.20	9.80	4.19	5.75
TOTAL	98.74	98.58	98.19	114.88	108.71	96.78	98.59	97.91	92.72	96.04	100.43	96.34	94.19	97.80	99.77	96.01	98.17
CAT. #																	
Na	21.13	34.19	30.12	30.05	24.08	15.27	45.93	49.81	56.98	57.47	30.92	34.29	34.96	32.88	32.35	33.83	2.29
Mg	45.08	48.73	61.40	40.31	55.78	51.75	18.40	16.63	33.77	29.33	21.35	36.25	29.15	32.37	33.30	17.11	1.84
Al	212.23	223.84	216.17	153.73	215.93	153.20	118.15	100.46	122.25	115.17	92.49	155.35	131.18	155.37	144.38	94.90	8.44
Si	368.73	354.42	348.43	420.44	355.22	406.67	463.32	473.49	431.21	445.09	485.89	411.22	442.97	416.47	425.53	486.27	39.59
P	0.32	0.12	1.04	0.18	0.51	0.64	0.21	0.25	0.74	0.00	0.46	0.06	0.00	0.00	0.00	0.45	0.00
S	6.76	1.90	3.15	2.18	7.36	6.09	4.30	2.20	3.18	---	2.52	2.92	---	---	---	2.15	0.08
K	34.29	17.35	11.03	20.55	23.14	39.52	13.92	17.85	25.50	24.51	17.56	32.00	26.05	29.64	22.00	21.89	2.48
Ca	5.23	17.74	15.32	10.33	11.97	8.52	20.50	8.81	8.07	6.10	9.60	11.08	9.11	11.20	11.71	8.92	0.80
Ti	3.13	2.93	2.97	2.85	3.28	1.57	1.72	2.89	5.43	3.95	2.80	4.38	2.26	2.49	2.54	2.68	0.23
Cr	0.22	0.16	0.35	0.15	0.23	0.28	0.13	0.18	0.36	---	0.27	0.34	---	---	---	0.24	0.01
Mn	0.64	0.55	0.86	0.38	0.82	0.71	0.24	0.47	0.84	0.00	0.41	0.66	0.00	0.00	0.05	0.43	0.03
Fe	58.13	56.21	71.66	45.81	65.30	63.36	22.91	33.99	57.05	52.73	26.74	52.60	43.99	54.18	55.08	23.96	2.72
TOTAL	755.89	758.14	762.50	726.96	763.62	747.58	709.73	708.83	745.38	681.62	691.00	741.71	675.68	680.42	671.84	892.83	58.49
A	0.6023	0.6024	0.5511	0.5271	0.5709	0.4419	0.4884	0.3272	0.2707	0.2575	0.4317	0.4800	0.4628	0.4927	0.4770	0.4408	0.3986
F	0.5632	0.5356	0.5386	0.5319	0.5393	0.5504	0.5546	0.6460	0.6282	0.6426	0.5560	0.5920	0.6014	0.6260	0.6232	0.5834	0.5965
M	0.4368	0.4644	0.4614	0.4681	0.4607	0.4496	0.4454	0.3540	0.3718	0.3574	0.4440	0.4080	0.3986	0.3740	0.3768	0.4166	0.4035

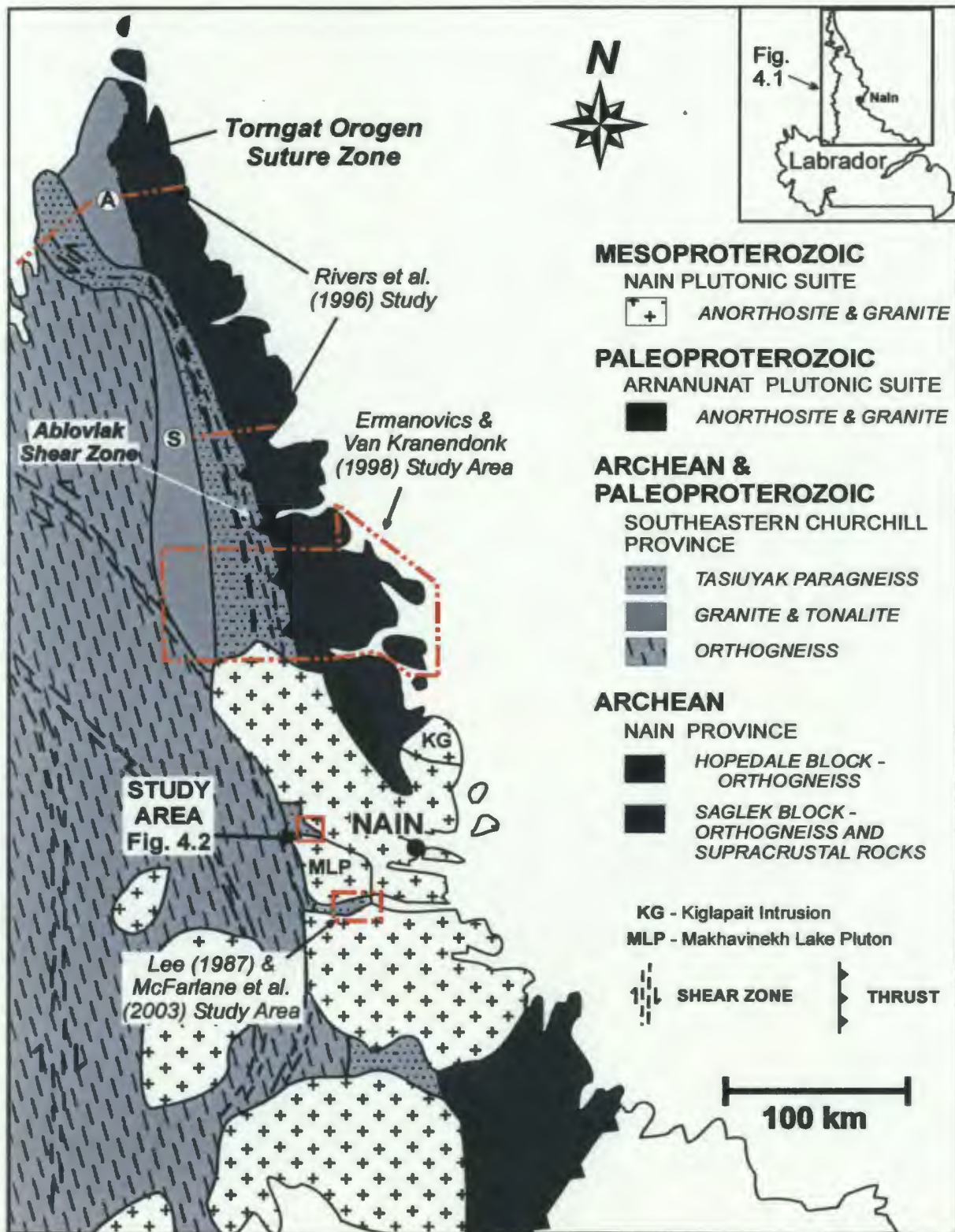


Figure 4.1: Simplified geological map of the major structural and intrusive units in northern Labrador (modified after Hall et al., 1995). Transects labelled A and S represent Abloviak and Saglek transects from the metamorphic study of Rivers et al. (1996).

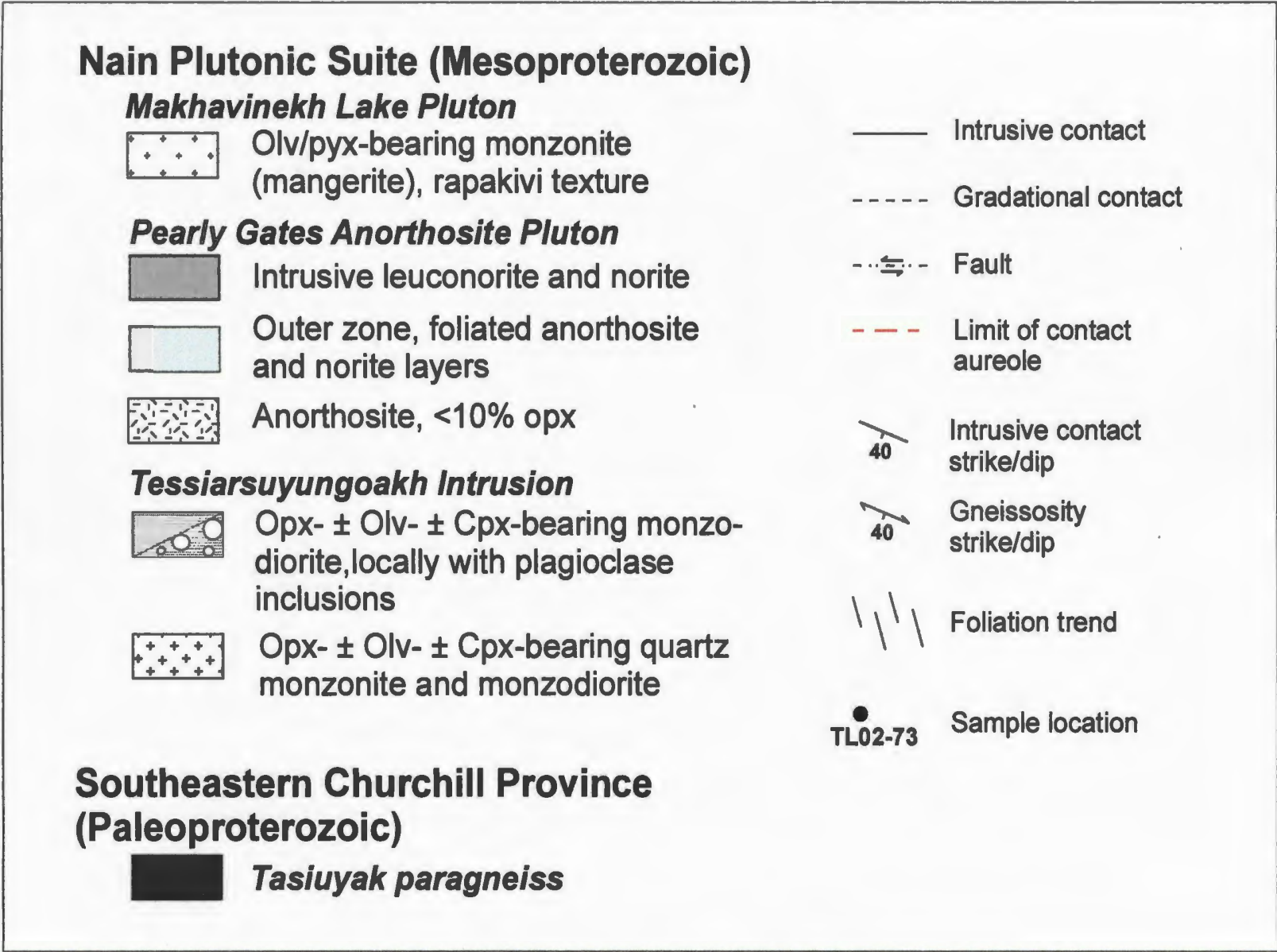


Figure 4.2: Geological map of the study area.

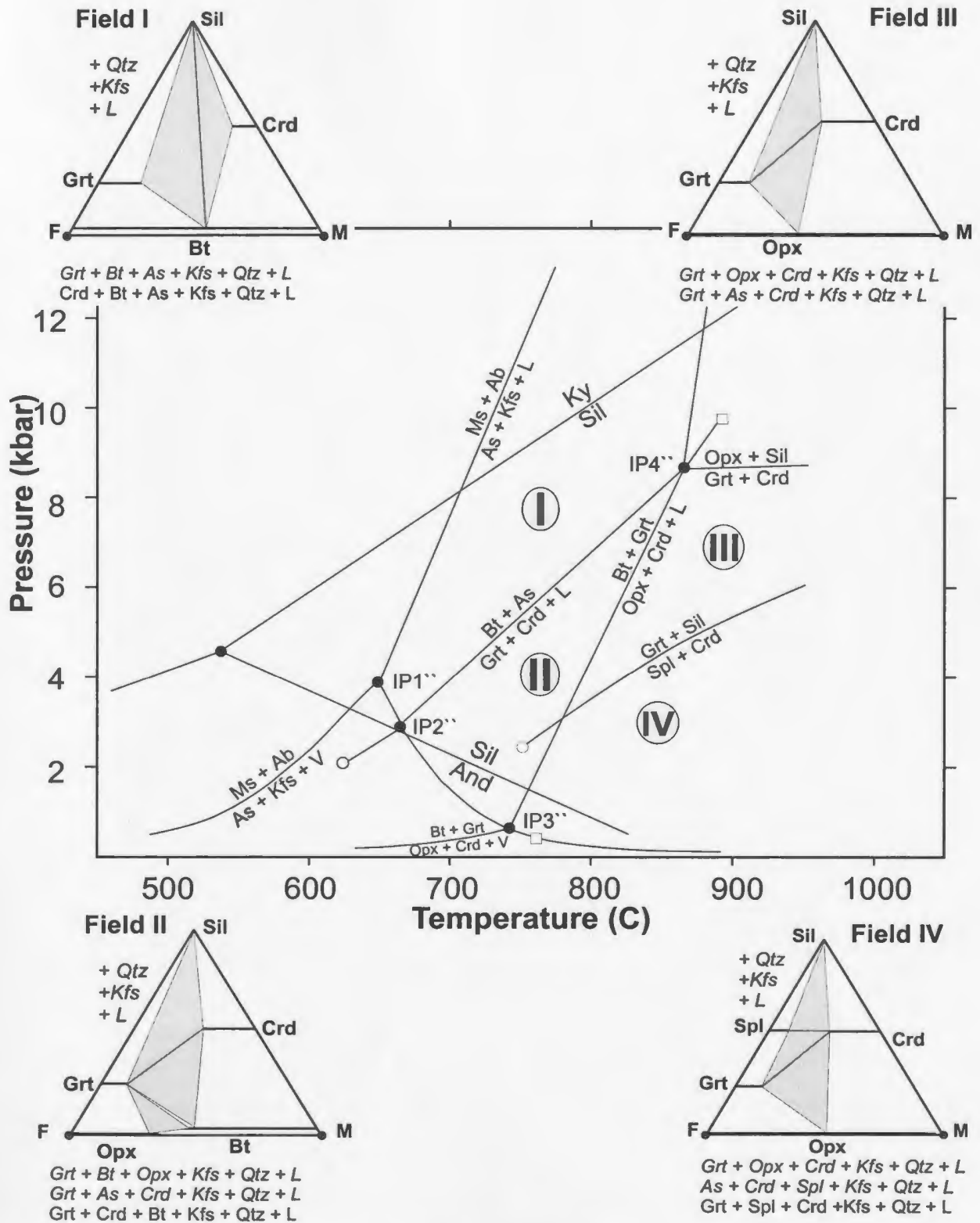


Figure 4.3: Generalized petrogenetic grid of the NaKFMASH system for anatectic pelites (modified after Spear et al., 1999). Divariant melt and dehydration reaction fields are represented by roman numerals I to IV and correlate to AFM diagrams and assemblages with the same notation.

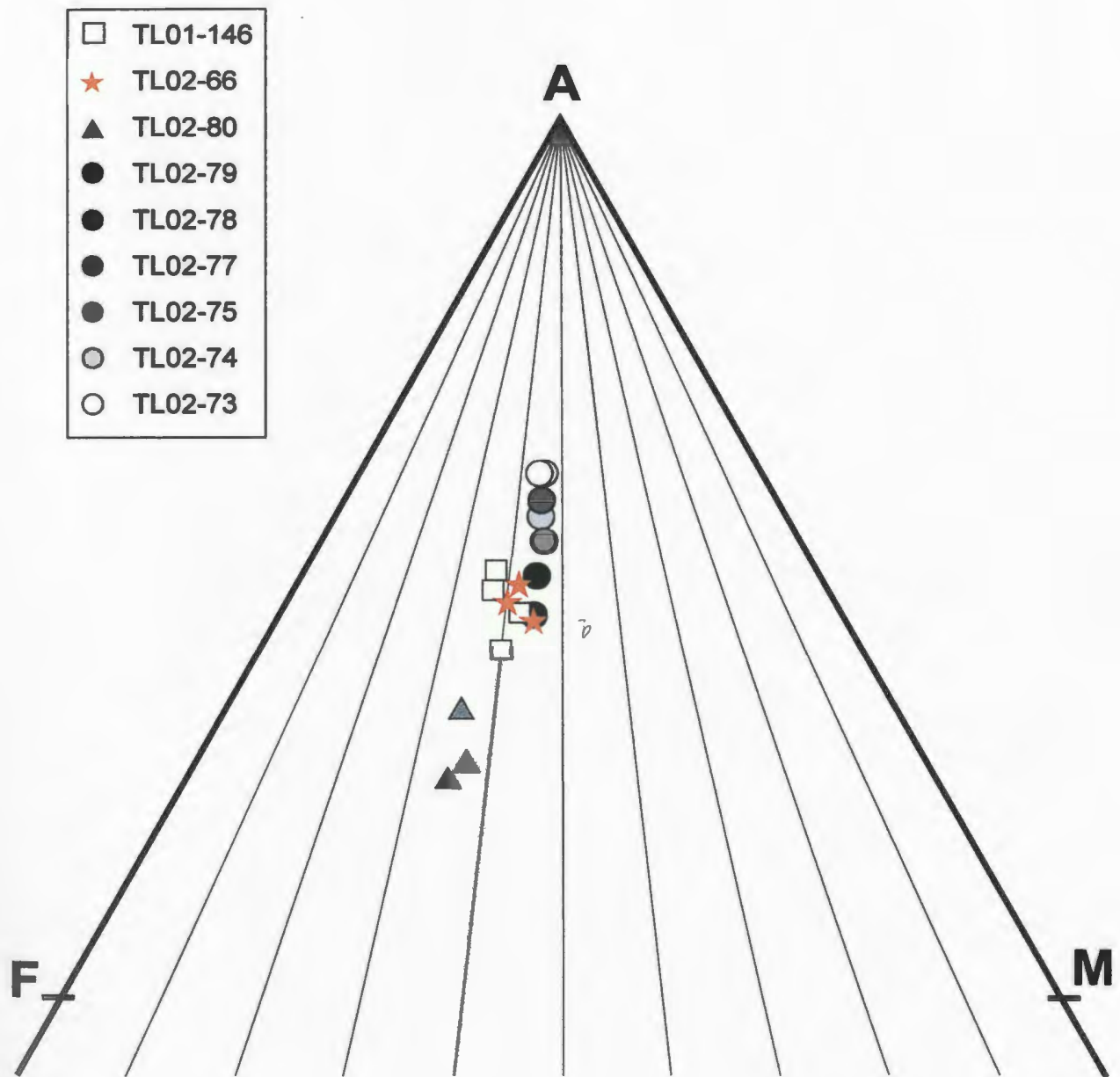


Figure 4.4: Bulk compositions of samples from the Tasiuyak paragneiss plotted on an AFM diagram projected from K-feldspar. White squares represent sample sections TL01-146c,d,j,k (regional assemblage); grey triangles represent sample sections TL02-80a,b,c; red stars represent sample sections TL02-66A and -66Bb,c; circles represent samples TL02-73 to -79 grading from white to black, respectively (contact metamorphic assemblages). Plotted values are recorded in Table 4.2.

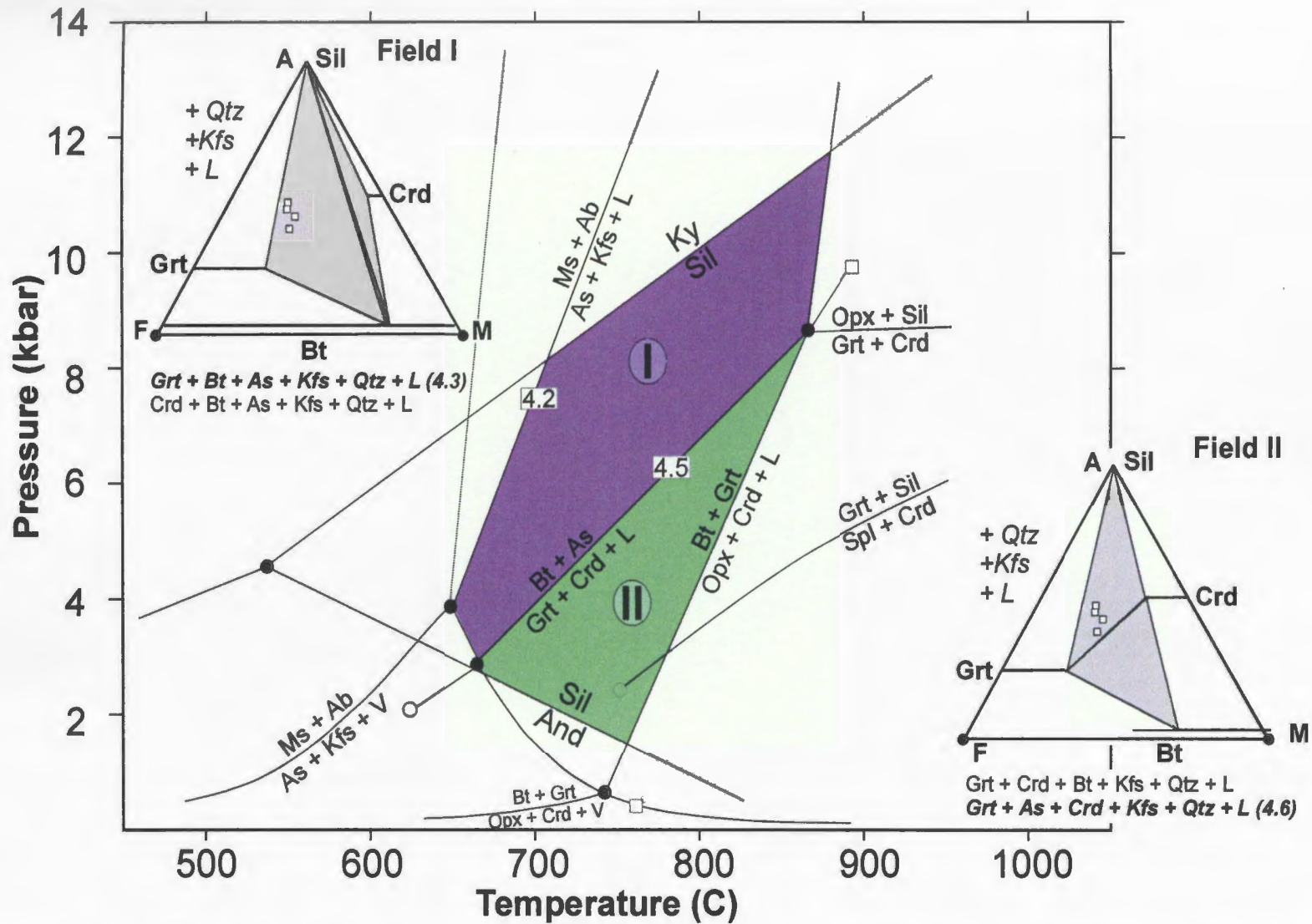


Figure 4.5: Generalized P - T diagram with univariant lines and divariant fields of the NaKFMASH system from Spear et al. (1999). The continuous biotite melt and dehydration reaction Field I is represented in purple. Divariant Field II in pale green represents the reaction $\text{Grt} + \text{As} = \text{Crd} + \text{L}$. Associated AFM mineral composition diagrams show plotted bulk compositions for sample sections TL01-146c, d, j and k. Univariant lines labelled 4.2 and 4.5 correspond to reactions 4.2 and 4.5 referred to in the text.

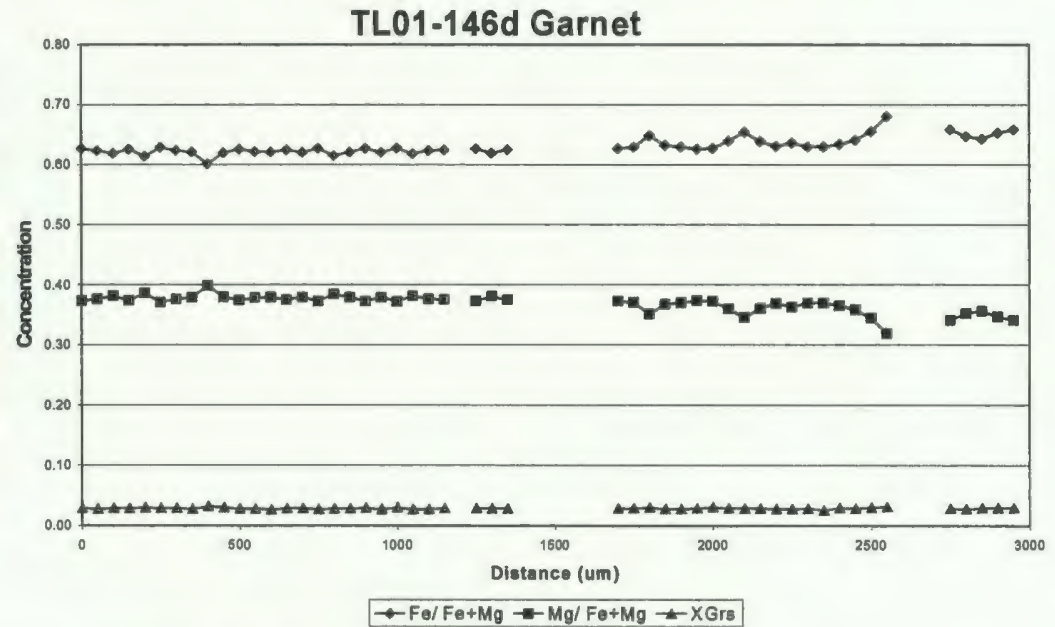
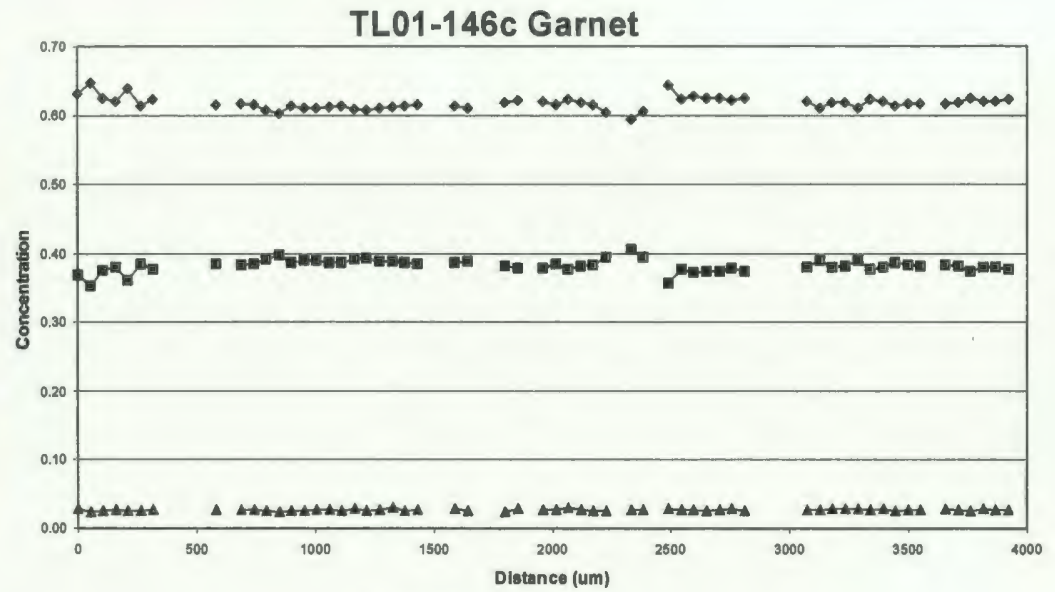
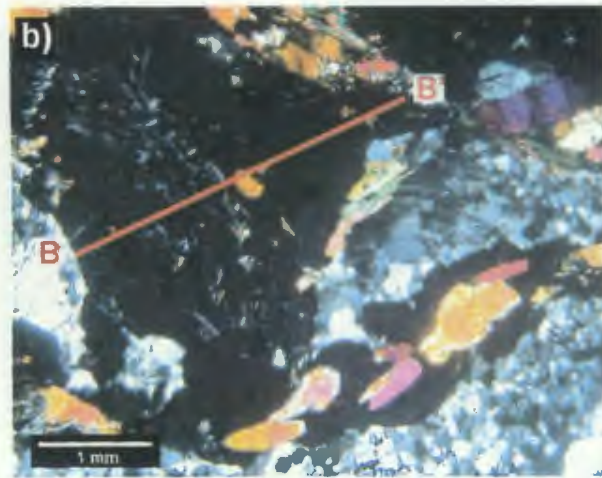
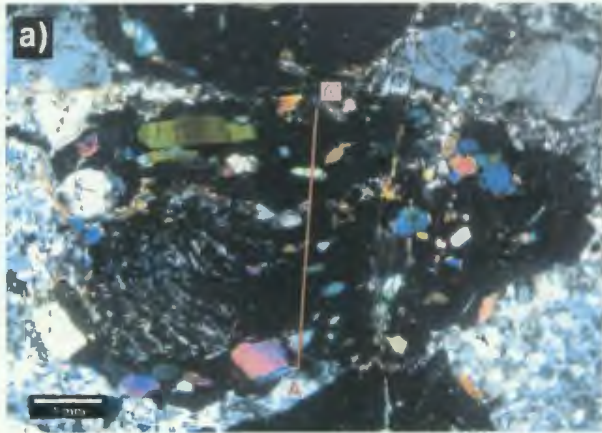


Figure 4.6a, b: Mineral and chemical composition plots for TL01-146c and d garnet.

444

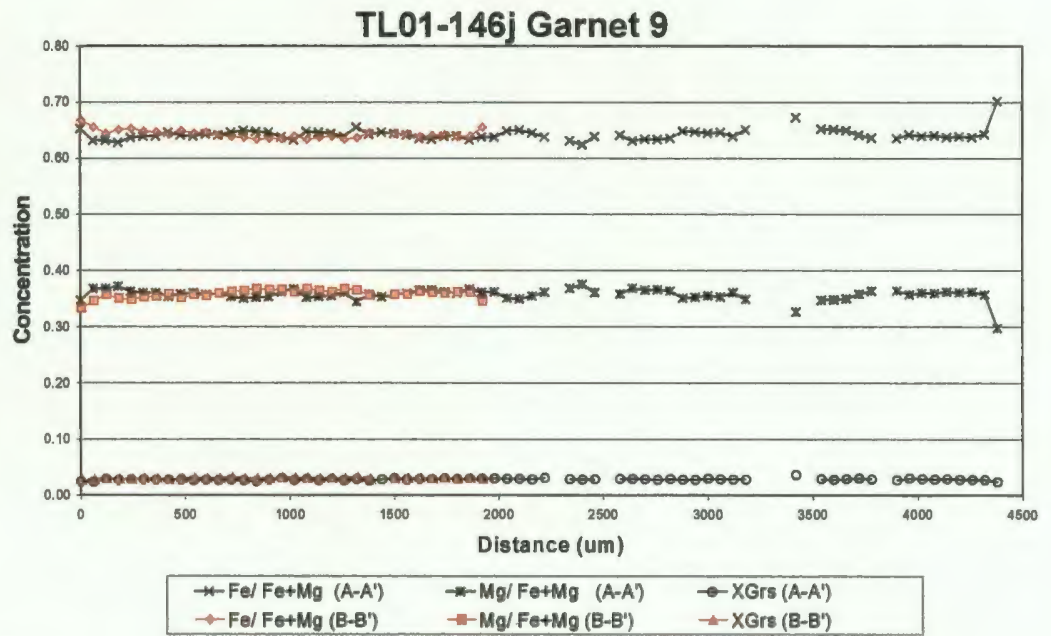
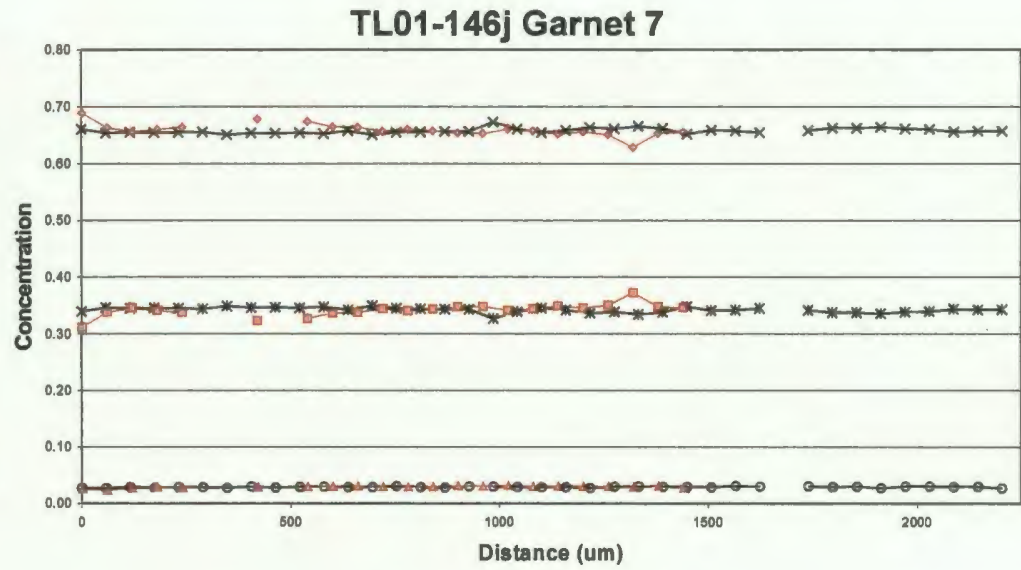
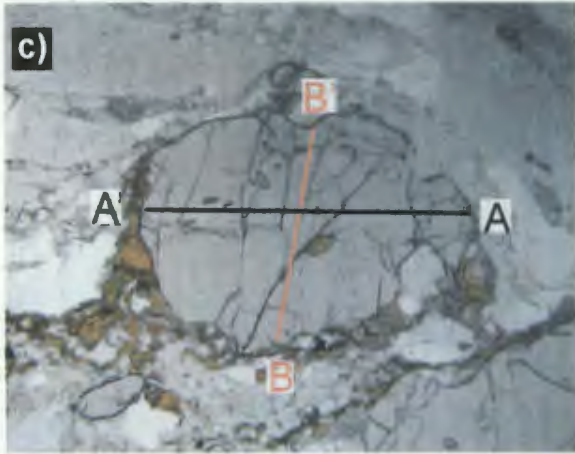


Figure 4.6c, d: Mineral and chemical composition for TL01-146j garnet.

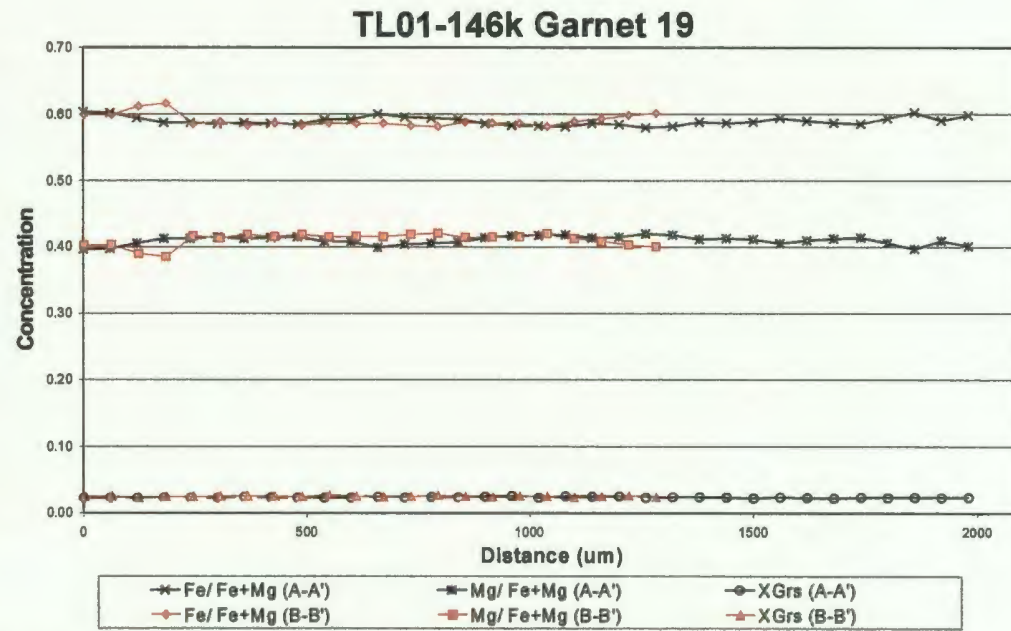
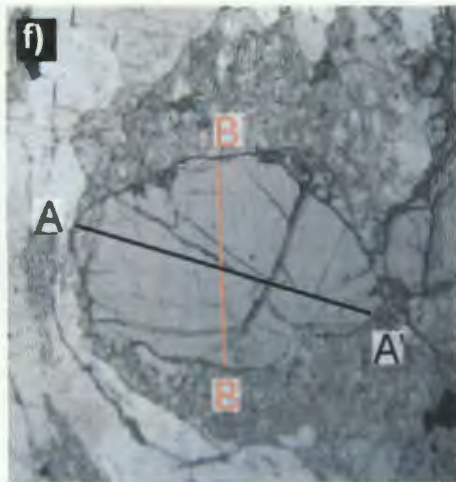
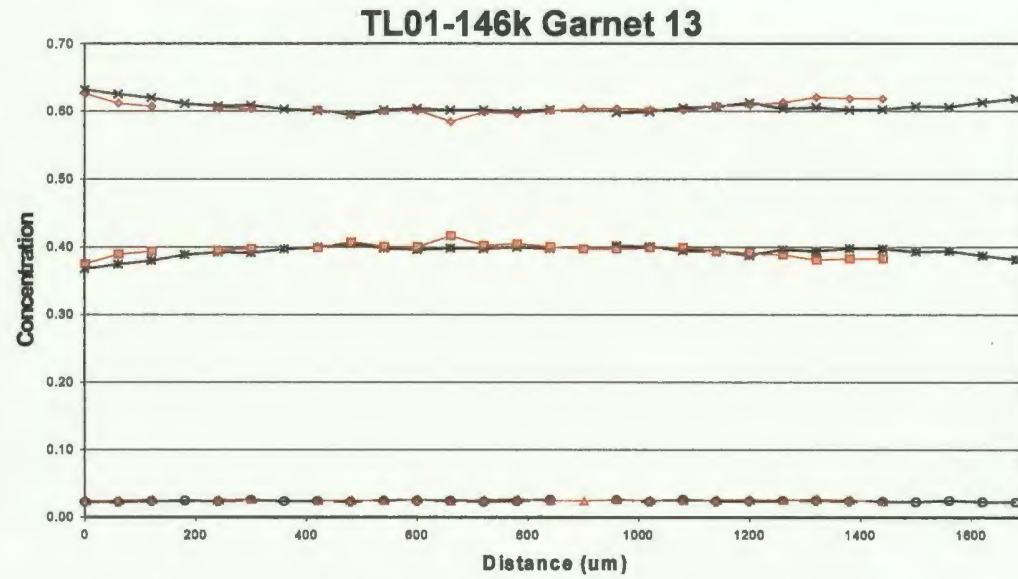
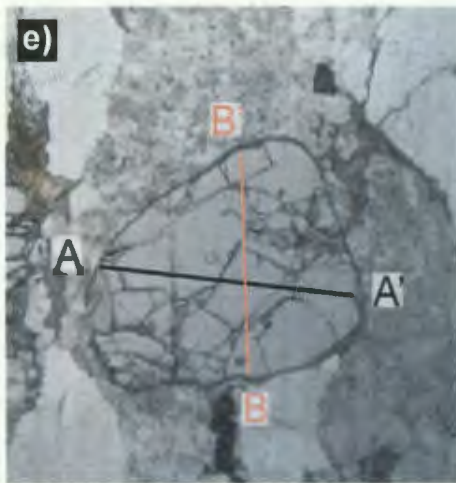


Figure 4.6e, f: Mineral and chemical composition for TL01-146k garnet.

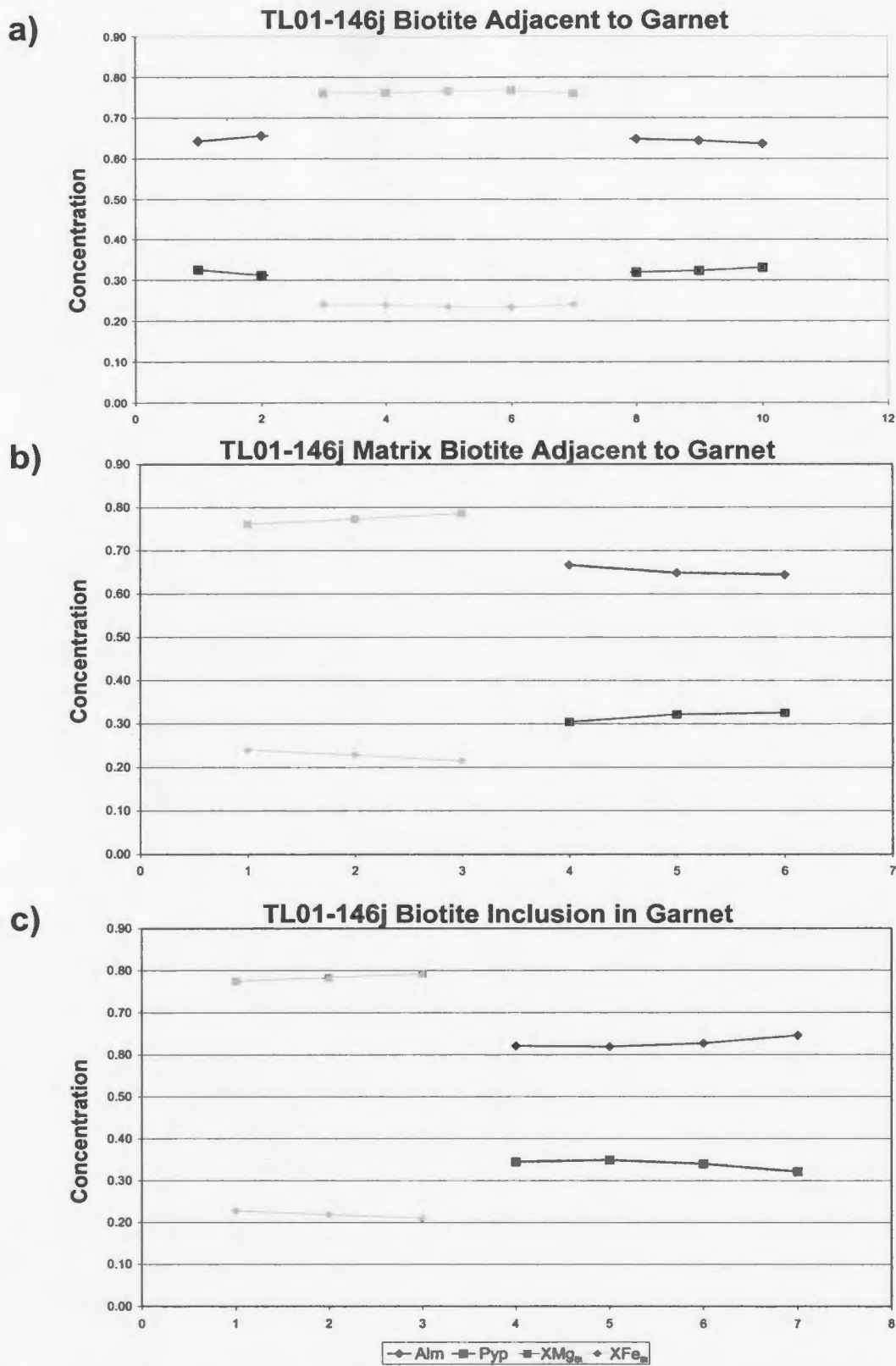


Figure 4.7a-c: Mineral and chemical composition for matrix biotite adjacent to Grt2 and biotite inclusion in Grt2. Black symbols represent almandine and pyrope compositions for garnet and grey symbols represent Fe/Fe+Mg and Mg/Fe+Mg compositions of biotite.

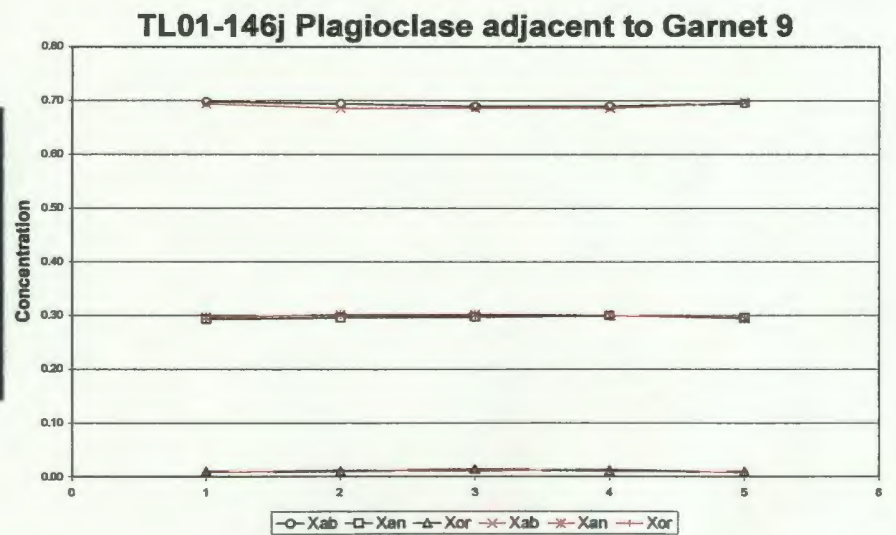
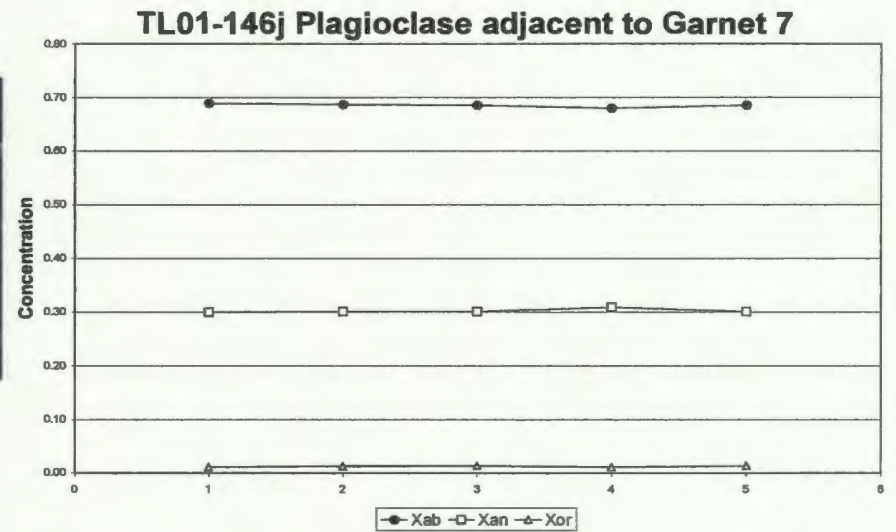
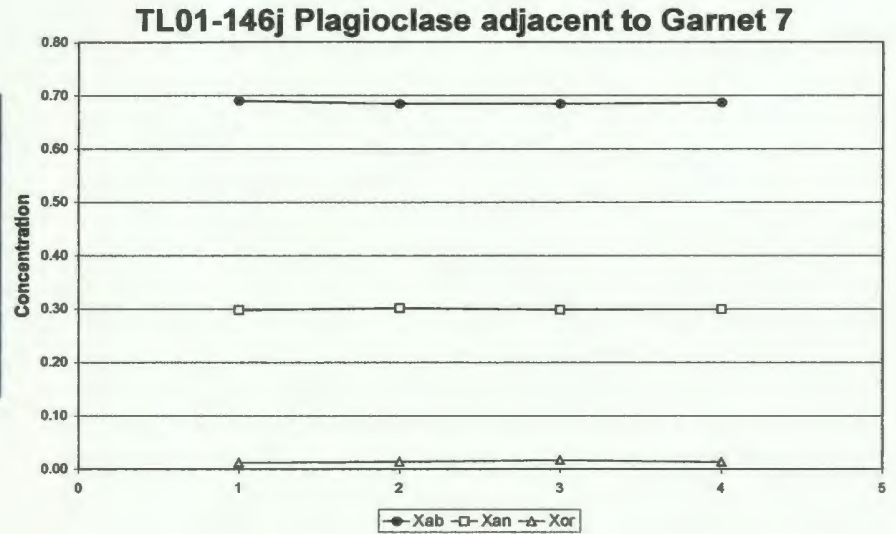


Figure 4.8a-c: Mineral and chemical composition for plagioclase adjacent to garnet.

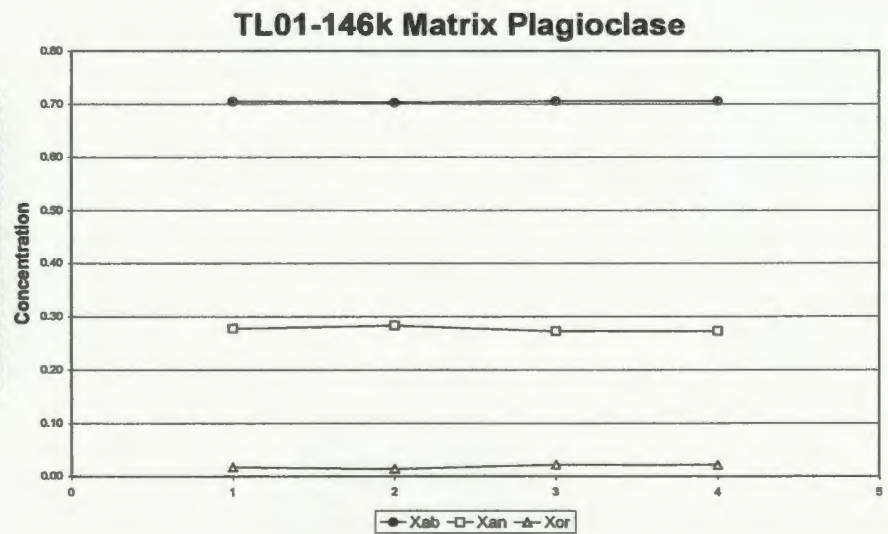
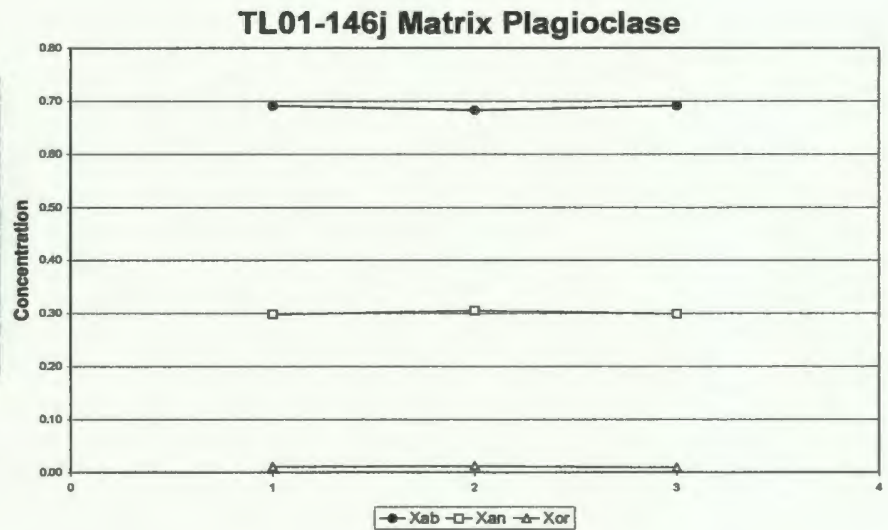
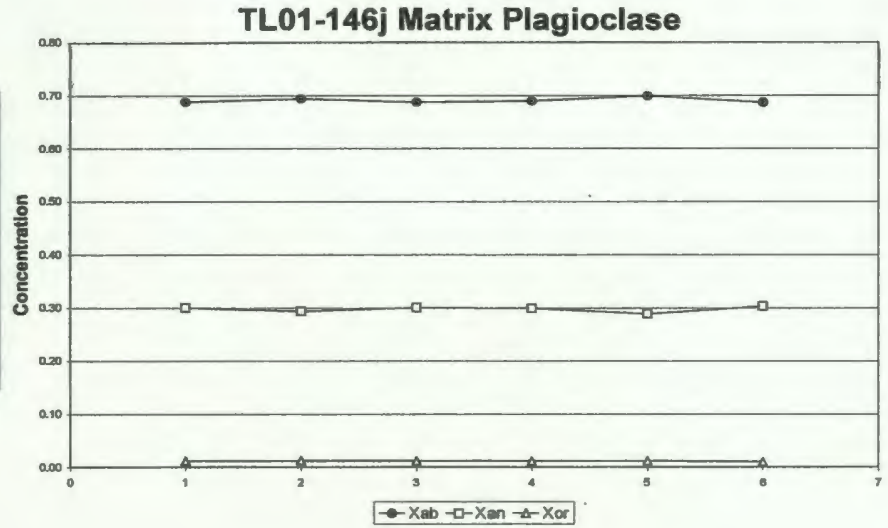


Figure 4.8d-f: Mineral and chemical composition for plagioclase in the quartzfeldspathic matrix.

4-49

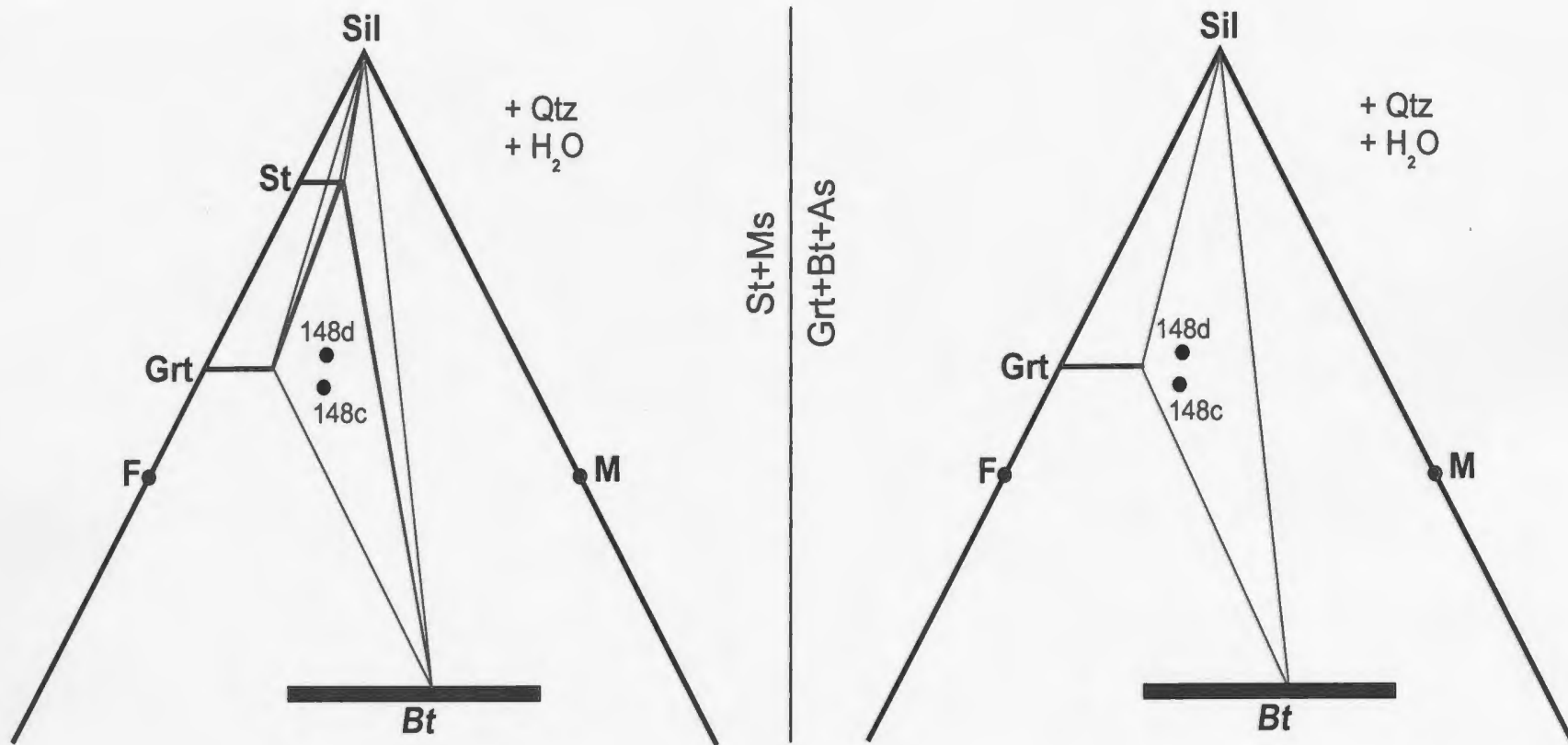


Figure 4.9: AFM diagrams projected from muscovite representing the staurolite-out terminal reaction. (Plotted bulk composition of TL01-146c and 146d only, which contain Sil1).

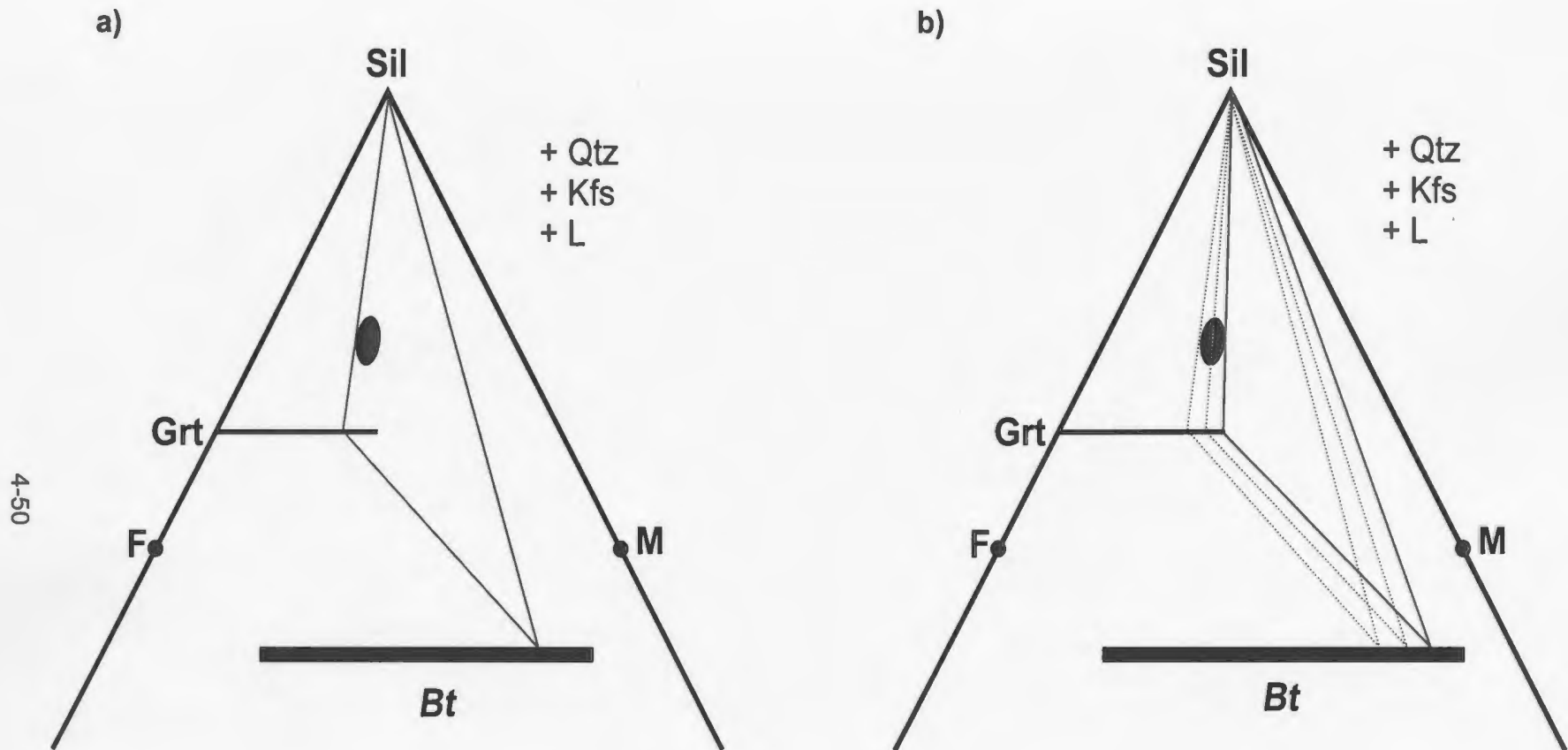


Figure 4.10: AFM diagrams projected from K-feldspar representing the assemblage garnet-sillimanite-biotite. The black area is the bulk composition of TL01-146. a) location of the present Grt-Sil-Bt triangle based on mineral chemistry. b) possible peak mineral compositions if Fe-Mg in garnet and biotite were reset after peak conditions (triangle shifts to the right).

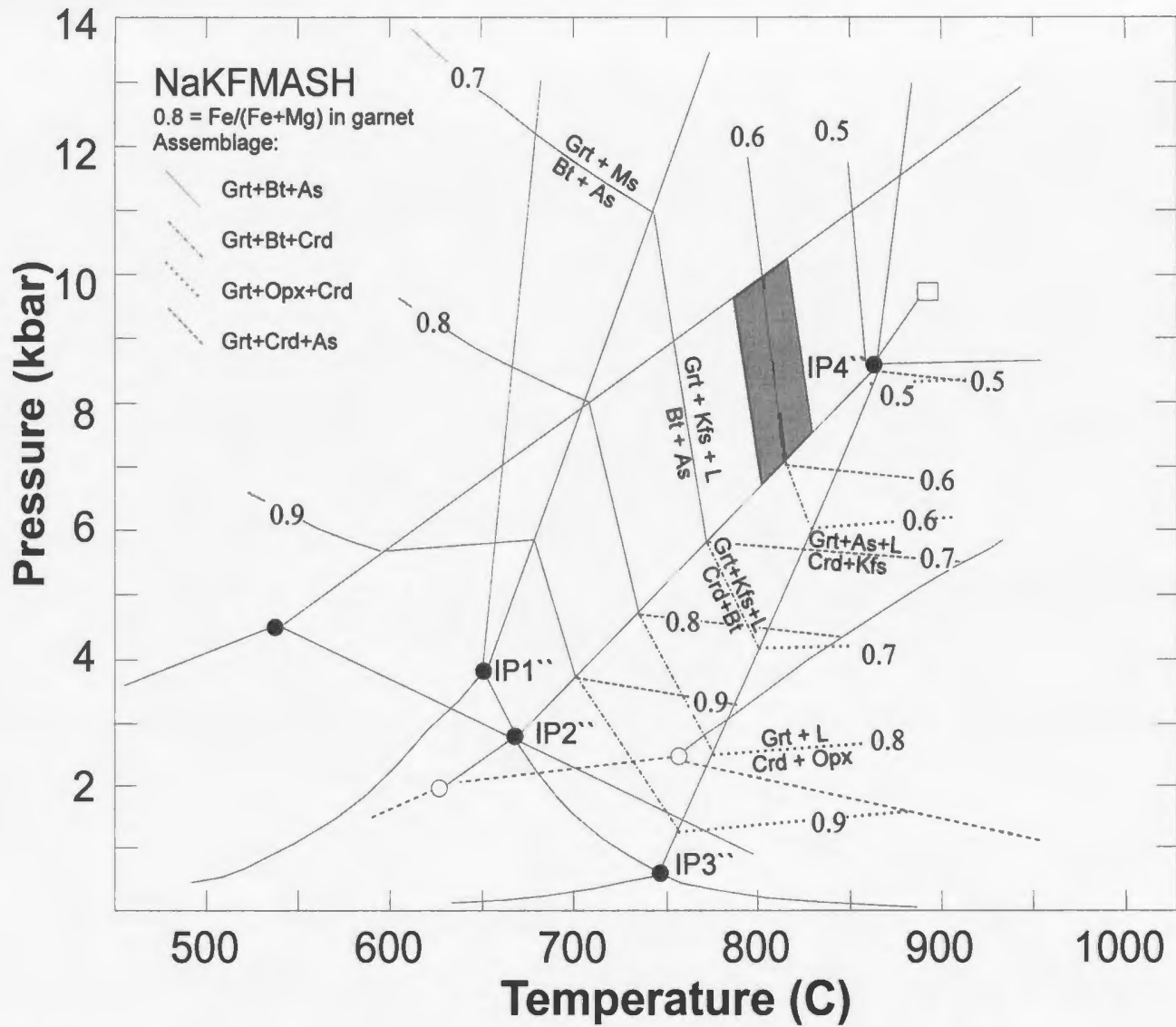


Figure 4.11: Fe/Fe+Mg garnet compositional isopleths plotted on the petrogenetic grid of the NaKFMASH system (modified from Spear et al., 1999). Large dark grey region shows the range in Fe/Fe+Mg compositions for regional metamorphic garnet.

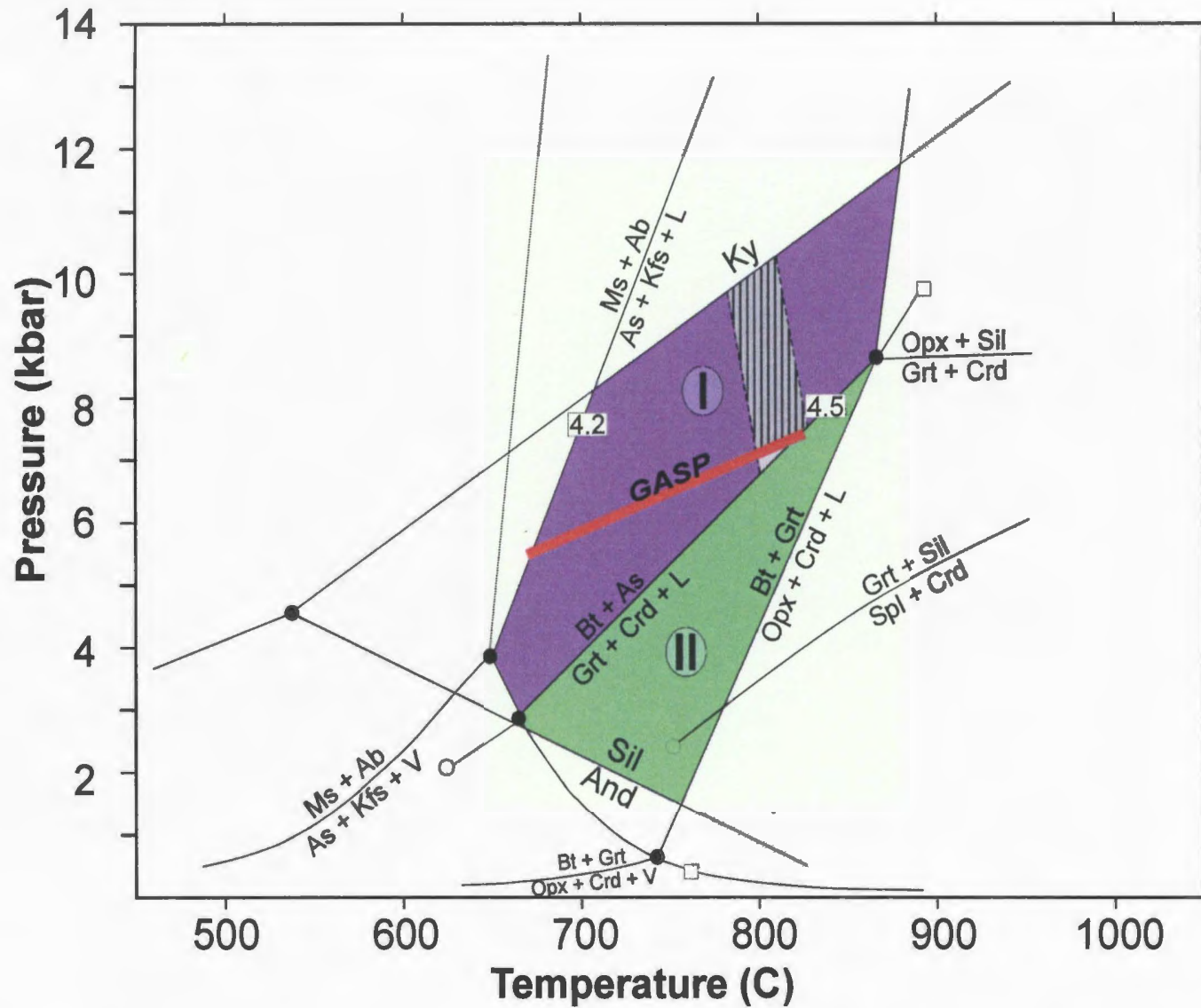


Figure 4.12: NaKFMASH petrogenetic grid from Spear et al. (1999). The regional peak P - T conditions are represented by the striped region, and constrained by the diavariant Field I, plotted GASP geobarometric isopleths and Fe/Fe+Mg garnet isopleths from Figure 4.9.

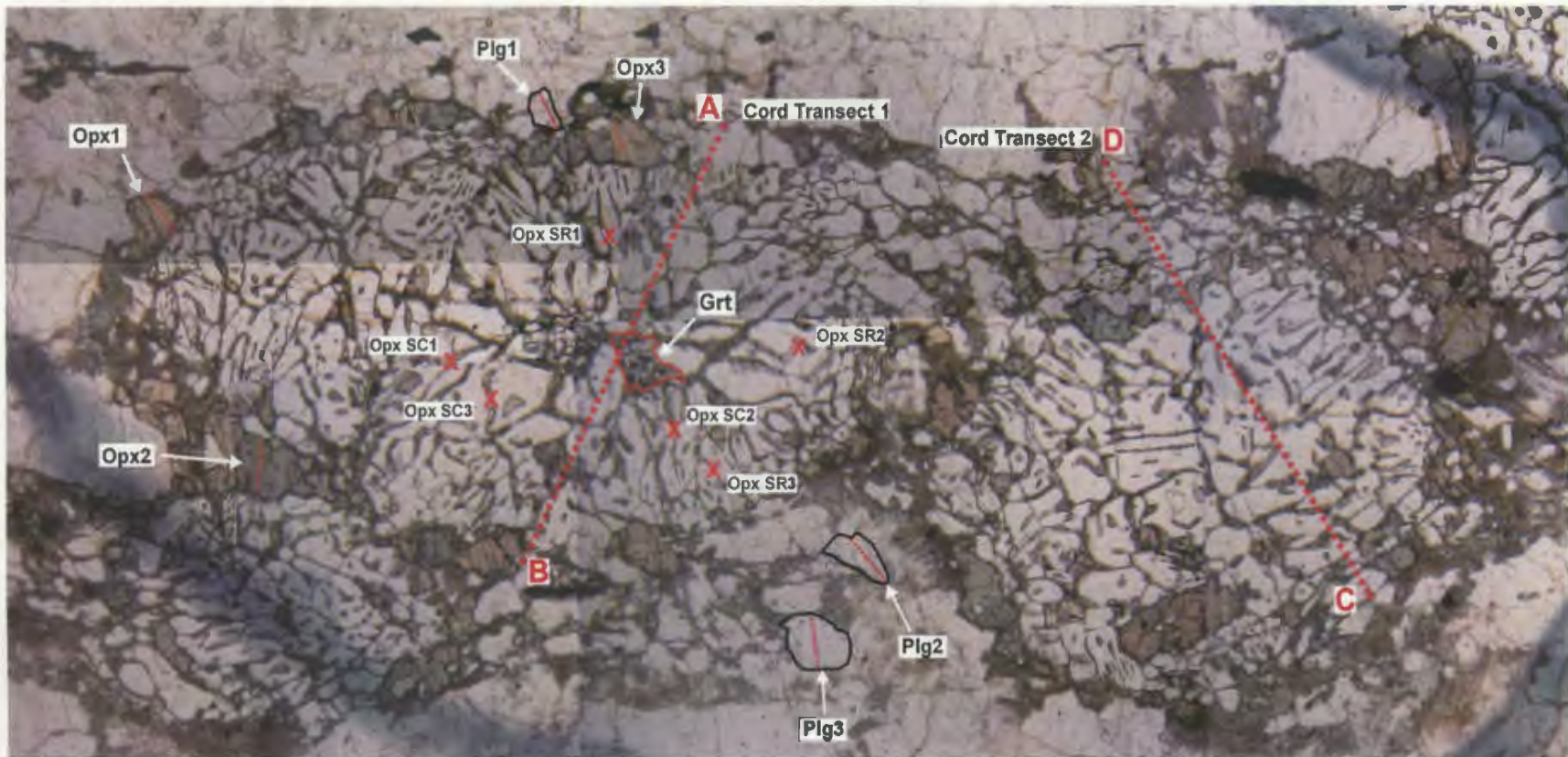


Figure 4.13: Photomicrograph of analyzed cordierite - orthopyroxene symplectites in sample TL01-147 from the contact aureole in the Tasiuyak paragneiss. An "x" represents spot analysis locations of orthopyroxene worms. Dotted lines represent transect locations. Analytical data of labelled minerals and transects are located in Table A.2 of Appendix A.

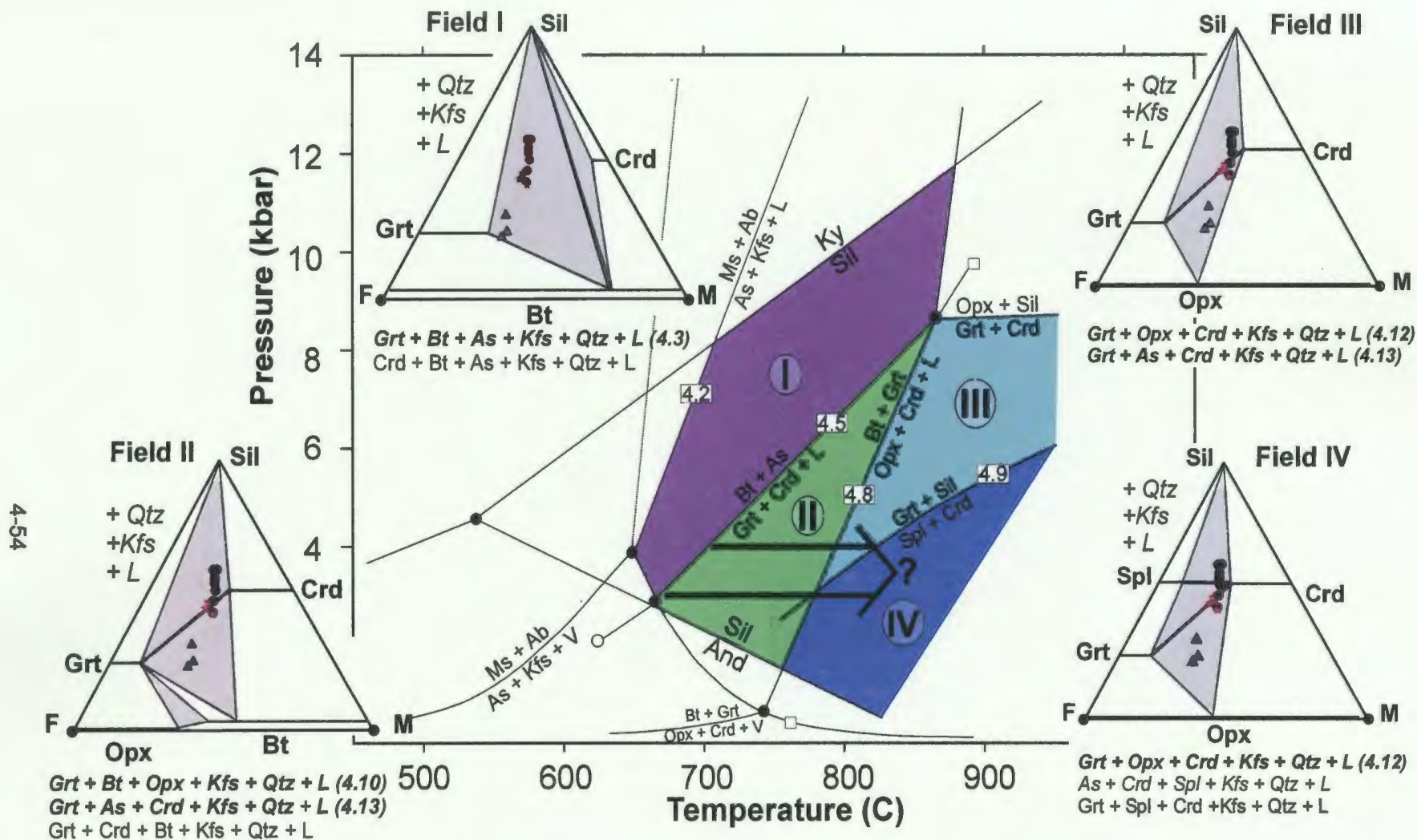


Figure 4.14: *P-T* gradient range for the Tasiuyak paragneiss contact assemblage in the NaKFMASH system from Spear et al. (1999). Divariant melt and dehydration reaction fields are represented by roman numerals I to IV and correlate to AFM diagrams and assemblages with the same notation. These AFM diagrams show bulk compositions for samples TL02-66 (red stars), TL02-80 (grey triangles), and TL02-73 to -79 (black circles) from Figure 4.3. Numbers listed as 4.x on univariant lines and listed Field assemblages correspond to reactions referred to in the text. The arrow represents the possible *T*-gradient estimates (and isobaric *P*-estimates) across the contact aureole surrounding the MLP based on petrographic evidence, bulk composition and mineral chemistry.

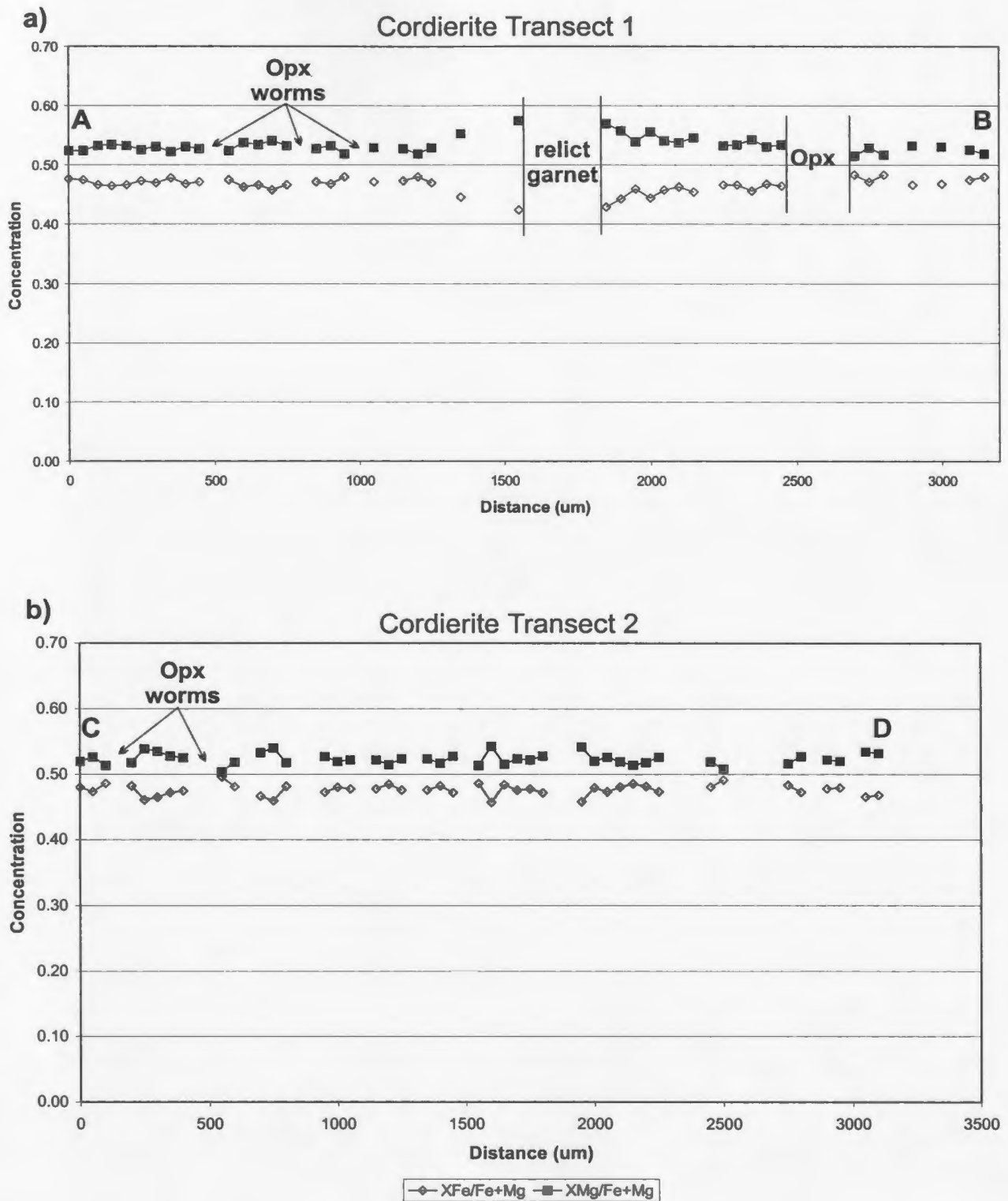


Figure 4.15: Chemical zoning patterns of symplectic cordierite from sample TL01-147. Transects 1 and 2 are shown in Figure 4.13.

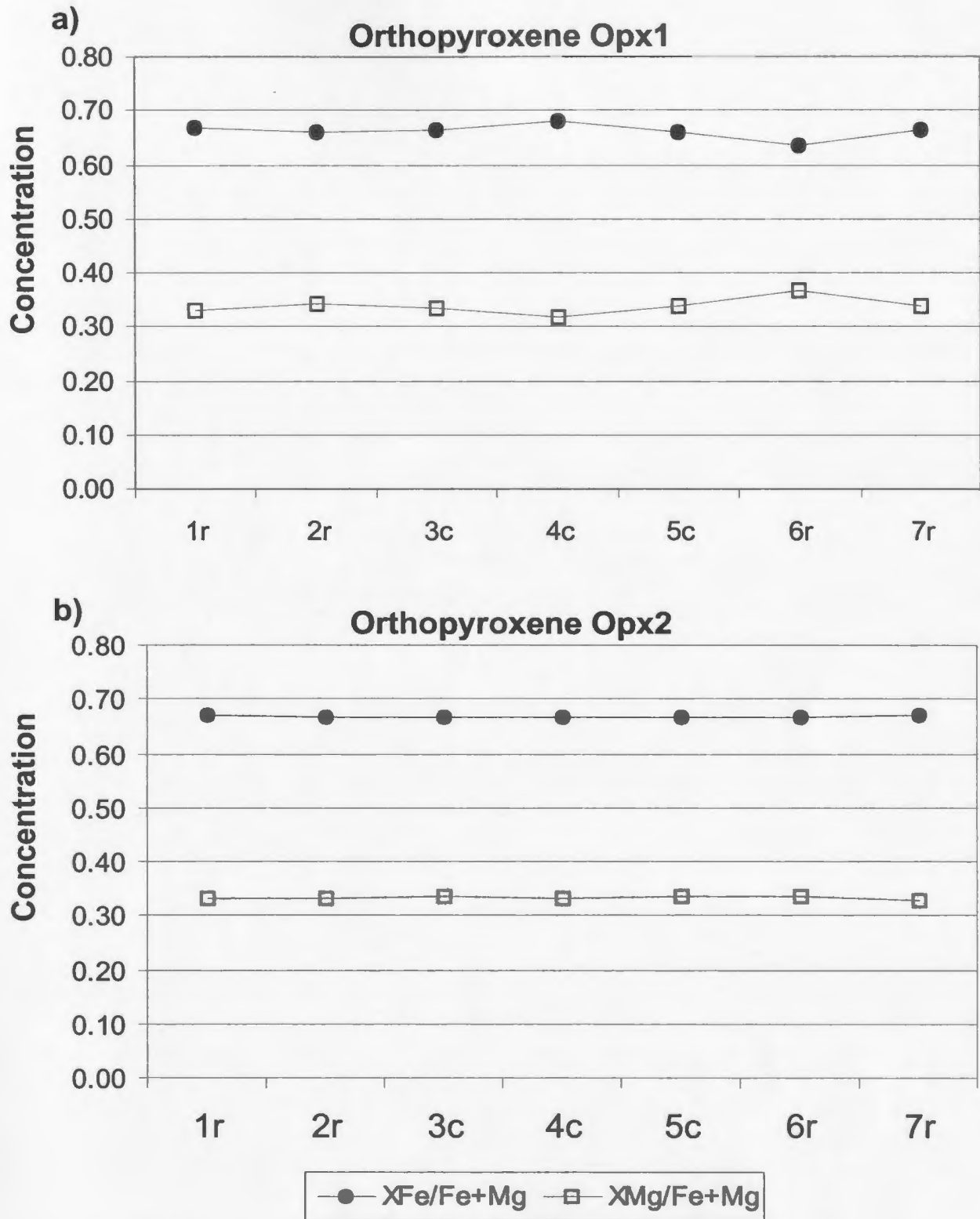
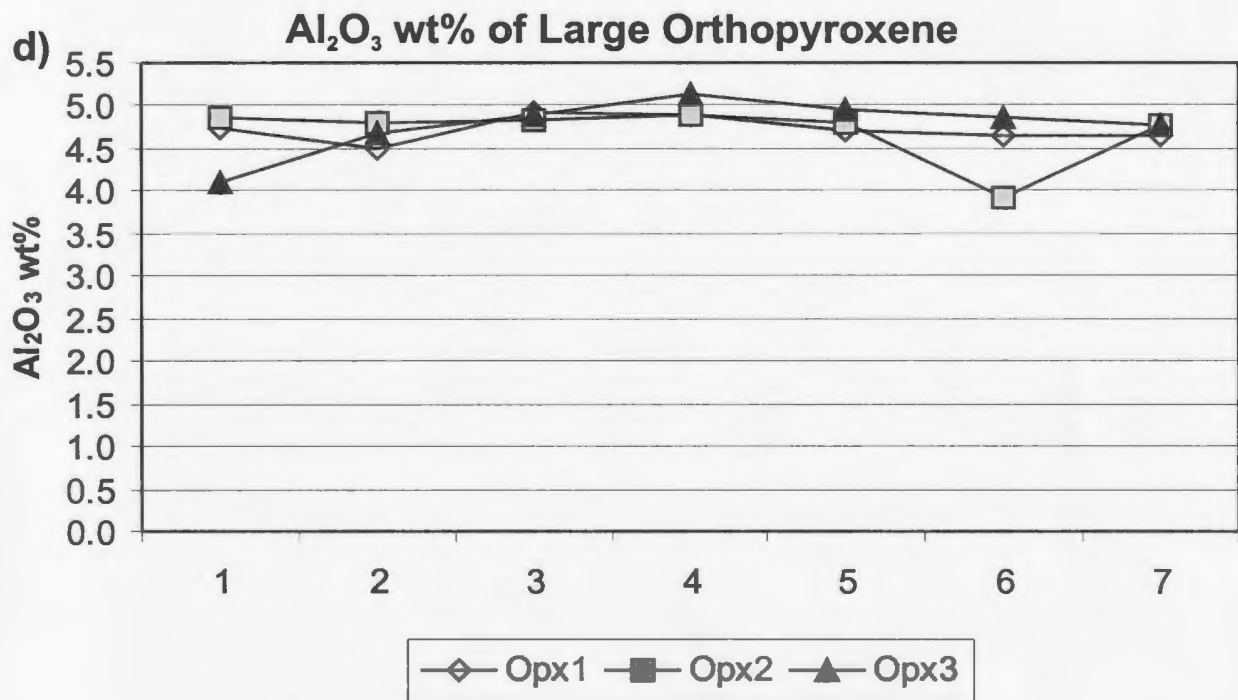
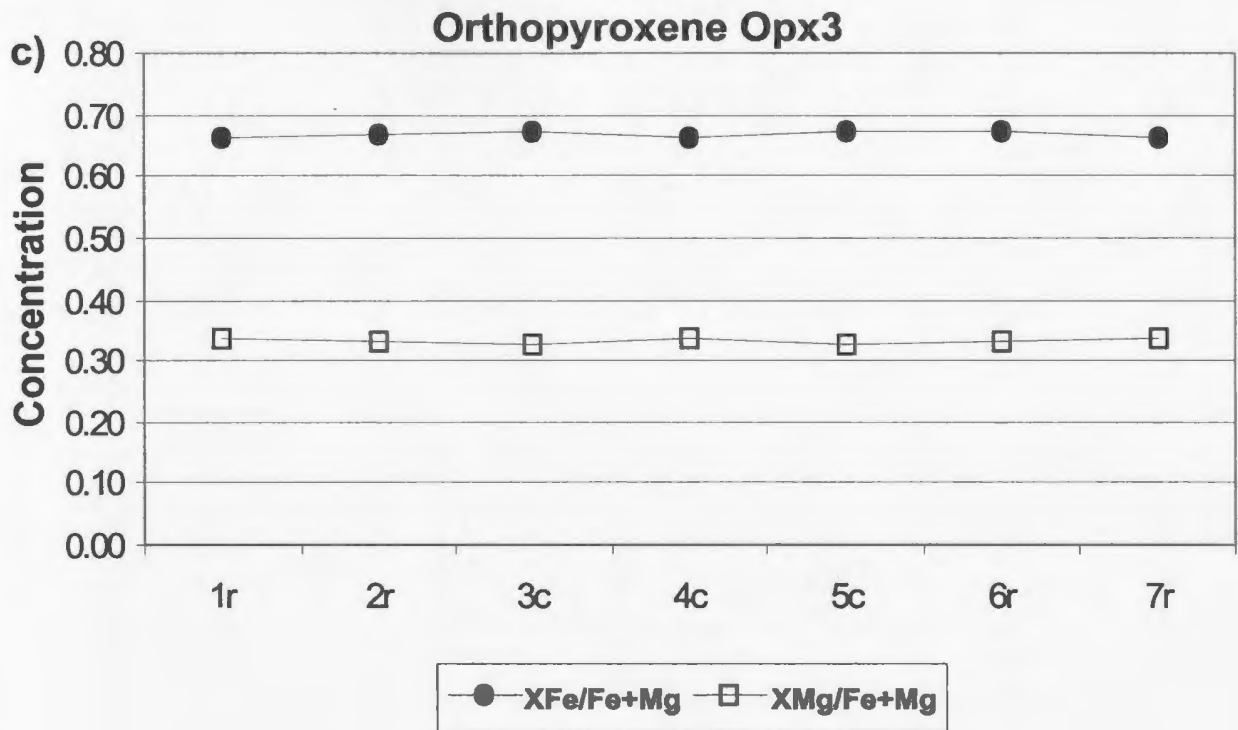


Figure 4.16: Compositional zoning of large orthopyroxene at outer rim of corona. Plots a) through c) represent Fe-Mg compositions of orthopyroxene grains, Opx1, Opx2 and Opx3; and plots Al₂O₃ (wt %) of these grains. (All orthopyroxene grains are shown in Figure 4.13.)



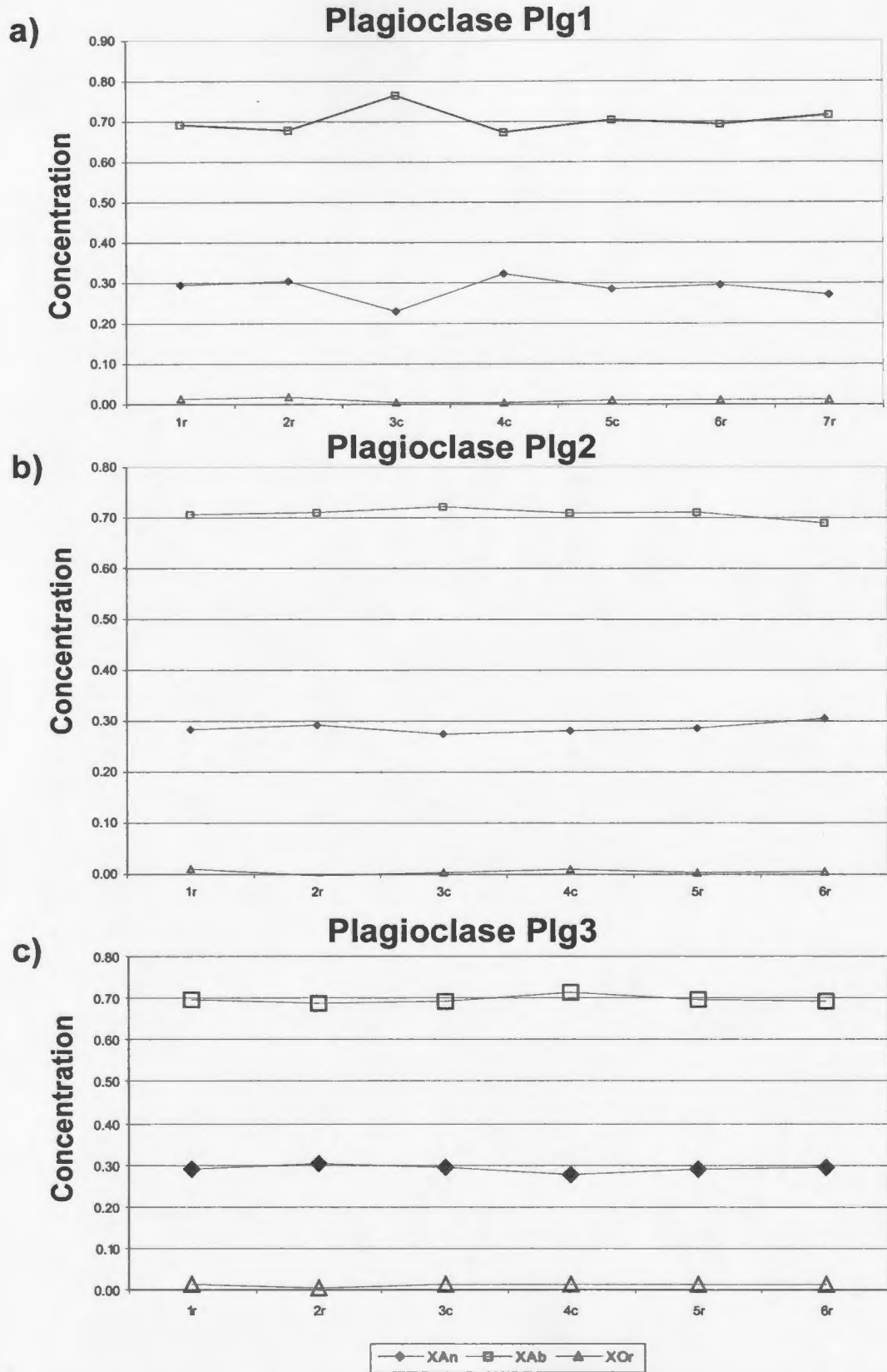


Figure 4.17: Mineral composition zoning of three large plagioclase grains at the outer rim of corona in Figure 4.13.

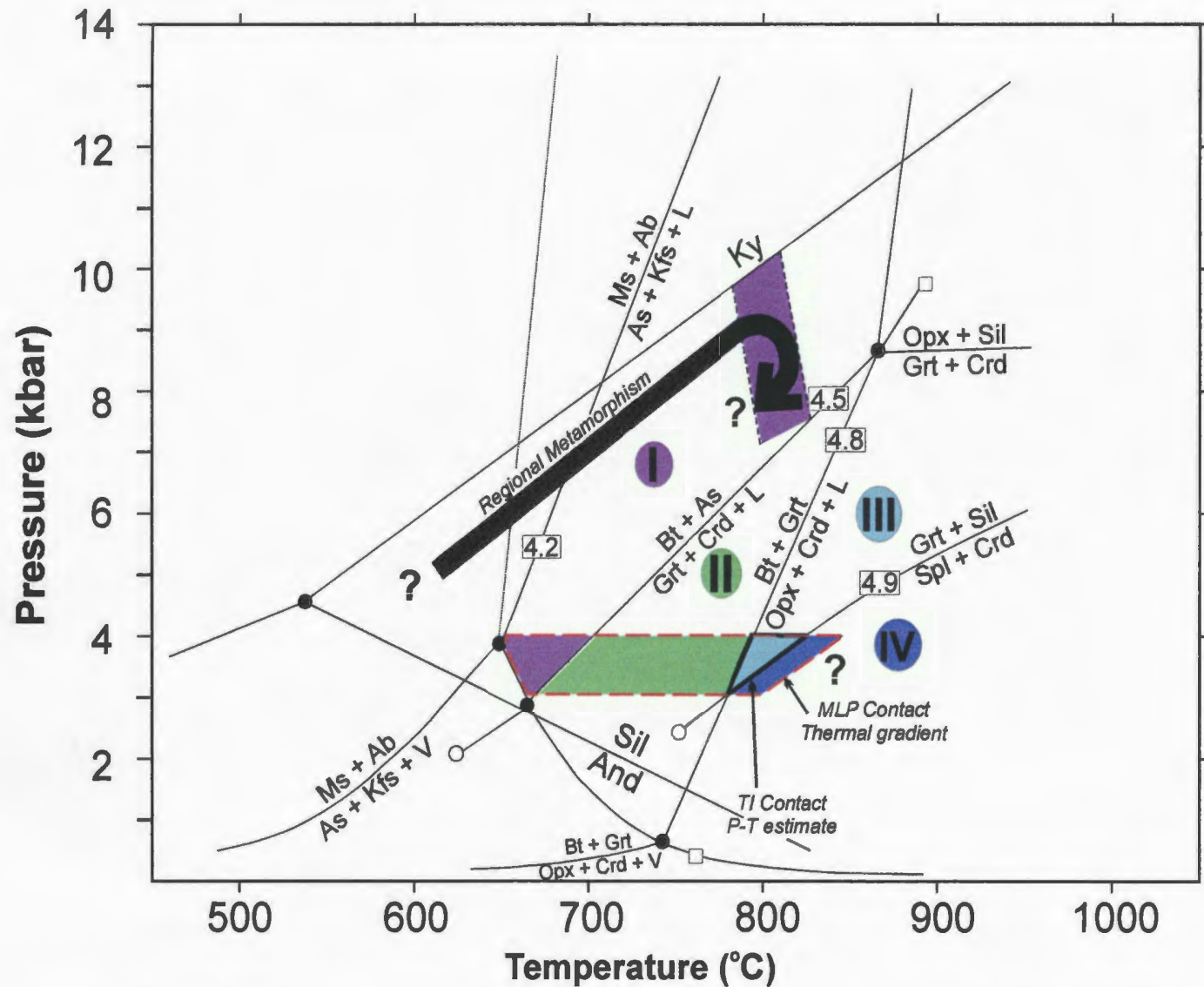


Figure 4.18: *P-T* estimates for the regional and contact metamorphic events. Thick arrow represents the approximate *P-T* path of regional metamorphism of the Tasiuyak paragneiss. The triangle with a solid black outline represents the *P-T* estimate from sample TL02-66 directly adjacent to the TI contact. The trapezoid with a red dashed outline represents the thermal gradient along the contact aureole surrounding the MLP in the study area.



Plate 4.1: Migmatitic Tasiuyak paragneiss with regional metamorphic assemblage. Note arrow pointing to leucosome rimming garnet (+ biotite + sillimanite) in a restitic layer. Location of sample TL01-146, outside of study area. Pen is 15 cm long.



Plate 4.2: Location of sample TL02-66b, adjacent to T1 in the northern part of study area. Here, the Tasiuyak paragneiss contains the regional metamorphic assemblage of garnet + biotite. Incipient development of contact metamorphic assemblage cordierite + orthopyroxene + spinel is not visible at outcrop-scale. Pencil is 15 cm long.



Plate 4.3: Photograph of the paragneiss in the contact aureole surrounding the Makhavinekh Lake Pluton (~2000 m from this contact). The contact metamorphic assemblage of cordierite + orthopyroxene + spinel has partially replaced the regional metamorphic assemblage of garnet + biotite + sillimanite.

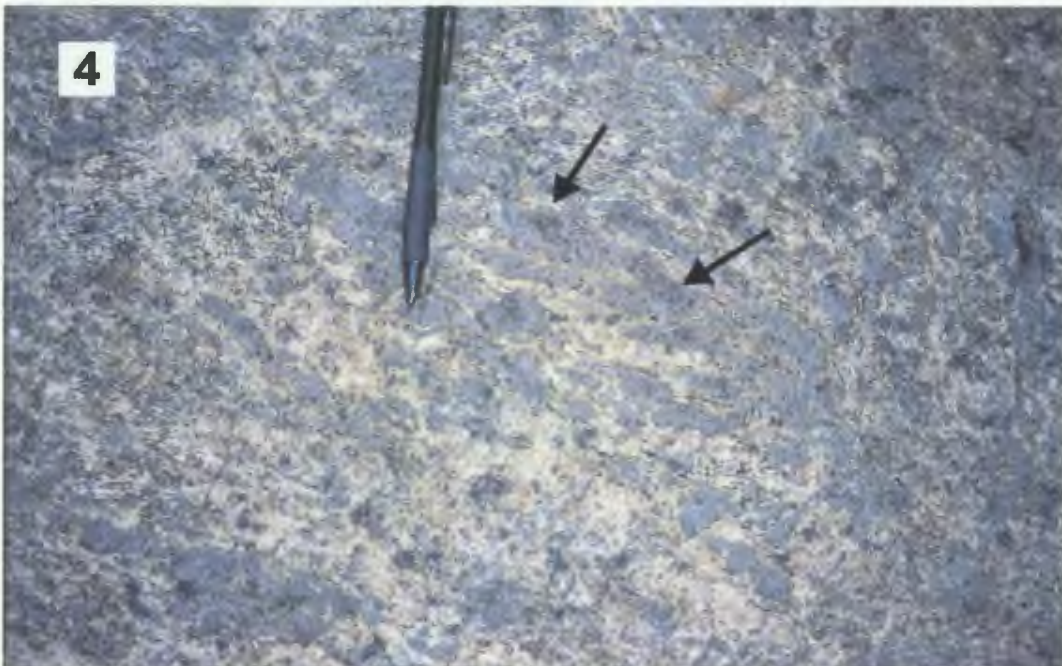


Plate 4.4: Photograph of the paragneiss ~700 m from the contact of the Makhavinekh Lake Pluton. Here, the contact metamorphic assemblage of cordierite + orthopyroxene + spinel has almost completely replaced the regional metamorphic assemblage of garnet + biotite + sillimanite. Arrows point to patches of relict garnet.

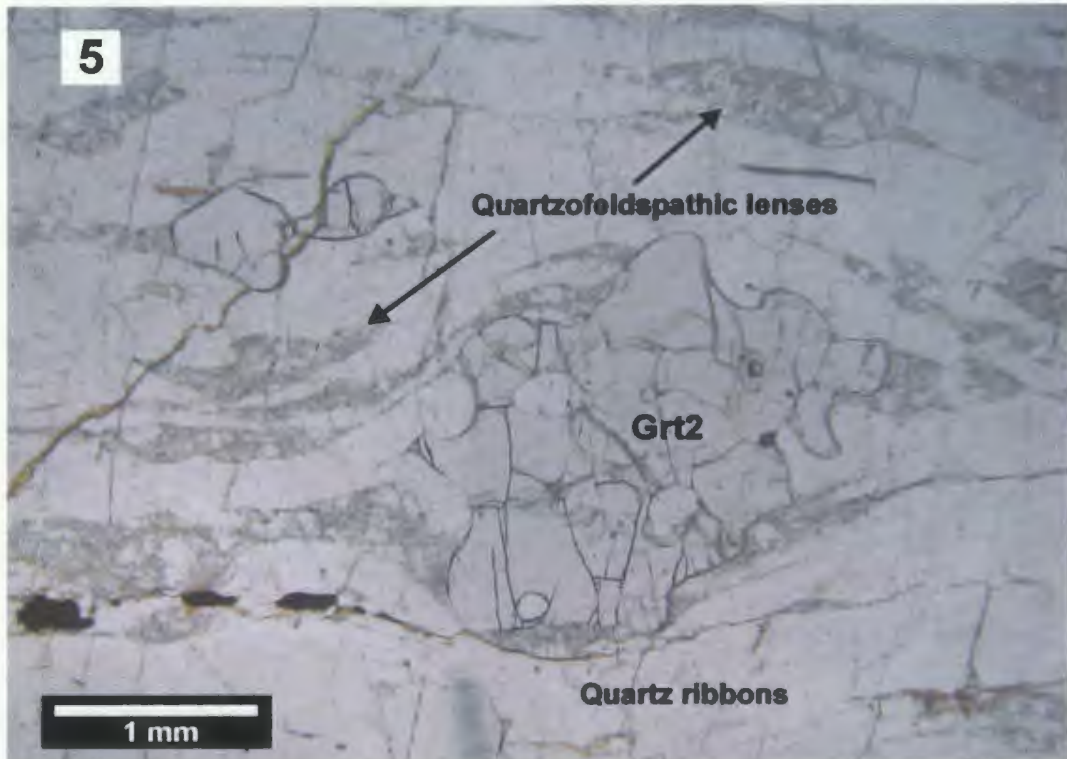


Plate 4.5: Quartz ribbon textural Domain I with minor amounts of attenuated quartzofeldspathic material. Anhedral, millimetre-sized Grt2 formed within quartzofeldspathic zones.

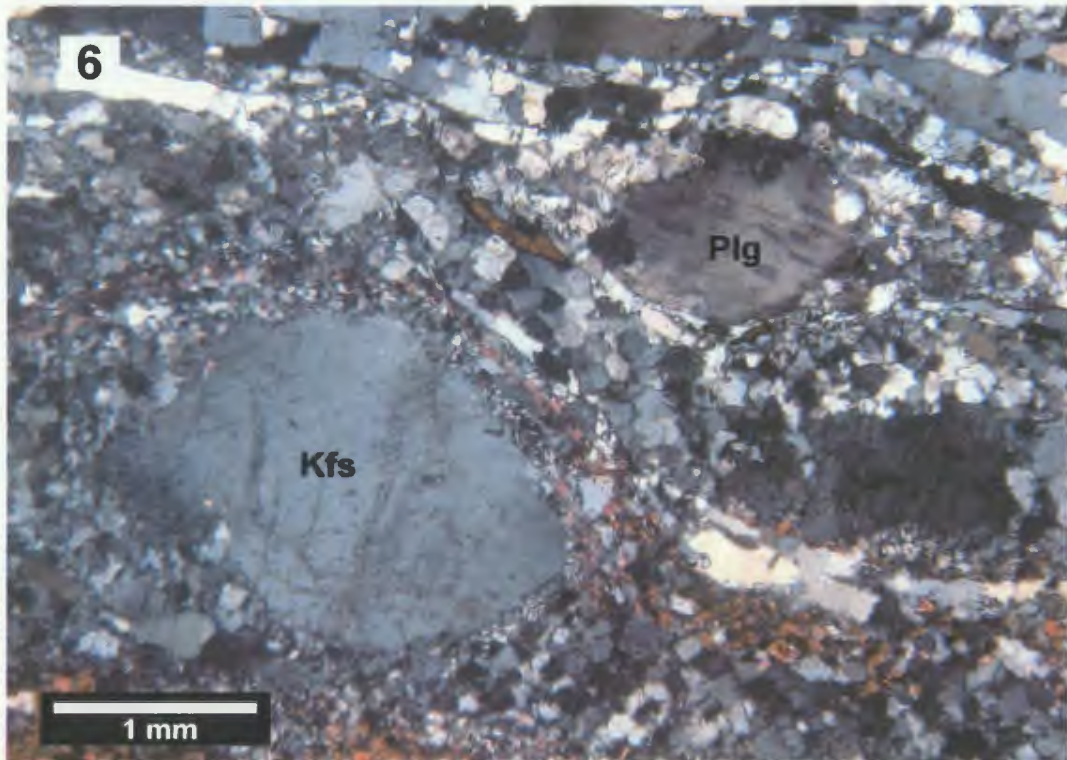


Plate 4.6: Porphyroblastic, perthitic feldspars in quartzofeldspathic Domain II. Remnant feldspars are augen-shaped and recrystallized along grain boundaries.

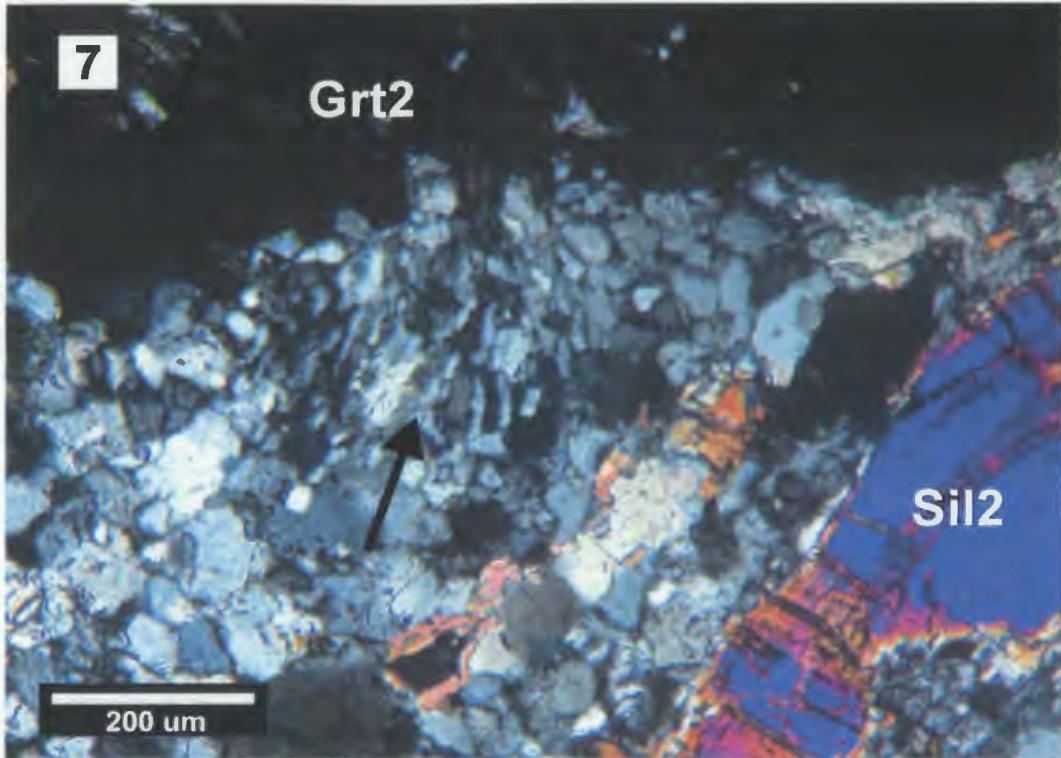


Plate 4.7: Vermicular quartz and feldspars adjacent to Grt2 rim (arrow). Note embayment of the vermicular material into Grt2.

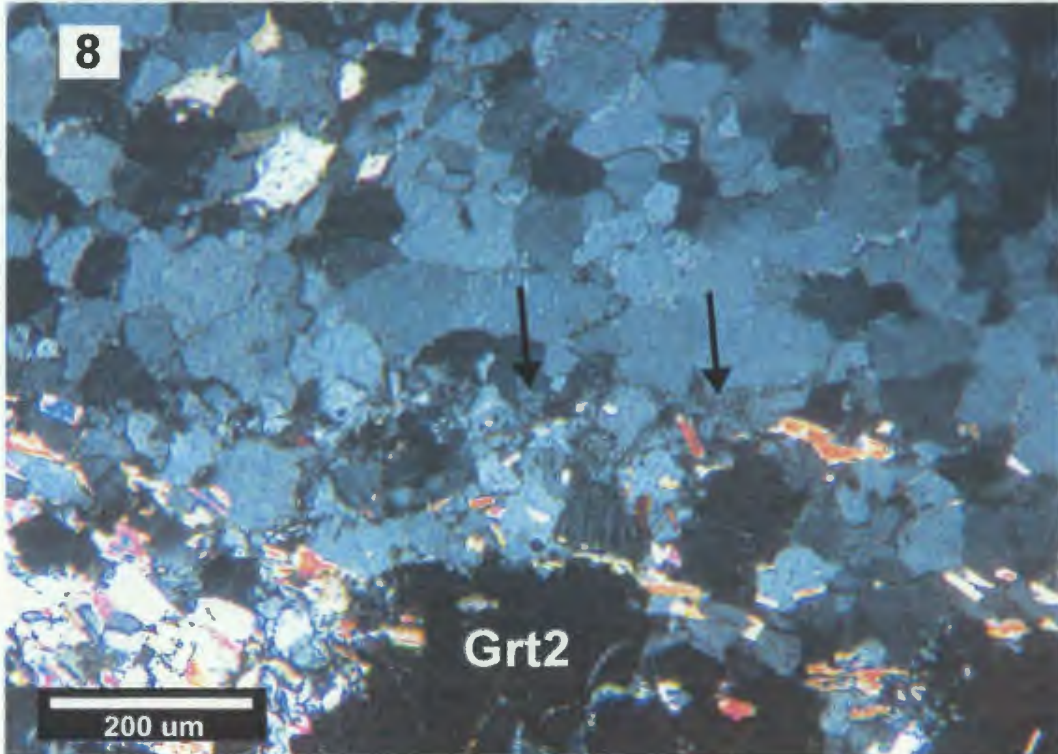


Plate 4.8: Arrows point to vermicular quartz and feldspars in biotite-rich layer of Domain II.

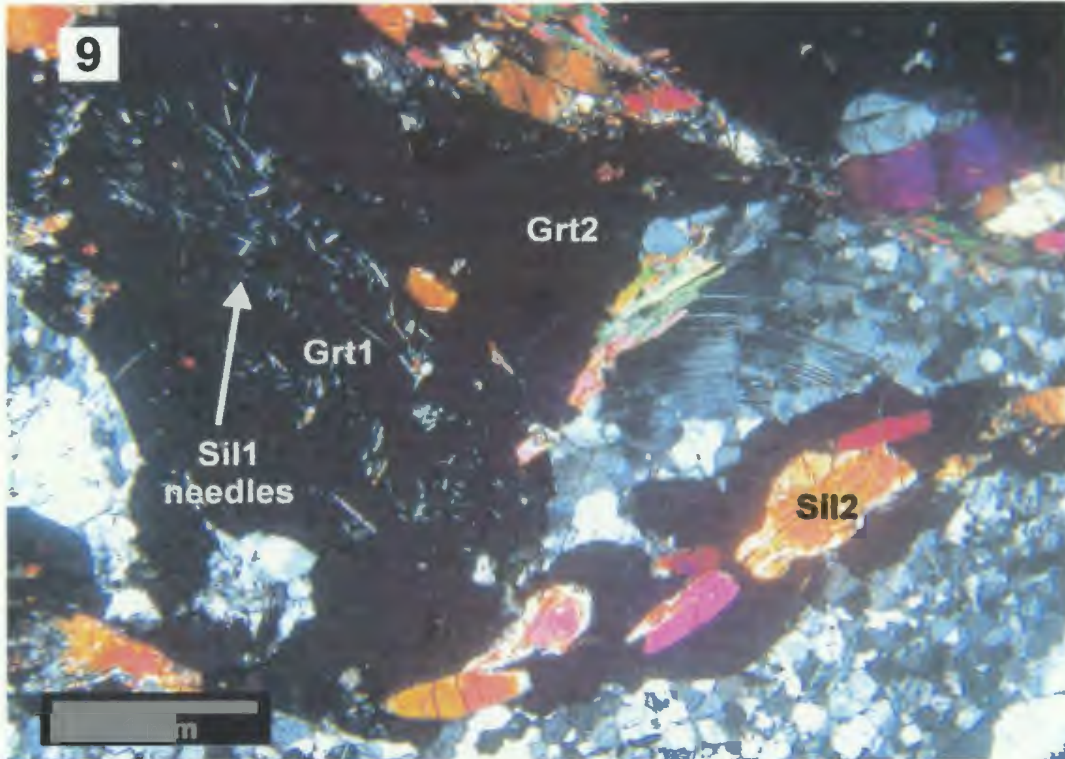


Plate 4.9: Randomly oriented sillimanite inclusions (Sil1) in Grt1 surrounded by Grt2 and coarse-grained, relict sillimanite (Sil2), which is parallel to the foliation.

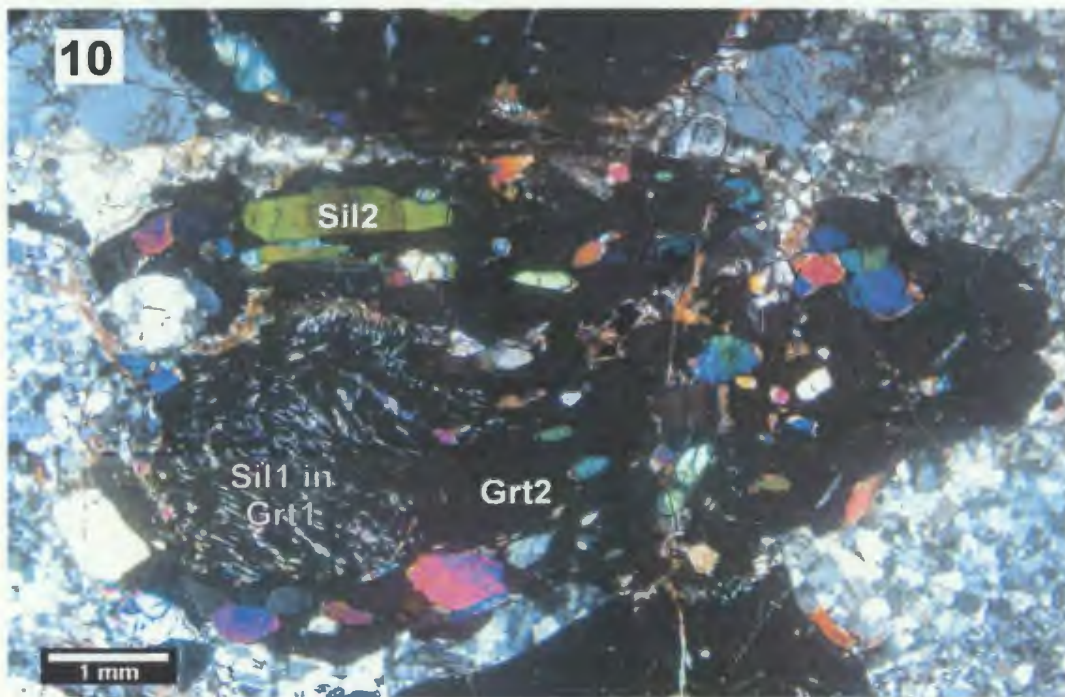


Plate 4.10: Foliation-parallel sillimanite inclusions (Sil1) in rotated Grt1 surrounded by Grt2 and coarse-grained, relict sillimanite (Sil2), which is parallel to the foliation.

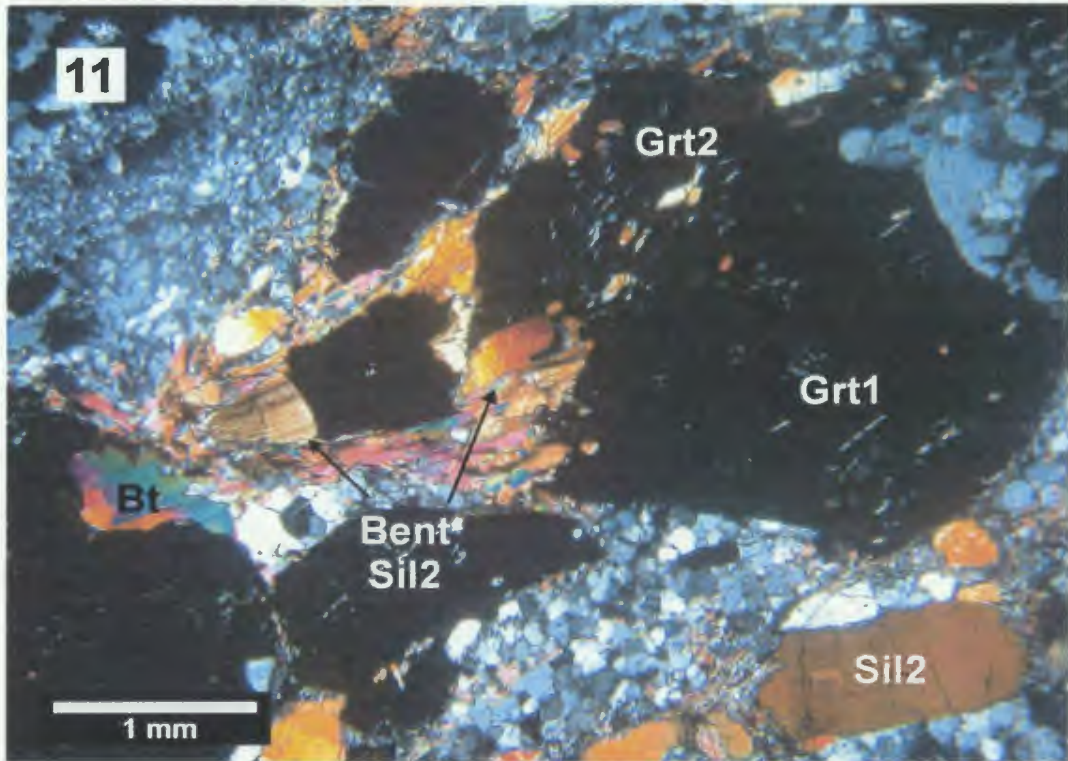


Plate 4.11: Bent Sil2 overgrown by Grt2 abutting Grt1. Coarse-grained Sil2 without overgrowth seen at right lower corner of this photomicrograph. Retrograde biotite formed along Grt2 rim.

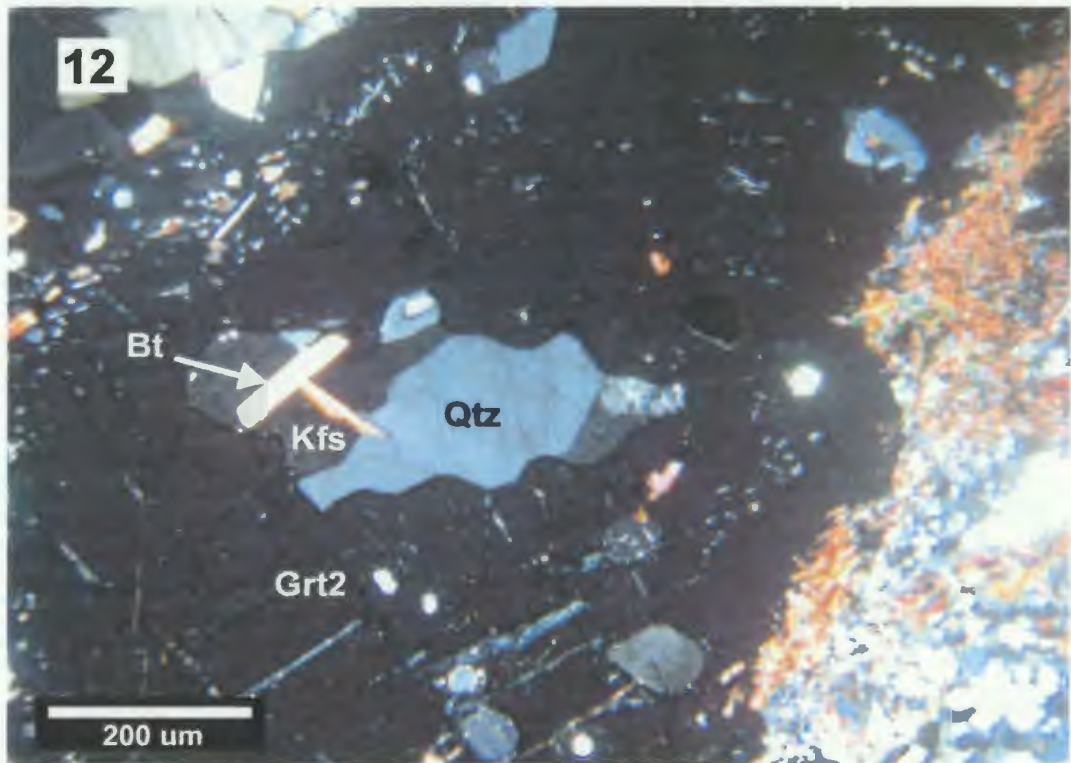


Plate 4.12: Inclusion of crystallized melt within Grt2 containing biotite, quartz, and K-feldspar.

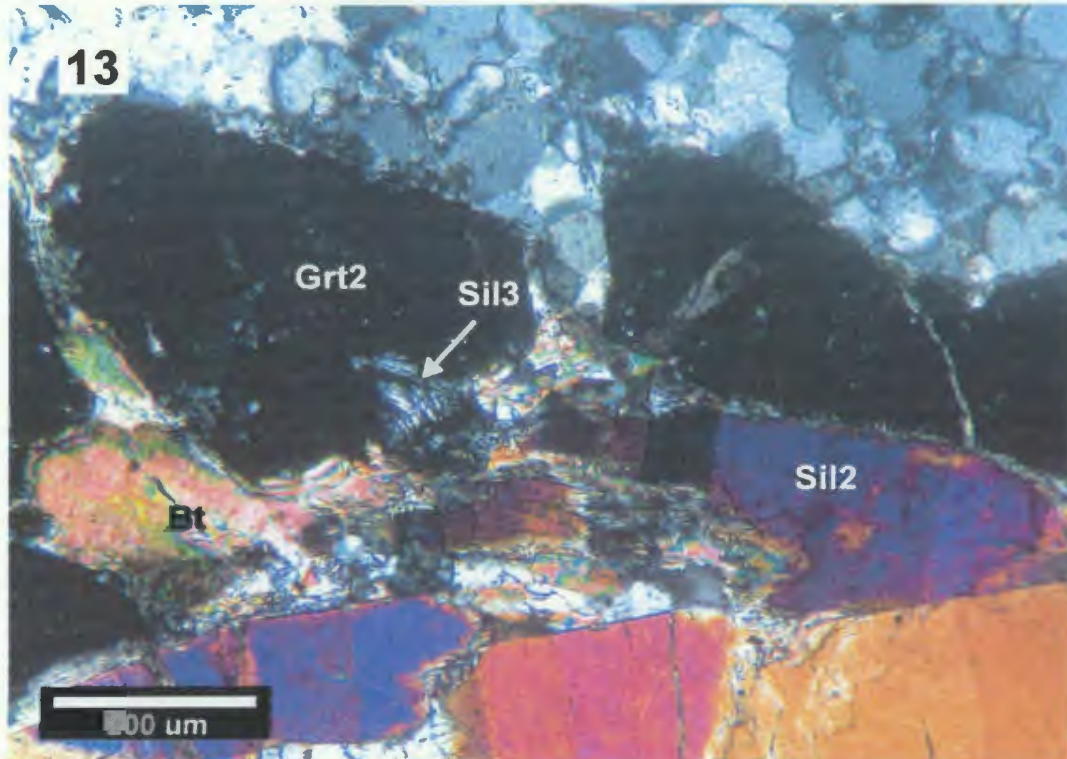


Plate 4.13: Photomicrograph showing corroded margins of Sil2 and Grt2, and retrograde biotite, Sil3 and quartz along grain boundaries and fractures. Irregular Grt2 rims adjacent to felsic matrix show resorption.

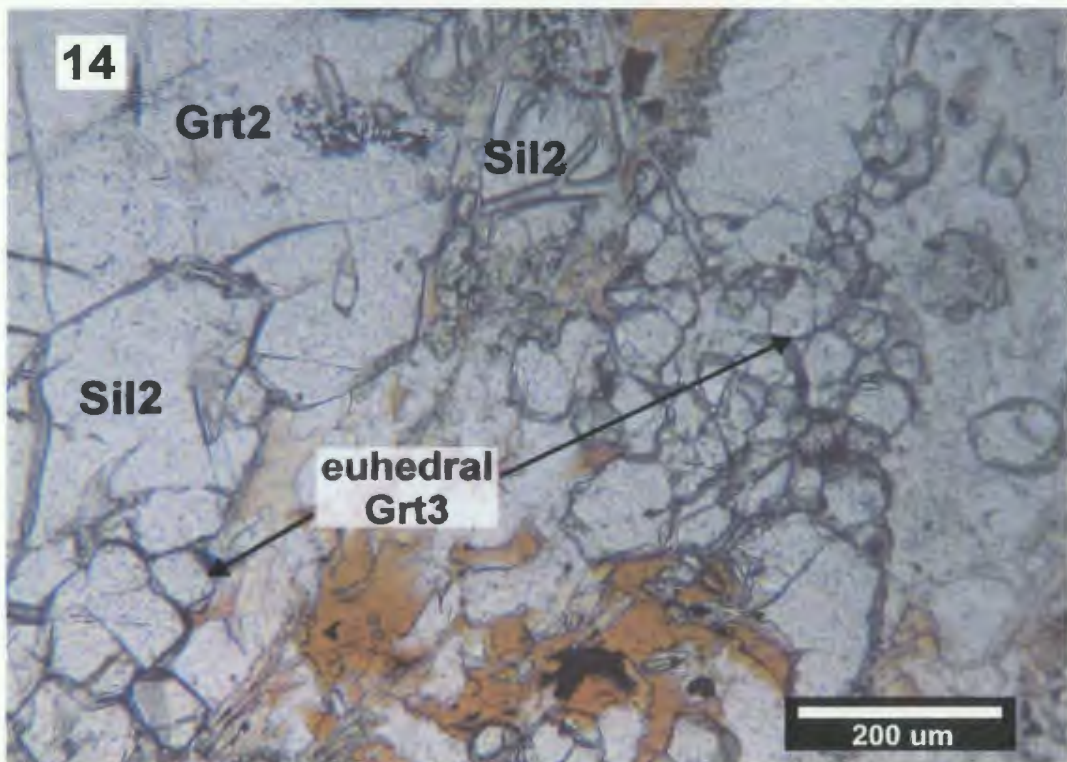


Plate 4.14: Small, euhedral Grt3 adjacent to xenomorphic Grt2 rims and Sil2 rims.

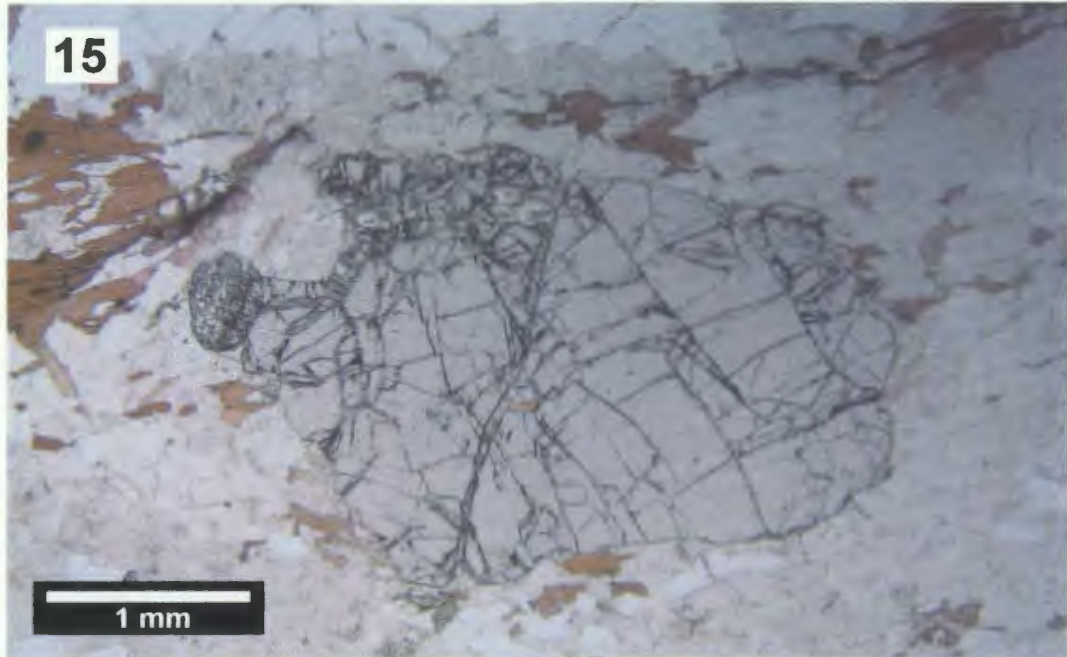


Plate 4.15: Sample TL02-80 showing preservation of the regional metamorphic assemblage. Grt2 is highly fractured and biotite adjacent to garnet is randomly oriented.

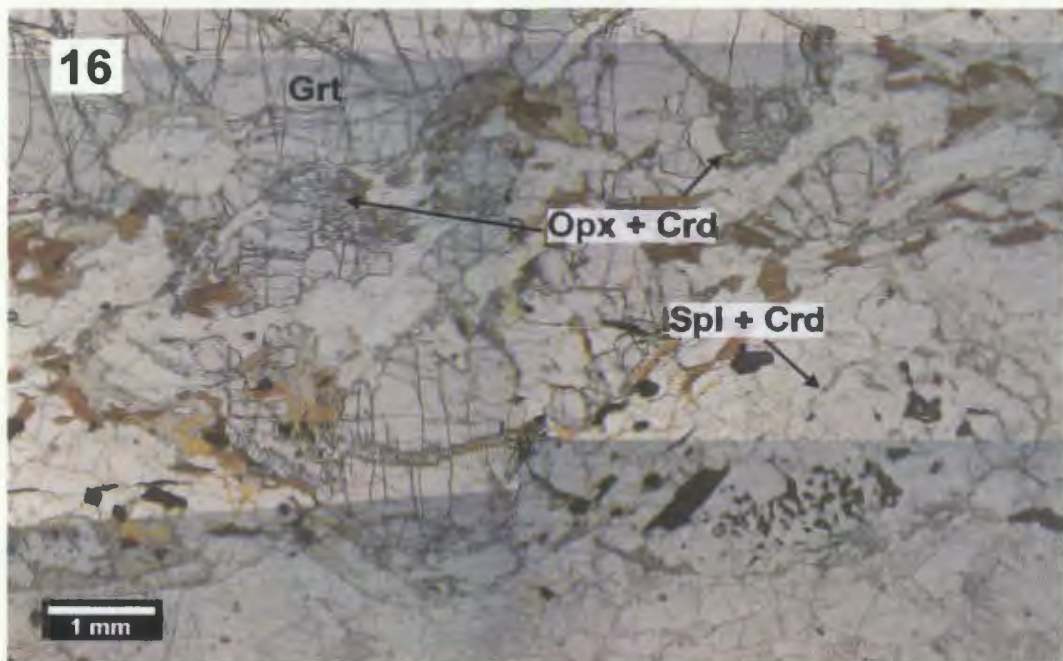


Plate 4.16: Sample TL02-66b showing minor contact metamorphic minerals superimposed on the regional assemblage. Sillimanite has been completely replaced by symplectic spinel and cordierite. There is only minor replacement of garnet rims by orthopyroxene and cordierite.

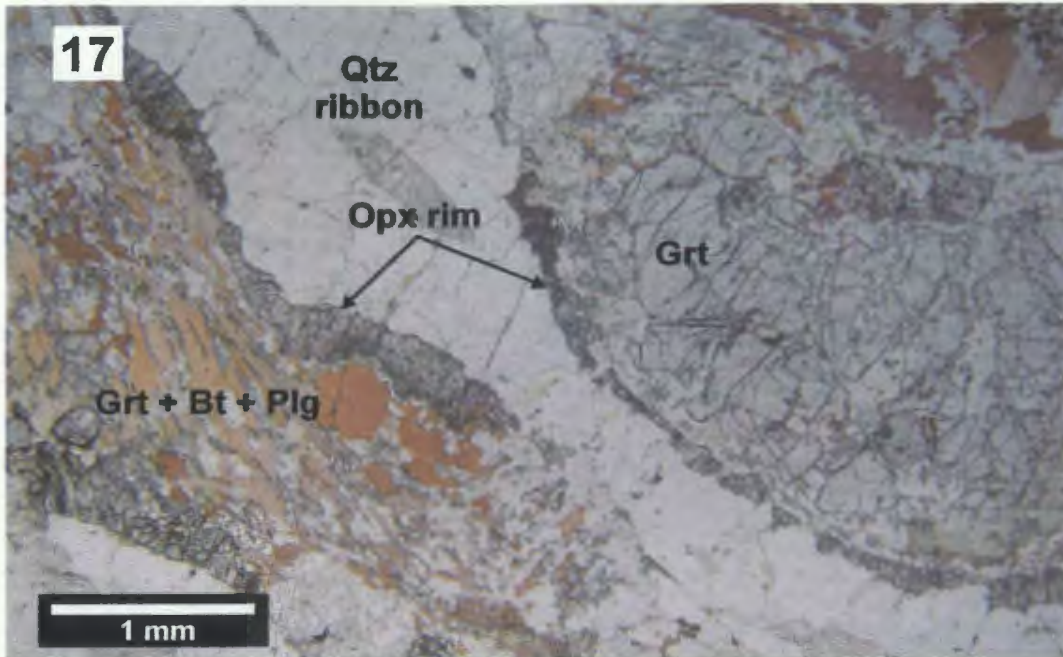


Plate 4.17: Sample TL02-79 showing minor contact metamorphic effects. Orthopyroxene rims developed along quartz ribbon in contact with biotite and garnet.

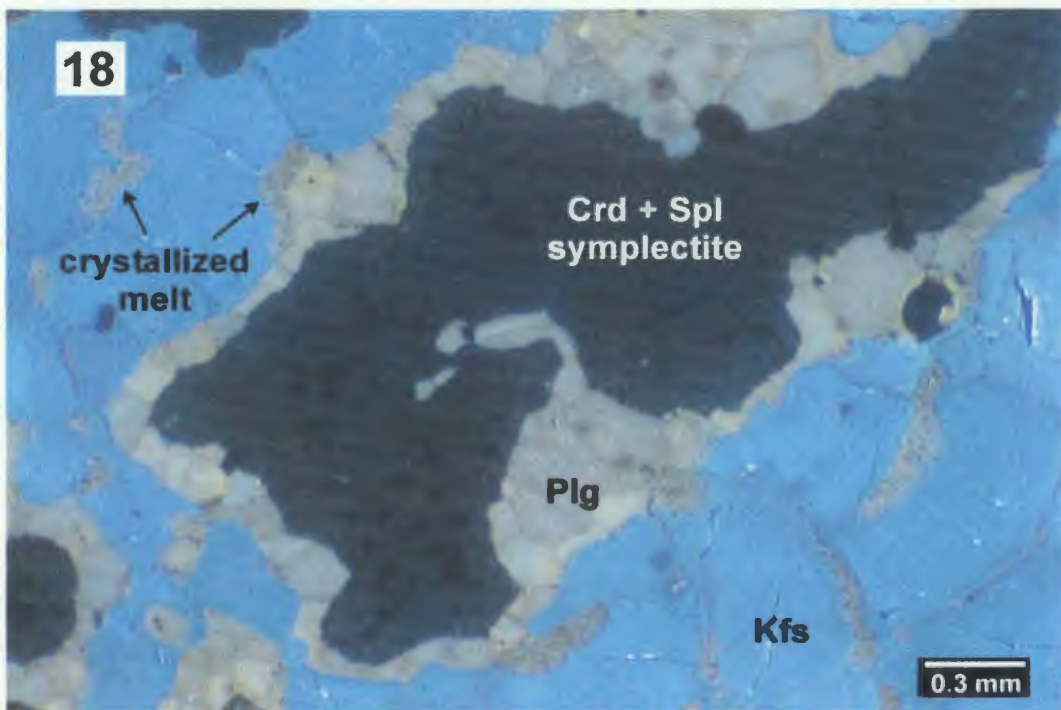


Plate 4.18: Cathodoluminescence photomicrograph of sample TL02-74 showing crystallized melt (plagioclase in yellow and quartz in black) along feldspar grain boundaries. Recrystallized plagioclase with triple-junctions at grain boundaries rimming cordierite and spinel symplectite.

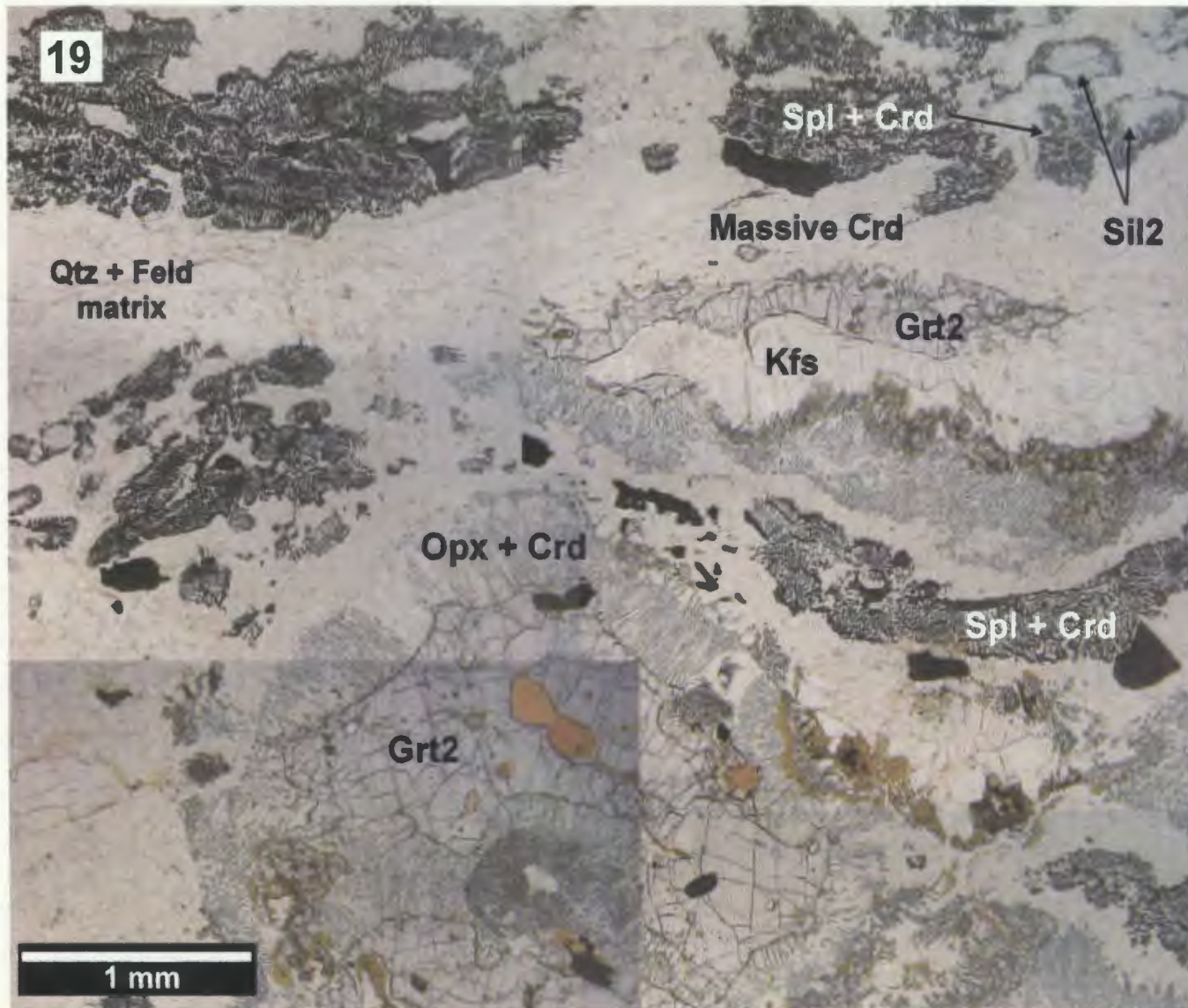


Plate 4.19: Photomicrograph of sample TL02-77. Porphyroblastic Grt2 partially replaced by orthopyroxene + cordierite. Relict Sil2 surrounded by symplectitic spinel + cordierite. Massive cordierite separating spinel + cordierite symplectite from relict Grt2 .

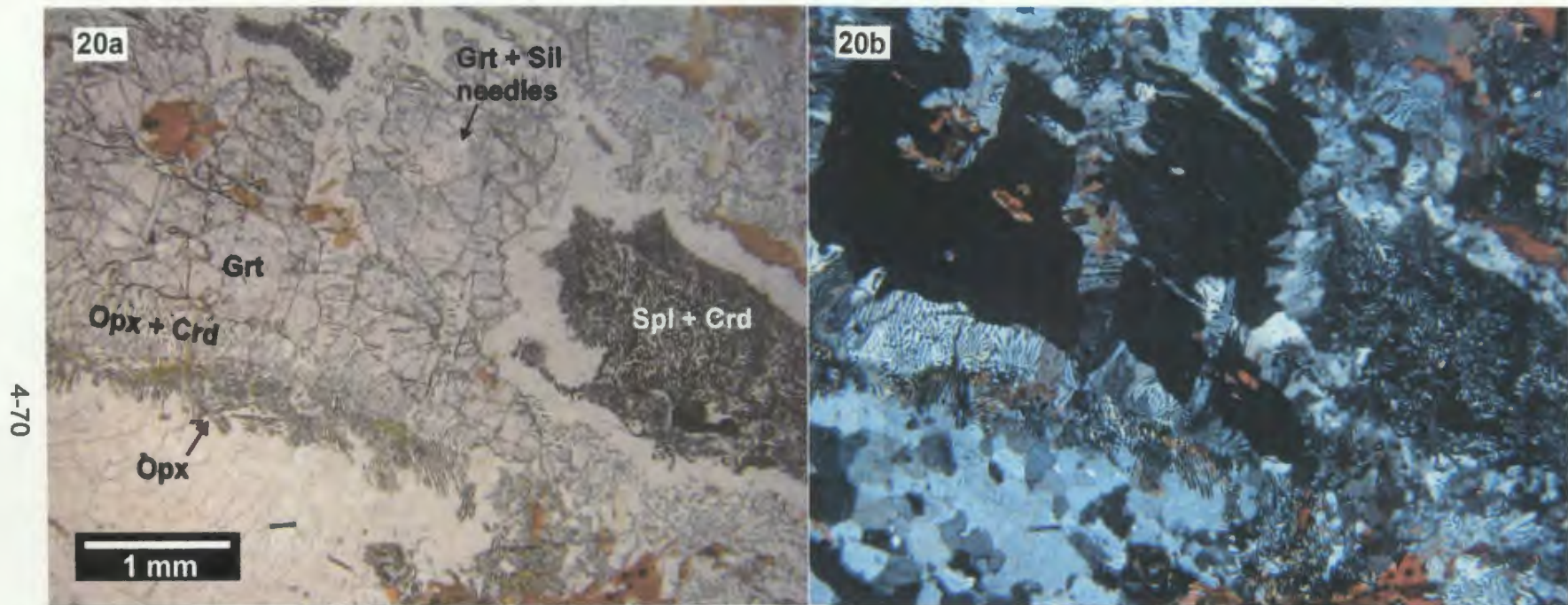


Plate 4.20: Photomicrograph of sample TL02-78. a) Porphyroblastic Grt2 partially replaced by orthopyroxene + cordierite. Grt1 with Sil1 inclusions is partially replaced by spinel + cordierite. Orthopyroxene needles formed at outer rim of corona. b) Large, anhedral cordierite with inclusions of wormy orthopyroxene. The cordierite + orthopyroxene symplectite shows disequilibrium textures. The quartzofeldspathic matrix shows partial recrystallization textures such as irregular, embayed boundaries and subgrain development.

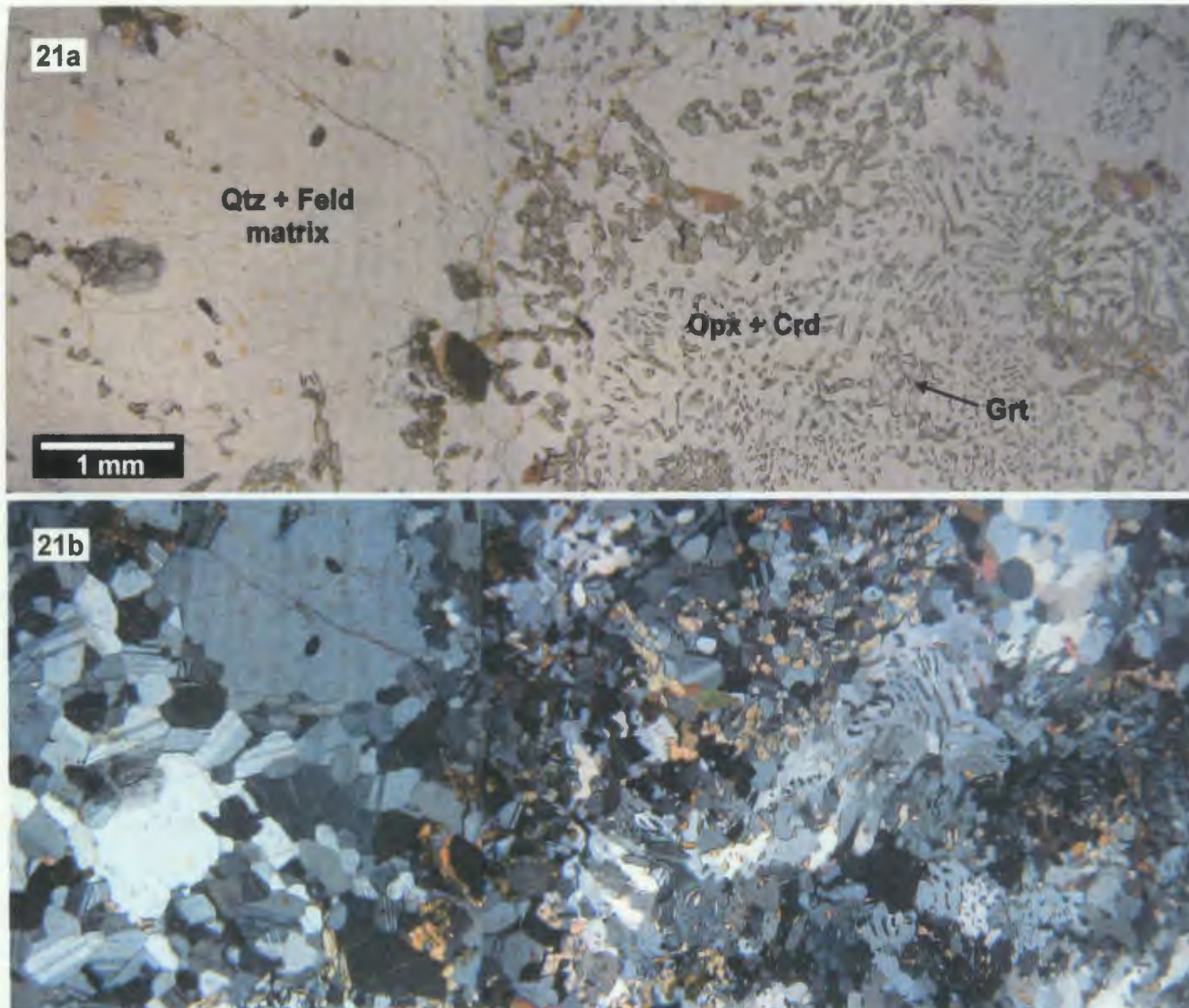


Plate 4.21: Photomicrograph of sample TL02-74. a) garnet is almost completely consumed, surrounded by orthopyroxene + cordierite symplectite and an outer rim of polygonal orthopyroxene. b) symplectitic cordierite and orthopyroxene are polygonal at the rim of the corona, whereas both phases still exhibit disequilibrium textures in the core (near relict garnet). The quartzofeldspathic matrix shows polygonal plagioclase and large, anhedral K-feldspar and quartz suggesting static recrystallization.

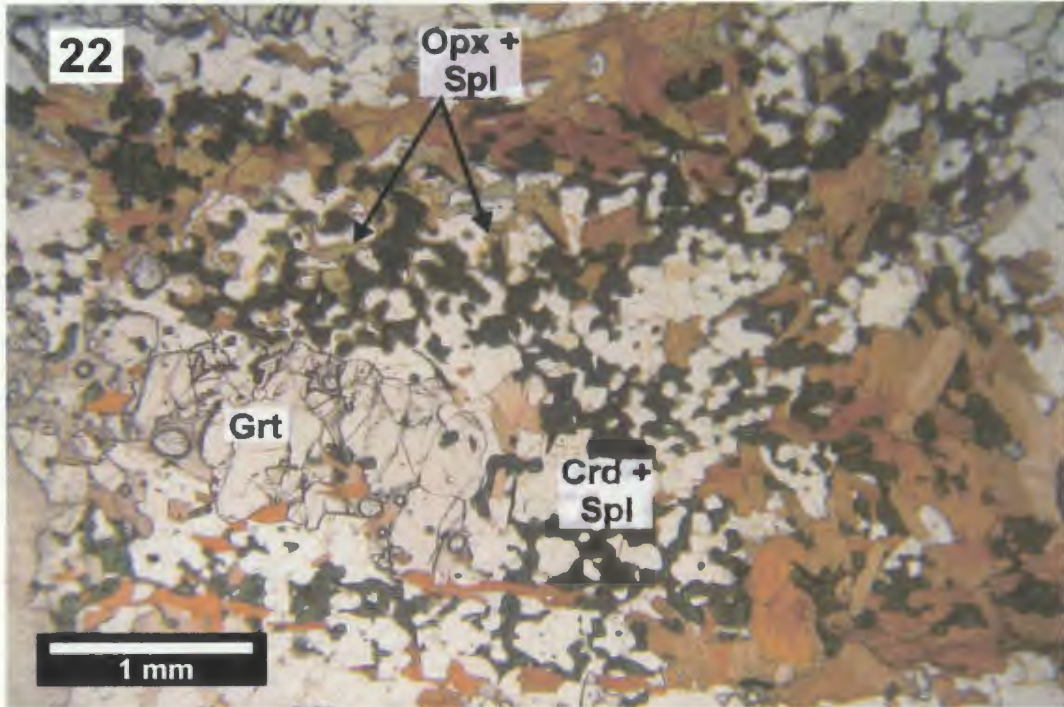


Plate 4.22: Sample TL02-48, garnet and biotite are partially replaced by coarse-grained intergrowths of spinel + cordierite and spinel rimmed by orthopyroxene.

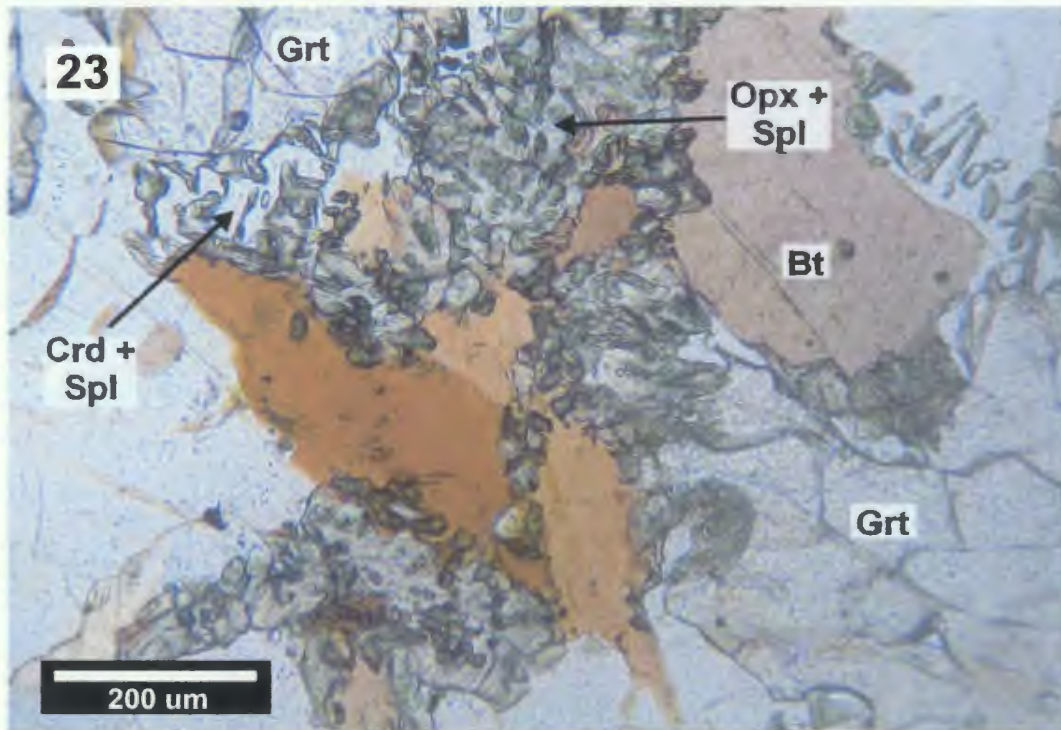


Plate 4.23: Photomicrograph of sample TL02-29 showing symplectic orthopyroxene + spinel after biotite and cordierite + spinel after garnet.

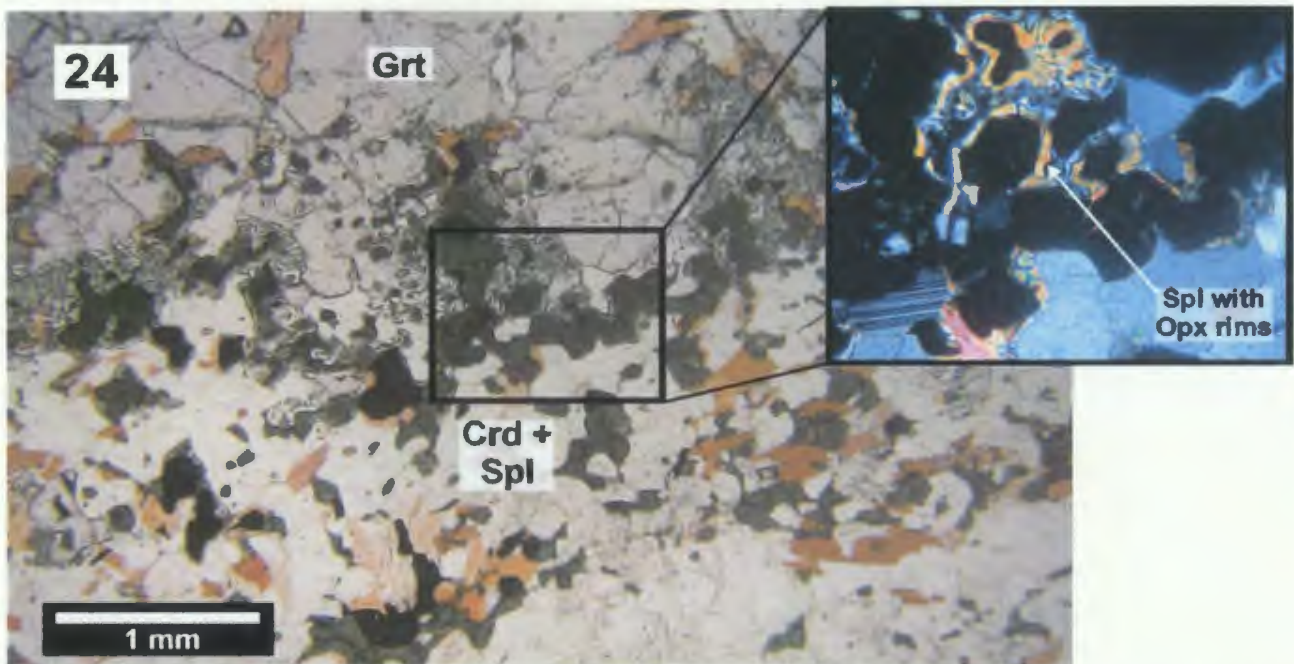


Plate 4.24: Sample TL02-29, garnet and biotite are partially replaced by cordierite + spinel, in which the latter is typically rimmed by orthopyroxene (orange-yellow rimming black spinel, inset box).

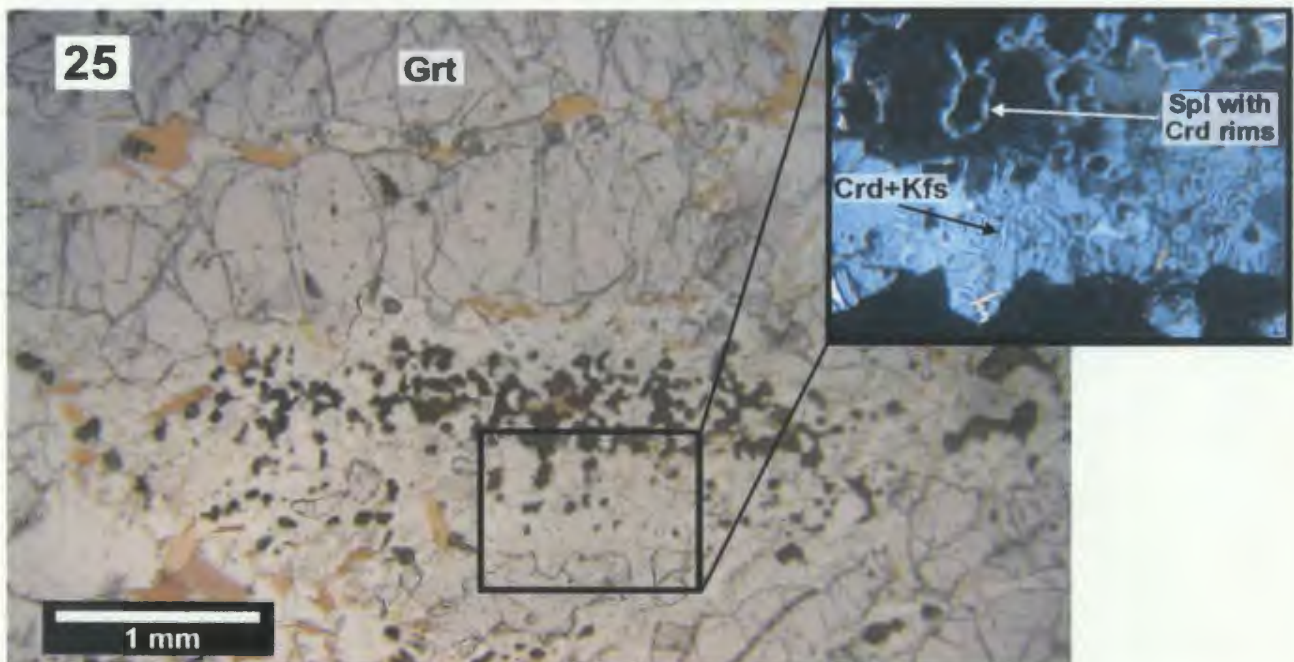


Plate 4.25: Sample TL02-44, garnet and biotite are partially replaced by cordierite + K-feldspar + spinel, in which the latter is typically rimmed by cordierite (grey-blue rimming black spinel, inset box).

CHAPTER 5 - COMPILATION OF CONCLUSIONS FROM THE THESIS RESEARCH

5.1 SUMMARY OF THESIS GOALS

The thesis study area includes a portion of the western margin of the Nain Plutonic Suite and the adjacent country rocks. The main goals of this research, as defined in Chapter 1, were to: 1) establish the emplacement history of the Pearly Gates Anorthosite pluton and the spatially related Tessiarsuyungoakh intrusion; and 2) define the contact metamorphism of the Tasiuyak paragneiss. These goals were met by detailed field investigations which were used to compile a 1:20 000 geological map (Map 1 and Map 2). The first goal was also met by using field structures, petrography and U-Pb geochronology to determine the timing and mode of emplacement. The second goal was achieved by determining the regional metamorphic evolution to provide a better understanding of the development of the contact metamorphic mineral assemblages. Both the regional and contact metamorphic mineral assemblages were subjected to a detailed petrographic study to establish textural relationships and some analytical microprobe work to determine bulk composition and mineral chemistry. This information was then used in conjunction with petrogenetic grids to provide *P-T* conditions for each of the two metamorphic events.

5.2 SUMMARY OF CONCLUSIONS

U-Pb TIMS dating that formed part of this study has produced the oldest zircon crystallization ages for the Nain Plutonic Suite. They are: 1) the 1370 ± 5 Ma prismatic zircons included in plagioclase phenocrysts from the Pearly Gates Anorthosite pluton that most likely formed at depth; 2) the oldest intrusive age at 1363 ± 3 Ma for the monzonite and 1360 ± 4 Ma for the monzodiorite of the Tessiarsuyungoakh intrusion; and 3) the oldest intrusive age of anorthosite at 1355 ± 1.3 Ma from the Fraser Canyon Anorthosite. A norite body and norite dyke, both of which are undeformed, intruded the Pearly Gates Anorthosite pluton at 1342 ± 1.2 and 1341 ± 1.8 , respectively. The geological history of the study area determined by this thesis research is summarized below.

The regional metamorphic assemblage of the ca. 1850 Ma (Bertrand et al., 1993) Tasiuyak paragneiss preserves evidence of the prograde reaction history. This includes: a) the formation of Grt1 with Sil1 inclusions before the onset of partial melting; b) growth of Sil2 during muscovite dehydration melting; c) growth of Grt2 at the expense of Sil2 during biotite dehydration melting; and d) limited development of retrograde biotite and Sil3 after garnet during melt crystallization. Peak *P-T* conditions are constrained in the range of 7.2 to 10.2 kbar and 800° to 830°C.

At ca. 1370 Ma, plagioclase phenocrysts with inclusions of prismatic zircon formed. This is suggested to have occurred at depth, prior to emplacement of the Pearly Gates Anorthosite pluton at a mid-crustal level.

At ca. 1360 Ma, reactivation of older structures in the Tasiuyak paragneiss provided conduit systems into which monzonitic and monzodioritic magma ascended. These magmas intruded as sheets into the paragneiss and formed the composite Tessiarsuyungoakh intrusion. Screens of paragneiss exposed in the Tessiarsuyungoakh intrusion contain the high-temperature contact metamorphic assemblage cordierite + spinel ± orthopyroxene, which replaced garnet + biotite (± sillimanite). In addition, the Tasiuyak paragneiss directly adjacent (< 20 m) to this intrusion exhibits incipient development of the contact metamorphic assemblage cordierite + orthopyroxene + spinel after garnet + biotite + sillimanite. This mineralogical and textural evidence, and the narrow width of the contact aureole imply that the Tessiarsuyungoakh intrusion had a short-lived history of emplacement and crystallization and was probably a small body. The *P-T* estimate of the contact metamorphism at the Tessiarsuyungoakh intrusion contact is between 3 and 4 kbar and 775° and 800°C.

At ca. 1355 Ma, noritic magma with plagioclase phenocrysts was emplaced into the T1 and formed the Fraser Canyon Anorthosite. The Pearly Gates Anorthosite pluton was either emplaced at this time or shortly thereafter. The outer zone of the anorthosite bodies with compositional layers of anorthosite and norite is interpreted as a relatively fast cooled margin. The inner zone of massive anorthosite is interpreted to have cooled relatively slowly, and as

plagioclase phenocrysts continued to grow they possibly filtered out the noritic magma towards the partially crystallized margins of the chamber. Syn-emplacement deformation, possibly associated with stoping, sheared the crystallized margins of the Pearly Gates Anorthosite pluton and the adjacent Tessiarsuyungoakh intrusion. However this deformation had little effect on the partially crystallized inner zone of the Pearly Gates Anorthosite. By ca. 1340 Ma, the Pearly Gates Anorthosite pluton had completely crystallized, was intruded by noritic magma and deformation in the area had ceased.

At ca. 1322 Ma (McFarlane et al., 2003), intrusion of the large Makhavinekh Lake pluton produced a substantial high-temperature metamorphic contact aureole in the Tasiuyak paragneiss. The development of the contact metamorphic assemblage of cordierite + orthopyroxene + spinel after garnet + biotite + sillimanite can be seen up to 4 km from the Makhavinekh Lake pluton contact. The temperature gradient along the contact aureole probably ranged from 675°C at the limit of the contact aureole, to at least 850°C at the Makhavinekh Lake pluton contact and isobaric conditions are estimated to have been between 3 to 4 kbar.

REFERENCES:

- Amelin, Y., Li, C. and Naldrett, A.J. 1999. Geochronology of the Voisey's Bay intrusion, Labrador, Canada, by precise U-Pb dating of coexisting baddeleyite, zircon, and apatite. *Lithos*, 47: 33-51.
- Ashwal, L.D. 1993. *Anorthosites*. Springer-Verlag, Berlin, 422 p.
- Barton, J.M., Jr. and Barton, E.S. 1975. Age and geochemical studies of the Snyder Breccia, central Labrador. *Canadian Journal of Earth Sciences*, 12: 361-370.
- Berg, J.H. 1977a. Dry granulite mineral assemblages in the contact aureoles of the Nain Complex, Labrador. *Contributions to Mineralogy and Petrology*, 64: 33-52.
- Berg, J.H. 1977b. Regional geobarometry in the contact aureoles of the anorthositic Nain Complex, Labrador. *Journal of Petrology*, 18: 399-430.
- Berg, J.H. 1979. Physical constraints and tectonic setting of the Nain complex. *Geological Association of Canada Abstracts*, p. 39.
- Berg, J.H. and Docka, J. 1983. Geothermometry in the Kiglapait contact aureole, Labrador. *American Journal of Science*, 283: 414-434.
- Berg, J.H., Emslie, R.F., Hamilton, M.A., Morse, S.A., Ryan, A.B. and Wiebe, R.A. 1994. Anorthositic, granitoid and related rocks of the Nain Plutonic Suite. Field excursion to the Nain area. International Geological Correlation Programme IGCP Projects 290 and 315, 69 p.
- Berman, R.G. 1988. Internally consistent thermodynamic data for minerals in the Na₂O-K₂O-CaO-MgO-FeO-Fe₂O₃-Al₂O₃-SiO₂-TiO₂-H₂O-CO₂. *Journal of Petrology*, 29: 445-522.

- Berman, R.G. 1991. Thermobarometry using multi-equilibrium calculations. A new technique, with Petrological applications. *Canadian Mineralogist*, 29: 833-855.
- Berman, R.G. and Aranovich, L.Y. 1996. Optimized standard state and solution properties of minerals: I, Model calibration for olivine, orthopyroxene, cordierite, garnet, and ilmenite in the system FeO-MgO-CaO-Al₂O₃-TiO₂-SiO₂. *Contributions to Mineralogy and Petrology*, 126: 1-24.
- Bertrand, J-M, Roddick, J.C., Van Kranendonk, M.J. and Ermanovics, I. 1993. U-Pb geochronology of deformation and metamorphism across a central transect of the Early Proterozoic Torngat Orogen, North River map area, Labrador. *Canadian Journal of Earth Sciences*, 30: 1470-1489.
- Bolle, O., Demaiffe, D. and Duchesne, J-C. 2003. Petrogenesis of jotunitic and acidic members of an AMC suite (Rogaland anorthosite province, SW Norway): a Sr and Nd isotopic assessment. *Precambrian Research*, 124: 185-214.
- Connelly, J.N. 1993. U-Pb geochronological research agreement: final report for the Newfoundland Department of Mines and Energy, Labrador Mapping Section. Unpublished report on file with the Geological Survey, Department of Mines and Energy, St. John's, Newfoundland and Labrador.
- Connelly, J.N. and Ryan, B. 1994. Late Archean and Proterozoic events in the central Nain craton. *In* Lithoprobe Eastern Canadian Shield Onshore-Offshore Transect (ECSOOT), Lithoprobe Report no. 36, p.53-61.
- Connelly, J.N. and Ryan, B. 1996. Late Archean evolution of the Nain Province, Nain, Labrador: imprint of a collision. *Canadian Journal of Earth Sciences*, 33: 1325-1342.

- Dickin, A.P. 1995. Lead isotopes. *In* Radiogenic Isotope Geology. Cambridge, New York, 452 p.
- Duchesne, J-C. 1984. Massif anorthosites: another partisan review. *In* Feldspars, Feldspathoids and Their Parageneses. W.S. Brown (Ed.), Reidel, Boston, pp. 411-433.
- Dymek, R.G. and Gromet, L.P. 1984. Nature and origin of orthopyroxene megacrysts from the St. Urbain anorthosite massif, Quebec. *Canadian Mineralogist*, 22: 297-326.
- Emslie, R.F. 1975. Pyroxene megacrysts from anorthositic rocks: new clues to the sources and evolution of the parent magmas, *Canadian Mineralogist*, 13: 138-145.
- Emslie, R.F. 1985. Proterozoic anorthosite massifs. *In* The Deep Proterozoic crust in the North Atlantic Provinces. A.C. Tobi and J.L.R. Touret (Eds.), Reidel, Boston, pp. 39-60.
- Emslie, R.F. and Loveridge, W.D. 1992. Fluorite-bearing early and middle Proterozoic granites, Okak Bay area, Labrador: geochronology, geochemistry and petrogenesis. *Lithos*, 28: 87-109.
- Emslie, R.F. and Stirling, J.A.R. 1993. Rapakivi and related granitoids of the Nain Plutonic Suite: Geochemistry, mineral assemblages and fluid equilibria. *The Canadian Mineralogist*, 31: 821-847.
- Emslie, R.F., Hamilton, M.A. and Thériault, R.J. 1994. Petrogenesis of a Mid-Proterozoic Anorthosite-Mangerite-Charnockite-Granite (AMCG) Complex: Isotopic and chemical evidence from the Nain Plutonic Suite. *Journal of Geology*, 102: 539-558.
- Ermanovics, I. and van Kranendonk, M. 1990. The Torngat Orogen in the North River-Nutak transect area of Nain and Churchill provinces. *Geoscience Canada*, 17: 279-283.

- Ermanovics, I. and van Kranendonk, M. 1998. Geology of the Archean Nain Province and Paleoproterozoic Torngat Orogen in a transect of the North River-Nutak map areas, Newfoundland (Labrador) and Quebec. Geological Survey of Canada Bulletin 497, 156p.
- Fram, M.S. and Longhi, J. 1992. Phase equilibria of dikes associated with Proterozoic anorthosite complexes, *American Mineralogist*, 77: 605-616.
- Hall, J., Wardle, R.J., Gower, C.F., Kerr, A., Coflin, K., Keen, C.E. and Carroll, P. 1995. Proterozoic orogens of the northeastern Canadian Shield: new information from the Lithoprobe ECSOOT crustal reflection seismic survey. *Canadian Journal of Earth Sciences*, 32: 1119-1131.
- Hamilton, M.A., Emslie, R.F. and Roddick, J.C. 1994. Detailed emplacement chronology of basic magmas of the mid-Proterozoic Nain Plutonic Suite, Labrador: insights from U-Pb systematics in zircon and baddeleyite. *International Conference on Geochronology, Cosmochronology and Isotope Geology VIII, June 5-11, 1994, USGS Circular 1107*, p. 124.
- Hamilton, M.A. 1997. New U-Pb geochronological results from the Mesoproterozoic Nain Plutonic Suite, Labrador, and implications for the origin and emplacement of massif anorthosites and related rocks. COPENA conference, 1997 Abstract and Proceedings.
- Hamilton, M.A., Ryan, A.B., Emslie, R.F. and Ermanovics, I.F. 1998. Identification of Paleoproterozoic anorthositic and monzonitic rocks in the vicinity of the Mesoproterozoic Nain Plutonic Suite, Labrador: U-Pb evidence. *In Radiogenic Age and Isotopic Studies, Report 11, Geological Survey of Canada, Current Research 1998-F*, p. 23-40.
- Hoffman P.F. 1988. United plates of America, the birth of a craton: Early Proterozoic assembly and growth of Laurentia. *Annual Review of Earth and Planetary Sciences*, 16: 543-603.

- Hoffman P.F. 1990. Dynamics of the tectonic assembly of northeastern Laurentia in geon 18 (1.9-1.8 Ga). *Geoscience Canada*, 17: 222-226.
- Krogh, T.E. 1973. A low-contamination method for hydrothermal decomposition of zircon and extraction of U and Pb for isotopic age determinations. *Geochimica et Cosmochimica Acta*, 37: 485-494.
- Krogh T.E. and Davis, G.L. 1973. The significance of inherited zircons on the age and origin of igneous rocks; an investigation of the ages of the Labrador adamellites. *Carnegie Institution of Washington – Yearbook no. 72*, p. 610-613.
- Krogh, T.E. 1982a. Improved accuracy of U-Pb zircon dating by selection of more concordant fractions using a high gradient magnetic separation technique. *Geochimica et Cosmochimica Acta*, 46: 631-635.
- Krogh, T.E. 1982b. Improved accuracy of U-Pb zircon ages by the creation of more concordant systems using the air abrasion technique. *Geochimica et Cosmochimica Acta*, 46: 637-649.
- Lee, D.V. 1987. Geothermobarometry and petrologic history of a contact metamorphosed section of the Tasiuyak Gneiss, west of Nain, Labrador. Unpublished B.Sc. Honours thesis, Memorial University of Newfoundland, St. John's, Newfoundland and Labrador, 111 p.
- Longhi, J., Fram, M.S., Vander Auwera, J. and Monteith, J.N. 1993. Pressure effects, kinetics, and rheology of anorthositic and related magmas. *American Mineralogist*, 78: 1016-1030.

- Longhi, J., Vander Auwera, J., Fram, M.S. and Duchesne, J-C. 1999. Some phase equilibrium constraints on the origin of Proterozoic (massif) anorthosites and related rocks. *Journal of Petrology*, 40: 339-362.
- McFarlane, C.R.M., Carlson, W.D. and Connelly, J.N. 2003. Prograde, peak, and retrograde P-T paths from aluminum in orthopyroxene: High-temperature contact metamorphism in the aureole of the Makhavinekh Lake Pluton, Nain Plutonic Suite, Labrador. *Journal of Metamorphic Geology*, 21: 405-423.
- Mengel, F. and Rivers, T. 1991. Decompression reactions and P-T conditions in high-grade rocks, northern Labrador: P-T-t paths from individual samples and implications for Early Proterozoic tectonic evolution. *Journal of Petrology*, 32: 139-167.
- Morse, S.A. 1975. Plagioclase lamellae in hypersthene, Tikkoatokhakh Bay, Labrador. *Earth and Planetary Science Letters*, 26: 331-336.
- Morse, S.A. 1982. A partisan review of Proterozoic anorthosites. *American Mineralogist*, 67: 1087-1100.
- Rivers, T., Mengel, F., Scott, D.J., Campbell, L.M. and Goulet, N. 1996. Torngat Orogen – a Palaeoproterozoic example of a narrow doubly vergent collisional orogen. *In Precambrian Crustal Evolution in the North Atlantic Region*, T.S. Brewer (Ed.), Geological Society Special Publication No. 112, pp. 117-136.
- Royse, K.R. and Park, R.G. 2000. Emplacement of the Nain anorthosite: diapiric versus conduit ascent. *Canadian Journal of Earth Sciences*, 37: 1195-1207.

- Royse, K.R. and Ryan, B. 1995. Structural evolution and emplacement of the Nain Plutonic Suite in the Dog Island area. *In* Current Research 1995, Newfoundland Department of Mines and Energy, Geological Survey, Report 95-1, pp. 37-45.
- Ryan, B. 1990. Preliminary geological map of the Nain Plutonic Suite and surrounding rocks (Nain - Nutak, NTS 14 S.W.). Newfoundland Department of Mines and Energy, Geological Survey, Map 90-44, Scale 1:500 000.
- Ryan, B. 1991. Makhavinekh Lake pluton, Labrador, Canada: geological setting, subdivisions, mode of emplacement, and a comparison with Finnish rapakivi granites. *Precambrian Research*, 51: 193-225.
- Ryan, B. 1991. New perspectives on the Nain Plutonic Suite and its country rocks. *In* Current Research 1991, Newfoundland Department of Mines and Energy, Geological Survey, Report 91-1, pp. 231-255.
- Ryan, B., Krogh, T.E., Heaman, L. Schärer, U., Philippe, S. and Oliver, G. 1991. On recent geochronological studies in the Nain Province, Churchill Province and Nain Plutonic Suite, north-central Labrador. *In* Current Research 1991, Newfoundland Department of Mines and Energy, Geological Survey, Report 91-1, pp. 257-261.
- Ryan, B. 1993. Further results of mapping gneissic and plutonic rocks of the Nain area, Labrador. *In* Current Research 1993, Newfoundland Department of Mines and Energy, Geological Survey, Report 93-1, pp. 61-75.
- Ryan, B. 1997. The Mesoproterozoic Nain Plutonic Suite in Eastern Canada, and the setting of the Voisey's Bay Ni-Cu-Co sulphide deposit. *Geoscience Canada*, 24: 173-188.

- Ryan, B. and Hamilton, M.A. 1998. Paleoproterozoic anorthosites among Mesoproterozoic anorthosites: the field identification of two similar plutonic terranes in northern Labrador. GAC-MAC Joint Annual Meeting, Abstracts vol. 23, p. A163.
- Ryan, B. 2001. A provisional subdivision of the Nain Plutonic Suite in its type-area, Nain, Labrador (NTS map-area 14C/12). *In* Current Research. Newfoundland Department of Mines and Energy, Geological Survey, Report 2001-1, pp. 127-157.
- Ryan, B. and James, D. 2003. The Geology of Labrador between Tikkoatokak Bay and the Quebec border (NTS 14D, north half): A reconnaissance examination. *In* Current Research, Newfoundland Department of Mines and Energy, Geological Survey, Report 03-1, pp. 137-165.
- Scoates, J.S. and Chamberlain, K.R. 1997. Orogenic to post-orogenic origin for the 1.76 Ga Horse Creek Anorthosite Complex, Wyoming, USA. *Journal of Geology*, 105: 331-343.
- Scoates, J.S. and Chamberlain, K.R. 2003. Geochronologic, geochemical and isotopic constraints on the origin of monzonitic and related rocks in the Laramie anorthosite complex, Wyoming, USA. *Precambrian Research*, 124: 269-304.
- Scott, D.J. 1998. An overview of the U-Pb geochronology of the Paleoproterozoic Torngat Orogen, Northeastern Canada. *Precambrian Research*, 91: 91-107.
- Scott, D.J. and Machado, N. 1994. U-Pb geochronology of the northern Torngat Orogen: results from work in 1993. Eastern Canadian Shield Onshore-Offshore Transect (ECSOOT), Report of Transect Meeting. *Lithoprobe Report* 36, pp. 141-155.
- Simmons, K.R., Wiebe, R.A., Snyder, G.A. and Simmons, E.C. 1986. U-Pb zircon age for the Newark Island Layered Intrusion, Nain Anorthosite Complex, Labrador. *Geological*

- Society of America, 1986 Annual Meeting and Exposition, Abstracts with Programs, p. 751.
- Simmons, K.R. and Simmons, E.C. 1987. Petrogenetic implications of Pb- and Sr-isotopic compositions for rocks from the Nain Anorthosite Complex, Labrador. Geological Society of America, 1987 Annual Meeting and Exposition, Abstracts with Programs, p. 845.
- Spear, F.S., Kohn, M.J. and Cheney, J.T. 1999. P-T paths from anatexis pelites. *Contributions to Mineralogy and Petrology*, 134: 17-32.
- Speer, J.A. 1982. Metamorphism of the pelitic rocks of the Snyder Group in the contact aureole of the Kiglapait layered intrusion, Labrador; effects of buffering partial pressures of water. *Canadian Journal of Earth Sciences*, 19: 1888-1909.
- Stacey, J.S. and Kramers, J.D. 1975. Approximation of terrestrial lead isotope evolution by a two-stage model. *Earth and Planetary Science Letters*, 26: 207-221.
- Taylor, F.C. 1977a. Geological map of Tasisuak Lake, NTS 14D. Geological Survey of Canada, Map 1438A, Scale 1:250 000.
- Taylor, S.R., Campbell, I.H., McCulloch, M.T. and McLennan, S.M. 1984. A lower crustal origin for massif-type anorthosites. *Nature*, 311: 372-374.
- Tilton, G.R. 1960. Volume diffusion as a mechanism for discordant lead ages. *Journal of Geophysical Research*, 65: 2933-2945.
- Van Kranendonk, M.J. 1996. Tectonic evolution of the Paleoproterozoic Torngat Orogen: Evidence from pressure-temperature-time-deformation paths in the North River map area, Labrador. *Tectonics*, 15: 843-869.

- Van Kranendonk M.J. and Wardle, R.J. 1997. Crustal-scale flexural slip folding during late tectonic amplification of an orogenic boundary perturbation in the Paleoproterozoic Torngat Orogen, northeastern Canada. *Canadian Journal of Earth Sciences*, 34: 1545-1565.
- Van Kranendonk M.J., Wardle, R.J., Mengel, F.C., Campbell, L.M. and Reid, L. 1994. New results and summary of the Archaean and Palaeoproterozoic geology of the Burwell domain, northern Torngat Orogen, Labrador, Quebec, and Northwest Territories. *In Current Research 1994-C*, Geological Survey of Canada, pp. 321-332.
- Vielzeuf, D. and Schmidt, M.W. 2001. Melting relations in hydrous systems revisited: application to metapelites, metagreywackes and metabasalts. *Contributions to Mineralogy and Petrology*, 141: 251-267.
- Wardle, R.J. 1983. Nain-Churchill province cross-section, Nachvak Fiord, northern Labrador. *In Current Research*, Newfoundland Department of Mines and Energy, Mineral Development Division, Report 83-1, pp. 68-90.
- Wardle, R.J. and Van Kranendonk M.J. 1996. The Palaeoproterozoic Southeastern Churchill Province of Labrador-Quebec, Canada: orogenic development as a consequence of oblique collision and indentation. *In Precambrian Crustal Evolution in the North Atlantic Region*, T.S. Brewer (Ed.), Geological Society Special Publication, No. 112, pp. 137-153.
- Watson, D. 1980. Preliminary report on Labradorite occurrences near Nain, Labrador. Newfoundland Department of Mines and Energy, Mineral Development Division, Open File LAB 234, 10 p.
- Wetherill, G.W. 1956a. An interpretation of the Rhodesia and Witwatersrand age patterns. *Geochimica et Cosmochimica Acta*, 9: 290-292.

- Wetherill, G.W. 1956b. Discordant uranium-lead ages. *Transactions - American Geophysical Union*, 37: 320-327.
- Wheeler, E.P. 1942. Anorthosite and related rocks about Nain, Labrador. *Journal of Geology*, 50: 611-642.
- Wheeler, E.P. 1960. Anorthosite-adamellite complex of Nain, Labrador. *Bulletin of the Geological Society of America*, 71: 1755-1762.
- Wheeler, E.P. 1969. Minor intrusives associated with the Nain anorthosite. *In* *Origin of Anorthosite and Related Rocks*. Y.W. Isachsen (Ed.), New York State Museum Science Service, Memoir 18, Albany, New York, pp. 189-206.
- Wiebe, R.A. 1979. Anorthositic dikes, southern Nain complex, Labrador. *American Journal of Science*, 279: 394-410.
- Wiebe, R.A. 1986. Lower crustal cumulate nodules in Proterozoic dikes of the Nain complex: evidence for the origin of Proterozoic anorthosites, *Journal of Petrology*, 27: 1253-1276.
- Wiebe, R.A. 1990. Evidence for unusually feldspathic liquids in the Nain complex, Labrador. *American Mineralogist*, 75: 1-12.
- Xue, S. and Morse, S.A. 1993. Geochemistry of the Nain massif anorthosite, Labrador: Magma diversity in five intrusions. *Geochimica et Cosmochimica Acta*, 57: 3925-3948.

APPENDIX A

Table A.1: Analytical data for garnet, plagioclase and biotite from sample TL01-146.

TL01-146c GARNET

Distance (um)	OXIDES						CATION NUMBER					CHEMICAL COMPOSITION DATA				
	FeO	MgO	CaO	Al ₂ O ₃	SiO ₂	Total	Fe	Mg	Ca	Al	Si	Fe/ Fe+Mg	Mg/ Fe+Mg	XAlm	XPy	XGr
0	28.9181	9.4647	1.0702	22.0580	39.1944	100.71	1.8505	1.0795	0.0877	1.9893	2.9992	0.6316	0.3684	0.6132	0.3577	0.0291
53	30.1822	9.2577	0.9122	22.4696	39.6119	102.43	1.9054	1.0416	0.0738	1.9991	2.9903	0.6466	0.3534	0.6308	0.3448	0.0244
106	28.9084	9.7488	0.9349	21.9276	39.2665	100.79	1.8478	1.1106	0.0766	1.9752	3.0011	0.6246	0.3754	0.6088	0.3659	0.0252
159	28.7063	9.8895	1.0118	22.2031	39.3999	101.21	1.8247	1.1204	0.0824	1.9889	2.9946	0.6196	0.3804	0.6027	0.3701	0.0272
212	28.7157	9.1053	0.9259	21.4280	38.4010	98.58	1.8803	1.0626	0.0777	1.9774	3.0067	0.6389	0.3611	0.6225	0.3518	0.0257
265	28.3572	9.9901	0.9606	22.1666	39.4083	100.88	1.8053	1.1335	0.0783	1.9887	2.9999	0.6143	0.3857	0.5984	0.3757	0.0260
318	28.9410	9.8437	1.0170	21.8992	39.2461	100.95	1.8479	1.1202	0.0832	1.9706	2.9964	0.6226	0.3774	0.6056	0.3671	0.0273
371	0.2609	0.7989	0.0292	61.3365	36.8568	99.28	0.0143	0.0778	0.0020	4.7251	2.4091	0.1553	0.8447	0.6056	0.3671	0.0273
424	0.2058	0.8323	0.0001	61.5422	36.9398	99.52	0.0112	0.0809	0.0000	4.7280	2.4079	0.1216	0.8784	0.6056	0.3671	0.0273
477	0.1475	0.9033	0.0001	61.5281	36.9379	99.52	0.0080	0.0878	0.0000	4.7262	2.4074	0.0835	0.9165	0.6056	0.3671	0.0273
530	0.1670	0.8459	0.0001	61.3954	36.5771	98.99	0.0092	0.0826	0.0000	4.7424	2.3973	0.1002	0.8998	0.6056	0.3671	0.0273
583	29.0675	10.2223	1.0432	22.0768	39.6530	102.06	1.8347	1.1499	0.0844	1.9637	2.9927	0.6147	0.3853	0.5978	0.3747	0.0275
636	25.7382	7.2795	0.9535	21.6137	38.1636	93.75	1.7460	0.8801	0.0829	2.0663	3.0957	0.6649	0.3351	0.6056	0.3671	0.0273
689	28.8506	10.0582	1.0157	21.8277	39.4978	101.25	1.8349	1.1401	0.0828	1.9564	3.0038	0.6168	0.3832	0.6001	0.3728	0.0271
742	28.7493	10.0811	1.0438	22.2753	39.4083	101.56	1.8216	1.1385	0.0847	1.9891	2.9858	0.6154	0.3846	0.5983	0.3739	0.0278
795	27.8856	10.0858	0.9678	22.2048	39.4101	100.55	1.7772	1.1456	0.0790	1.9943	3.0033	0.6080	0.3920	0.5920	0.3816	0.0263
848	28.2348	10.4764	0.8992	22.0627	39.5659	101.24	1.7897	1.1835	0.0730	1.9708	2.9988	0.6019	0.3981	0.5875	0.3885	0.0240
901	28.4621	10.0779	0.9430	21.9466	39.2562	100.69	1.8176	1.1471	0.0772	1.9752	2.9977	0.6131	0.3869	0.5975	0.3771	0.0254
954	28.4700	10.1988	0.9308	22.0407	39.2855	100.93	1.8135	1.1579	0.0760	1.9786	2.9924	0.6103	0.3897	0.5951	0.3800	0.0249
1007	28.4888	10.2072	1.0074	21.8916	39.2834	100.88	1.8165	1.1600	0.0823	1.9672	2.9952	0.6103	0.3897	0.5939	0.3792	0.0269
1060	28.7343	10.1853	1.0461	22.2527	39.1568	101.38	1.8252	1.1531	0.0851	1.9921	2.9742	0.6128	0.3872	0.5958	0.3764	0.0278
1113	28.8039	10.1619	0.9578	22.1434	39.6046	101.67	1.8224	1.1459	0.0776	1.9744	2.9963	0.6140	0.3860	0.5983	0.3762	0.0255
1166	28.4922	10.2601	1.0686	22.2441	39.7986	101.86	1.7962	1.1528	0.0863	1.9763	3.0001	0.6091	0.3909	0.5918	0.3798	0.0284
1219	28.3151	10.3005	0.9730	22.1071	39.5330	101.23	1.7959	1.1644	0.0791	1.9760	2.9983	0.6067	0.3933	0.5909	0.3831	0.0260
1272	28.8066	10.2865	1.0048	22.0675	39.1098	101.28	1.8328	1.1665	0.0819	1.9787	2.9754	0.6111	0.3889	0.5948	0.3786	0.0266
1325	28.1043	9.9903	1.1108	22.0642	39.1420	100.41	1.7979	1.1390	0.0910	1.9892	2.9941	0.6122	0.3878	0.5938	0.3762	0.0301
1378	28.8936	10.2157	0.9777	22.0727	39.3342	101.49	1.8337	1.1555	0.0795	1.9742	2.9850	0.6134	0.3866	0.5975	0.3765	0.0259
1431	28.5746	10.0152	0.9955	22.1445	39.2344	100.96	1.8206	1.1373	0.0813	1.9884	2.9891	0.6155	0.3845	0.5990	0.3742	0.0268
1484	0.2819	0.9349	0.0001	60.1572	36.8553	98.23	0.0156	0.0920	0.0000	4.6827	2.4342	0.1450	0.8550	0.5990	0.3742	0.0268
1537	0.2773	0.8349	0.0001	61.4993	36.5900	99.20	0.0152	0.0814	0.0000	4.7431	2.3944	0.1573	0.8427	0.5990	0.3742	0.0268
1590	28.2454	9.9949	1.0491	22.2262	39.4570	100.97	1.7957	1.1325	0.0854	1.9914	2.9996	0.6132	0.3868	0.5959	0.3758	0.0283
1643	28.3678	10.1388	0.9739	22.1013	39.6469	101.23	1.7990	1.1460	0.0791	1.9753	3.0065	0.6109	0.3891	0.5949	0.3790	0.0262

A-1

1696	0.8109	0.9350	0.0001	60.2998	37.1916	99.24	0.0445	0.0914	0.0000	4.6587	2.4380	0.3274	0.6726	0.5990	0.3742	0.0268
1749	4.1343	2.5572	0.5674	20.1674	29.2347	56.66	0.4068	0.4484	0.0715	2.7963	3.4394	0.4757	0.5243	0.5990	0.3742	0.0268
1802	28.5683	9.8835	0.9018	22.1914	39.5161	101.06	1.8162	1.1199	0.0735	1.9882	3.0040	0.6186	0.3814	0.6035	0.3721	0.0244
1855	29.0618	9.9516	1.0646	22.3058	39.4554	101.84	1.8386	1.1221	0.0863	1.9888	2.9849	0.6210	0.3790	0.6034	0.3683	0.0283
1908	0.3269	0.9659	0.0001	61.2980	36.9072	99.50	0.0178	0.0940	0.0000	4.7143	2.4084	0.1592	0.8408	0.5990	0.3742	0.0268
1961	28.5902	9.7947	0.9742	22.1350	39.1864	100.68	1.8268	1.1155	0.0797	1.9932	2.9941	0.6209	0.3791	0.6045	0.3691	0.0264
2014	28.4016	9.9919	1.0149	21.9708	39.2836	100.66	1.8138	1.1373	0.0830	1.9774	2.9999	0.6146	0.3854	0.5978	0.3748	0.0274
2067	29.0305	9.8731	1.1138	22.0854	39.2674	101.37	1.8466	1.1193	0.0908	1.9798	2.9868	0.6226	0.3774	0.6041	0.3662	0.0297
2120	28.9149	10.0091	1.0319	22.2507	39.3621	101.57	1.8335	1.1312	0.0838	1.9883	2.9845	0.6184	0.3816	0.6014	0.3711	0.0275
2173	29.0313	10.1573	0.9932	21.7940	39.3494	101.33	1.8473	1.1520	0.0810	1.9544	2.9941	0.6159	0.3841	0.5997	0.3740	0.0263
2226	28.5685	10.4861	0.9749	21.9953	39.2453	101.27	1.8152	1.1875	0.0794	1.9696	2.9818	0.6045	0.3955	0.5889	0.3853	0.0258
2279	26.3486	4.8717	0.1786	13.8166	22.6751	67.89	2.6638	0.8778	0.0231	1.9685	2.7412	0.7521	0.2479	0.5990	0.3742	0.0268
2332	27.8205	10.6420	1.0488	22.1515	39.6818	101.34	1.7584	1.1988	0.0849	1.9731	2.9991	0.5946	0.4054	0.5780	0.3941	0.0279
2385	27.6143	10.1065	1.0074	22.0109	39.4013	100.14	1.7657	1.1517	0.0825	1.9834	3.0125	0.6052	0.3948	0.5886	0.3839	0.0275
2438	19.8829	2.4437	0.0335	17.2421	22.5529	62.16	2.0808	0.4558	0.0045	2.5430	2.8222	0.8203	0.1797	0.5990	0.3742	0.0268
2491	30.0363	9.3311	1.0958	21.9792	38.9219	101.36	1.9211	1.0637	0.0898	1.9812	2.9768	0.6436	0.3564	0.6248	0.3460	0.0292
2544	28.9640	9.8244	1.0305	22.3218	39.3738	101.51	1.8376	1.1109	0.0838	1.9958	2.9870	0.6232	0.3768	0.6060	0.3664	0.0276
2597	28.9740	9.6186	1.0074	22.1459	39.4543	101.20	1.8437	1.0909	0.0821	1.9860	3.0021	0.6283	0.3717	0.6112	0.3616	0.0272
2650	28.7122	9.6424	0.9551	21.9516	39.0890	100.35	1.8424	1.1028	0.0785	1.9851	2.9993	0.6256	0.3744	0.6093	0.3647	0.0260
2703	29.4322	9.8903	1.0221	21.9517	39.3550	101.65	1.8698	1.1198	0.0832	1.9653	2.9896	0.6254	0.3746	0.6085	0.3644	0.0271
2756	28.3216	9.6670	1.0500	21.7869	38.8839	99.71	1.8278	1.1119	0.0868	1.9815	3.0006	0.6218	0.3782	0.6039	0.3674	0.0287
2809	29.1946	9.8147	0.9726	21.8723	39.1533	101.01	1.8654	1.1177	0.0796	1.9695	2.9915	0.6253	0.3747	0.6091	0.3649	0.0260
2862	0.3100	0.8004	0.0001	61.0832	36.9407	99.13	0.0170	0.0781	0.0000	4.7125	2.4181	0.1788	0.8212	0.5990	0.3742	0.0268
2915	0.1229	0.9273	0.0001	61.6003	37.0233	99.67	0.0067	0.0899	0.0000	4.7237	2.4089	0.0694	0.9306	0.5990	0.3742	0.0268
2968	0.1501	0.7382	0.0001	61.3755	36.5510	98.81	0.0082	0.0722	0.0000	4.7477	2.3990	0.1020	0.8980	0.5990	0.3742	0.0268
3021	0.4240	1.0424	0.0430	58.2194	36.3925	96.12	0.0239	0.1049	0.0031	4.6345	2.4581	0.1856	0.8144	0.5990	0.3742	0.0268
3074	28.7917	9.9134	1.0374	22.0227	39.3371	101.10	1.8337	1.1253	0.0846	1.9766	2.9957	0.6197	0.3803	0.6025	0.3697	0.0278
3127	28.4506	10.2008	1.0263	22.2200	39.6305	101.53	1.7998	1.1501	0.0832	1.9809	2.9978	0.6101	0.3899	0.5934	0.3792	0.0274
3180	27.7753	9.5904	1.0316	22.3885	39.7334	100.52	1.7678	1.0879	0.0841	2.0082	3.0240	0.6190	0.3810	0.6013	0.3701	0.0286
3233	29.0984	10.0609	1.0567	22.1001	39.6117	101.93	1.8394	1.1335	0.0856	1.9688	2.9942	0.6187	0.3813	0.6014	0.3706	0.0280
3286	28.1369	10.0870	1.0739	22.1215	39.4128	100.83	1.7911	1.1444	0.0876	1.9845	3.0000	0.6102	0.3898	0.5925	0.3786	0.0290
3339	28.8594	9.7909	1.0073	21.9205	39.2553	100.83	1.8439	1.1149	0.0825	1.9738	2.9991	0.6232	0.3768	0.6063	0.3666	0.0271
3392	28.9883	9.9730	1.0707	22.0547	39.4606	101.55	1.8393	1.1278	0.0870	1.9721	2.9939	0.6199	0.3801	0.6022	0.3693	0.0285
3445	28.7950	10.1615	0.9373	22.4172	39.3851	101.70	1.8217	1.1457	0.0760	1.9986	2.9794	0.6139	0.3861	0.5986	0.3765	0.0250
3498	28.9515	10.0944	0.9927	22.4687	39.7317	102.24	1.8215	1.1319	0.0800	1.9922	2.9891	0.6167	0.3833	0.6005	0.3731	0.0264
3551	28.7203	9.9866	1.0416	22.0533	39.3219	101.12	1.8282	1.1330	0.0849	1.9784	2.9931	0.6174	0.3826	0.6002	0.3720	0.0279
3604	0.7010	0.8690	0.0001	61.0265	36.6435	99.24	0.0384	0.0849	0.0000	4.7149	2.4021	0.3114	0.6886	0.5990	0.3742	0.0268
3657	28.8329	10.0556	1.0621	22.2364	39.3602	101.55	1.8282	1.1364	0.0863	1.9870	2.9843	0.6167	0.3833	0.5992	0.3725	0.0283
3710	28.7529	9.9514	0.9965	21.9681	39.4634	101.13	1.8296	1.1286	0.0812	1.9700	3.0027	0.6185	0.3815	0.6020	0.3713	0.0267

3763	28.7933	9.6819	0.9644	21.9040	39.4572	100.80	1.8383	1.1017	0.0789	1.9709	3.0124	0.6253	0.3747	0.6089	0.3649	0.0261
3816	28.7228	9.8772	1.0495	22.2216	39.2350	101.11	1.8287	1.1208	0.0856	1.9939	2.9870	0.6200	0.3800	0.6025	0.3693	0.0282
3869	28.8780	9.9193	0.9926	21.8414	39.3573	100.99	1.8421	1.1277	0.0811	1.9634	3.0020	0.6203	0.3797	0.6038	0.3696	0.0266
3922	29.0884	9.8920	0.9904	21.8869	39.4201	101.28	1.8515	1.1222	0.0808	1.9633	3.0003	0.6226	0.3774	0.6062	0.3674	0.0265

TL01-146d GARNET

Distance (um)	OXIDES						CATION NUMBER					CHEMICAL COMPOSITION DATA				
	FeO	MgO	CaO	Al ₂ O ₃	SiO ₂	Total	Fe	Mg	Ca	Al	Si	Fe/ Fe+Mg	Mg/ Fe+Mg	XAlm	XPyp	XGr
0	29.3158	9.7906	1.0824	21.7882	39.1101	101.09	1.8738	1.1153	0.0886	1.9626	2.9892	0.6269	0.3731	0.6088	0.3624	0.0288
50	28.9644	9.8059	1.0322	22.1802	39.1504	101.13	1.8460	1.1139	0.0843	1.9922	2.9837	0.6237	0.3763	0.6064	0.3659	0.0277
100	28.6219	9.9000	1.0658	21.8228	39.3028	100.71	1.8293	1.1277	0.0873	1.9656	3.0037	0.6186	0.3814	0.6009	0.3704	0.0287
150	28.9639	9.7108	1.0578	21.9406	39.3355	101.01	1.8480	1.1043	0.0865	1.9728	3.0010	0.6260	0.3740	0.6081	0.3634	0.0285
200	28.3215	9.9913	1.1080	21.9571	39.5655	100.94	1.8021	1.1331	0.0903	1.9690	3.0105	0.6140	0.3860	0.5956	0.3745	0.0298
250	29.3910	9.7321	1.0950	22.1621	39.3432	101.72	1.8653	1.1008	0.0890	1.9822	2.9857	0.6289	0.3711	0.6106	0.3603	0.0291
300	28.4428	9.6188	1.0667	21.7302	39.4587	100.32	1.8227	1.0986	0.0876	1.9625	3.0237	0.6239	0.3761	0.6058	0.3651	0.0291
350	28.5668	9.7776	1.0213	22.0623	39.4370	100.87	1.8210	1.1108	0.0834	1.9819	3.0060	0.6211	0.3789	0.6039	0.3684	0.0277
400	27.9462	10.3988	1.2004	23.8750	41.3677	104.79	1.6987	1.1266	0.0935	2.0452	3.0067	0.6012	0.3988	0.5820	0.3860	0.0320
450	28.7534	9.8830	1.1368	21.9512	39.2908	101.02	1.8334	1.1232	0.0929	1.9726	2.9958	0.6201	0.3799	0.6012	0.3683	0.0305
500	28.7524	9.6465	1.0162	22.1624	39.4624	101.04	1.8307	1.0947	0.0829	1.9886	3.0044	0.6258	0.3742	0.6085	0.3639	0.0276
550	29.1208	9.9461	1.0487	22.2563	39.5290	101.90	1.8414	1.1209	0.0850	1.9833	2.9889	0.6216	0.3784	0.6043	0.3678	0.0279
600	28.9915	9.9174	0.9811	22.2209	39.4015	101.51	1.8395	1.1215	0.0798	1.9870	2.9894	0.6212	0.3788	0.6049	0.3688	0.0262
650	29.0247	9.7758	1.0646	22.0061	39.1449	101.02	1.8532	1.1124	0.0871	1.9801	2.9886	0.6249	0.3751	0.6071	0.3644	0.0285
700	28.7500	9.8573	1.0585	21.7779	39.4465	100.89	1.8346	1.1211	0.0865	1.9585	3.0100	0.6207	0.3793	0.6031	0.3685	0.0284
750	29.1619	9.7211	1.0155	22.2416	39.1692	101.31	1.8567	1.1031	0.0828	1.9956	2.9820	0.6273	0.3727	0.6102	0.3626	0.0272
800	28.7014	10.0661	1.0480	22.2233	39.5350	101.57	1.8174	1.1360	0.0850	1.9831	2.9934	0.6154	0.3846	0.5981	0.3739	0.0280
850	29.3119	10.0319	1.0672	21.8956	39.3090	101.62	1.8625	1.1361	0.0869	1.9607	2.9867	0.6211	0.3789	0.6036	0.3682	0.0282
900	28.6697	9.5522	1.0839	21.9055	39.0977	100.31	1.8408	1.0931	0.0892	1.9822	3.0018	0.6274	0.3726	0.6089	0.3616	0.0295
950	28.5471	9.7816	0.9960	22.1787	39.2371	100.74	1.8224	1.1129	0.0815	1.9953	2.9951	0.6209	0.3791	0.6041	0.3689	0.0270
1000	28.8035	9.5759	1.1117	21.9289	39.2619	100.68	1.8430	1.0920	0.0911	1.9774	3.0039	0.6279	0.3721	0.6090	0.3609	0.0301
1050	28.7919	9.9699	1.0155	21.9609	39.2814	101.02	1.8356	1.1328	0.0829	1.9731	2.9945	0.6184	0.3816	0.6016	0.3713	0.0272
1100	28.9075	9.7881	1.0166	21.9211	39.3133	100.95	1.8450	1.1135	0.0831	1.9718	3.0004	0.6236	0.3764	0.6066	0.3661	0.0273
1150	29.2361	9.8552	1.0774	22.0865	39.4016	101.66	1.8553	1.1146	0.0876	1.9752	2.9898	0.6247	0.3753	0.6068	0.3645	0.0287
1200	0.8476	0.9099	0.0001	61.9709	37.9954	101.72	0.0453	0.0867	0.0000	4.6716	2.4303	0.3432	0.6568	0.6068	0.3645	0.0287
1250	28.9611	9.6744	1.0648	21.9682	39.3477	101.02	1.8475	1.1000	0.0870	1.9750	3.0015	0.6268	0.3732	0.6088	0.3625	0.0287
1300	28.6252	9.8737	1.0617	22.0972	39.3052	100.96	1.8243	1.1215	0.0867	1.9846	2.9953	0.6193	0.3807	0.6016	0.3698	0.0286
1350	29.0365	9.7631	1.0630	22.1111	39.3144	101.29	1.8479	1.1074	0.0867	1.9831	2.9917	0.6253	0.3747	0.6075	0.3640	0.0285
1400	9.0049	17.0738	0.2889	14.3523	38.4191	79.14	0.6669	2.2538	0.0274	1.4980	3.4024	0.2283	0.7717	0.6068	0.3645	0.0287
1450	8.9267	17.5899	0.3387	14.8851	39.5459	81.29	0.6424	2.2561	0.0312	1.5096	3.4030	0.2216	0.7784	0.6068	0.3645	0.0287

A-3

1500	8.9483	17.2437	0.2914	14.3982	38.4552	79.34	0.8610	2.2701	0.0276	1.4988	3.3966	0.2255	0.7745	0.6068	0.3645	0.0287
1550	42.2592	2.3468	0.0001	0.6394	0.8194	46.06	10.1924	1.0088	0.0000	0.2173	0.2363	0.9099	0.0901	0.6068	0.3645	0.0287
1600	8.7098	18.7253	0.3048	15.3671	40.0790	83.19	0.6119	2.3447	0.0274	1.5215	3.3669	0.2070	0.7930	0.6068	0.3645	0.0287
1650	7.8042	18.8264	0.3122	14.4112	39.4065	80.76	0.5626	2.4188	0.0288	1.4641	3.3968	0.1887	0.8113	0.6068	0.3645	0.0287
1700	28.7341	9.5856	1.0397	21.8471	38.8647	100.07	1.8510	1.1006	0.0858	1.9834	2.9938	0.6271	0.3729	0.6094	0.3623	0.0282
1750	28.7572	9.5006	1.0601	21.8602	39.0769	100.26	1.8482	1.0883	0.0873	1.9800	3.0031	0.6294	0.3706	0.6112	0.3599	0.0289
1800	27.9868	8.5120	1.0403	23.5321	37.0646	98.14	1.8364	0.9955	0.0875	2.1761	2.9082	0.6485	0.3515	0.6290	0.3410	0.0300
1850	29.4858	9.6220	1.0395	21.8249	39.0573	101.03	1.8870	1.0975	0.0852	1.9684	2.9889	0.6323	0.3677	0.6147	0.3575	0.0278
1900	29.4202	9.7143	1.0408	22.2341	38.9302	101.34	1.8762	1.1041	0.0850	1.9982	2.9687	0.6295	0.3705	0.6121	0.3602	0.0277
1950	28.9278	9.6904	1.0653	22.0308	39.5137	101.23	1.8403	1.0987	0.0868	1.9751	3.0058	0.6262	0.3738	0.6082	0.3631	0.0287
2000	29.0783	9.6848	1.1398	22.1066	39.3336	101.34	1.8502	1.0983	0.0929	1.9823	2.9926	0.6275	0.3725	0.6083	0.3611	0.0305
2050	29.4709	9.3080	1.0774	21.7601	39.1278	100.74	1.8910	1.0645	0.0886	1.9677	3.0022	0.6398	0.3602	0.6212	0.3497	0.0291
2100	30.4588	9.0365	1.0671	22.2763	39.3408	102.18	1.9328	1.0220	0.0868	1.9921	2.9851	0.6541	0.3459	0.6355	0.3360	0.0285
2150	29.4252	9.3252	1.0529	21.7998	38.8232	100.43	1.8951	1.0704	0.0869	1.9786	2.9898	0.6390	0.3610	0.6209	0.3507	0.0285
2200	29.1704	9.5776	1.0230	22.0553	39.2298	101.06	1.8620	1.0896	0.0837	1.9840	2.9943	0.6308	0.3692	0.6134	0.3590	0.0276
2250	29.5767	9.4753	1.0344	22.0410	39.2415	101.37	1.8856	1.0766	0.0845	1.9803	2.9915	0.6366	0.3634	0.6189	0.3534	0.0277
2300	29.1108	9.5881	1.0558	21.9634	39.3681	101.09	1.8568	1.0900	0.0863	1.9743	3.0027	0.6301	0.3699	0.6122	0.3594	0.0285
2350	28.6661	9.4450	0.9388	22.0353	39.3135	100.40	1.8366	1.0785	0.0771	1.9895	3.0118	0.6300	0.3700	0.6138	0.3604	0.0258
2400	29.4901	9.5348	1.1071	22.0603	39.1574	101.35	1.8805	1.0837	0.0904	1.9825	2.9858	0.6344	0.3656	0.6156	0.3548	0.0296
2450	29.4095	9.2356	1.0549	21.8389	39.1085	100.65	1.8881	1.0568	0.0868	1.9759	3.0023	0.6411	0.3589	0.6228	0.3486	0.0286
2500	30.3651	8.9638	1.1312	22.0237	39.0657	101.55	1.9405	1.0210	0.0926	1.9835	2.9853	0.6552	0.3448	0.6354	0.3343	0.0303
2550	31.0926	8.1858	1.1529	21.7677	39.0978	101.30	1.9987	0.9378	0.0949	1.9720	3.0053	0.6806	0.3194	0.6593	0.3094	0.0313
2600	7.1142	23.2715	0.4092	11.9676	45.0186	87.78	0.4689	2.7336	0.0348	1.1116	3.5478	0.1464	0.8536	0.6068	0.3645	0.0287
2650	82.7274	0.2124	0.0001	0.2836	0.6421	83.87	11.6461	0.0533	0.0000	0.0563	0.1081	0.9954	0.0046	0.6068	0.3645	0.0287
2700	26.2529	10.1567	1.1598	26.2332	43.7022	107.50	1.5307	1.0555	0.0866	2.1556	3.0469	0.5919	0.4081	0.6068	0.3645	0.0287
2750	30.3082	8.8078	1.0722	21.9119	38.7347	100.83	1.9519	1.0110	0.0885	1.9887	2.9828	0.6588	0.3412	0.6397	0.3313	0.0290
2800	29.8250	9.1131	1.0202	22.0137	38.8892	100.86	1.9148	1.0428	0.0839	1.9917	2.9855	0.6474	0.3526	0.6296	0.3429	0.0276
2850	29.5648	9.2110	1.0965	21.9594	38.9259	100.76	1.8982	1.0541	0.0902	1.9870	2.9885	0.6430	0.3570	0.6239	0.3465	0.0296
2900	29.7636	8.8654	1.0884	21.9780	38.8714	100.57	1.9163	1.0173	0.0898	1.9942	2.9926	0.6532	0.3468	0.6338	0.3365	0.0297
2950	30.7857	8.9605	1.1143	22.0721	39.0676	102.00	1.9622	1.0179	0.0910	1.9826	2.9775	0.6584	0.3416	0.6389	0.3314	0.0296

- indicates poor results

TL01-146] GARNET 7

Distance (um)	OXIDES								CATION NUMBERS						CHEMICAL COMPOSITION DATA					
	FeO	MgO	CaO	MnO	TiO ₂	Al ₂ O ₃	SiO ₂	Total	Fe	Mg	Ca	Mn	Al	Si	Fe/Mg (A-A')	Mg/ Fe+Mg (A-A')	XAlm	XPyp	XGrS	XSps
0	30.3640	8.7555	1.0084	0.2229	0.0002	21.6947	38.5139	100.56	1.9647	1.0097	0.0836	0.0146	1.9783	2.9799	0.6605	0.3395	0.6394	0.3286	0.0272	0.0048
58	29.9814	8.9185	1.0010	0.1750	0.0002	21.8177	38.3325	100.23	1.9434	1.0303	0.0831	0.0115	1.9930	2.9711	0.6535	0.3465	0.6334	0.3358	0.0271	0.0037
116	29.3701	8.6879	1.0446	0.1807	0.0002	21.9069	38.3351	99.53	1.9117	1.0079	0.0871	0.0119	2.0095	2.9836	0.6548	0.3452	0.6333	0.3339	0.0289	0.0039
174	29.7898	8.8347	1.0136	0.1703	0.0002	21.5847	38.5518	99.95	1.9341	1.0223	0.0843	0.0112	1.9749	2.9929	0.6542	0.3458	0.6337	0.3350	0.0276	0.0037
232	29.6547	8.7765	1.0416	0.1739	0.0002	21.7409	38.4450	99.83	1.9266	1.0162	0.0867	0.0114	1.9905	2.9866	0.6547	0.3453	0.6336	0.3342	0.0285	0.0037
290	30.0131	8.8411	1.0563	0.1632	0.0002	21.7359	38.1801	99.99	1.9516	1.0246	0.0880	0.0108	1.9918	2.9686	0.6557	0.3443	0.6347	0.3332	0.0286	0.0035
348	29.9346	9.0124	1.0298	0.2217	0.0002	22.1141	38.7216	101.03	1.9220	1.0314	0.0847	0.0144	2.0010	2.9729	0.6508	0.3492	0.6296	0.3379	0.0277	0.0047
406	29.9190	8.8854	1.1045	0.2259	0.0002	21.8714	38.5509	100.56	1.9320	1.0226	0.0914	0.0148	1.9904	2.9768	0.6539	0.3461	0.6312	0.3341	0.0299	0.0048
464	29.5722	8.8065	1.0249	0.1834	0.0002	21.9081	38.2944	99.79	1.9217	1.0200	0.0853	0.0121	2.0064	2.9757	0.6533	0.3467	0.6323	0.3356	0.0281	0.0040
522	29.6171	8.7796	1.0658	0.1553	0.0002	21.8100	38.2126	99.64	1.9286	1.0190	0.0889	0.0102	2.0015	2.9755	0.6543	0.3457	0.6330	0.3345	0.0292	0.0033
580	29.7920	8.9066	1.1024	0.2012	0.0002	21.6474	38.4103	100.06	1.9335	1.0302	0.0917	0.0132	1.9799	2.9808	0.6524	0.3476	0.6301	0.3357	0.0299	0.0043
638	29.8491	8.7194	1.0660	0.2186	0.0002	21.6562	38.5309	100.04	1.9372	1.0086	0.0886	0.0144	1.9807	2.9901	0.6576	0.3424	0.6354	0.3308	0.0291	0.0047
696	29.5270	8.9029	1.0484	0.1135	0.0002	21.6183	38.1727	99.38	1.9273	1.0357	0.0877	0.0075	1.9886	2.9794	0.6505	0.3495	0.6302	0.3387	0.0287	0.0025
754	29.5622	8.7391	1.1321	0.1979	0.0002	21.7870	38.3528	99.77	1.9221	1.0127	0.0943	0.0130	1.9963	2.9817	0.6549	0.3451	0.6318	0.3329	0.0310	0.0043
812	29.7443	8.7597	1.0508	0.2213	0.0002	21.5758	38.3765	99.73	1.9365	1.0165	0.0876	0.0146	1.9796	2.9877	0.6558	0.3442	0.6338	0.3327	0.0287	0.0048
870	30.2548	8.8818	1.0368	0.1285	0.0002	21.8382	38.3038	100.44	1.9592	1.0251	0.0860	0.0084	1.9929	2.9659	0.6565	0.3435	0.6364	0.3330	0.0279	0.0027
928	29.8109	8.7447	1.1195	0.2225	0.0002	21.9370	38.5538	100.39	1.9271	1.0075	0.0927	0.0146	1.9985	2.9802	0.6567	0.3433	0.6335	0.3312	0.0305	0.0048
986	30.4555	8.3072	1.0845	0.1629	0.0002	21.5793	38.1259	99.72	1.9904	0.9676	0.0908	0.0108	1.9875	2.9795	0.6729	0.3271	0.6505	0.3163	0.0297	0.0035
1044	30.2670	8.7201	1.0828	0.2418	0.0002	21.7857	38.3742	100.47	1.9604	1.0067	0.0899	0.0159	1.9886	2.9721	0.6607	0.3393	0.6380	0.3276	0.0293	0.0052
1102	29.6995	8.7971	1.0518	0.1727	0.0002	21.7831	38.1930	99.70	1.9339	1.0209	0.0877	0.0114	1.9989	2.9738	0.6545	0.3455	0.6333	0.3343	0.0287	0.0037
1160	30.1708	8.7898	1.0688	0.1856	0.0002	21.7368	38.2987	100.25	1.9577	1.0165	0.0889	0.0122	1.9877	2.9716	0.6582	0.3418	0.6366	0.3305	0.0289	0.0040
1218	30.3322	8.6358	1.0193	0.2742	0.0002	21.7017	38.4373	100.40	1.9664	0.9978	0.0847	0.0180	1.9827	2.9796	0.6634	0.3366	0.6412	0.3253	0.0276	0.0059
1276	30.2121	8.6921	1.1078	0.2047	0.0002	21.9147	38.3211	100.45	1.9565	1.0032	0.0919	0.0134	2.0000	2.9674	0.6610	0.3390	0.6383	0.3273	0.0300	0.0044
1334	30.4427	8.5821	1.1204	0.1490	0.0002	21.6200	38.0477	99.96	1.9852	0.9974	0.0936	0.0098	1.9869	2.9668	0.6656	0.3344	0.6433	0.3232	0.0303	0.0032
1392	30.1225	8.6363	1.0858	0.1692	0.0002	21.7064	38.3974	100.12	1.9561	0.9996	0.0903	0.0111	1.9865	2.9816	0.6618	0.3382	0.6399	0.3270	0.0295	0.0036
1450	29.5257	8.8534	1.0786	0.1688	0.0002	21.6923	38.0958	99.41	1.9275	1.0301	0.0902	0.0112	1.9957	2.9738	0.6517	0.3483	0.6301	0.3367	0.0295	0.0037
1508	30.2237	8.7828	1.0724	0.2239	0.0002	21.7813	38.2046	100.29	1.9616	1.0160	0.0892	0.0147	1.9923	2.9650	0.6588	0.3412	0.6366	0.3297	0.0289	0.0048
1566	30.0943	8.7827	1.1550	0.2387	0.0002	21.7869	38.3331	100.39	1.9500	1.0143	0.0959	0.0157	1.9895	2.9700	0.6578	0.3422	0.6340	0.3298	0.0312	0.0051
1624	29.9947	8.8825	1.1101	0.1857	0.0002	21.8665	38.2652	100.30	1.9438	1.0259	0.0922	0.0122	1.9970	2.9652	0.6545	0.3455	0.6323	0.3337	0.0300	0.0040
1682	29.8935	3.1137	1.2382	0.4363	0.1899	9.9657	18.1394	62.98	3.5079	0.6512	0.1861	0.0519	1.6481	2.5453	0.8434	0.1566	0.7978	0.1481	0.0423	0.0118
1740	29.7040	8.6575	1.1236	0.2059	0.0002	21.7541	38.0834	99.53	1.9388	1.0072	0.0940	0.0136	2.0011	2.9724	0.6581	0.3419	0.6349	0.3298	0.0308	0.0045
1798	29.8937	8.5555	1.0605	0.1922	0.0002	21.6638	38.1367	99.50	1.9528	0.9961	0.0888	0.0127	1.9944	2.9790	0.6622	0.3378	0.6402	0.3265	0.0291	0.0042
1856	29.9674	8.5776	1.1031	0.1927	0.0002	21.9394	38.3463	100.13	1.9444	0.9919	0.0917	0.0127	2.0061	2.9751	0.6622	0.3378	0.6395	0.3262	0.0302	0.0042
1914	30.0577	8.5352	0.9976	0.1793	0.0002	21.6431	38.2352	99.65	1.9611	0.9925	0.0834	0.0118	1.9901	2.9830	0.6640	0.3360	0.6432	0.3255	0.0274	0.0039
1972	30.0600	8.6391	1.1203	0.1902	0.0002	21.8028	38.3272	100.14	1.9516	0.9996	0.0932	0.0125	1.9948	2.9754	0.6613	0.3387	0.6384	0.3270	0.0305	0.0041
2030	29.9821	8.6570	1.1143	0.2223	0.0002	21.8183	38.3187	100.11	1.9466	1.0018	0.0927	0.0146	1.9963	2.9749	0.6602	0.3398	0.6370	0.3278	0.0303	0.0048
2088	29.7630	8.7664	1.0841	0.2181	0.0002	21.6463	38.2823	99.76	1.9378	1.0173	0.0904	0.0144	1.9862	2.9804	0.6557	0.3443	0.6333	0.3325	0.0295	0.0047
2146	29.9257	8.7614	1.0982	0.1696	0.0002	21.7580	38.3048	100.02	1.9441	1.0144	0.0914	0.0112	1.9920	2.9755	0.6571	0.3429	0.6351	0.3314	0.0299	0.0037
2204	30.0336	8.7949	0.9995	0.2181	0.0002	21.8889	38.0910	100.03	1.9526	1.0191	0.0832	0.0144	2.0055	2.9612	0.6571	0.3429	0.6362	0.3320	0.0271	0.0047
Distance (um)	FeO	MgO	CaO	MnO	TiO ₂	Al ₂ O ₃	SiO ₂	Total	Fe	Mg	Ca	Mn	Al	Si	Fe/Mg (B-B')	Mg/ Fe+Mg (B-B')	XAlm	XPyp	XGrS	XSps
0	31.2469	7.9240	0.9226	0.2513	0.0294	21.6419	38.2589	100.28	2.0367	0.9205	0.0770	0.0166	1.9880	2.9819	0.6887	0.3113	0.6676	0.3017	0.0252	0.0054
60	30.2881	8.6501	0.8387	0.1699	0.0002	21.7094	38.3691	100.03	1.9688	1.0022	0.0698	0.0112	1.9888	2.9824	0.6627	0.3373	0.6451	0.3284	0.0229	0.0037
120	30.0463	8.8684	0.9664	0.2072	0.0002	21.8121	38.2853	100.19	1.9493	1.0254	0.0803	0.0136	1.9942	2.9700	0.6553	0.3447	0.6352	0.3342	0.0262	0.0044
180	30.2265	8.7556	1.0160	0.2178	0.0002	21.8933	38.5204	100.63	1.9526	1.0081	0.0841	0.0143	1.9932	2.9756	0.6595	0.3405	0.6383	0.3295	0.0275	0.0047
240	30.0915	8.5679	0.9827	0.1766	0.0002	21.8809	38.4284	100.13	1.9523	0.9907	0.0817	0.0116	2.0007	2.9813	0.6634	0.3366	0.6430	0.3283	0.0269	0.0038
300	28.1950	8.9760	0.9593	0.1830	0.0002	19.7510	34.9974	93.06	1.9779	1.1223	0.0862	0.0130	1.9527	2.9358	0.6380	0.3620	0.6182	0.3508	0.0289	0.0041

A-5

360	22.5526	10.4828	0.8590	0.1974	0.0281	17.3225	34.0978	85.54	1.6835	1.3947	0.0821	0.0149	1.8224	3.0437	0.5469	0.4531	0.5302	0.4392	0.0259	0.0047
420	30.4587	8.1200	1.0240	0.2565	0.0002	21.6166	38.2070	99.68	1.9911	0.9460	0.0858	0.0170	1.9914	2.9865	0.6779	0.3221	0.6550	0.3112	0.0282	0.0056
480	8.1864	8.5507	1.9280	0.0001	0.0002	26.1221	49.4900	94.28	0.4925	0.9168	0.1486	0.0000	2.2146	3.5601	0.3495	0.6505	0.3161	0.5885	0.0954	0.0000
540	30.7636	8.3611	1.0573	0.2638	0.0002	21.6976	38.1338	100.28	2.0025	0.9700	0.0882	0.0174	1.9904	2.9682	0.6737	0.3263	0.6506	0.3151	0.0287	0.0057
600	30.4367	8.6393	1.0875	0.1955	0.0002	21.5715	38.1030	100.03	1.9834	1.0034	0.0908	0.0129	1.9810	2.9690	0.6641	0.3359	0.6418	0.3247	0.0294	0.0042
660	30.2118	8.6218	1.1025	0.2533	0.0002	21.8565	38.6551	100.70	1.9502	0.9919	0.0912	0.0166	1.9883	2.9838	0.6629	0.3371	0.6394	0.3252	0.0299	0.0054
720	30.2135	8.8782	1.0664	0.2489	0.0002	21.6278	38.3402	100.38	1.9591	1.0260	0.0886	0.0163	1.9764	2.9727	0.6563	0.3437	0.6340	0.3320	0.0287	0.0053
780	30.2290	8.7333	1.0551	0.2065	0.0002	21.8089	38.1893	100.22	1.9630	1.0108	0.0878	0.0136	1.9959	2.9655	0.6601	0.3399	0.6383	0.3287	0.0286	0.0044
840	30.0528	8.8057	1.0601	0.1975	0.0002	21.6308	38.2465	99.99	1.9547	1.0208	0.0883	0.0130	1.9827	2.9746	0.6569	0.3431	0.6353	0.3318	0.0287	0.0042
900	29.8505	8.8839	1.1340	0.1932	0.0002	21.8031	38.0996	99.96	1.9411	1.0296	0.0945	0.0127	1.9981	2.9625	0.6534	0.3466	0.6307	0.3345	0.0307	0.0041
960	29.8496	8.9264	1.0982	0.1545	0.0002	21.6582	38.1982	99.89	1.9419	1.0350	0.0915	0.0102	1.9857	2.9715	0.6523	0.3477	0.6308	0.3362	0.0297	0.0033
1020	30.1084	8.7283	1.1507	0.1717	0.0002	21.6909	38.3603	100.21	1.9540	1.0096	0.0957	0.0113	1.9838	2.9769	0.6593	0.3407	0.6364	0.3288	0.0312	0.0037
1080	29.9748	8.7917	1.0841	0.1649	0.0002	21.6504	38.4828	100.15	1.9443	1.0164	0.0901	0.0108	1.9791	2.9848	0.6567	0.3433	0.6351	0.3320	0.0294	0.0035
1140	29.7187	8.9159	1.1095	0.1965	0.0002	21.7299	38.3555	100.03	1.9288	1.0313	0.0923	0.0129	1.9875	2.9767	0.6516	0.3484	0.6292	0.3364	0.0301	0.0042
1200	29.8350	8.8134	1.0828	0.1641	0.0002	21.6663	38.5980	100.16	1.9331	1.0178	0.0899	0.0108	1.9784	2.9904	0.6551	0.3449	0.6335	0.3335	0.0295	0.0035
1260	29.6119	8.9365	1.0702	0.1857	0.0002	21.7363	38.3647	99.91	1.9229	1.0343	0.0890	0.0122	1.9892	2.9789	0.6502	0.3498	0.6287	0.3382	0.0291	0.0040
1320	29.1771	9.6970	1.0474	0.1433	0.0002	23.2495	40.4853	103.80	1.8055	1.0695	0.0830	0.0090	2.0276	2.9958	0.6280	0.3720	0.6085	0.3605	0.0280	0.0030
1380	29.7114	8.8655	1.1012	0.1706	0.0002	21.6009	38.3401	99.79	1.9330	1.0280	0.0918	0.0112	1.9805	2.9826	0.6528	0.3472	0.6309	0.3355	0.0300	0.0037
1440	29.8854	8.8459	0.9898	0.1832	0.0002	21.6716	38.2987	99.87	1.9437	1.0254	0.0825	0.0121	1.9863	2.9785	0.6546	0.3454	0.6344	0.3347	0.0269	0.0039

TL01-146] GARNET 9

Distance (um)	OXIDES								CATION NUMBERS						CHEMICAL COMPOSITION DATA					
	FeO	MgO	CaO	MnO	TiO ₂	Al ₂ O ₃	SiO ₂	Total	Fe	Mg	Ca	Mn	Al	Si	Fe/ Fe+Mg (A-A')	Mg/ Fe+Mg (A-A')	XAlm	XPy	XGr	XSp
	0	29.8296	8.8826	0.9174	0.1882	0.0002	21.8772	38.7054	100.40	1.9262	1.0223	0.0759	0.0123	1.9908	2.9886	0.6533	0.3467	0.6343	0.3366	0.0250
60	29.1069	9.5095	0.8981	0.1981	0.0002	21.6965	38.6715	100.08	1.8803	1.0949	0.0743	0.0130	1.9753	2.9873	0.6320	0.3680	0.6140	0.3575	0.0243	0.0042
120	29.0361	9.4799	1.0829	0.2153	0.0002	21.8586	38.7514	100.42	1.8691	1.0876	0.0893	0.0140	1.9829	2.9828	0.6322	0.3678	0.6108	0.3554	0.0292	0.0046
180	28.4980	9.4678	1.0013	0.2061	0.0002	21.7495	38.0512	98.97	1.8602	1.1015	0.0837	0.0136	2.0007	2.9700	0.6281	0.3719	0.6081	0.3601	0.0274	0.0044
240	28.9308	9.2454	1.0344	0.1649	0.0002	21.7801	38.4937	99.65	1.8766	1.0688	0.0860	0.0108	1.9910	2.9857	0.6371	0.3629	0.6169	0.3513	0.0283	0.0036
300	29.6566	9.3721	1.0580	0.1623	0.0002	21.9238	38.6688	100.84	1.9061	1.0736	0.0871	0.0106	1.9858	2.9719	0.6397	0.3603	0.6194	0.3489	0.0283	0.0034
360	29.5193	9.3239	1.0280	0.1740	0.0002	22.0046	38.6702	100.72	1.8981	1.0685	0.0847	0.0113	1.9940	2.9732	0.6398	0.3602	0.6198	0.3489	0.0277	0.0037
420	29.5862	9.0639	1.0186	0.1583	0.0002	21.8550	38.4189	100.10	1.9161	1.0462	0.0845	0.0104	1.9947	2.9753	0.6468	0.3532	0.6267	0.3422	0.0276	0.0034
480	29.5342	9.2527	1.0427	0.1669	0.0002	22.0348	38.6511	100.68	1.8999	1.0608	0.0859	0.0109	1.9976	2.9731	0.6417	0.3583	0.6214	0.3470	0.0281	0.0036
540	29.2613	9.2363	0.9906	0.1375	0.0002	21.8699	39.0179	100.51	1.8810	1.0582	0.0816	0.0089	1.9813	2.9992	0.6400	0.3600	0.6209	0.3493	0.0269	0.0029
600	29.6749	9.2097	1.0379	0.1867	0.0002	21.9458	38.5029	100.56	1.9137	1.0585	0.0858	0.0122	1.9945	2.9691	0.6439	0.3561	0.6233	0.3448	0.0279	0.0040
660	29.5215	9.2520	1.0077	0.1875	0.0002	21.9016	38.6582	100.53	1.9021	1.0625	0.0832	0.0122	1.9887	2.9784	0.6416	0.3584	0.6216	0.3472	0.0272	0.0040
720	29.2853	8.9781	1.0233	0.2111	0.0002	21.7939	38.5776	99.87	1.8981	1.0371	0.0850	0.0139	1.9907	2.9899	0.6467	0.3533	0.6256	0.3418	0.0280	0.0046
780	29.9909	9.0678	0.9919	0.1675	0.0002	21.9111	38.5086	100.64	1.9348	1.0426	0.0820	0.0109	1.9921	2.9707	0.6498	0.3502	0.6302	0.3396	0.0267	0.0036
840	29.3481	8.9409	0.9265	0.1627	0.0002	21.6976	38.1992	99.28	1.9155	1.0401	0.0775	0.0108	1.9958	2.9813	0.6481	0.3519	0.6293	0.3417	0.0255	0.0035
900	29.2891	8.9615	1.0129	0.1415	0.0002	21.6697	38.2872	99.36	1.9094	1.0412	0.0846	0.0093	1.9908	2.9846	0.6471	0.3529	0.6272	0.3420	0.0278	0.0031
960	29.6358	9.4297	1.1428	0.2291	0.0002	21.8279	38.7963	101.06	1.9011	1.0781	0.0939	0.0149	1.9733	2.9760	0.6381	0.3619	0.6156	0.3491	0.0304	0.0048
1020	28.8439	9.3848	1.0050	0.1423	0.0002	22.0083	38.5542	99.94	1.8636	1.0807	0.0832	0.0093	2.0039	2.9786	0.6330	0.3670	0.6137	0.3559	0.0274	0.0031
1080	29.6626	9.0298	1.0709	0.2482	0.0002	21.6271	38.4578	100.10	1.9233	1.0435	0.0890	0.0163	1.9762	2.9818	0.6483	0.3517	0.6261	0.3397	0.0290	0.0053
1140	29.7932	9.1366	1.0000	0.2024	0.0002	21.8525	38.5806	100.57	1.9219	1.0505	0.0826	0.0132	1.9866	2.9759	0.6466	0.3534	0.6264	0.3424	0.0269	0.0043
1200	29.3059	9.0503	1.0656	0.1976	0.0002	21.8602	38.4723	99.95	1.8987	1.0450	0.0884	0.0130	1.9959	2.9805	0.6450	0.3550	0.6235	0.3432	0.0290	0.0043
1260	29.5145	9.3521	1.0047	0.1659	0.0002	22.5880	39.4029	102.03	1.8678	1.0548	0.0815	0.0106	2.0145	2.9817	0.6391	0.3609	0.6196	0.3499	0.0270	0.0035
1320	30.0110	8.8318	1.0807	0.2075	0.0002	22.0483	38.5887	100.77	1.9337	1.0142	0.0892	0.0135	2.0021	2.9731	0.6560	0.3440	0.6339	0.3325	0.0292	0.0044
1380	29.5352	9.2024	0.9705	0.1274	0.0002	21.6956	38.5036	100.03	1.9132	1.0624	0.0805	0.0084	1.9805	2.9823	0.6430	0.3570	0.6243	0.3467	0.0263	0.0027
1440	29.4829	9.0210	1.0541	0.1966	0.0002	21.6621	38.3939	99.81	1.9153	1.0445	0.0877	0.0129	1.9832	2.9824	0.6471	0.3529	0.6258	0.3413	0.0287	0.0042
1500	29.4086	9.1121	1.1406	0.1754	0.0002	21.7084	38.5466	100.09	1.9038	1.0514	0.0946	0.0115	1.9805	2.9839	0.6442	0.3558	0.6219	0.3434	0.0309	0.0038
1560	29.3063	9.1792	1.0385	0.1905	0.0002	21.9840	38.5707	100.27	1.8917	1.0560	0.0859	0.0125	1.9998	2.9771	0.6418	0.3582	0.6210	0.3467	0.0282	0.0041
1620	29.0919	9.3647	1.0791	0.1928	0.0002	22.0719	38.7125	100.51	1.8709	1.0733	0.0889	0.0126	2.0003	2.9769	0.6355	0.3645	0.6143	0.3524	0.0292	0.0041

1680	29.0252	9.3816	1.0616	0.1215	0.0002	21.7877	38.4347	99.81	1.8806	1.0834	0.0881	0.0080	1.9895	2.9778	0.6345	0.3655	0.8146	0.3540	0.0288	0.0026
1740	29.1708	9.2481	1.1275	0.1937	0.0002	21.8742	38.5019	100.12	1.8859	1.0656	0.0934	0.0127	1.9930	2.9765	0.6390	0.3610	0.8168	0.3485	0.0305	0.0042
1800	29.5038	9.2934	1.0812	0.1308	0.0002	21.7080	38.5482	100.27	1.9069	1.0706	0.0895	0.0086	1.9773	2.9792	0.6404	0.3598	0.8200	0.3481	0.0291	0.0028
1860	28.7728	9.3568	1.1013	0.1817	0.0002	21.7853	38.6272	99.83	1.8616	1.0790	0.0913	0.0119	1.9864	2.9884	0.6331	0.3669	0.8118	0.3545	0.0300	0.0039
1920	29.0577	9.2258	1.0880	0.1951	0.0002	21.7780	38.4783	99.82	1.8834	1.0658	0.0903	0.0128	1.9891	2.9820	0.6386	0.3614	0.8170	0.3492	0.0296	0.0042
1980	29.1035	9.2657	1.1204	0.1352	0.0002	22.0356	38.6820	100.34	1.8748	1.0638	0.0925	0.0088	2.0005	2.9797	0.6380	0.3620	0.8167	0.3499	0.0304	0.0029
2040	29.7811	9.0350	1.1118	0.1663	0.0002	21.6591	38.2660	100.02	1.9341	1.0458	0.0925	0.0109	1.9823	2.9716	0.6490	0.3510	0.8273	0.3392	0.0300	0.0035
2100	29.2738	8.8293	1.0746	0.1859	0.0002	22.0083	38.6996	100.07	1.8922	1.0172	0.0890	0.0122	2.0048	2.9911	0.6504	0.3498	0.8285	0.3379	0.0298	0.0041
2160	29.4356	9.0757	1.0555	0.1753	0.0002	21.7327	38.3962	99.87	1.9103	1.0497	0.0878	0.0115	1.9876	2.9796	0.6454	0.3546	0.8244	0.3431	0.0287	0.0038
2220	28.4951	9.0548	1.1294	0.2194	0.0278	21.7362	38.0647	98.73	1.8651	1.0583	0.0947	0.0145	2.0052	2.9792	0.6384	0.3616	0.8154	0.3485	0.0312	0.0048
2280	0.1823	0.0002	0.1091	0.0001	0.0002	0.0002	9.8211	10.11	0.0918	0.0002	0.0705	0.0001	0.0002	5.9185	0.9978	0.0022	0.5648	0.0012	0.4338	0.0008
2340	28.8320	9.4285	1.0783	0.1300	0.0002	21.8721	38.4443	99.79	1.8669	1.0881	0.0895	0.0085	1.9959	2.9766	0.6318	0.3682	0.8115	0.3564	0.0293	0.0028
2400	29.2031	9.8480	1.0788	0.2023	0.0002	22.3236	39.1827	101.84	1.8518	1.1130	0.0876	0.0130	1.9950	2.9710	0.8246	0.3754	0.8041	0.3631	0.0288	0.0042
2460	29.4879	9.3445	1.0841	0.2601	0.0002	21.9749	38.5608	100.71	1.8977	1.0718	0.0894	0.0169	1.9930	2.9673	0.8391	0.3609	0.8170	0.3485	0.0291	0.0055
2520	22.8778	7.4480	1.3158	0.1351	0.0002	21.1612	37.5300	90.27	1.5798	0.9247	0.1174	0.0095	2.0775	3.1282	0.6308	0.3692	0.8004	0.3514	0.0448	0.0038
2580	29.3081	9.1806	1.0995	0.1995	0.0002	21.9760	38.6775	100.44	1.8885	1.0543	0.0908	0.0130	1.9956	2.9800	0.6417	0.3583	0.8199	0.3461	0.0298	0.0043
2640	28.7803	9.4312	1.0911	0.1533	0.0002	21.7872	38.4099	99.65	1.8663	1.0900	0.0906	0.0101	1.9910	2.9783	0.6313	0.3687	0.8105	0.3566	0.0296	0.0033
2700	29.2027	9.4285	1.0939	0.1502	0.0002	22.0178	38.6736	100.57	1.8781	1.0807	0.0901	0.0098	1.9955	2.9740	0.6348	0.3652	0.8140	0.3533	0.0295	0.0032
2760	28.8968	9.3812	1.0342	0.2353	0.0002	21.8219	38.5188	99.87	1.8705	1.0800	0.0858	0.0154	1.9906	2.9812	0.6340	0.3660	0.8129	0.3539	0.0281	0.0050
2820	28.7740	9.2367	1.0799	0.1455	0.0002	21.8418	38.4090	99.49	1.8685	1.0690	0.0896	0.0096	1.9988	2.9824	0.6381	0.3639	0.8153	0.3520	0.0296	0.0032
2880	29.4758	8.9381	1.0391	0.1983	0.0002	21.9238	38.5899	100.17	1.9060	1.0301	0.0881	0.0130	1.9979	2.9839	0.6492	0.3508	0.8280	0.3394	0.0284	0.0043
2940	29.8199	9.1046	1.0413	0.2127	0.0002	21.8832	38.5293	100.57	1.9243	1.0471	0.0881	0.0139	1.9883	2.9731	0.6476	0.3524	0.8265	0.3409	0.0280	0.0045
3000	29.8309	9.1454	1.1196	0.2218	0.0002	21.7054	38.4818	100.29	1.9173	1.0547	0.0928	0.0145	1.9793	2.9759	0.6451	0.3549	0.8228	0.3425	0.0301	0.0047
3060	29.8834	9.1476	1.0987	0.1877	0.0002	21.9814	38.8075	101.11	1.9170	1.0459	0.0903	0.0122	1.9872	2.9789	0.6470	0.3530	0.8254	0.3412	0.0295	0.0040
3120	28.8071	9.0660	1.0317	0.1290	0.0002	21.7481	38.2938	98.88	1.8680	1.0551	0.0863	0.0085	2.0013	2.9900	0.6390	0.3610	0.8190	0.3498	0.0286	0.0028
3180	29.5256	8.8704	1.0553	0.2075	0.0002	21.7001	38.8080	99.97	1.9141	1.0249	0.0877	0.0138	1.9826	2.9929	0.6513	0.3487	0.8296	0.3371	0.0288	0.0045
3240	0.2688	0.1858	0.1123	0.0001	0.0002	0.5830	97.6988	98.81	0.0137	0.0181	0.0073	0.0000	0.0404	5.9516	0.4757	0.5243	0.3795	0.4183	0.2022	0.0000
3300	0.2184	0.1459	0.0002	0.0001	0.0002	0.5318	96.9069	97.80	0.0112	0.0134	0.0000	0.0000	0.0385	5.9588	0.4553	0.5447	0.4553	0.5447	0.0000	0.0000
3360	0.8793	0.3811	0.1589	0.0001	0.0312	6.3002	85.9459	93.69	0.0478	0.0389	0.0109	0.0000	0.4828	5.5885	0.5843	0.4357	0.5000	0.3860	0.1140	0.0000
3420	27.3968	7.4585	1.2172	0.1310	0.0002	19.8589	34.3474	90.41	1.9745	0.9580	0.1124	0.0096	2.0170	2.9800	0.8733	0.3287	0.8464	0.3138	0.0368	0.0031
3480	10.5809	2.4448	0.6509	0.1412	0.2042	13.3221	19.6753	47.02	1.3877	0.5714	0.1094	0.0188	2.4823	3.0856	0.7083	0.2917	0.8648	0.2738	0.0524	0.0090
3540	29.4889	8.8114	1.0819	0.1480	0.0002	21.7879	38.6214	99.94	1.9111	1.0179	0.0898	0.0096	1.9901	2.9932	0.8525	0.3475	0.8311	0.3381	0.0297	0.0032
3600	29.8255	8.9312	1.0453	0.1848	0.0002	21.7368	38.3710	100.07	1.9350	1.0327	0.0869	0.0108	1.9874	2.9787	0.8520	0.3480	0.8312	0.3369	0.0283	0.0035
3660	30.2400	9.1378	1.1099	0.2014	0.0002	21.7492	38.7752	101.21	1.9420	1.0459	0.0913	0.0131	1.9884	2.9776	0.8500	0.3500	0.8280	0.3382	0.0295	0.0042
3720	29.4802	9.2381	1.1372	0.1534	0.0002	21.7844	38.5899	100.34	1.9040	1.0832	0.0941	0.0100	1.9809	2.9787	0.6417	0.3583	0.8199	0.3482	0.0308	0.0033
3780	29.2415	9.3660	1.0862	0.1830	0.0002	21.8273	38.5658	100.25	1.8879	1.0778	0.0898	0.0107	1.9860	2.9774	0.6386	0.3634	0.8157	0.3515	0.0293	0.0035
3840	17.9830	0.1384	0.1327	0.5688	0.1800	0.4861	1.1982	20.62	9.3372	0.1284	0.0884	0.2993	0.3415	0.7435	0.9886	0.0134	0.9478	0.0128	0.0090	0.0304
3900	28.7592	9.2383	1.0096	0.1755	0.0002	21.7234	38.7099	99.81	1.8636	1.0867	0.0838	0.0115	1.9838	2.9994	0.6360	0.3640	0.8159	0.3528	0.0277	0.0038
3960	29.0581	9.0647	1.1288	0.1819	0.0002	21.7888	38.4634	99.69	1.8880	1.0486	0.0939	0.0120	1.9930	2.9851	0.6427	0.3573	0.8203	0.3449	0.0309	0.0039
4020	29.4802	9.3081	1.0995	0.1497	0.0002	21.7244	38.4706	100.21	1.9054	1.0730	0.0911	0.0098	1.9801	2.9752	0.6397	0.3603	0.8188	0.3485	0.0296	0.0032
4080	29.0792	9.1504	1.0662	0.1390	0.0002	21.8910	38.3803	99.51	1.8910	1.0605	0.0888	0.0092	1.9878	2.9844	0.8407	0.3593	0.8201	0.3478	0.0291	0.0030
4140	29.1682	9.2902	1.1031	0.2077	0.0002	21.9415	38.4805	100.17	1.8847	1.0699	0.0913	0.0136	1.9981	2.9717	0.6379	0.3621	0.8180	0.3497	0.0298	0.0044
4200	29.0821	9.2081	1.0583	0.1845	0.0002	21.8078	38.4889	99.61	1.8894	1.0680	0.0879	0.0121	1.9784	2.9865	0.6383	0.3607	0.8184	0.3489	0.0288	0.0040
4260	29.0545	9.2553	1.0399	0.1986	0.0002	21.7448	38.6791	99.97	1.8790	1.0868	0.0862	0.0130	1.9818	2.9911	0.6379	0.3621	0.8171	0.3503	0.0283	0.0043
4320	29.3050	9.1383	1.0379	0.2177	0.0002	21.8055	38.4182	99.92	1.8998	1.0558	0.0862	0.0143	1.9922	2.9779	0.8428	0.3572	0.8217	0.3454	0.0282	0.0047
4380	31.5015	7.4901	0.8889	0.1983	0.0002	21.2011	37.8310	98.91	2.0885	0.8850	0.0755	0.0133	1.9808	2.9832	0.7024	0.2978	0.8820	0.2890	0.0247	0.0043
															Fe/ (B-B')	Mg/ (B-B')	XAlm	XPyp	XGrS	XSpS
0	30.3537	8.4704	0.9427	0.2054	0.0002	21.8007	38.4184	99.99	1.9753	0.9824	0.0786	0.0135	1.9810	2.9893	0.6679	0.3321	0.8477	0.3221	0.0258	0.0044
60	29.9587	8.8505	1.0354	0.1747	0.0002	21.4837	38.3873	99.87	1.9494	1.0285	0.0883	0.0115	1.9702	2.9855	0.6551	0.3449	0.8342	0.3340	0.0281	0.0037
120	29.3427	9.0981	1.0581	0.1853	0.0002	21.8035	38.7085	100.19	1.8955	1.0475	0.0874	0.0121	1.9849	2.9900	0.6441	0.3559	0.8230	0.3443	0.0287	0.0040
180	29.8198	8.9810	1.0392	0.1858	0.0002	21.8229	38.3957	100.24	1.9311	1.0366	0.0862	0.0122	1.9918	2.9732	0.6507	0.3493	0.8298	0.3381	0.0281	0.0040

240	30.0117	8.9533	0.9980	0.1584	0.0002	21.6324	38.2520	100.01	1.9507	1.0372	0.0831	0.0104	1.9816	2.9731	0.6529	0.3471	0.6331	0.3366	0.0270	0.0034
300	29.5918	9.0147	1.0807	0.2279	0.0002	21.8737	38.5018	100.29	1.9134	1.0389	0.0895	0.0149	1.9932	2.9768	0.6481	0.3519	0.6260	0.3399	0.0293	0.0049
360	29.3806	8.9927	1.0682	0.2354	0.0002	21.8919	38.5626	100.13	1.9005	1.0367	0.0885	0.0154	1.9956	2.9827	0.6470	0.3530	0.6249	0.3409	0.0291	0.0051
420	29.5229	9.2225	0.9763	0.1576	0.0002	20.7146	36.7407	97.33	1.9789	1.1018	0.0838	0.0107	1.9568	2.9448	0.6424	0.3576	0.6232	0.3470	0.0264	0.0034
480	29.5724	8.9584	1.0699	0.1633	0.0002	21.8402	38.5899	100.19	1.9127	1.0327	0.0887	0.0107	1.9908	2.9846	0.6494	0.3506	0.6282	0.3392	0.0291	0.0035
540	29.3448	9.1002	1.1320	0.2255	0.0002	21.8546	38.3979	100.06	1.9007	1.0505	0.0939	0.0148	1.9949	2.9739	0.6440	0.3560	0.6212	0.3433	0.0307	0.0048
600	29.5606	9.0973	1.0994	0.2063	0.0002	22.0053	38.6144	100.58	1.9045	1.0446	0.0907	0.0135	1.9980	2.9748	0.6458	0.3542	0.6238	0.3421	0.0297	0.0044
660	29.2004	9.1716	1.1017	0.1930	0.0002	21.8415	38.3066	99.82	1.8947	1.0607	0.0916	0.0127	1.9973	2.9722	0.6411	0.3589	0.6192	0.3467	0.0299	0.0042
720	29.2231	9.2963	1.1884	0.2696	0.0002	21.8473	38.5237	100.35	1.8864	1.0695	0.0983	0.0176	1.9874	2.9735	0.6382	0.3618	0.6141	0.3482	0.0320	0.0057
780	29.0876	9.3100	1.0864	0.1666	0.0002	21.9927	38.7013	100.34	1.8737	1.0689	0.0897	0.0109	1.9965	2.9810	0.6367	0.3633	0.6157	0.3512	0.0295	0.0036
840	28.8521	9.3828	1.0998	0.1391	0.0002	21.8473	38.5424	99.86	1.8666	1.0819	0.0912	0.0091	1.9919	2.9817	0.6331	0.3669	0.6122	0.3549	0.0299	0.0030
900	28.9216	9.3276	1.0638	0.1440	0.0002	21.9101	38.5921	99.96	1.8693	1.0745	0.0881	0.0094	1.9957	2.9826	0.6350	0.3650	0.6146	0.3533	0.0290	0.0031
960	29.1119	9.4246	1.1265	0.1919	0.0002	21.8442	38.5613	100.26	1.8788	1.0840	0.0931	0.0125	1.9867	2.9757	0.6341	0.3659	0.6123	0.3533	0.0303	0.0041
1020	28.9729	9.1712	1.1304	0.1674	0.0002	21.8742	38.4781	99.79	1.8773	1.0591	0.0938	0.0110	1.9974	2.9813	0.6393	0.3607	0.6173	0.3483	0.0308	0.0036
1080	29.1610	9.4888	1.0893	0.1680	0.0002	21.9180	38.5840	100.41	1.8789	1.0896	0.0899	0.0110	1.9902	2.9727	0.6329	0.3671	0.6121	0.3550	0.0293	0.0036
1140	28.8590	9.2488	1.0753	0.1947	0.0002	21.7196	38.4576	99.56	1.8739	1.0704	0.0895	0.0128	1.9876	2.9860	0.6365	0.3635	0.6151	0.3513	0.0294	0.0042
1200	28.9126	9.1686	1.0728	0.1845	0.0002	21.7716	38.5044	99.61	1.8762	1.0604	0.0892	0.0121	1.9910	2.9878	0.6389	0.3611	0.6176	0.3491	0.0294	0.0040
1260	28.9883	9.4254	1.1034	0.1515	0.0002	21.9636	38.5859	100.22	1.8696	1.0834	0.0912	0.0099	1.9963	2.9757	0.6331	0.3669	0.6122	0.3547	0.0299	0.0032
1320	29.0284	9.3278	1.1667	0.1981	0.0002	21.8717	38.5399	100.13	1.8753	1.0740	0.0966	0.0130	1.9913	2.9771	0.6358	0.3642	0.6131	0.3511	0.0316	0.0042
1380	29.4784	9.0967	1.0685	0.2258	0.0002	21.8957	38.4794	100.24	1.9059	1.0483	0.0885	0.0148	1.9951	2.9749	0.6451	0.3549	0.6234	0.3429	0.0289	0.0048
1440	11.9240	20.8123	0.9919	0.0001	0.7527	18.8962	40.1568	93.53	0.7626	2.3724	0.0813	0.0000	1.7032	3.0711	0.2433	0.7567	0.2371	0.7376	0.0253	0.0000
1500	29.8389	9.2691	1.0651	0.1361	0.0002	22.0602	38.4520	100.82	1.9204	1.0632	0.0878	0.0089	2.0009	2.9592	0.6437	0.3563	0.6234	0.3452	0.0285	0.0029
1560	29.2499	9.1015	1.0604	0.1843	0.0002	21.8236	38.6336	100.05	1.8917	1.0491	0.0879	0.0121	1.9891	2.9878	0.6433	0.3567	0.6221	0.3450	0.0289	0.0040
1620	29.1797	9.2888	1.1233	0.1482	0.0002	22.0002	38.4840	100.22	1.8839	1.0689	0.0929	0.0097	2.0017	2.9710	0.6380	0.3620	0.6166	0.3498	0.0304	0.0032
1680	29.2325	9.2080	1.0512	0.1697	0.0002	21.7689	38.7442	100.17	1.8876	1.0597	0.0870	0.0111	1.9810	2.9916	0.6405	0.3595	0.6198	0.3480	0.0286	0.0036
1740	29.0672	9.1102	1.0831	0.2057	0.0002	22.0153	38.5780	100.06	1.8783	1.0492	0.0897	0.0135	2.0049	2.9810	0.6416	0.3584	0.6198	0.3462	0.0296	0.0045
1800	28.7273	9.1157	1.0094	0.1562	0.0002	21.5182	38.1444	98.67	1.8824	1.0646	0.0847	0.0104	1.9871	2.9887	0.6388	0.3612	0.6188	0.3500	0.0278	0.0034
1860	29.4813	9.3252	1.0789	0.2434	0.0002	21.8561	38.5082	100.49	1.9018	1.0721	0.0892	0.0159	1.9869	2.9703	0.6395	0.3605	0.6177	0.3482	0.0290	0.0052
1920	29.8262	8.7977	1.0151	0.2079	0.0002	21.8072	38.5677	100.22	1.9310	1.0152	0.0842	0.0136	1.9897	2.9857	0.6554	0.3446	0.6344	0.3335	0.0277	0.0045

TL01-146k GARNET 13

Distance (um)	OXIDES								CATION NUMBERS					CHEMICAL COMPOSITION DATA						
	FeO	MgO	CaO	MnO	TiO ₂	Al ₂ O ₃	SiO ₂	Total	Fe	Mg	Ca	Mn	Al	Si	Fe/ Fe+Mg (A-A')	Mg/ Fe+Mg (A-A')	XAlm	XPy	XGr	XSp
	0	28.6375	9.3530	0.8116	0.1565	0.0002	21.6180	38.3375	98.91	1.8688	1.0878	0.0678	0.0103	1.9881	2.9915	0.6321	0.3679	0.6158	0.3585	0.0223
60	28.2592	9.4994	0.8314	0.1455	0.0002	21.8254	38.1389	98.70	1.8455	1.1057	0.0696	0.0096	2.0087	2.9783	0.6253	0.3747	0.6090	0.3649	0.0230	0.0032
120	27.5181	9.4655	0.8550	0.1967	0.0002	21.6143	38.2859	97.94	1.8051	1.1066	0.0719	0.0131	1.9981	3.0031	0.6199	0.3801	0.6024	0.3693	0.0240	0.0044
180	27.5369	9.8265	0.8901	0.2046	0.0002	21.6579	38.5039	98.62	1.7933	1.1406	0.0743	0.0135	1.9877	2.9984	0.6112	0.3888	0.5935	0.3775	0.0246	0.0045
240	27.7733	10.0550	0.8629	0.1482	0.0002	21.8648	38.5904	99.29	1.7970	1.1596	0.0715	0.0097	1.9938	2.9857	0.6078	0.3922	0.5915	0.3817	0.0235	0.0032
300	27.8638	10.0551	0.9509	0.1369	0.0002	21.8206	38.4580	99.29	1.8050	1.1609	0.0789	0.0090	1.9921	2.9790	0.6086	0.3914	0.5911	0.3801	0.0258	0.0029
360	27.6335	10.2067	0.8817	0.2044	0.0002	21.9873	38.7367	99.65	1.7801	1.1719	0.0728	0.0133	1.9961	2.9839	0.6030	0.3970	0.5859	0.3857	0.0240	0.0044
420	27.8514	10.3816	0.9066	0.1311	0.0002	22.0992	38.7801	100.15	1.7862	1.1867	0.0745	0.0085	1.9974	2.9740	0.6008	0.3992	0.5845	0.3883	0.0244	0.0028
480	26.8347	10.2499	0.8449	0.1285	0.0002	22.0625	38.5532	98.67	1.7392	1.1840	0.0702	0.0084	2.0151	2.9878	0.5950	0.4050	0.5794	0.3944	0.0234	0.0028
540	27.2941	10.1296	0.8991	0.1195	0.0002	21.8578	38.5315	98.83	1.7707	1.1712	0.0747	0.0078	1.9984	2.9890	0.6019	0.3981	0.5855	0.3873	0.0247	0.0026
600	27.6257	10.1650	0.9138	0.1665	0.0002	21.8768	38.8011	99.55	1.7811	1.1681	0.0755	0.0109	1.9878	2.9914	0.6039	0.3961	0.5867	0.3848	0.0249	0.0036
660	27.7613	10.3158	0.9278	0.1676	0.0002	21.9191	38.8620	99.95	1.7836	1.1812	0.0764	0.0109	1.9846	2.9855	0.6016	0.3984	0.5844	0.3870	0.0250	0.0036
720	27.5437	10.2159	0.8553	0.1261	0.0002	22.0551	38.8708	99.67	1.7717	1.1712	0.0705	0.0082	1.9993	2.9897	0.6020	0.3980	0.5863	0.3876	0.0233	0.0027
780	27.0051	10.1004	0.8803	0.0921	0.0002	21.4501	38.1395	97.67	1.7729	1.1818	0.0740	0.0061	1.9846	2.9941	0.6000	0.4000	0.5842	0.3894	0.0244	0.0020
840	27.4612	10.1714	0.9615	0.1294	0.0002	21.9830	38.6545	99.36	1.7730	1.1704	0.0795	0.0085	2.0002	2.9842	0.6024	0.3976	0.5849	0.3861	0.0262	0.0028
900	23.5033	7.2133	0.7688	0.1695	0.0002	16.4269	30.1150	78.20	1.9550	1.0694	0.0819	0.0143	1.9257	2.9954	0.6464	0.3536	0.6265	0.3427	0.0262	0.0046
960	27.8084	10.4888	0.9712	0.1246	0.0002	21.9977	38.7522	100.14	1.7840	1.1993	0.0798	0.0081	1.9888	2.9728	0.5980	0.4020	0.5809	0.3905	0.0260	0.0026
1020	26.9438	10.1067	0.8503	0.1410	0.0002	21.4273	38.2950	97.76	1.7661	1.1808	0.0714	0.0094	1.9794	3.0016	0.5993	0.4007	0.5833	0.3900	0.0236	0.0031

1080	27.8747	10.2022	0.9860	0.1673	0.0002	22.1319	38.7032	100.07	1.7903	1.1679	0.0811	0.0109	2.0033	2.9724	0.6052	0.3948	0.5869	0.3829	0.0266	0.0036
1140	28.1916	10.2799	0.8865	0.1449	0.0002	21.8865	38.7442	100.12	1.8122	1.1777	0.0730	0.0094	1.9810	2.9780	0.6081	0.3939	0.5899	0.3833	0.0238	0.0031
1200	27.9949	9.9393	0.8862	0.1578	0.0328	21.9371	38.7819	99.73	1.8043	1.1418	0.0732	0.0103	1.9926	2.9889	0.6124	0.3876	0.5956	0.3769	0.0242	0.0034
1260	27.5361	10.1453	0.9131	0.1669	0.0002	21.8077	38.4446	99.01	1.7861	1.1729	0.0759	0.0110	1.9935	2.9819	0.6036	0.3964	0.5864	0.3851	0.0249	0.0036
1320	28.2188	10.2988	0.9474	0.1521	0.0002	21.9851	38.7861	100.39	1.8090	1.1768	0.0778	0.0099	1.9864	2.9734	0.6059	0.3941	0.5888	0.3829	0.0253	0.0032
1380	27.4898	10.2020	0.8857	0.1193	0.0002	21.9560	38.7148	99.37	1.7742	1.1735	0.0732	0.0078	1.9970	2.9878	0.6019	0.3981	0.5858	0.3875	0.0242	0.0028
1440	27.3876	10.1336	0.8821	0.1027	0.0002	21.8892	38.5742	98.95	1.7748	1.1704	0.0716	0.0087	1.9990	2.9890	0.6028	0.3974	0.5870	0.3871	0.0237	0.0022
1500	28.0187	10.1729	0.8582	0.1484	0.0002	21.9993	38.6155	99.81	1.8052	1.1682	0.0707	0.0097	1.9975	2.9750	0.6071	0.3929	0.5911	0.3825	0.0232	0.0032
1560	27.7931	10.1295	0.9227	0.1748	0.0002	21.8795	38.4294	99.33	1.7993	1.1688	0.0765	0.0115	1.9962	2.9749	0.6082	0.3938	0.5888	0.3824	0.0250	0.0038
1820	27.8451	9.8694	0.8499	0.1388	0.0002	21.8390	38.3001	98.84	1.8118	1.1445	0.0709	0.0091	2.0026	2.9799	0.6129	0.3871	0.5967	0.3769	0.0234	0.0030
1680	28.1213	9.7380	0.8378	0.1189	0.0002	22.0314	38.8131	99.46	1.8184	1.1220	0.0694	0.0077	2.0076	2.9855	0.6184	0.3818	0.6026	0.3718	0.0230	0.0026

Distance (um)	OXIDES								CATION NUMBERS						CHEMICAL COMPOSITION DATA					
	FeO	MgO	CaO	MnO	TiO ₂	Al ₂ O ₃	SiO ₂	Total	Fe	Mg	Ca	Mn	Al	Si	Fe/ Fe+Mg (B-B')	Mg/ Fe+Mg (B-B')	XAlm	XPyp	XGrS	XSpS
0	28.4068	9.5800	0.8513	0.1489	0.0002	21.8523	38.2490	98.87	1.8533	1.1116	0.0712	0.0098	1.9908	2.9839	0.6251	0.3749	0.6085	0.3649	0.0234	0.0032
60	27.8311	9.9377	0.8805	0.1157	0.0002	21.8892	38.6886	99.34	1.7998	1.1453	0.0729	0.0076	1.9946	2.9913	0.6111	0.3889	0.5948	0.3786	0.0241	0.0025
120	27.7169	10.0812	0.9294	0.1746	0.0002	21.7774	38.4833	99.16	1.7967	1.1647	0.0772	0.0115	1.9894	2.9829	0.6067	0.3933	0.5891	0.3819	0.0253	0.0038
180	0.1083	0.0004	0.0001	0.0001	0.0002	0.0004	0.0003	0.11	11.6973	0.0752	0.0186	0.0142	0.0540	0.0413	0.9936	0.0064	0.9909	0.0064	0.0016	0.0012
240	28.0234	10.2585	0.9242	0.1083	0.0002	21.9287	38.6014	99.84	1.8053	1.1779	0.0763	0.0071	1.9909	2.9736	0.6052	0.3948	0.5887	0.3841	0.0249	0.0023
300	27.6457	10.2281	0.9522	0.1866	0.0002	21.7730	38.4534	99.24	1.7908	1.1807	0.0790	0.0122	1.9874	2.9782	0.6026	0.3974	0.5847	0.3855	0.0258	0.0040
360	0.4481	0.1349	0.0720	0.0001	0.0002	0.5420	96.8045	98.00	0.0230	0.0124	0.0047	0.0000	0.0393	5.9505	0.6497	0.3503	0.5736	0.3092	0.1172	0.0000
420	27.5612	10.2185	0.8654	0.1521	0.0002	21.7832	38.4983	99.08	1.7863	1.1804	0.0719	0.0100	1.9896	2.9835	0.6021	0.3979	0.5859	0.3872	0.0236	0.0033
480	27.4290	10.5535	0.9022	0.1392	0.0002	22.0703	38.9722	100.07	1.7565	1.2045	0.0740	0.0090	1.9917	2.9842	0.5932	0.4068	0.5770	0.3957	0.0243	0.0030
540	27.0995	10.1567	0.8566	0.1340	0.0002	21.7040	38.4582	98.41	1.7646	1.1787	0.0715	0.0068	1.9917	2.9944	0.5995	0.4005	0.5836	0.3898	0.0236	0.0029
600	27.7882	10.3771	0.9482	0.1378	0.0002	21.9823	38.7188	99.95	1.7860	1.1887	0.0781	0.0090	1.9911	2.9757	0.6004	0.3998	0.5833	0.3882	0.0255	0.0029
660	27.0926	10.8189	0.8686	0.1215	0.0002	22.6009	39.8665	101.37	1.7046	1.2132	0.0699	0.0077	2.0040	2.9993	0.5842	0.4158	0.5691	0.4050	0.0233	0.0026
720	27.4724	10.3657	0.9246	0.1298	0.0318	21.8798	38.6780	99.47	1.7719	1.1904	0.0784	0.0085	1.9888	2.9829	0.5982	0.4018	0.5815	0.3907	0.0251	0.0028
780	27.2590	10.3792	0.9626	0.1088	0.0002	21.9723	38.6550	99.34	1.7587	1.1935	0.0796	0.0071	1.9978	2.9622	0.5957	0.4043	0.5787	0.3927	0.0282	0.0023
840	27.1007	10.1346	0.8527	0.1456	0.0002	21.8798	37.9733	97.89	1.7768	1.1841	0.0718	0.0097	2.0030	2.9767	0.6001	0.3999	0.5840	0.3893	0.0235	0.0032
900	27.4287	10.1161	0.8682	0.1003	0.0002	21.8525	38.1400	98.30	1.7921	1.1781	0.0727	0.0066	1.9938	2.9799	0.6034	0.3966	0.5877	0.3863	0.0238	0.0022
960	27.7540	10.2193	0.9257	0.1123	0.0002	22.0803	38.8910	99.78	1.7880	1.1721	0.0783	0.0073	2.0025	2.9773	0.6038	0.3962	0.5872	0.3853	0.0251	0.0024
1020	27.1933	10.0948	0.8883	0.1558	0.0002	21.8509	38.1732	98.15	1.7779	1.1763	0.0742	0.0103	1.9949	2.9844	0.6016	0.3982	0.5851	0.3871	0.0244	0.0034
1080	27.1959	10.1285	0.8778	0.1360	0.0002	21.7762	38.0053	98.12	1.7791	1.1809	0.0735	0.0090	2.0078	2.9729	0.6010	0.3990	0.5847	0.3881	0.0242	0.0030
1140	27.7597	10.0549	0.9128	0.1592	0.0002	21.8424	38.8067	99.34	1.7958	1.1592	0.0756	0.0104	1.9912	2.9862	0.6077	0.3923	0.5905	0.3812	0.0249	0.0034
1200	27.7092	9.9831	0.9070	0.1488	0.0002	21.9216	38.5000	99.17	1.7952	1.1527	0.0753	0.0096	2.0015	2.9825	0.6090	0.3910	0.5919	0.3801	0.0248	0.0032
1260	27.8541	9.9009	0.8971	0.0787	0.0002	21.8925	38.4509	99.07	1.8071	1.1448	0.0748	0.0052	2.0018	2.9829	0.6122	0.3878	0.5961	0.3776	0.0246	0.0017
1320	28.3942	9.7732	0.9520	0.2197	0.0002	22.0803	38.8605	100.28	1.8238	1.1188	0.0783	0.0143	1.9969	2.9847	0.6198	0.3802	0.6009	0.3886	0.0258	0.0047
1380	29.0304	10.0632	0.9379	0.1449	0.0002	22.4584	39.4441	102.08	1.8323	1.1320	0.0758	0.0093	1.9977	2.9770	0.6181	0.3819	0.6009	0.3712	0.0249	0.0030
1440	28.1774	9.7735	0.8251	0.1505	0.0002	22.0394	38.9762	99.94	1.8120	1.1202	0.0680	0.0098	1.9973	2.9970	0.6180	0.3820	0.6020	0.3722	0.0226	0.0033

TL01-148k GARNET 19

Distance (um)	OXIDES								CATION NUMBERS						CHEMICAL COMPOSITION DATA					
	FeO	MgO	CaO	MnO	TiO ₂	Al ₂ O ₃	SiO ₂	Total	Fe	Mg	Ca	Mn	Al	Si	Fe/ Fe+Mg (A-A')	Mg/ Fe+Mg (A-A')	XAlm	XPyp	XGrS	XSpS
0	28.0574	10.3328	0.8467	0.1496	0.0002	21.9659	39.0087	100.36	1.7983	1.1791	0.0694	0.0097	1.9819	2.9862	0.6037	0.3963	0.5881	0.3880	0.0227	0.0032
60	28.0583	10.3932	0.8684	0.1800	0.0002	22.0712	38.9627	100.53	1.7937	1.1842	0.0711	0.0117	1.9884	2.9784	0.6023	0.3977	0.5860	0.3889	0.0232	0.0038
120	27.8099	10.6418	0.8688	0.1389	0.0002	22.1302	38.8275	100.22	1.7828	1.2159	0.0713	0.0089	1.9993	2.9610	0.5945	0.4055	0.5790	0.3949	0.0232	0.0029
180	28.0323	10.2652	0.8441	0.0960	0.0002	21.4139	38.0477	96.70	1.7188	1.2079	0.0714	0.0064	1.9923	3.0036	0.5873	0.4127	0.5720	0.4021	0.0238	0.0021
240	28.6896	10.5179	0.8439	0.1777	0.0002	21.9482	38.6008	98.78	1.7274	1.2133	0.0700	0.0117	2.0019	2.9874	0.5874	0.4126	0.5715	0.4014	0.0232	0.0039
300	27.2323	10.8190	0.8715	0.1585	0.0002	22.1147	38.9512	100.15	1.7411	1.2328	0.0714	0.0101	1.9926	2.9778	0.5855	0.4145	0.5898	0.4035	0.0234	0.0033
360	27.2814	10.7405	0.9252	0.1683	0.0002	22.2990	39.2037	100.80	1.7340	1.2178	0.0754	0.0108	1.9989	2.9818	0.5875	0.4125	0.5708	0.4008	0.0248	0.0038
420	27.1928	10.7724	0.8940	0.1685	0.0002	22.0579	38.8120	99.90	1.7435	1.2310	0.0734	0.0109	1.9931	2.9757	0.5881	0.4139	0.5700	0.4024	0.0240	0.0038

480	27.1725	10.8220	0.8778	0.1811	0.0002	22.1333	38.8505	100.04	1.7393	1.2346	0.0720	0.0117	1.9966	2.9737	0.5849	0.4151	0.5688	0.4038	0.0235	0.0038
540	27.4196	10.6054	0.8777	0.1806	0.0002	22.1298	38.7829	100.00	1.7580	1.2119	0.0721	0.0117	1.9996	2.9734	0.5919	0.4081	0.5757	0.3969	0.0236	0.0038
600	27.4732	10.6172	0.8827	0.1178	0.0002	22.1756	38.8619	100.13	1.7586	1.2113	0.0724	0.0076	2.0005	2.9746	0.5921	0.4079	0.5766	0.3972	0.0237	0.0025
660	28.2360	10.5211	0.9395	0.2357	0.0002	22.2902	39.2780	101.50	1.7882	1.1875	0.0762	0.0151	1.9894	2.9744	0.6009	0.3991	0.5830	0.3872	0.0248	0.0049
720	27.5563	10.4868	0.8799	0.1866	0.0002	22.2817	39.0059	100.40	1.7594	1.1933	0.0720	0.0121	2.0049	2.9779	0.5959	0.4041	0.5794	0.3929	0.0237	0.0040
780	27.7134	10.6017	0.9298	0.1585	0.0002	22.2782	38.9622	100.64	1.7667	1.2046	0.0759	0.0102	2.0015	2.9701	0.5946	0.4054	0.5778	0.3940	0.0248	0.0033
840	27.4285	10.5771	0.8964	0.2154	0.0002	21.5400	38.1005	98.76	1.7859	1.2275	0.0748	0.0142	1.9765	2.9664	0.5927	0.4073	0.5757	0.3957	0.0241	0.0046
900	27.2923	10.8118	0.9433	0.1060	0.0002	22.0903	38.8422	100.09	1.7470	1.2335	0.0774	0.0069	1.9928	2.9731	0.5861	0.4139	0.5700	0.4025	0.0253	0.0023
960	27.1496	10.8871	0.9721	0.1512	0.0002	22.2512	38.8836	100.30	1.7331	1.2387	0.0795	0.0098	2.0018	2.9681	0.5832	0.4168	0.5662	0.4047	0.0260	0.0032
1020	27.0072	10.8619	0.8725	0.1341	0.0002	22.0026	38.8365	99.72	1.7330	1.2422	0.0717	0.0087	1.9897	2.9799	0.5825	0.4175	0.5672	0.4065	0.0235	0.0028
1080	26.9942	10.9102	0.9498	0.0920	0.0351	22.0568	38.8551	99.89	1.7289	1.2454	0.0779	0.0060	1.9909	2.9757	0.5813	0.4187	0.5653	0.4072	0.0255	0.0020
1140	27.5904	10.9301	0.9522	0.1399	0.0002	22.1957	39.0735	100.88	1.7536	1.2382	0.0775	0.0090	1.9882	2.9697	0.5861	0.4139	0.5697	0.4022	0.0252	0.0029
1200	26.8143	10.6762	0.9484	0.1514	0.0002	22.0449	38.6289	99.26	1.7282	1.2263	0.0783	0.0099	2.0023	2.9769	0.5849	0.4151	0.5680	0.4030	0.0257	0.0033
1260	26.8968	10.9257	0.8785	0.1482	0.0002	22.1730	38.9316	99.95	1.7203	1.2454	0.0720	0.0096	1.9986	2.9774	0.5801	0.4199	0.5645	0.4087	0.0236	0.0032
1320	27.1159	10.9298	0.9135	0.1650	0.0002	22.1734	38.8937	100.19	1.7324	1.2446	0.0748	0.0107	1.9965	2.9714	0.5819	0.4181	0.5657	0.4064	0.0244	0.0035
1380	27.2198	10.6769	0.9075	0.1653	0.0002	22.2157	39.1483	100.33	1.7359	1.2136	0.0741	0.0107	1.9966	2.9854	0.5885	0.4115	0.5721	0.4000	0.0244	0.0035
1440	26.7700	10.5701	0.8733	0.0798	0.0002	21.5938	38.4096	98.30	1.7429	1.2265	0.0728	0.0053	1.9813	2.9902	0.5870	0.4130	0.5719	0.4025	0.0239	0.0017
1500	27.2439	10.6970	0.8439	0.1058	0.0002	21.8553	38.3733	99.12	1.7627	1.2335	0.0700	0.0069	1.9928	2.9688	0.5883	0.4117	0.5736	0.4014	0.0228	0.0022
1560	27.7081	10.6040	0.9096	0.1576	0.0278	22.0134	38.9623	100.38	1.7715	1.2083	0.0745	0.0102	1.9834	2.9786	0.5945	0.4055	0.5781	0.3943	0.0243	0.0033
1620	27.7416	10.8114	0.8831	0.1779	0.0002	22.2404	39.1763	101.03	1.7611	1.2233	0.0718	0.0114	1.9897	2.9739	0.5901	0.4099	0.5741	0.3988	0.0234	0.0037
1680	27.0645	10.6799	0.8378	0.1612	0.0002	22.0313	38.8406	99.62	1.7387	1.2228	0.0689	0.0105	1.9946	2.9836	0.5871	0.4129	0.5718	0.4021	0.0227	0.0035
1740	27.2458	10.8171	0.8908	0.1367	0.0002	22.1081	38.8255	100.02	1.7447	1.2346	0.0731	0.0089	1.9952	2.9730	0.5856	0.4144	0.5699	0.4033	0.0239	0.0029
1800	27.5866	10.5836	0.8830	0.1487	0.0002	22.0705	38.8564	100.13	1.7673	1.2084	0.0725	0.0096	1.9926	2.9766	0.5939	0.4061	0.5780	0.3952	0.0237	0.0031
1860	27.7027	10.2529	0.8820	0.1949	0.0002	22.0752	38.9213	100.03	1.7772	1.1723	0.0725	0.0127	1.9958	2.9858	0.6025	0.3975	0.5856	0.3863	0.0239	0.0042
1920	27.3446	10.6416	0.8783	0.1866	0.0002	21.8022	38.5140	99.37	1.7659	1.2248	0.0727	0.0122	1.9842	2.9741	0.5905	0.4095	0.5742	0.3982	0.0236	0.0040
1980	27.3603	10.2907	0.8806	0.1621	0.0002	22.0544	39.1465	99.89	1.7535	1.1755	0.0723	0.0105	1.9920	3.0001	0.5987	0.4013	0.5822	0.3903	0.0240	0.0035
															Fe/	Mg/				
															Fe+Mg	Fe+Mg				
															(B-B')	(B-B')	XAlm	XPyP	XGrS	XSpS
0	27.7507	10.4479	0.8796	0.1273	0.0002	22.0626	38.9157	100.18	1.7776	1.1928	0.0722	0.0083	1.9917	2.9808	0.5984	0.4016	0.5826	0.3910	0.0237	0.0027
61	27.8612	10.5166	0.8974	0.1519	0.0002	22.1232	38.8769	100.43	1.7817	1.1986	0.0735	0.0098	1.9938	2.9728	0.5978	0.4022	0.5816	0.3912	0.0240	0.0032
122	28.1019	10.0360	0.8034	0.1886	0.0002	21.9436	38.4558	99.53	1.8173	1.1567	0.0666	0.0124	1.9998	2.9737	0.6111	0.3889	0.5953	0.3789	0.0218	0.0041
183	28.4608	9.9638	0.8662	0.2112	0.0002	21.8584	38.5510	99.91	1.8367	1.1460	0.0716	0.0138	1.9880	2.9749	0.6158	0.3842	0.5986	0.3735	0.0233	0.0045
244	27.2968	10.8948	0.8704	0.1066	0.0002	22.1831	39.0023	100.35	1.7414	1.2387	0.0711	0.0069	1.9943	2.9752	0.5843	0.4157	0.5694	0.4051	0.0232	0.0023
305	27.1277	10.6857	0.8948	0.1295	0.0002	21.9372	38.7739	99.55	1.7450	1.2251	0.0737	0.0084	1.9887	2.9824	0.5875	0.4125	0.5717	0.4014	0.0241	0.0028
366	27.0947	10.9099	0.9066	0.1695	0.0002	22.0530	39.0505	100.18	1.7305	1.2419	0.0742	0.0110	1.9850	2.9824	0.5822	0.4178	0.5660	0.4062	0.0243	0.0036
427	27.0836	10.7504	0.9004	0.1460	0.0002	22.0146	38.9985	99.89	1.7348	1.2273	0.0739	0.0095	1.9872	2.9869	0.5857	0.4143	0.5696	0.4030	0.0243	0.0031
488	27.3166	10.9917	0.8855	0.1287	0.0002	22.1310	38.7255	100.18	1.7476	1.2533	0.0726	0.0083	1.9954	2.9625	0.5824	0.4176	0.5671	0.4067	0.0236	0.0027
549	27.3951	10.8628	0.9932	0.1464	0.0002	22.2548	39.0356	100.69	1.7433	1.2320	0.0810	0.0094	1.9958	2.9703	0.5859	0.4141	0.5686	0.4019	0.0264	0.0031
610	27.3376	10.8825	0.9079	0.1662	0.0002	22.0706	38.6996	100.06	1.7517	1.2428	0.0745	0.0108	1.9931	2.9652	0.5850	0.4150	0.5688	0.4035	0.0242	0.0035
671	27.1428	10.7838	0.8595	0.1017	0.0002	21.9263	38.8343	99.65	1.7437	1.2347	0.0707	0.0066	1.9851	2.9832	0.5854	0.4146	0.5706	0.4041	0.0231	0.0022
732	27.0870	10.9273	0.8953	0.1307	0.0002	22.0025	38.9412	99.98	1.7337	1.2466	0.0734	0.0085	1.9847	2.9804	0.5817	0.4183	0.5662	0.4071	0.0240	0.0028
793	27.0661	10.9878	0.9541	0.1526	0.0002	22.2155	38.9348	100.31	1.7267	1.2493	0.0780	0.0099	1.9973	2.9701	0.5802	0.4198	0.5636	0.4077	0.0255	0.0032
854	27.2128	10.7519	0.8942	0.1725	0.0002	21.8523	38.6323	99.52	1.7530	1.2345	0.0738	0.0113	1.9839	2.9758	0.5868	0.4132	0.5705	0.4018	0.0240	0.0037
915	27.1580	10.7691	0.8541	0.1346	0.0002	21.8941	38.8663	99.68	1.7445	1.2329	0.0703	0.0088	1.9820	2.9853	0.5859	0.4141	0.5708	0.4034	0.0230	0.0029
976	27.1096	10.7729	0.9060	0.1153	0.0002	21.9753	39.0614	99.94	1.7354	1.2291	0.0743	0.0075	1.9825	2.9900	0.5854	0.4146	0.5697	0.4035	0.0244	0.0025
1037	27.1734	10.9999	0.8975	0.1494	0.0002	22.0397	39.0400	100.30	1.7341	1.2512	0.0734	0.0097	1.9822	2.9792	0.5809	0.4191	0.5651	0.4078	0.0239	0.0032
1098	27.2172	10.6888	0.8291	0.1209	0.0002	21.7945	38.7228	99.37	1.7547	1.2282	0.0685	0.0079	1.9802	2.9852	0.5883	0.4117	0.5736	0.4015	0.0224	0.0026
1159	27.5350	10.6316	0.8967	0.1520	0.0002	21.9226	38.8821	100.02	1.7659	1.2152	0.0737	0.0099	1.9813	2.9817	0.5924	0.4076	0.5762	0.3965	0.0240	0.0032
1220	28.0544	10.5977	0.9424	0.1362	0.0002	21.8872	38.9883	100.61	1.7926	1.2069	0.0771	0.0088	1.9710	2.9790	0.5976	0.4024	0.5810	0.3912	0.0250	0.0029
1281	27.6466	10.3115	0.8490	0.1189	0.0002	21.7028	38.4701	99.10	1.7922	1.1914	0.0705	0.0078	1.9827	2.9820	0.6007	0.3993	0.5853	0.3891	0.0230	0.0025

- indicates poor results

BIOTITE ADJACENT TO GARNET

Label	OXIDE													CATION NUMBER													CHEMICAL COMPOSITION		
	K ₂ O	Na ₂ O	CaO	MgO	FeO	MnO	TiO ₂	Al ₂ O ₃	SiO ₂	F-	Cl-	Total	K	Na	Ca	Mg	Fe	Mn	Ti	Al ^{VI}	Al ^{IV}	Al	Si	F	Cl	X _{Mg} /X _{Fe}	X _{Fe} /X _{Mg}		
146j#1-2	8.4053	0.7375	0.1567	17.1028	10.4696	0.1124	4.4767	14.6160	38.8128	1.7457	0.0906	97.73	1.7771	0.2117	0.0249	3.7744	1.2964	0.0141	0.4984	0.2972	2.2533	2.5505	5.7467	0.8175	0.0227	0.7443	0.2557		
146j#1-3	5.2861	0.2233	0.0604	16.3319	13.9935	0.0578	2.6208	16.5292	33.6893	1.3144	0.0625	90.17	1.0738	0.0689	0.0103	3.8763	1.8835	0.0078	0.3138	0.4668	2.8353	3.1021	5.3647	0.6520	0.0169	0.6753	0.3247		
146j#1-4-1	9.0896	0.3663	0.1245	15.9298	8.9689	0.0658	4.3314	14.8425	36.6037	1.8488	0.1045	92.06	1.8159	0.1115	0.0209	3.7266	1.1773	0.0087	0.5112	0.4537	2.2549	2.7086	5.7451	0.9177	0.0278	0.7599	0.2401		
146j#1-4-2	9.5774	0.8721	0.3079	17.2296	9.6696	0.2388	4.9213	14.4535	38.2295	1.8275	0.1022	97.43	1.8199	0.2519	0.0491	3.8254	1.2046	0.0301	0.5513	0.2322	2.3053	2.5375	5.6947	0.8609	0.0258	0.7605	0.2395		
146j#1-4-3	9.6446	0.5733	0.1172	17.4722	9.5931	0.0590	4.7828	14.3357	38.3895	2.1646	0.0934	97.23	1.8443	0.1666	0.0188	3.9039	1.2026	0.0075	0.5391	0.2874	2.2453	2.5327	5.7547	1.0282	0.0237	0.7645	0.2355		
146j#1-4-4	9.3857	0.4428	0.0524	17.7414	9.5954	0.0669	4.5485	14.5579	39.2248	2.2847	0.0921	97.97	1.7754	0.1273	0.0083	3.9213	1.1899	0.0084	0.5070	0.3607	2.1835	2.5442	5.8165	1.0621	0.0231	0.7672	0.2328		
146j#1-4-5	9.5798	0.4252	0.0415	16.7304	9.4413	0.0569	4.6912	13.8979	37.3629	2.1587	0.0975	94.48	1.8893	0.1275	0.0069	3.8552	1.2207	0.0075	0.5454	0.3086	2.2237	2.5323	5.7763	1.0555	0.0255	0.7595	0.2405		
146j#7-3bt1	9.7421	0.9452	0.0935	19.0827	9.2720	0.0874	4.4729	15.8376	40.0678	2.0662	0.0756	101.54	1.7676	0.2606	0.0142	4.0455	1.1029	0.0105	0.4784	0.3202	2.3011	2.6213	5.8989	0.9295	0.0182	0.7858	0.2142		
146j#7-3bt2	9.7612	0.7430	0.1386	18.0173	9.4610	0.0775	4.4954	14.9215	38.7680	2.1317	0.0679	98.58	1.8364	0.2125	0.0216	3.9606	1.1689	0.0097	0.4988	0.3111	2.2825	2.5936	5.7175	0.9843	0.0170	0.7724	0.2276		
146j#7-3bt3	9.6726	0.9338	0.2089	17.9989	10.0837	0.1638	4.6106	14.7458	38.5403	2.5801	0.0997	99.62	1.8261	0.2680	0.0331	3.9705	1.2481	0.0205	0.5131	0.2761	2.2960	2.5721	5.7040	1.1983	0.0250	0.7608	0.2382		
146j#7-4bt1	9.9814	0.9267	0.2189	19.0537	9.5825	0.1210	4.8396	15.5258	40.4138	2.2682	0.0808	102.82	1.8002	0.2540	0.0332	4.0153	1.1330	0.0145	0.4933	0.3010	2.2861	2.5871	5.7139	1.0142	0.0217	0.7799	0.2201		
146j#7-4bt2	9.9151	0.5134	0.1676	16.6972	9.3360	0.1040	4.3251	14.5592	37.7140	2.5520	0.0780	95.66	1.8848	0.1530	0.0276	3.8245	1.1998	0.0135	0.4998	0.4324	2.2044	2.6368	5.7956	1.2403	0.0203	0.7612	0.2388		
146j#7-4bt3	9.3902	0.2380	0.1156	17.5735	9.4147	0.0001	3.8783	14.9436	39.1455	2.3530	0.0651	97.12	1.7905	0.0690	0.0185	3.9154	1.1769	0.0000	0.4360	0.4841	2.1485	2.8326	5.8515	1.1124	0.0165	0.7689	0.2311		
146j#7-4bt4	9.8883	0.6259	0.0889	18.5967	9.3701	0.0537	4.3108	15.1584	39.7740	2.3228	0.0615	100.26	1.8290	0.1760	0.0154	4.0193	1.1363	0.0068	0.4701	0.3576	2.2326	2.5902	5.7674	1.0652	0.0151	0.7796	0.2204		
146j#9-3bt	9.7951	0.7637	0.0948	21.4349	8.1149	0.0520	2.2532	15.5365	41.9150	2.7588	0.0682	102.79	1.7606	0.2087	0.0143	4.5018	0.9562	0.0062	0.2388	0.4861	2.0940	2.5801	5.9060	1.2294	0.0163	0.8248	0.1752		
146j#9-5bt1	9.6365	1.1904	0.2457	18.0990	9.9953	0.1578	4.9963	16.4875	40.4310	2.3375	0.0956	103.67	1.7249	0.3239	0.0369	3.7855	1.1730	0.0187	0.5272	0.4002	2.3265	2.7267	5.6735	1.0374	0.0227	0.7634	0.2366		
146j#9-5bt2	9.9528	1.0388	0.3289	18.0302	10.2690	0.1166	5.5813	15.3450	39.5198	2.5011	0.0947	102.78	1.8162	0.2881	0.0501	3.8444	1.2285	0.0141	0.6004	0.2404	2.3467	2.5871	5.8533	1.1316	0.0230	0.7578	0.2422		
146j#9-5bt3	9.4856	0.4398	0.1901	16.7623	9.5689	0.0710	4.7184	14.1947	37.3878	2.5748	0.1042	95.47	1.8940	0.1304	0.0314	3.8568	1.2351	0.0093	0.5477	0.3541	2.2284	2.5825	5.7718	1.2571	0.0273	0.7574	0.2428		
146j#9-5bt4	9.4623	0.8718	0.1443	18.3567	10.2188	0.0820	5.0170	15.4149	39.9754	2.4055	0.0842	101.99	1.7257	0.2417	0.0221	3.9117	1.2215	0.0075	0.5394	0.3125	2.2848	2.5973	5.7152	1.0877	0.0156	0.7620	0.2380		
146j#9-5bt5	9.6373	0.8639	0.2090	17.9615	9.7031	0.1568	4.8246	15.9223	39.9155	2.2981	0.0884	101.60	1.7588	0.2452	0.0320	3.8302	1.1609	0.0190	0.5191	0.3953	2.2894	2.6847	5.7106	1.0398	0.0214	0.7674	0.2328		
146k#21-1bt1	9.4872	0.8048	0.2977	16.8237	10.5454	0.1646	4.7545	14.5143	37.2876	1.9701	0.0883	96.74	1.8314	0.2361	0.0320	3.7947	1.3345	0.0211	0.5411	0.2312	2.3574	2.5886	5.8426	0.9429	0.0221	0.7398	0.2602		
146k#21-1bt2	8.8407	0.0003	0.0723	15.8822	10.6703	0.0001	4.2843	14.0207	36.4336	1.9862	0.0934	92.03	1.7448	0.0001	0.0123	3.7473	1.4128	0.0000	0.5035	0.3830	2.2327	2.6157	5.7673	0.9844	0.0251	0.7282	0.2738		
146k#21-1bt3	9.5953	0.7414	0.3948	17.8792	10.0584	0.1060	4.5378	15.3057	36.8797	1.9113	0.0699	98.48	1.7836	0.2095	0.0816	3.6833	1.2258	0.0131	0.4973	0.2942	2.3344	2.6286	5.6856	0.8808	0.0173	0.7601	0.2389		
146k#21-2bt1	5.7038	0.4540	0.4837	6.8787	7.0214	0.1812	1.4092	19.9027	37.6952	0.9987	0.0491	82.78	1.1863	0.1435	0.0645	2.1577	0.9574	0.0250	0.1728	1.9705	1.8540	3.8245	6.1480	0.5139	0.0136	0.6927	0.3073		
146k#21-3bt1	9.9451	1.0421	0.1388	19.3095	9.7836	0.1055	4.9168	16.1083	41.0311	1.9551	0.0644	104.40	1.7516	0.2790	0.0205	3.9737	1.1297	0.0123	0.5105	0.2863	2.3349	2.8212	5.8851	0.8537	0.0151	0.7786	0.2214		
146k#21-3bt2	9.8888	0.8250	0.2376	17.9488	9.6102	0.1121	4.7823	14.9889	38.8677	2.1149	0.0920	99.27	1.8112	0.2344	0.0373	3.9207	1.1778	0.0139	0.5270	0.2848	2.3039	2.5885	5.6961	0.9803	0.0228	0.7690	0.2310		
146k#21-3bt3	8.8670	1.0259	0.3159	18.2952	9.5215	0.0979	4.7810	16.9032	40.4096	1.9104	0.0846	102.21	1.5839	0.2785	0.0474	3.8187	1.1151	0.0118	0.5035	0.4485	2.3412	2.7897	5.6588	0.8461	0.0201	0.7740	0.2260		

BIOTITE INCLUSIONS

Label	OXIDE													CATION NUMBER													CHEMICAL COMPOSITION		
	K ₂ O	Na ₂ O	CaO	MgO	FeO	MnO	TiO ₂	Al ₂ O ₃	SiO ₂	F-	Cl-	Total	K	Na	Ca	Mg	Fe	Mn	Ti	Al ^{VI}	Al ^{IV}	Al	Si	F	Cl	X _{Mg} /X _{Fe}	X _{Fe} /X _{Mg}		
146j#2-2incl1	10.0159	1.0534	0.3737	17.7257	10.4874	0.1275	5.7989	15.3885	38.7789	2.1574	0.0754	101.98	1.8358	0.2935	0.0575	3.7962	1.2602	0.0155	0.6266	0.1775	2.4281	2.6058	5.5719	0.9804	0.0183	0.7508	0.2492		
146j#2-2incl2	9.8675	1.0007	0.2239	17.5206	10.0866	0.1624	5.7781	15.3627	38.7561	2.2740	0.0642	101.10	1.8230	0.2810	0.0347	3.7822	1.2217	0.0199	0.6293	0.2353	2.3870	2.6223	5.6130	1.0416	0.0158	0.7559	0.2481		
146j#9-1incl1	9.6423	0.9940	0.2448	19.0691	8.9735	0.1583	5.2258	16.2559	40.8428	2.0827	0.1249	103.59	1.7088	0.2678	0.0384	3.9488	1.0426	0.0186	0.5460	0.3360	2.3257	2.6617	5.6743	0.9063	0.0294	0.7911	0.2089		
146j#9-1incl2	9.5564	0.6489	0.1322	18.4595	9.1487	0.0324	5.2047	15.7179	39.5654	2.3792	0.1143	100.96	1.7535	0.1804	0.0204	3.9578	1.1005	0.0039	0.5630	0.3560	2.3087	2.6647	5.6913	1.0824	0.0279	0.7824	0.2176		
146j#9-1incl3	9.5940	0.6149	0.1399	17.5175	9.1397	0.0875	4.8736	15.9545	39.4992	2.3304	0.0922	99.82	1.7778	0.1732	0.0218	3.7929	1.1103	0.0083	0.5324	0.4694	2.2621	2.7315	5.7379	1.0707	0.0227	0.7736	0.2284		
146j#9-2																													

PLAGIOCLASE ADJACENT TO GARNET

Label	OXIDE							CATION NUMBER						MINERAL COMPOSITION		
	CaO	Na ₂ O	K ₂ O	FeO	Al ₂ O ₃	SiO ₂	Total	Ca	Na	K	Fe	Al	Si	XAn	XAb	XOr
#7-1pl1	6.1880	7.9330	0.2148	0.0447	24.7410	59.7241	98.85	0.2985	0.6925	0.0123	0.0015	1.3128	2.6888	0.2975	0.6902	0.0123
#7-1pl2	6.3941	8.0168	0.2449	0.0657	25.6820	59.9788	100.38	0.3041	0.6900	0.0139	0.0022	1.3437	2.6626	0.3017	0.6845	0.0138
#7-1pl3	6.1722	7.8188	0.2923	0.0208	25.5108	60.3043	100.12	0.2937	0.6733	0.0166	0.0007	1.3355	2.6785	0.2986	0.6845	0.0169
#7-1pl4	6.2949	7.9700	0.2345	0.0824	25.0738	60.0218	99.68	0.3013	0.6903	0.0134	0.0028	1.3201	2.6813	0.2998	0.6869	0.0133
#7-2pl1	6.2711	7.9781	0.1948	0.1337	25.2824	60.2675	100.13	0.2987	0.6876	0.0110	0.0045	1.3246	2.6792	0.2995	0.6895	0.0110
#7-2pl2	6.2047	7.8309	0.2195	0.0002	25.4268	60.3021	99.98	0.2956	0.6750	0.0125	0.0000	1.3324	2.6811	0.3007	0.6866	0.0127
#7-2pl3	6.2251	7.8433	0.2351	0.0480	25.4622	60.1708	99.98	0.2967	0.6765	0.0133	0.0016	1.3350	2.6768	0.3008	0.6858	0.0135
#7-2pl4	6.3881	7.7741	0.1910	0.0034	25.2896	60.1242	99.77	0.3051	0.6719	0.0109	0.0001	1.3287	2.6802	0.3088	0.6801	0.0110
#7-2pl5	6.2545	7.8777	0.2401	0.0483	24.8711	60.5414	99.83	0.2985	0.6804	0.0136	0.0016	1.3057	2.6968	0.3008	0.6855	0.0137
#9-1pl1	6.0315	7.9493	0.1611	0.0002	25.1492	59.7906	99.08	0.2899	0.6915	0.0092	0.0000	1.3298	2.6825	0.2927	0.6981	0.0093
#9-1pl2	6.2258	8.0723	0.1771	0.0002	25.5033	60.5469	100.53	0.2952	0.6926	0.0100	0.0000	1.3301	2.6792	0.2959	0.6941	0.0100
#9-1pl3	6.3247	8.0894	0.2384	0.0002	25.0644	60.8376	100.55	0.2999	0.6942	0.0135	0.0000	1.3074	2.6926	0.2976	0.6890	0.0134
#9-1pl4	6.2299	7.9182	0.1880	0.0002	25.4987	60.0554	99.89	0.2972	0.6836	0.0107	0.0000	1.3382	2.6742	0.2997	0.6895	0.0108
#9-1pl5	6.0969	7.9167	0.1577	0.0069	25.6269	60.4531	100.26	0.2895	0.6802	0.0089	0.0002	1.3384	2.6790	0.2958	0.6951	0.0091
#9-1pl6	6.3135	8.1454	0.1511	0.0726	25.2024	60.7316	100.62	0.2992	0.6986	0.0085	0.0024	1.3139	2.6864	0.2973	0.6942	0.0084
#9-1pl7	6.1267	7.6781	0.2072	0.1034	25.1009	60.1700	99.39	0.2934	0.6654	0.0118	0.0035	1.3224	2.6896	0.3023	0.6856	0.0122
#9-1pl8	6.3042	7.9034	0.1902	0.0002	25.1510	60.3787	99.93	0.3006	0.6820	0.0108	0.0000	1.3192	2.6871	0.3026	0.6865	0.0109
#9-1pl9	6.2586	7.9073	0.2381	0.0002	24.8164	60.8454	100.07	0.2979	0.6811	0.0135	0.0000	1.2993	2.7030	0.3002	0.6862	0.0136
#9-1pl10	6.1778	8.0749	0.1465	0.0002	25.3071	60.9382	100.64	0.2923	0.6914	0.0083	0.0000	1.3171	2.6911	0.2947	0.6970	0.0084
#21-1pl1	6.1784	7.7516	0.1903	0.1246	24.3011	59.1185	97.66	0.3016	0.6847	0.0111	0.0043	1.3049	2.6934	0.3024	0.6865	0.0111
#21-1pl2	5.9961	8.0883	0.1724	0.0700	24.8934	59.5331	98.75	0.2895	0.7067	0.0099	0.0024	1.3221	2.6828	0.2877	0.7024	0.0098
#21-1pl3	5.8418	8.0170	0.1772	0.0173	24.3422	58.5402	96.94	0.2873	0.7135	0.0104	0.0006	1.3169	2.6872	0.2841	0.7056	0.0103

PLAGIOCLASE IN MATRIX

Label	OXIDE							CATION NUMBER						MINERAL COMPOSITION		
	CaO	Na ₂ O	K ₂ O	FeO	Al ₂ O ₃	SiO ₂	Total	Ca	Na	K	Fe	Al	Si	XAn	XAb	XOr
146j_1mtrx1	6.2888	7.9729	0.1996	0.0002	25.2722	60.3641	100.10	0.2995	0.6870	0.0113	0.0000	1.3238	2.6828	0.3002	0.6885	0.0113
146j_1mtrx2	6.2965	8.2175	0.2180	0.0002	25.3686	60.8199	100.92	0.2976	0.7029	0.0123	0.0000	1.3190	2.6831	0.2938	0.6940	0.0121
146j_1mtrx3	6.1668	7.7973	0.2003	0.0587	25.6466	60.6944	100.56	0.2919	0.6679	0.0113	0.0020	1.3353	2.6813	0.3006	0.6878	0.0116
146j_1mtrx4	6.3347	8.0717	0.1982	0.0002	25.2134	60.4136	100.23	0.3014	0.6950	0.0112	0.0000	1.3197	2.6830	0.2991	0.6898	0.0111
146j_1mtrx5	6.1337	8.2124	0.2141	0.0416	25.5088	60.6416	100.75	0.2903	0.7034	0.0121	0.0014	1.3281	2.6789	0.2886	0.6993	0.0120
146j_1mtrx6	6.2877	7.8719	0.1737	0.0002	25.5173	61.0724	100.92	0.2966	0.6719	0.0098	0.0000	1.3239	2.6884	0.3032	0.6868	0.0100
146j_2mtrx1	6.3892	8.1853	0.1911	0.0002	25.9808	61.0101	101.76	0.2995	0.6943	0.0107	0.0000	1.3397	2.6693	0.2982	0.6912	0.0107
146j_2mtrx2	6.3764	7.8925	0.2160	0.0002	25.8498	60.9321	101.27	0.3000	0.6720	0.0121	0.0000	1.3378	2.6756	0.3048	0.6829	0.0123
146j_2mtrx3	6.3627	8.1313	0.1683	0.0569	25.3782	59.9974	100.09	0.3034	0.7017	0.0096	0.0019	1.3313	2.6705	0.2990	0.6915	0.0095
146k_1mtrx1	5.8346	8.1806	0.3091	0.0208	24.6025	59.1813	98.13	0.2837	0.7199	0.0179	0.0007	1.3161	2.6861	0.2777	0.7047	0.0175
146k_1mtrx2	5.8737	8.0492	0.2417	0.0795	25.2862	60.9513	100.48	0.2782	0.6900	0.0136	0.0026	1.3176	2.6948	0.2834	0.7028	0.0139
146k_1mtrx3	5.6886	8.1385	0.3811	0.0206	24.7711	61.1768	100.18	0.2703	0.6998	0.0216	0.0007	1.2947	2.7130	0.2726	0.7057	0.0218
146k_1mtrx4	5.6770	8.1065	0.3723	0.0726	25.4183	61.1349	100.78	0.2681	0.6929	0.0209	0.0024	1.3207	2.6952	0.2730	0.7057	0.0213

Table A.2: Analytical data for cordierite, orthopyroxene, plagioclase and garnet for sample TL01-147.

CORDERITE TRANSECT 1

Distance (um)	OXIDE						CATION NUMBER					XMg/ Fe+Mg	XFe/ Fe+Mg
	FeO	MgO	MnO	Al ₂ O ₃	SiO ₂	Total	Fe	Mg	Mn	Al	Si		
0	11.1954	6.9005	0.3399	32.7052	48.8725	100.01	0.9603	1.0550	0.0296	3.9537	5.0124	0.5235	0.4765
50	11.0461	6.8335	0.0913	32.7699	49.2627	100.00	0.9455	1.0425	0.0080	3.9528	5.0414	0.5244	0.4756
100	10.7221	6.8603	0.2702	32.7320	49.3992	99.98	0.9167	1.0454	0.0234	3.9437	5.0496	0.5328	0.4672
150	10.9770	7.0668	0.1952	32.8574	49.2998	100.40	0.9368	1.0749	0.0170	3.9518	5.0304	0.5343	0.4657
200	11.1542	7.1425	0.3072	33.3156	49.5778	101.50	0.9419	1.0749	0.0263	3.9645	5.0052	0.5330	0.4670
250	10.8387	6.7583	0.1227	32.9772	49.2918	99.99	0.9269	1.0302	0.0107	3.9747	5.0405	0.5264	0.4736
300	11.2888	7.1478	0.2735	33.2141	49.6798	101.60	0.9510	1.0733	0.0234	3.9435	5.0043	0.5302	0.4698
350	11.0772	6.7938	0.1484	32.7835	49.3217	100.12	0.9476	1.0358	0.0129	3.9521	5.0444	0.5222	0.4778
400	10.9614	6.9570	0.1529	33.1118	49.4819	100.67	0.9306	1.0529	0.0132	3.9623	5.0234	0.5308	0.4692
450	11.2262	7.0499	0.3178	33.0868	48.9817	100.66	0.9569	1.0710	0.0275	3.9744	4.9917	0.5281	0.4719
500	23.0773	5.9014	0.1243	14.0541	24.4982	67.66	3.2787	1.4945	0.0179	2.8142	4.1619	0.3131	0.6869
550	10.9767	6.8030	0.2839	32.4095	48.0420	98.52	0.9555	1.0554	0.0251	3.9759	5.0001	0.5248	0.4752
600	10.5471	6.8693	0.2342	33.1579	49.5292	100.34	0.8973	1.0418	0.0203	3.9759	5.0385	0.5372	0.4628
650	10.7219	6.8945	0.2795	32.6360	48.5961	99.13	0.9228	1.0577	0.0243	3.9587	5.0009	0.5340	0.4660
700	10.9002	7.2117	0.1846	33.4176	49.9619	101.68	0.9161	1.0803	0.0158	3.9582	5.0207	0.5411	0.4589
750	10.8326	6.9486	0.2550	33.3928	49.7900	101.22	0.9149	1.0460	0.0218	3.9746	5.0279	0.5334	0.4666
800	9.2238	1.4950	0.2327	10.2141	13.8707	35.04	2.4785	0.7161	0.0633	3.8681	4.4564	0.2242	0.7758
850	11.2476	7.0440	0.1165	33.4251	49.6574	101.49	0.9495	1.0599	0.0099	3.9770	5.0126	0.5275	0.4725
900	10.9091	6.9695	0.1405	32.9597	49.4027	100.38	0.9300	1.0590	0.0122	3.9599	5.0357	0.5324	0.4676
950	11.5273	6.9869	0.2470	33.5580	50.9777	103.30	0.9558	1.0326	0.0207	3.9216	5.0543	0.5193	0.4807
1000	3.4752	1.5550	0.1391	11.3301	11.5831	28.08	1.0805	0.8618	0.0438	4.9643	4.3058	0.4437	0.5563
1050	10.9559	6.8873	0.1747	32.8572	49.0575	99.93	0.9390	1.0523	0.0152	3.9690	5.0276	0.5284	0.4716
1100	18.6513	7.5141	0.1131	15.4596	37.6214	79.36	2.1060	1.5123	0.0129	2.4603	5.0795	0.4180	0.5820
1150	11.1091	6.9407	0.1159	33.6686	49.9186	101.75	0.9335	1.0397	0.0099	3.9875	5.0157	0.5269	0.4731
1200	11.0350	6.6964	0.1774	32.7611	48.9444	99.61	0.9471	1.0244	0.0155	3.9627	5.0228	0.5196	0.4804
1250	10.7074	6.7679	0.0731	32.3893	48.4500	98.39	0.9306	1.0485	0.0065	3.9674	5.0349	0.5298	0.4702
1300	9.8722	3.9062	0.0607	9.1241	75.1829	98.15	0.8102	0.5714	0.0051	1.0553	7.3770	0.4136	0.5864
1350	10.1136	7.0319	0.1907	33.5957	49.1523	100.08	0.8619	1.0682	0.0165	4.0352	5.0087	0.5534	0.4466
1400	0.3971	-0.0450	0.1384	25.9350	63.5723	90.00	0.0318	-0.0065	0.0113	2.9222	6.0768	-0.2544	1.2544
1450	0.2473	-0.0588	-0.0032	25.1161	60.2384	85.54	0.0207	-0.0089	-0.0003	2.9688	6.0408	-0.7468	1.7468
1500	0.3729	0.0428	-0.0255	26.6786	64.4274	91.50	0.0294	0.0060	-0.0021	2.9583	6.0609	0.1695	0.8305

A-13

1550	10.0803	7.6735	0.5194	34.7948	51.9561	105.02	0.8141	1.1045	0.0425	3.9600	5.0168	0.5757	0.4243
1600	28.1010	2.7942	6.8154	18.0293	25.4938	81.23	3.5892	0.6362	0.8817	3.2456	3.8934	0.1506	0.8494
1650	36.6139	3.5731	1.5079	21.1193	37.7561	100.57	3.6474	0.6345	0.1521	2.9652	4.4973	0.1482	0.8518
1700	36.4624	3.6062	1.6929	20.8626	37.9454	100.57	3.6341	0.6407	0.1709	2.9306	4.5221	0.1499	0.8501
1750	0.6927	0.2267	-0.0227	28.0839	67.4048	96.39	0.0516	0.0302	-0.0017	2.9463	5.9994	0.3688	0.6312
1800	37.6714	3.4187	1.6674	21.3689	38.1982	102.32	3.6996	0.5985	0.1659	2.9577	4.4855	0.1392	0.8608
1850	10.2699	7.6334	0.2687	33.7357	50.2935	102.20	0.8556	1.1337	0.0227	3.9615	5.0105	0.5699	0.4301
1900	10.1909	7.2051	0.1008	32.7937	49.3041	99.59	0.8724	1.0994	0.0087	3.9566	5.0468	0.5576	0.4424
1950	10.8196	7.1262	0.0831	32.8610	49.0539	99.94	0.9261	1.0872	0.0072	3.9641	5.0204	0.5400	0.4600
2000	10.4507	7.3382	0.1239	33.2427	49.5746	100.73	0.8858	1.1087	0.0107	3.9713	5.0244	0.5559	0.4441
2050	11.0925	7.3394	0.1616	33.0239	49.0657	100.68	0.9437	1.1129	0.0140	3.9596	4.9911	0.5411	0.4589
2100	11.0863	7.2256	0.1895	33.4468	48.9934	100.94	0.9405	1.0926	0.0164	3.9989	4.9697	0.5374	0.4626
2150	10.7945	7.2625	0.1871	33.6358	50.3386	102.22	0.9027	1.0826	0.0159	3.9647	5.0339	0.5453	0.4547
2200	16.3618	8.7917	0.2050	30.0992	47.3164	102.77	1.3875	1.3289	0.0176	3.5975	4.7979	0.4892	0.5108
2250	10.5989	6.7927	0.0335	32.3898	48.9340	98.75	0.9164	1.0467	0.0030	3.9467	5.0585	0.5332	0.4668
2300	11.0281	7.0916	0.1129	33.6352	50.6074	102.48	0.9153	1.0491	0.0095	3.9344	5.0222	0.5341	0.4659
2350	10.6289	7.0874	0.1393	33.1668	50.1020	101.12	0.8975	1.0667	0.0119	3.9467	5.0580	0.5431	0.4569
2400	11.1957	7.1113	0.1156	32.9558	49.0087	100.39	0.9545	1.0806	0.0101	3.9597	4.9956	0.5310	0.4690
2450	10.6681	6.8844	0.0978	33.6863	49.0343	100.37	0.9068	1.0430	0.0084	4.0352	4.9832	0.5349	0.4651
2500	22.5311	8.3011	0.1283	19.3237	33.9754	84.26	2.4390	1.6017	0.0141	2.9481	4.3977	0.3964	0.6036
2550	37.1964	10.3471	0.5597	5.0535	47.1333	100.29	3.7176	1.8434	0.0567	0.7119	5.6327	0.3315	0.6685
2600	36.1934	10.5153	0.5814	6.4788	46.2843	100.05	3.5952	1.8618	0.0585	0.9071	5.4972	0.3412	0.6588
2650	15.2240	0.2652	0.0822	0.8869	1.2259	17.68	12.9144	0.4010	0.0707	1.0604	1.2435	0.0301	0.9699
2700	10.9659	6.5717	0.3400	31.6191	47.5120	97.01	0.9681	1.0341	0.0305	3.9341	5.0151	0.5165	0.4835
2750	10.8263	6.8061	0.2379	32.3003	48.6894	98.86	0.9359	1.0487	0.0209	3.9351	5.0325	0.5284	0.4716
2800	11.4272	6.8585	0.0209	32.7994	49.0687	100.17	0.9762	1.0443	0.0018	3.9491	5.0121	0.5169	0.4831
2850	10.7735	5.0293	0.1482	13.1854	72.1180	101.25	0.8699	0.7238	0.0122	1.5005	6.9624	0.4542	0.5458
2900	11.0889	7.1104	0.0994	32.8508	49.5440	100.69	0.9414	1.0760	0.0086	3.9306	5.0292	0.5333	0.4667
2950	37.5730	9.8600	0.7083	3.9824	47.5334	99.66	3.7764	1.7664	0.0722	0.5642	5.7125	0.3187	0.6813
3000	10.9203	6.9312	0.1209	32.4571	49.1115	99.54	0.9375	1.0607	0.0105	3.9272	5.0414	0.5308	0.4692
3050	12.0338	5.7594	0.1695	32.9554	37.0329	87.95	1.1861	1.0118	0.0170	4.5777	4.3643	0.4603	0.5397
3100	10.9913	6.8282	0.1750	32.7913	49.3408	100.13	0.9399	1.0409	0.0152	3.9524	5.0454	0.5255	0.4745
3150	11.3475	6.8842	0.0447	32.9862	49.7041	100.97	0.9626	1.0409	0.0039	3.9432	5.0409	0.5195	0.4805

CORDIERITE TRANSECT 2

Distance (um)	OXIDE						CATION NUMBER					XMg/ Fe+Mg	XFe/ Fe+Mg
	FeO	MgO	MnO	Al ₂ O ₃	SiO ₂	Total	Fe	Mg	Mn	Al	Si		
0	10.9665	6.6619	0.2318	32.8724	49.1609	99.89	0.9405	1.0184	0.0201	3.9731	5.0409	0.5199	0.4801
50	11.1741	6.9688	0.1608	32.5380	49.2170	100.06	0.9575	1.0643	0.0140	3.9293	5.0423	0.5264	0.4736
100	11.0162	6.5298	0.2120	32.1455	48.2910	98.19	0.9621	1.0166	0.0188	3.9569	5.0430	0.5138	0.4862
150	2.2604	0.4209	0.0651	35.6573	39.4883	77.89	0.2346	0.0779	0.0069	5.2164	4.9010	0.2492	0.7508
200	10.7641	6.4820	-0.0101	32.5507	48.8270	98.61	0.9320	1.0004	-0.0009	3.9720	5.0549	0.5177	0.4823
250	11.2179	7.3650	0.0751	36.2873	53.8537	108.80	0.8786	1.0281	0.0060	4.0052	5.0429	0.5392	0.4608
300	10.7133	6.9134	0.2927	33.1511	49.7973	100.87	0.9075	1.0439	0.0251	3.9576	5.0436	0.5349	0.4651
350	10.7813	6.7654	0.1605	32.1866	48.4642	98.36	0.9375	1.0487	0.0141	3.9449	5.0394	0.5280	0.4720
400	10.8876	6.7621	0.1567	32.4092	49.1066	99.32	0.9383	1.0386	0.0137	3.9360	5.0597	0.5254	0.4746
450	21.2728	0.1850	0.4388	0.7258	1.4540	24.08	13.9095	0.2157	0.2906	0.6689	1.1369	0.0153	0.9847
500	11.9942	7.7673	0.2799	34.2479	52.6284	106.92	0.9581	1.1058	0.0227	3.8552	5.0261	0.5358	0.4642
550	11.2683	6.4227	0.2149	32.5133	49.0015	99.42	0.9722	0.9878	0.0188	3.9534	5.0550	0.5040	0.4960
600	11.2138	6.7826	0.1077	32.9931	49.2845	100.38	0.9570	1.0317	0.0093	3.9684	5.0292	0.5188	0.4812
650	37.1525	10.2609	0.4761	4.1005	47.6133	99.60	3.7323	1.8374	0.0485	0.5805	5.7192	0.3299	0.6701
700	10.7809	6.9065	0.2983	32.5967	49.3907	99.97	0.9222	1.0530	0.0258	3.9300	5.0520	0.5331	0.4669
750	10.3753	6.8414	0.1341	32.3514	49.1956	98.90	0.8928	1.0493	0.0117	3.9234	5.0616	0.5403	0.4597
800	11.3296	6.8314	0.2185	32.2443	48.4856	99.11	0.9788	1.0520	0.0191	3.9258	5.0084	0.5180	0.4820
850	29.0422	8.1632	0.4972	9.0769	43.5202	90.30	3.0978	1.5521	0.0537	1.3646	5.5506	0.3338	0.6662
900	36.9044	10.0896	0.5570	4.8538	47.7284	100.13	3.6780	1.7924	0.0563	0.6818	5.6877	0.3276	0.6724
950	10.9390	6.8430	0.2346	32.9073	48.8703	99.79	0.9372	1.0451	0.0204	3.9737	5.0067	0.5272	0.4728
1000	11.0949	6.7340	0.2153	32.3144	48.2051	98.56	0.9662	1.0454	0.0191	3.9662	5.0196	0.5197	0.4803
1050	10.8786	6.6701	0.0829	32.6939	49.1334	99.46	0.9353	1.0221	0.0072	3.9612	5.0505	0.5222	0.4778
1100	36.8921	10.3641	0.6241	4.8626	46.9831	99.73	3.6926	1.8491	0.0633	0.6860	5.6229	0.3337	0.6663
1150	10.7634	6.5981	0.2676	32.1374	48.7224	98.49	0.9360	1.0227	0.0236	3.9390	5.0664	0.5221	0.4779
1200	11.1682	6.6547	0.0377	32.5609	48.3801	98.80	0.9686	1.0287	0.0033	3.9797	5.0166	0.5151	0.4849
1250	10.9383	6.7556	0.0965	32.6676	48.8294	99.29	0.9429	1.0380	0.0084	3.9689	5.0330	0.5240	0.4760
1300	32.8980	7.6806	0.6436	4.8813	40.3314	86.43	3.8244	1.5915	0.0758	0.7998	5.6061	0.2939	0.7061
1350	10.5640	6.5203	0.1997	32.2862	47.3409	96.91	0.9338	1.0272	0.0179	4.0218	5.0031	0.5238	0.4762
1400	10.6215	6.3865	0.3644	32.3060	48.8051	98.48	0.9219	0.9881	0.0321	3.9519	5.0651	0.5173	0.4827
1450	10.8050	6.7773	0.1446	31.7571	48.5536	98.04	0.9435	1.0548	0.0128	3.9084	5.0696	0.5278	0.4722
1500	10.9059	5.2638	0.1698	26.5166	39.9778	82.83	1.1417	0.9822	0.0180	3.9122	5.0040	0.4625	0.5375
1550	11.3047	6.7004	0.3403	32.8981	48.8666	100.11	0.9671	1.0217	0.0296	3.9663	4.9985	0.5137	0.4863

A-15

1600	10.6314	7.0826	0.4950	32.5450	48.7833	99.54	0.9147	1.0862	0.0432	3.9462	5.0184	0.5428	0.4572
1650	10.7192	6.4034	0.2322	32.0422	48.7577	98.15	0.9345	0.9951	0.0206	3.9369	5.0825	0.5157	0.4843
1700	11.0169	6.8067	0.2434	32.7797	49.0073	99.85	0.9459	1.0418	0.0212	3.9666	5.0313	0.5241	0.4759
1750	10.8513	6.6495	0.0329	32.4951	48.7709	98.80	0.9389	1.0256	0.0029	3.9627	5.0459	0.5221	0.4779
1800	10.5819	6.6451	0.3036	32.3479	48.2148	98.09	0.9228	1.0329	0.0269	3.9755	5.0271	0.5281	0.4719
1850	37.6047	10.5876	0.5878	3.7793	49.5068	102.07	3.6779	1.8458	0.0582	0.5210	5.7894	0.3342	0.6658
1900	20.7000	6.4898	0.2495	18.9316	40.2679	86.64	2.1906	1.2242	0.0267	2.8238	5.0955	0.3585	0.6415
1950	10.7509	7.1345	0.0928	32.9038	49.2165	100.10	0.9183	1.0863	0.0081	3.9612	5.0268	0.5419	0.4581
2000	10.8998	6.6357	0.1630	32.7394	49.8694	100.31	0.9290	1.0080	0.0141	3.9326	5.0820	0.5204	0.4796
2050	10.8463	6.7668	0.0732	32.4500	48.8313	98.97	0.9374	1.0424	0.0065	3.9524	5.0459	0.5265	0.4735
2100	10.8388	6.5711	0.0187	33.0176	48.9684	99.41	0.9315	1.0065	0.0017	3.9990	5.0318	0.5193	0.4807
2150	10.9370	6.4943	0.0848	32.4275	48.7213	98.66	0.9485	1.0038	0.0075	3.9630	5.0517	0.5142	0.4858
2200	11.2255	6.7750	0.0297	32.3480	48.8580	99.24	0.9690	1.0424	0.0026	3.9354	5.0429	0.5182	0.4818
2250	10.6022	6.6148	0.2120	32.0773	48.7328	98.24	0.9231	1.0265	0.0188	3.9360	5.0732	0.5265	0.4735
2300	15.1489	5.0607	0.1303	21.1551	31.6010	73.10	1.8644	1.1102	0.0162	3.6692	4.6500	0.3732	0.6268
2350	37.7283	10.2247	0.4732	3.8567	47.1275	99.41	3.8165	1.8435	0.0485	0.5499	5.7003	0.3257	0.6743
2400	22.6046	8.6581	0.3039	21.8221	36.4937	89.88	2.2986	1.5693	0.0314	3.1275	4.4373	0.4057	0.5943
2450	10.5839	6.4112	0.2975	31.9103	48.6192	97.82	0.9246	0.9984	0.0263	3.9290	5.0787	0.5192	0.4808
2500	11.1180	6.4510	0.0039	32.3691	48.8640	98.81	0.9626	0.9956	0.0003	3.9498	5.0586	0.5084	0.4916
2550	10.6479	5.1339	0.3748	26.5082	39.3650	82.03	1.1243	0.9662	0.0401	3.9446	4.9697	0.4622	0.5378
2600	11.4712	7.6153	0.2031	33.5727	52.0311	104.89	0.9344	1.1057	0.0168	3.8541	5.0676	0.5420	0.4580
2650	23.4570	7.7273	0.0537	19.1577	33.2401	83.64	2.5929	1.5225	0.0060	2.9846	4.3932	0.3700	0.6300
2700	36.6419	10.2215	0.4990	4.0772	47.3361	98.78	3.7121	1.8458	0.0512	0.5822	5.7341	0.3321	0.6679
2750	10.8188	6.4818	0.1238	32.2359	48.9478	98.61	0.9381	1.0019	0.0108	3.9398	5.0753	0.5164	0.4836
2800	10.4598	6.5459	0.1648	33.1350	49.3109	99.62	0.8961	0.9996	0.0143	4.0010	5.0514	0.5273	0.4727
2850	18.5623	2.9057	0.0782	10.8803	16.0150	48.44	3.7431	1.0445	0.0159	3.0921	3.8615	0.2182	0.7818
2900	10.9058	6.6784	0.3281	32.4706	48.9529	99.34	0.9399	1.0259	0.0287	3.9441	5.0447	0.5219	0.4781
2950	11.1448	6.7879	-0.0609	32.6781	48.4244	98.97	0.9639	1.0464	-0.0054	3.9831	5.0076	0.5205	0.4795
3000	22.6584	7.3416	0.1163	22.6073	32.7281	85.45	2.4120	1.3931	0.0126	3.3918	4.1658	0.3661	0.6339
3050	10.9456	7.0457	0.1405	32.9781	49.3104	100.42	0.9332	1.0706	0.0122	3.9623	5.0264	0.5343	0.4657
3100	10.3634	6.6093	0.1727	32.8196	49.0880	99.05	0.8930	1.0151	0.0150	3.9854	5.0571	0.5320	0.4680
3150	0.4940	0.0417	-0.0424	24.6384	62.5343	87.67	0.0407	0.0062	-0.0036	2.8584	6.1548	0.1314	0.8686
3200	0.2587	-0.0459	0.0042	24.6085	62.3034	87.13	0.0215	-0.0068	0.0003	2.8706	6.1656	-0.4592	1.4592
3250	-0.0113	0.1321	0.0174	24.5102	62.0774	86.73	-0.0009	0.0195	0.0015	2.8695	6.1659	1.0484	-0.0484
3300	0.0557	0.0504	0.0867	24.2546	61.2497	85.70	0.0047	0.0075	0.0074	2.8773	6.1644	0.6173	0.3827
3350	0.0628	0.1475	-0.0854	24.7661	62.5293	87.42	0.0051	0.0216	-0.0071	2.8712	6.1500	0.8090	0.1910

3400	0.2281	0.0209	-0.0540	24.5294	61.9218	86.65	0.0191	0.0032	-0.0045	2.8820	6.1722	0.1419	0.8581
3450	0.1353	-0.0354	0.0710	24.3407	61.4828	85.99	0.0113	-0.0053	0.0060	2.8700	6.1502	-0.8750	1.8750

: indicates poor results

ORTHOPYROXENE LARGE GRAINS

Label	OXIDE								CATION NUMBER						XFe/ Fe+Mg	XMg/ Fe+Mg
	FeO	MgO	MnO	CaO	TiO ₂	Al ₂ O ₃	SiO ₂	Total	Fe	Mg	Mn	Ca	Al	Si		
LR1 1r	36.5677	10.1526	0.6053	0.1939	0.4885	4.7504	46.8707	99.63	2.4579	1.2163	0.0412	0.0167	0.4500	3.7669	0.6690	0.3310
LR1 2r	35.9501	10.4110	0.9525	0.1961	0.1057	4.5052	47.7740	99.89	2.4017	1.2397	0.0644	0.0168	0.4242	3.8163	0.6596	0.3404
LR1 3c	37.4124	10.5437	0.4931	0.0437	0.3944	4.9320	47.2769	101.10	2.4818	1.2467	0.0331	0.0037	0.4611	3.7499	0.6656	0.3344
LR1 4c	37.3772	9.8208	0.7254	0.1748	0.2809	4.8988	45.9212	99.20	2.5410	1.1900	0.0499	0.0152	0.4694	3.7327	0.6811	0.3189
LR1 5c	36.9026	10.6535	0.7103	0.0818	0.2376	4.7138	46.8736	100.17	2.4785	1.2754	0.0483	0.0070	0.4462	3.7643	0.6602	0.3398
LR1 6r	32.9699	10.6517	0.7321	0.0501	0.3298	4.6522	47.6160	97.00	2.2195	1.2781	0.0499	0.0043	0.4414	3.8329	0.6346	0.3654
LR1 7r	37.0572	10.5430	0.5914	0.0681	0.3862	4.6358	46.9542	100.24	2.4811	1.2582	0.0401	0.0058	0.4374	3.7590	0.6635	0.3365
LR2 r1	36.5464	10.1247	0.4706	0.2827	0.2665	4.8582	47.4539	100.00	2.4410	1.2054	0.0318	0.0242	0.4573	3.7898	0.6694	0.3306
LR2 r2	36.7798	10.2756	0.6195	0.1873	0.4262	4.8158	47.9336	101.04	2.4312	1.2107	0.0415	0.0159	0.4486	3.7886	0.6676	0.3324
LR2 c3	36.2489	10.2390	0.6228	0.1708	0.2051	4.8414	47.3159	99.64	2.4337	1.2253	0.0423	0.0147	0.4581	3.7984	0.6651	0.3349
LR2 c4	36.3627	10.1212	0.5784	0.1851	0.3475	4.8818	46.8060	99.28	2.4500	1.2155	0.0395	0.0160	0.4636	3.7708	0.6684	0.3316
LR2 c5	36.1961	10.1861	0.5133	0.1962	0.3721	4.7892	46.4025	98.66	2.4556	1.2317	0.0353	0.0170	0.4579	3.7641	0.6660	0.3340
LR2 r6	36.4177	10.3013	0.6620	0.2289	0.2620	3.9079	47.6839	99.46	2.4481	1.2343	0.0451	0.0197	0.3703	3.8328	0.6648	0.3352
LR2 r7	37.2960	10.2482	0.7373	0.1431	0.1575	4.7609	47.2238	100.57	2.4960	1.2225	0.0500	0.0123	0.4491	3.7790	0.6712	0.3288
LR3 r1	36.0004	10.2861	0.6245	0.2837	0.3153	4.0909	46.8199	98.42	2.4475	1.2464	0.0430	0.0247	0.3920	3.8059	0.6626	0.3374
LR3 r2	36.6098	10.2160	0.4711	0.1035	0.2607	4.6727	47.2246	99.56	2.4601	1.2236	0.0321	0.0089	0.4425	3.7944	0.6678	0.3322
LR3 c3	36.9363	10.1296	0.4719	0.0556	0.2729	4.8800	47.1204	99.87	2.4767	1.2107	0.0320	0.0048	0.4612	3.7779	0.6717	0.3283
LR3 c4	36.7032	10.4210	0.4549	0.0809	0.4582	5.1494	47.2340	100.50	2.4414	1.2355	0.0306	0.0069	0.4827	3.7567	0.6640	0.3360
LR3 c5	36.9106	9.9832	0.6809	0.0269	0.3702	4.9433	46.6715	99.59	2.4867	1.1988	0.0465	0.0023	0.4694	3.7596	0.6747	0.3253
LR3 r6	36.8376	10.1436	0.6308	0.1365	0.3600	4.8542	47.1235	100.09	2.4674	1.2110	0.0428	0.0117	0.4582	3.7740	0.6708	0.3292
LR3 r7	37.1668	10.5499	0.4783	0.2194	0.1603	4.7784	47.3554	100.71	2.4766	1.2530	0.0323	0.0187	0.4488	3.7731	0.6640	0.3360

ORTHOPYROXENE SMALL GRAINS

Label	OXIDE								CATION NUMBER						XFe/ Fe+Mg	XMg/ Fe+Mg
	FeO	MgO	MnO	CaO	TiO ₂	Al ₂ O ₃	SiO ₂	Total	Fe	Mg	Mn	Ca	Al	Si		
SR1 1	17.5309	8.7641	0.2509	0.2850	0.0578	26.7390	43.7891	102.67	1.0584	0.9414	0.0153	0.0220	2.2710	3.1536	0.5288	0.4712
SR1 2	14.6724	2.8865	0.2140	0.1580	0.0725	22.4594	12.9838	56.92	1.7360	0.6088	0.0256	0.0240	3.7453	1.8369	0.7404	0.2596
SR2 1	37.9090	9.9567	0.4614	0.0859	0.4221	4.4755	47.0499	100.27	2.5434	1.1907	0.0314	0.0074	0.4232	3.7744	0.6811	0.3189
SR2 2	36.6900	10.0482	0.6815	0.1841	0.1953	4.2970	47.3076	99.19	2.4774	1.2093	0.0452	0.0159	0.4089	3.8194	0.6720	0.3280
SR3 1	10.8972	6.7017	0.0981	0.1129	0.1527	31.8207	48.5170	97.94	0.6344	0.6954	0.0058	0.0084	2.6107	3.3771	0.4771	0.5229
SR3 2	32.7177	3.9319	0.3421	0.1105	0.2279	3.8982	24.7582	65.79	3.6478	0.7814	0.0386	0.0158	0.6125	3.3006	0.8236	0.1764
SC1 1	15.4011	8.1740	0.4149	0.0941	-0.0104	26.5872	47.6289	100.55	0.9136	0.8643	0.0249	0.0072	2.2229	3.3784	0.5139	0.4861
SC1 2	36.8897	10.0223	0.9906	0.1059	0.4500	3.6306	47.7516	99.73	2.4809	1.2014	0.0675	0.0091	0.3441	3.8398	0.6737	0.3263
SC2 1	22.0341	6.0772	0.0681	0.2072	0.2130	13.8222	25.5103	74.16	2.0606	1.0130	0.0063	0.0248	1.8218	2.8525	0.6704	0.3296
SC2 2	33.4760	9.5437	0.7577	0.0453	-0.0124	5.6066	44.9621	95.25	2.3420	1.1901	0.0537	0.0041	0.5528	3.7612	0.6631	0.3369
SC3 1	36.8615	10.0636	0.6133	0.1239	0.4061	4.8854	46.7117	99.54	2.4825	1.2080	0.0418	0.0107	0.4637	3.7615	0.6727	0.3273
SC3 2	21.8289	9.3392	0.1373	0.1209	0.1492	21.6595	38.1624	98.23	1.4468	1.1033	0.0092	0.0103	2.0233	3.0245	0.5674	0.4326

Note: L - large grains, S - small grains, R - rim of symplectite, r - rim of grain, C - core of symplectite, c - core of grain.

: indicates poor results

PLAG LARGE GRAINS

Label	OXIDE						CATION NUMBERS					COMPOSITION DATA		
	Na ₂ O	K ₂ O	CaO	Al ₂ O ₃	SiO ₂	Total	Na	K	Ca	Al	Si	XAn	XAb	XOr
LR1 r1	7.3515	0.2161	5.6647	23.6005	60.0364	96.87	0.6498	0.0126	0.2767	1.2681	2.7368	0.2946	0.6919	0.0134
LR1 r2	7.3717	0.2967	5.9841	23.4817	59.4756	96.61	0.6564	0.0174	0.2944	1.2710	2.7311	0.3041	0.6780	0.0180
LR1 c3	8.4037	0.0763	4.5679	22.8004	61.7002	97.55	0.7349	0.0044	0.2207	1.2120	2.7826	0.2299	0.7655	0.0046
LR1 c4	7.4156	0.0686	6.4236	24.5282	61.8432	100.28	0.6351	0.0039	0.3040	1.2770	2.7315	0.3224	0.6735	0.0041
LR1 c5	8.1729	0.1822	5.9924	23.7867	61.5231	99.66	0.7060	0.0104	0.2861	1.2491	2.7410	0.2854	0.7042	0.0104
LR1 r6	8.0835	0.2045	6.2389	23.8723	61.7872	100.19	0.6936	0.0115	0.2958	1.2452	2.7342	0.2955	0.6930	0.0115
LR1 r7	8.5022	0.2224	5.8328	24.7328	62.4171	101.71	0.7199	0.0124	0.2729	1.2731	2.7257	0.2715	0.7162	0.0123
LR2 r1	7.9509	0.1763	5.7766	24.2404	62.0761	100.22	0.6813	0.0099	0.2735	1.2627	2.7434	0.2835	0.7062	0.0103
LR2 r2	7.9547	-0.0416	5.9218	23.5935	60.3032	97.73	0.6996	-0.0024	0.2878	1.2614	2.7352	0.2922	0.7103	-0.0024
LR2 c3	8.7642	0.0613	6.0386	24.5526	63.4924	102.91	0.7334	0.0034	0.2793	1.2490	2.7403	0.2749	0.7218	0.0033
LR2 c4	7.9656	0.1647	5.7217	25.0607	64.1650	103.08	0.6622	0.0090	0.2628	1.2664	2.7510	0.2814	0.7090	0.0096
LR2 r5	8.5118	0.0612	6.2082	24.1554	61.8420	100.78	0.7283	0.0034	0.2935	1.2564	2.7289	0.2863	0.7104	0.0033
LR2 r6	7.9532	0.0933	6.3709	24.6169	62.7048	101.74	0.6713	0.0052	0.2972	1.2631	2.7296	0.3052	0.6894	0.0053
LR3 r1	7.8053	0.2272	5.8364	23.9345	62.1623	99.97	0.6692	0.0128	0.2765	1.2475	2.7488	0.2885	0.6982	0.0134
LR3 r2	7.6822	0.1102	6.1387	24.1959	61.9646	100.09	0.6593	0.0062	0.2912	1.2624	2.7428	0.3044	0.6891	0.0065
LR3 c3	7.7575	0.1987	5.9627	23.5598	63.6174	101.10	0.6578	0.0111	0.2794	1.2145	2.7822	0.2946	0.6937	0.0117
LR3 c4	8.0812	0.2418	5.6463	24.1806	62.3610	100.51	0.6906	0.0136	0.2666	1.2562	2.7485	0.2746	0.7114	0.0140
LR3 r5	7.5368	0.2024	5.6604	23.8635	61.4809	98.74	0.6544	0.0116	0.2716	1.2595	2.7531	0.2897	0.6980	0.0124
LR3 r6	7.3626	0.1849	5.6958	24.1400	61.7549	99.14	0.6361	0.0105	0.2719	1.2678	2.7515	0.2960	0.6925	0.0114

A-19

Note: L - large grains, R - rim of symplectite, r - rim of grain, c - core of grain.

GARNET

Label	OXIDE									CATION NUMBER						CHEMICAL COMPOSITION DATA					
	FeO	MgO	MnO	CaO	Al ₂ O ₃	SiO ₂	TiO ₂	Cr ₂ O ₃	Total	Fe	Mg	Mn	Ca	Al	Si	Fe/Mg	Mg/Fe	XAlm	XPrp	XGr	XSp
Grt_1	37.6191	3.4884	1.4701	0.8700	21.1608	38.1070	0.3377	0.3000	103.35	2.4680	0.4079	0.0977	0.0731	1.9566	2.9893	0.8582	0.1418	0.8101	0.1339	0.0240	0.0321
Grt_2	36.7463	3.0735	1.9174	0.8381	21.2721	38.7119	0.0943	0.0433	102.70	2.4124	0.3597	0.1275	0.0705	1.9682	3.0388	0.8702	0.1298	0.8122	0.1211	0.0237	0.0429
Grt_3	37.0150	3.5044	1.5713	0.9629	21.3067	38.2375	0.1719	-0.0215	102.75	2.4329	0.4108	0.1046	0.0811	1.9737	3.0051	0.8556	0.1444	0.8031	0.1355	0.0268	0.0345
Grt_4	36.9613	3.3900	1.4872	0.8686	21.1277	37.9159	0.0602	0.0872	101.90	2.4510	0.4007	0.0999	0.0738	1.9746	3.0064	0.8595	0.1405	0.8101	0.1324	0.0244	0.0330
Grt_5	36.9842	3.4834	1.4848	0.8127	21.2007	38.4301	-0.0558	0.0993	102.40	2.4316	0.4084	0.0976	0.0685	1.9656	3.0228	0.8562	0.1438	0.8089	0.1359	0.0228	0.0325
Grt_6	37.0444	3.2077	1.6576	1.1342	21.7017	38.1276	0.3763	0.2549	103.50	2.4208	0.3736	0.1097	0.0950	1.9988	2.9792	0.8663	0.1337	0.8072	0.1246	0.0317	0.0366

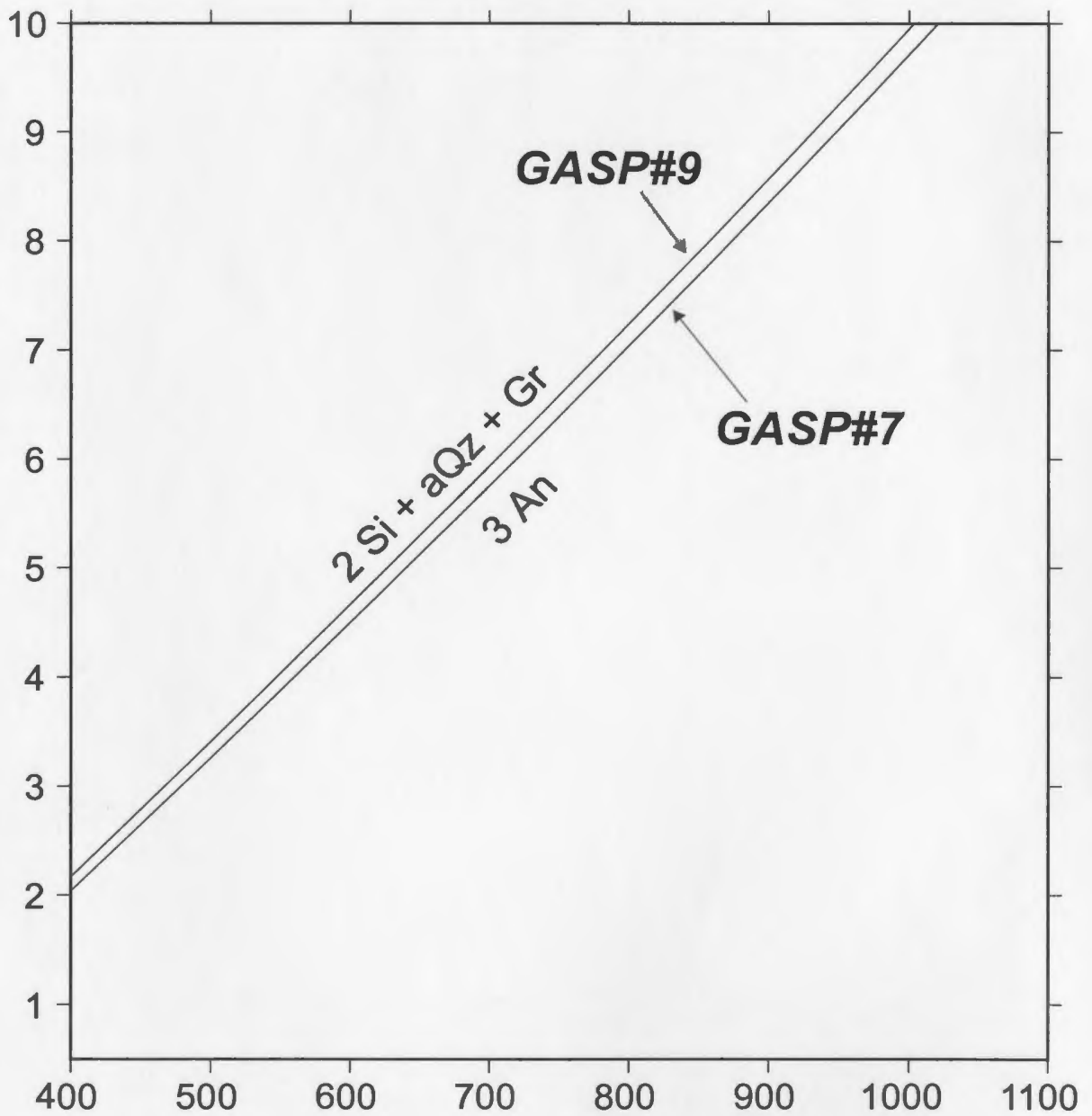


Figure A.1: TWQ (v. 2.02) plot of the pressure dependant GASP reaction. The generated reaction lines represent two separate analyses of plagioclase and adjacent garnet from the regional metamorphic sample TL01-146.

